

# Loughborough University Institutional Repository

---

## *Laser based tracking and spin measurement*

This item was submitted to Loughborough University's Institutional Repository by the/an author.

**Additional Information:**

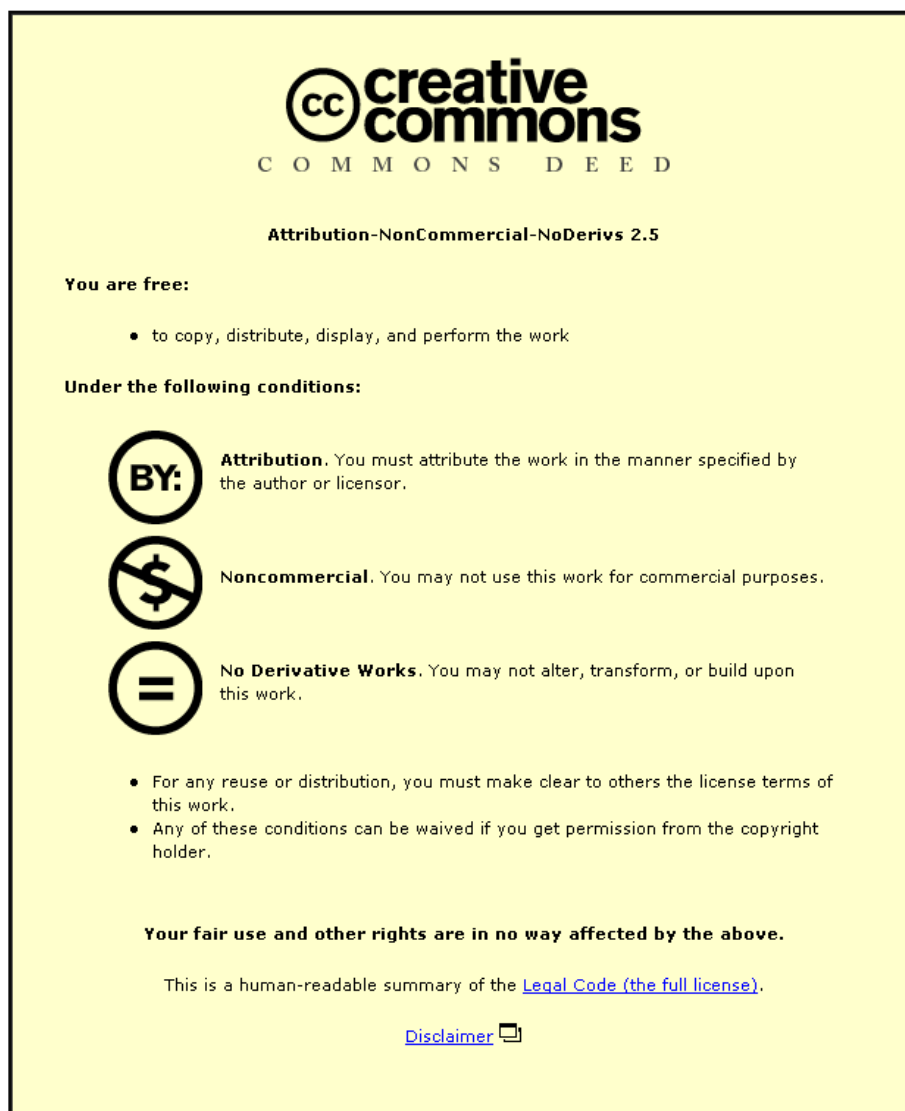
- A Doctoral Thesis. Submitted in partial fulfilment of the requirements for the award of Doctor of Philosophy of Loughborough University.

**Metadata Record:** <https://dspace.lboro.ac.uk/2134/10800>

**Publisher:** © Jouni A. Ronkainen

Please cite the published version.

This item was submitted to Loughborough University as a PhD thesis by the author and is made available in the Institutional Repository (<https://dspace.lboro.ac.uk/>) under the following Creative Commons Licence conditions.



For the full text of this licence, please go to:  
<http://creativecommons.org/licenses/by-nc-nd/2.5/>



**University Library**

Author/Filing Title ..... RONKAINEN, J.A. .....

Class Mark ..... T .....

**Please note that fines are charged on ALL  
overdue items.**

--	--	--

0403668247





Laser based tracking and spin measurement

**LASER BASED TRACKING AND SPIN MEASUREMENT**

by


Jouni Ronkainen

A thesis submitted in partial fulfilment of the  
requirements for the degree of

Doctor of Philosophy

Loughborough University

2008

 Loughborough University Pilkington Library
Date 24/9/09
Class T
Acc No. 0403668247

## Abstract

The sports ball market is extremely competitive and in the US alone valued in excess of \$1305 million (SGMA 2008). Original equipment manufacturers (OEMs) are continually trying to create a competitive edge over their rivals. In order to research and develop sports balls it is vital to quantitatively measure launch and flight characteristics of the ball, in an attempt to create a ball that has better flight and/or impact characteristics. A launch or flight monitor allows consistent measurement and benchmarking of the ball under test. Current top of the range soccer ball monitors are assessed for performance. Predominantly the sports engineering community uses high speed video (HSV) cameras in this benchmarking process. This technique however is extremely susceptible to errors in spin measurement. These errors are explored in detail and recommendations are given in order to improve the measurements.

The properties of laser light make it an ideal tool for accurate, non-contact measurements. It has gained such widespread use, that living in the 21<sup>st</sup> century it is inconceivable to avoid laser technology. In this thesis, optical laser techniques are pursued for ball launch angle, velocity and spin measurement. In order to successfully utilise these techniques a system that is capable of accurately steering the laser beam to the desired target is developed.

A novel laser tracking system (NLTS) has been designed, developed and proven to work successfully, allowing tracking capability of an arbitrarily moving soccer ball, that has no special fiducials. The system is demonstrated to be capable of measuring the position of the ball in space, therefore the NLTS is capable of acting as a launch monitor. The system is proven to track soccer balls in the laboratory and in a more realistic player testing environment. A valuable design feature is that the natural and ambient lighting conditions are inconsequential for the operation of the system. The tracking technique could be applied to any sports ball and could conceivably be transferred to other applications, e.g. military and automotive.

Single point vibrometry work and the NLTS are combined to add spin measurement capability. Actual and measured spin rate values show high levels of similarity when tracking a ball with angular, but no translational velocity. A purpose built 'pendulum rig' is used to carry out measurements on a ball with both translational and angular velocity. The testing highlights how influential the radial measurement distance from the spin axis is, regarding the outputted spin rate value. The current set-up would require further development to allow accurate spin rate measurement using the 'pendulum rig'. The main sources of error and recommendations for future developments of this device are outlined and discussed.

## Acknowledgements

First and foremost, I would like to thank my supervisor, Dr Andy Harland, for his assistance, support and belief that I could complete this project. He was always there to direct me along the right path.

I have a list of people to thank on my PhD journey, and will always be grateful for their assistance, working in the Sports Technology Research Group was fantastic since there was always an expert on hand, whether it was getting the signal acquisition system to function, teach me how to program or just brainstorm. I would like to thank Prof Roy Jones, Dr Jon Roberts, Dr Carolyn Steele, Dr Erin and Pauli Komi, Dr Jon Smith, Dr Laura Justham, Mr Stuart McLeod, Mr Roger Traynor and Mr Mark Capers for their assistance.

I know that Chris Holmes and Ross Cotton, both had to put up with me throughout their time as students, a big thank you must go to them for making the three years at Loughborough as both undergraduate and postgraduate as enjoyable as it was, times that I hope to never forget.

Previously I have seen the wrath of students forgetting to thank the technical staff in the group. I know I put them through a lot, forever making design modifications and expecting changes to be made immediately. Thanks to Mr Carr, Mr Carpenter and Mr Neal, and I am especially indebted to Mr Hallam with the NLTS work.

On a personal note I want to say thank you to my Grandpa and all my family, they have always supported me throughout my studies, and were always a great place to visit in order to avoid cooking and cleaning. Thank you to Kirsty for her continued love and support and I now hope that I can live up to my earning potential!



## **Publications arising from this work**

Ronkainen, J., and Harland. A., 2006. Soccer ball modal analysis using a scanning laser Doppler vibrometer (SLDV), *The Engineering of Sport*, **6**, (1), 11-14<sup>th</sup> July, Munich, Germany, pp. 357-62.

Ronkainen, J., and Harland, A., 2007. Soccer ball modal analysis using a scanning laser Doppler vibrometer (SLDV), *Journal of Sports Engineering*, **10**, (1), pp. 49-54.

Ronkainen, J., Holmes, C., Harland. A., and Jones, R., 2008. A comparative study of ball launch measurement systems; soccer case study. *The Engineering of Sport*, **7**, 2-6<sup>th</sup> June, Biarritz, France.

Ronkainen, J., Toon, D., Santry, J., and Waller, T., 2008. Testing protocol for quantitative comparison of top of the range soccer boots. *The Engineering of Sport*, **7**, 2-6<sup>th</sup> June, Biarritz, France.

## Laser based tracking and spin measurement

“For the vast majority of us, sport kindles memories of **triumphs** and **tragedies** in childhood, adolescence and adulthood: it cloaks a field of dreams. Be it **competitive** or social, organised or impromptu, a **team** game or a solo pursuit; whether we **dedicate** our lives to it or from time to time dip our toes in it, **sport touches us all.**”

Sebastian Coe

## Table of contents

<i>Abstract</i> .....	<i>iii</i>
<i>Acknowledgements</i> .....	<i>iv</i>
<i>Publications arising from this work</i> .....	<i>v</i>
<i>Nomenclature</i> .....	<i>xii</i>
<i>List of equations</i> .....	<i>xvi</i>
<i>List of figures</i> .....	<i>xvii</i>
<i>List of tables</i> .....	<i>xxii</i>
<b>1 Introduction</b> .....	<b>1</b>
1.1 Chapter overview .....	1
1.2 Context of research .....	1
1.3 Research aim and objectives .....	3
1.4 Summary of chapters .....	3
<b>2 Literature review: Optical engineering</b> .....	<b>6</b>
2.1 Chapter overview .....	6
2.2 Fundamentals .....	6
2.2.1 Electromagnetic wave .....	6
2.2.2 Propagation of light .....	8
2.2.3 Interference .....	8
2.2.4 Polarisation .....	9
2.2.5 Lenses .....	10
2.3 Laser optical engineering .....	10
2.3.1 Background .....	10
2.3.2 Laser operation .....	11
2.3.3 Collimation .....	13
2.3.4 Monochromaticity .....	13
2.3.5 Coherence .....	13
2.3.6 Laser safety .....	13
2.4 Laser Doppler anemometry to laser Doppler vibrometry .....	16
2.4.1 Laser Doppler anemometry .....	16
2.4.2 Laser Doppler vibrometry .....	17
2.5 Dual and Multiple beam vibrometry .....	22
2.5.1 The cross beam vibrometer .....	22
2.5.2 The laser torsional vibrometer .....	22
2.5.3 Other dual beam vibrometers .....	25
2.5.4 Multiple beam vibrometers .....	26
2.6 Scanning and laser tracking .....	29
2.6.1 The scanning technique .....	29

## Laser based tracking and spin measurement

2.6.2	Contributions by Imperial college London .....	31
2.6.3	Contributions by Ancona University .....	32
2.6.4	Contributions by Loughborough University .....	35
2.6.5	Contributions by Robert Bosch GmbH.....	37
2.6.6	Contributions by Polytec GmbH.....	38
2.6.7	Laser based scanning and tracking systems.....	38
<b>2.7</b>	<b>Limitations with laser Doppler vibrometry .....</b>	<b>40</b>
2.7.1	Speckle phenomenon .....	40
2.7.2	Pseudo-vibrations .....	42
2.7.3	Noise-floor .....	42
2.7.4	Other issues.....	42
<b>2.8</b>	<b>Chapter summary .....</b>	<b>44</b>
<b>3</b>	<b><i>Literature review: Sports engineering.....</i></b>	<b>45</b>
<b>3.1</b>	<b>Chapter overview .....</b>	<b>45</b>
<b>3.2</b>	<b>Sports ball specifications .....</b>	<b>45</b>
3.2.1	American football & rugby.....	46
3.2.2	Baseball .....	46
3.2.3	Golf.....	47
3.2.4	Soccer .....	48
3.2.5	Tennis & table tennis .....	48
<b>3.3</b>	<b>Reported launch parameters.....</b>	<b>49</b>
3.3.1	American football & rugby.....	49
3.3.2	Baseball .....	50
3.3.3	Golf.....	50
3.3.4	Soccer .....	51
3.3.5	Tennis & table tennis .....	51
<b>3.4</b>	<b>Why measure launch and flight characteristics? .....</b>	<b>52</b>
<b>3.5</b>	<b>Technologies for measuring sports balls.....</b>	<b>54</b>
3.5.1	Introduction .....	54
3.5.2	General Spin measurement .....	54
3.5.3	Spin measurement in controlled conditions .....	57
3.5.4	High speed video camera measurement.....	57
3.5.5	Multi and long exposure camera measurement.....	59
3.5.6	Radar based techniques.....	60
3.5.7	Devices in the ball .....	64
3.5.8	Purpose built devices .....	66
3.5.9	Case study: Srixon, golf science centre .....	68
<b>3.6</b>	<b>Chapter summary .....</b>	<b>71</b>
<b>4</b>	<b><i>Quantification of typical errors associated with high speed video measurements of sports ball spin.....</i></b>	<b>73</b>
<b>4.1</b>	<b>Chapter overview .....</b>	<b>73</b>
<b>4.2</b>	<b>Test equipment .....</b>	<b>73</b>
4.2.1	Experimental apparatus 'spin rig' .....	73
4.2.2	HSV and Flightpath .....	78
4.2.3	Rotational vibrometer .....	78

## Laser based tracking and spin measurement

<b>4.3</b>	<b>Testing protocol.....</b>	<b>79</b>
4.3.1	Objective for HSV camera ball spin measurement.....	79
4.3.2	Methodology.....	79
4.3.3	Statistical analysis.....	84
<b>4.4</b>	<b>Results .....</b>	<b>85</b>
4.4.1	Test 1 – Effects of camera orientation .....	85
4.4.2	Test 2 – Effects of radial lens distortion .....	86
4.4.3	Test 3 – Effects of camera orientation and radial lens distortion.....	86
<b>4.5</b>	<b>Discussion.....</b>	<b>87</b>
<b>4.6</b>	<b>Conclusions .....</b>	<b>90</b>
<b>4.7</b>	<b>Additional error sources.....</b>	<b>90</b>
4.7.1	Frame rate of HSV camera .....	90
4.7.2	Error associated with dot monitoring spin measurement.....	93
<b>4.8</b>	<b>Chapter summary .....</b>	<b>97</b>
<b>5</b>	<b><i>Launch parameter measurement.....</i></b>	<b>99</b>
<b>5.1</b>	<b>Chapter overview .....</b>	<b>99</b>
<b>5.2</b>	<b>Player Testing.....</b>	<b>99</b>
5.2.1	Previous work.....	99
5.2.2	Automated system for free kick measurement.....	102
<b>5.3</b>	<b>Mechanical kicking simulator testing.....</b>	<b>106</b>
5.3.1	Equipment.....	106
5.3.2	Testing protocol.....	107
5.3.3	Results and Discussion .....	108
5.3.4	Summary.....	117
<b>5.4</b>	<b>Chapter summary .....</b>	<b>117</b>
<b>6</b>	<b><i>Single point vibrometry for ball velocity and spin rate measurement .....</i></b>	<b>119</b>
<b>6.1</b>	<b>Chapter overview .....</b>	<b>119</b>
<b>6.2</b>	<b>Linear and angular velocity measurements within sport .....</b>	<b>119</b>
<b>6.3</b>	<b>Mathematical computer modelling of surface velocity .....</b>	<b>122</b>
6.3.1	Ball oscillations due to impact.....	122
6.3.2	Velocity contour map of a spinning soccer ball.....	127
<b>6.4</b>	<b>Graphical user interface (GUI) for a virtual vibrometer .....</b>	<b>129</b>
<b>6.5</b>	<b>Validation of ‘virtual vibrometer’ .....</b>	<b>130</b>
6.5.1	Methodology.....	130
6.5.2	Experimental results .....	135
<b>6.6</b>	<b>Comparison of virtual and actual vibrometer velocity measurements .....</b>	<b>139</b>
<b>6.7</b>	<b>Chapter summary .....</b>	<b>142</b>
<b>7</b>	<b><i>Laser tracking.....</i></b>	<b>144</b>
<b>7.1</b>	<b>Chapter overview .....</b>	<b>144</b>
<b>7.2</b>	<b>System Concept .....</b>	<b>144</b>
<b>7.3</b>	<b>Hardware.....</b>	<b>147</b>

## Laser based tracking and spin measurement

7.3.1	Image Acquisition.....	147
7.3.2	Light source and alignment.....	152
7.3.3	The scanning system.....	156
7.3.4	Operating system.....	158
<b>7.4</b>	<b>Software .....</b>	<b>159</b>
7.4.1	Common Vision Blox.....	159
7.4.2	Microsoft Visual Studio .NET.....	159
7.4.3	Coyote Application.....	160
<b>7.5</b>	<b>System Design.....</b>	<b>160</b>
7.5.1	The build.....	160
7.5.2	Alignment.....	161
7.5.3	Costs.....	161
<b>7.6</b>	<b>Soccer ball tracking application .....</b>	<b>162</b>
7.6.1	Image processing.....	163
7.6.2	Ball movement by hand.....	165
7.6.3	Player testing.....	166
7.6.4	Soccer ball launch monitor.....	171
<b>7.7</b>	<b>Tracking calibration .....</b>	<b>172</b>
7.7.1	Fixed scale factor.....	172
7.7.2	Adaptive scale factor.....	173
<b>7.8</b>	<b>Sources of error.....</b>	<b>174</b>
<b>7.9</b>	<b>Further developments.....</b>	<b>176</b>
7.9.1	FOV of the NLTS.....	176
7.9.2	Image processing stage.....	176
7.9.3	The DOE.....	177
7.9.4	System automation.....	177
7.9.5	Non-spherical target tracking application.....	178
<b>7.10</b>	<b>Chapter summary.....</b>	<b>178</b>
<b>8</b>	<b><i>Laser based spin measurement system.....</i></b>	<b><i>180</i></b>
<b>8.1</b>	<b>Chapter overview .....</b>	<b>180</b>
<b>8.2</b>	<b>Testing protocol.....</b>	<b>180</b>
8.2.1	Selected laser vibrometer.....	180
8.2.2	Line scan work and results.....	182
8.2.3	Circular scan work and results.....	187
8.2.4	NLTS combined with single point vibrometry.....	191
8.2.5	Pendulum rig study.....	196
<b>8.3</b>	<b>Sources of error.....</b>	<b>203</b>
<b>8.4</b>	<b>Chapter summary.....</b>	<b>205</b>
<b>9</b>	<b><i>Conclusions and recommendations for future work.....</i></b>	<b><i>206</i></b>
<b>9.1</b>	<b>Conclusions.....</b>	<b>206</b>
<b>9.2</b>	<b>Recommendations for future work.....</b>	<b>208</b>
<b>Appendix A</b>	<b>.....</b>	<b>212</b>
<b>Appendix B</b>	<b>.....</b>	<b>213</b>

Laser based tracking and spin measurement

*Appendix C*.....219  
*Appendix D*.....220  
*Appendix E*.....228  
*Appendix F*.....234  
*Appendix G*.....235  
*References* .....237

## Nomenclature

ANOVA	Analysis of variance
BLOB	Binary Large Object
B&K	Bruel and Kjaer
CAD	Computer aided design
CCD	Charge couple device
CD	Compact disc
CMOS	Complementary metal-oxide semiconductor
CODA	Dynamic Optoelectronic Dynamic Anthropometer
COR	Coefficient of restitution
CPU	Central processing unit
CVB	Common Vision Blox
CW	Continuous wave
DAQ	Digital acquisition
DC	Direct current
DLL	Dynamically linked libraries
DOE	Diffraction optical element
DOF	Degree of freedom
DPSS	Diode pumped solid state
DSP	Digital signal processing
DVD	Digital video disc
ECB	England and Wales Cricket Board
FE	Finite element
FEA	Finite element analysis
FEM	Finite element model
FFT	Fast Fourier Transform
FIFA	Fédération Internationale de Football Association
FOV	Field of view



## Laser based tracking and spin measurement

FPGA	Field programmable gate array
FPS	Frames per second
GB	Governing body
GigE	Gigabit Ethernet
GUI	Graphical user interface
He-Ne	Helium-Neon
HSV	High speed video
ICC	International Cricket Council
IEC	International Electrotechnical Commission
IRB	International Rugby Board
ITF	International Tennis Federation
iTLDV	Image based tracking laser Doppler vibrometry
ITTF	International table tennis federation
LASER	Light amplification by stimulated emission of radiation
LDA	Laser Doppler anemometry
LDV	Laser Doppler vibrometer or laser Doppler vibrometry
LED	Light emitting diode
LTV	Laser torsional vibrometer
LU	Loughborough University
LUT	Lookup table
MASER	Microwave amplification by stimulated emission of radiation
MLB	Major League Baseball
MPE	Maximum permissible exposure
NBA	National Basketball Association
NFL	National Football League
NIC	Network interface card
NLTS	Novel laser tracking system
ODS	Operational deflection shape
OEM	Original equipment manufacturer
PC	Personal computer

## Laser based tracking and spin measurement

PCI	Peripheral component interconnect
RAM	Random access memory
RPM	Revolutions per minute
R&A	Royal and Ancient Golf Club of St Andrews
SLDV	Scanning laser Doppler vibrometer
SNR	Signal to noise ratio
TLDV	Tracking laser Doppler vibrometer
TT	Trajectory Tracker
USB	Universal serial bus
USGA	United States Golf Association
VB.NET	Visual Basic .NET
VGA	Vector graphics array
2D	Two dimensional
3D	Three dimensional
~	Circa
$c$	Speed of light, $3 \times 10^8 \text{ ms}^{-1}$
$f$	Frequency, Hz
$\lambda$	Wavelength, m
$E$	Energy of photon/particle of light, J
$h$	Planck's constant, 6.626 Js
$\mu$	Refractive index of material
$U$	On-axis surface velocity of target, $\text{ms}^{-1}$
$\theta$	Angle, °
$f_D$	Doppler frequency, Hz
$N$	Target revolutions per second, RPS or integer number
$d$	Laser beam separation distance, m
$L$	Cavity length, m
$\Delta$	Change or difference between mathematical value

## Laser based tracking and spin measurement

$\pi$	Mathematical constant pi, 3.14159 (to 5 decimal places)
$\alpha$	Angle between direction of incident laser beams and the direction of the spin axis, ° (see Figure 2-15)
$\gamma$	Angle between plane of cross section of the target and the plane of the incident laser beams, ° (see Figure 2-16)
$r$	Perpendicular measurement distance between laser measurement point and the target spin axis, radial distance, metres
$v$	On-axis surface velocity of target, $\text{ms}^{-1}$
$\omega$	Angular velocity, radians $\text{s}^{-1}$
$V_T$	Translational velocity of the ball, $\text{ms}^{-1}$
$V_R$	Rotational velocity of the ball, RPM
$v_{ball}$	Velocity of the ball, $\text{ms}^{-1}$
$v_{foot}$	Velocity of the foot, $\text{ms}^{-1}$
$m_l$	Combined mass of the leg and foot, kg
$m_b$	Mass of the ball, kg
$O_S$	Object size, mm
$W_D$	Working distance, mm
$f_L$	Focal length, mm
$I_S$	Image sensor size, mm
$S_A$	Pendulum shaft angle, °
$V_A$	Vertical vibrometer angle of incidence on target, °

## List of equations

<i>Equation 2-1</i> .....	7
<i>Equation 2-2</i> .....	7
<i>Equation 2-3</i> .....	8
<i>Equation 2-4</i> .....	11
<i>Equation 2-5</i> .....	13
<i>Equation 2-6</i> .....	16
<i>Equation 2-7</i> .....	18
<i>Equation 2-8</i> .....	18
<i>Equation 2-9</i> .....	23
<i>Equation 2-10</i> .....	24
<i>Equation 5-1</i> .....	102
<i>Equation 6-1</i> .....	128
<i>Equation 7-1</i> .....	151
<i>Equation 8-1</i> .....	201
<i>Equation 8-2</i> .....	203

## List of figures

<i>Figure 2-1: The light spectrum, adapted from (First Sight Vision 2004).</i>	6
<i>Figure 2-2: Schematic of Young's double slit experiment.</i>	7
<i>Figure 2-3: The superposition principle.</i>	9
<i>Figure 2-4: Simple lenses, (a) biconvex lens, (b) biconcave lens, adapted from (Precision Graphics 2000).</i>	10
<i>Figure 2-5: Three level population inversion.</i>	12
<i>Figure 2-6: Basic laser design, Fabry-Perot interferometer.</i>	12
<i>Figure 2-7: Warning label for class 2 to 4 lasers.</i>	15
<i>Figure 2-8: LDA set-up (Halliwell and Hargrave 2003).</i>	16
<i>Figure 2-9: LDV set-up, adapted from (Halliwell and Hargrave 2003).</i>	17
<i>Figure 2-10: Heterodyne process, adapted from (Kurtus 2007).</i>	19
<i>Figure 2-11: The Michelson interferometer, adapted from (Michelson 1887).</i>	20
<i>Figure 2-12: Basic schematic of portable LDV.</i>	21
<i>Figure 2-13: Basic schematic of LDV set-up with a Bragg cell frequency shift.</i>	21
<i>Figure 2-14: The laser torsional vibrometer (Halliwell et al. 1984).</i>	23
<i>Figure 2-15: Plan view of target rotation.</i>	23
<i>Figure 2-16: Front view of target rotation.</i>	24
<i>Figure 2-17: Torsional vibrometer test set-up, adapted from (Miles et al. 1996).</i>	25
<i>Figure 2-18: Dual beam system, adapted from (Trethewey et al. 1993).</i>	26
<i>Figure 2-19: Three beam system, adapted from (Bokelberger et al. 1994a).</i>	27
<i>Figure 2-20: Underwater measurement system, adapted from (Vignola and Houston 1993).</i>	28
<i>Figure 2-21: Parallel beam arrangement, adapted from (Bell and Rothberg 2000a).</i>	29
<i>Figure 2-22: Scanning mirrors, adapted from (Halkon and Rothberg 2004).</i>	30
<i>Figure 2-23: Complex harmonic motion.</i>	31
<i>Figure 2-24: Misalignment between scan axis and rotating shaft axis, adapted from (Castellini and Paone 2000).</i>	32
<i>Figure 2-25: Transducer time history, (a) for vibrometer, (b) for accelerometer, adapted from (Castellini and Cupido 2001).</i>	34
<i>Figure 2-26: iTLDV set-up, adapted from (Castellini and Tomasini 2002).</i>	35
<i>Figure 2-27: Synchronised-SLDV system, adapted from (Halkon and Rothberg 2004).</i>	36
<i>Figure 2-28: Above – theoretical static line and area scan profile, Below – in situ real time tracking profile of target blade, adapted from (Halkon and Rothberg 2004).</i>	37
<i>Figure 2-29: PSV-400-3D system, three individual scanning heads.</i>	38
<i>Figure 2-30: Laser tracking protocol, (a) stationary target, (b) target moves, (c) laser pattern shifted to track target, adapted from (Cassinelli et al. 2005).</i>	39

## Laser based tracking and spin measurement

Figure 2-31: (a) Lissajous pattern on flat target with 3:2 lissajous ratio, (b) lissajous pattern on sphere with 4:3 lissajous ratio (Blais et al. 2001b) .....	40
Figure 2-32: Light striking an optically rough surface. ....	41
Figure 2-33: Airy disc appearance of backscattered light from retroreflective target. ....	41
Figure 2-34: SNR influenced by target colour, finish and angle of incidence (a) Laser incident perpendicular striking yellow surface – strongest SNR, (b) Laser incident at acute angle striking yellow surface – strong SNR, (c) Laser incident perpendicular striking black surface – strong SNR, (d) Laser incident at acute angle striking black surface – no signal. ....	43
Figure 3-1: Trackman data viewed on television, comparison of player's shots, adapted from (Trackman 2006) .....	54
Figure 3-2: Calibration disc used for spin rate measurement. ....	56
Figure 3-3: Circumferential lines for spin measurement, adapted from (Cotton 2006) .....	58
Figure 3-4: Dots for spin measurement, adapted from (Alaways and Hubbard 2001). ....	58
Figure 3-5: The Hawkeye system, Henin v Williams tennis shots analysis (Hawkeye 2008). ....	59
Figure 3-6: Animal locomotion, adapted from (Muybridge 1878). ....	60
Figure 3-7: Visualisation of baseball pitch, adapted from (Theobalt et al. 2004). ....	60
Figure 3-8: The Trackman system, adapted from (Stachura 2006). ....	63
Figure 3-9: Visualisation of the measurements made at the Davis cup by RacquetRadar, adapted from (EDH 2006). ....	64
Figure 3-10: Schematic of data acquisition and processing (Marinelli 2000). ....	65
Figure 3-11: Flight data recorder for a 'Nerf' football, adapted from (Nowak 2003). ....	65
Figure 3-12: Teamgeist II match ball (Soccer Ball World 2007). ....	66
Figure 3-13: The Quinspin system (Quinspin 2006). ....	68
Figure 3-14: Difference between two acquired images, adapted from (Tamaki et al. 2004) .....	68
Figure 3-15: Overview of the Srixon golf testing facility, adapted from (Srixon 2003). ....	69
Figure 4-1: 'Spin rig' set-up, (a) for soccer (b) for golf. ....	74
Figure 4-2: Slotted wheel attachment on motor shaft, (a) side view, (b) isometric view. ....	75
Figure 4-3: Calibration of 'spin rig' hardware, ball rotating at 600 RPM. ....	77
Figure 4-4: Plan view, circumferential line marking on golf ball. ....	80
Figure 4-5: Basic testing set-up. ....	80
Figure 4-6: Flightpath analysis of spin rate, using golf ball collage. ....	81
Figure 4-7: Standard spin analysis technique, LU. ....	82
Figure 4-8: Test 1 HSV camera angles, (black = 0°, red = 5°, blue = 10°, green = 15°, purple = 30°). ....	83
Figure 4-9: CAD image of golf ball dependent upon the angle of the camera in relation to the ball spin axis. ....	83
Figure 4-10: Four different golf ball locations in camera FOV (1024 × 256 pixels). ....	84
Figure 4-11: Test 1, Average spin rates showing ± 1 standard deviation. ....	85

## Laser based tracking and spin measurement

Figure 4-12: Test 2, Average spin rates showing $\pm 1$ standard deviation. ....	86
Figure 4-13: Test 3, Average spin rates showing $\pm 1$ standard deviation. ....	87
Figure 4-14: Flightpath analysis of CAD golf ball images. ....	89
Figure 4-15: Spin measurement using dot monitoring method. ....	94
Figure 5-1: Plan view of straight and swerve kick set-ups. ....	104
Figure 5-2: Plan view of mechanical kicking simulator testing set-up. ....	107
Figure 5-5: Composite images with balls spaced 20 ms apart, leg velocity at $23 \text{ ms}^{-1}$ , (a) straight kick, (b) swerve kick. ....	111
Figure 5-6: Optical device measurement images, (a) static image for straight kick, (b) dynamic image for straight kick (6 ms post launch), (c) static image for curve kick, (d) dynamic image for curve kick (6 ms post launch). ....	114
Figure 5-7: Radar device visual for balls striking an imaginary goal. ....	115
Figure 6-1: Bragg cell requirements for golf. ....	120
Figure 6-2: Translational velocity measurement of a golf ball, Hocknell (1998b). ....	121
Figure 6-3: Bragg cell requirements for soccer. ....	122
Figure 6-4: Soccer ball pre, during and post impact in FEA model, the contour plots of the balls are shown using z-axis velocity values. ....	123
Figure 6-5: Impact and post impact out of plane velocities ( $V_z$ ) measured at the nodes. ....	124
Figure 6-6: Post impact out of plane velocities ( $V_z$ ) measured at the nodes. ....	124
Figure 6-7: OFV-323 vibrometer range. ....	125
Figure 6-8: Spin loading scenario of FE soccer ball. ....	127
Figure 6-9: Soccer ball spinning at 601 RPM, (a) in the FE model, (b) on the 'spin rig'. ....	128
Figure 6-10: Velocity ( $V_z$ ) of the monitored nodes throughout the simulation. ....	128
Figure 6-11: Matlab simulated vibrometer set-up, (a) side view, (b) plan view. ....	129
Figure 6-12: GUI for the 'virtual vibrometer'. ....	130
Figure 6-13: Predicted 'saw tooth' velocity profile using the virtual vibrometer. ....	131
Figure 6-14: Plan view of test 1 set-up for velocity measurement. ....	133
Figure 6-16: Saw tooth profiles, (a) at $\theta = 75^\circ$ , (b) at $\theta = 105^\circ$ . ....	136
Figure 6-17: Average velocity versus displacement for linear actuator runner. ....	137
Figure 6-18: On-axis vibrometer velocity measurements to runner moving at, (a) $1 \text{ ms}^{-1}$ , (b) $3 \text{ ms}^{-1}$ , (c) $5 \text{ ms}^{-1}$ . ....	137
Figure 6-19: Measured velocity 'saw tooth' profiles from $\theta = 90^\circ$ to $\theta = 40^\circ$ . ....	139
Figure 6-20: Virtual and measured velocity 'saw tooth' profiles, vibrometer perpendicular to ball travel direction. ....	141
Figure 6-21: Virtual and actual velocity measurement comparison. ....	142
Figure 7-2: Plan view of core laser tracking system components. ....	147
Figure 7-3: Pulnix camera snapshots, (a) standard image capture, (b) interference filter ( $\lambda = 530 \text{ nm}$ ) in front of lens. ....	152
Figure 7-3: The absolute quantum efficiency of the Pulnix TM-6740GE camera. ....	153
Figure 7-4: Purchased sample DOE illumination patterns. ....	155

## Laser based tracking and spin measurement

Figure 7-5: 90° plate polarizer. ....	156
Figure 7-7: Image processing, (a) raw acquired 8-bit image, (b) zoomed in section showing gray scale pixel values, (c) processed image after LUT stage, (d) zoomed in section showing binary pixel values. ....	163
Figure 7-8: Summary of image processing , (a) raw 8-bit image, (b) 'edge' detect algorithm locates the edge of the ball, (c) the centre position of the ball is deduced. ....	165
Figure 7-9: Tracking a soccer ball, moved arbitrarily by hand, (a) lights on in laboratory, (b) lights off in laboratory.....	166
Figure 7-13: Laser tracking, launch monitor in action. ....	171
Figure 7-14: Calculated launch parameters. ....	172
Figure 7-15: Scale factor calibration, (a) horizontally, (b) vertically. ....	172
Figure 7-16: Change in FOV size due to stand off distance, (a) x and y-mirror voltage values (0,0), (b) x and y-mirror voltage values (4,-4).....	173
Figure 7-17: Adaptive scale factor, (a) changing diameter of the ball in the system FOV, (b) Calculated x and y-mirror voltage scale factor when the need to realign by one pixel.....	174
Figure 7-18: The 'Hough' transform, to locate the edge of the soccer ball. ....	175
Figure 7-19: The novel laser tracking system (NLTS).....	178
Figure 8-1: Scanning strategy, (a) line scan, (b) circular scan. ....	183
Figure 8-2: Line scan velocity measurements, (a) 60 scan points, (b) 120 scan points, (c) 180 scan points.....	184
Figure 8-3: Line scan results, 60 measurement points along the line. ....	185
Figure 8-4: Line scan results, 120 measurement points along the line.....	185
Figure 8-5: Line scan results, 180 measurement points along the line.....	186
Figure 8-6: Circular scan velocity measurements, (a) scan radius 8 cm, (b) scan radius 4 cm, (c) scan radius 2cm. ....	188
Figure 8-7: Circular scan spin rate results, (a) scan radius 8 cm, (b) scan radius 4 cm (c) scan radius 2 cm. ....	189
Figure 8-8: Spin axis definition using circular scan technique, zero = zero surface velocity value along the laser scan path, maximum = maximum positive and negative surface velocity along the laser scan path.....	190
Figure 8-9: Combination of NLTS and single point vibrometer set-up, (a) 3D schematic (b) isometric view of mirror attachment, (c) side view of mirror attachment, (d) juxtaposition of vibrometer and illumination laser beams.....	191
Figure 8-10: Vibrometer measurements, (a) spin rate 400 RPM, tracking 'inactive', (b) spin rate 400 RPM tracking 'active', (c) spin rate 500 RPM, tracking 'inactive', (d) spin rate 500 RPM, tracking 'active', (e) spin rate 600 RPM, tracking 'inactive', (f) spin rate 600 RPM, tracking 'active'.....	193
Figure 8-11: Spin rate values for 'active' and 'inactive' tracking at ~400 RPM. ....	194
Figure 8-12: Spin rate values for 'active' and 'inactive' tracking at ~500 RPM. ....	194
Figure 8-13: Spin rate values for 'active' and 'inactive' tracking at ~600 RPM. ....	195



## Laser based tracking and spin measurement

<i>Figure 8-14: Pendulum rig, (a) composite image of the rig in 'action', (b) side view of the rig components. ....</i>	<i>197</i>
<i>Figure 8-15: The laser vibrometer and projected NLTS 'cross' on the ball, (a) clockwise negative rotation, (b) zero position, (c) counter clockwise positive rotation. ....</i>	<i>198</i>
<i>Figure 8-16: Pendulum rig results, including the 'raw' vibrometer readings, (a) trial 1, (b) trial 10. ....</i>	<i>199</i>
<i>Figure 8-17: Pendulum rig results, showing 'filtered' results, (a) trial 7, (b) trial 8. ....</i>	<i>200</i>
<i>Figure 8-18: Radial measurement distance plotted alongside vibrometer measurements, (a) trial 1, (b) trial 10. ....</i>	<i>202</i>

## List of tables

<i>Table 2-1: Summary of IEC laser classes.....</i>	<i>15</i>
<i>Table 4-1: Average uncertainty in soccer ball spin measurement dependant on HSV frame rate. ....</i>	<i>92</i>
<i>Table 4-2: Average uncertainty in golf ball spin measurement dependant on HSV frame rate. ....</i>	<i>92</i>
<i>Table 4-3: Predicted soccer ball spin rate values, depending on the distance <math>x_1</math> and <math>x_2</math>.....</i>	<i>95</i>
<i>Table 4-4: Predicted soccer ball spin rate values, depending on the distance <math>y_1</math> and <math>y_2</math>.....</i>	<i>97</i>
<i>Table 5-1: Velocity measurements from player testing (Neilson 2003).....</i>	<i>101</i>
<i>Table 5-2: Spin rate measurements from player testing (Neilson 2003).....</i>	<i>101</i>
<i>Table 5-3: Driven kick and swerve kick results from player testing.....</i>	<i>105</i>
<i>Table 5-4: Success of measurement systems throughout testing. ....</i>	<i>116</i>
<i>Table 5-5: Range of possible soccer free kick launch characteristics.....</i>	<i>117</i>
<i>Table 6-1: Spin rate versus measured vibrometer velocity.....</i>	<i>125</i>
<i>Table 6-2: Dependence of radius on measured vibrometer velocities.....</i>	<i>126</i>
<i>Table 6-3: Vibrometer at <math>90^\circ</math> to ball travelling at <math>1 \text{ ms}^{-1}</math>. ....</i>	<i>135</i>
<i>Table 7-1: Bandwidth of typical machine vision interfaces, adapted from (Levis 2006). ....</i>	<i>148</i>
<i>Table 7-2: Pulnix camera 'binning' mode.....</i>	<i>150</i>
<i>Table 7-3: Price comparison of equal power diode pumped laser sources (Scitec 2007).....</i>	<i>153</i>
<i>Table 7-4: Itemised cost of the NLTS. ....</i>	<i>162</i>
<i>Table 8-1: Comparison of commercial single point vibrometers. ....</i>	<i>181</i>

# **1** Introduction

## **1.1 Chapter overview**

This chapter provides the reader with a basic introduction to the general area of study in this thesis. Specific research aim and objectives are defined, which are the main focus of the work to follow. A brief summary of the work within the subsequent chapters is given.

## **1.2 Context of research**

The sports ball market is extremely competitive and in the US alone valued in excess of \$1305 million (SGMA 2008). OEMs invest significant amounts of time and money researching and developing sports balls, using advanced materials and constructions in an attempt to create a ball that has better flight and/or impact characteristics. In order to research and develop sport balls it is vital to quantitatively measure the launch and flight characteristics of the ball. OEMs are currently using a wide range of systems to measure these parameters, allowing direct comparison between products. It is fair to state that almost all OEMs have their own testing protocols in place, to develop their latest range of balls.

Governing bodies (GBs), athletes/coaches and spectators/media are also extremely interested in sports ball launch and flight characteristics for their own specific interests in the game.

Spin measurement is a crucial part of ball launch characteristics and current techniques lack the ability to give spin measurement output with traceability. In cricket at the elite level the England Cricket Board (ECB) continue to search for methods from which they can objectively quantify spin. For many years, spin bowling coaches have used 'perceived wisdom' to analyse a spin bowler's action and the trajectory of the ball throughout flight and impact. The method is very subjective and

## Laser based tracking and spin measurement

is reliant upon the coaches' knowledge of the game. The ECB want to be able to "measure spin quantitatively so that they can compare academy players and professionals alike against the best players in the world" (Parsons 2005). Almost all ball sports involve some components of spin. Given the dramatic influence spin can have on a game due to the aerodynamic phenomenon known as the Magnus effect (Prandtl 1905) or ball bouncing effects, manufacturers are increasingly looking to design balls and implements that allow athletes greater control over the spin imparted.

Several systems exist for sports ball launch measurement, however often the ball under investigation needs to have special markings or the ball needs to be pre-orientated. Most devices appear to be built for use in specific sports, which can severely limit the functionality of the system, therefore a tool that is able to measure generic sports ball launch characteristics is pursued and an optical non-contact approach is thought to offer the most feasible approach to this task.

Throughout this thesis devices are referred to as either monitoring systems, predictive monitoring systems or tracking systems. Within literature these words seem to be used interchangeably, for brevity these devices are clearly defined due to distinct differences between the architecture of the systems. Monitoring systems are defined as whole field processing techniques which have the capability of locating a moving target with time. Predictive monitoring systems are pre-programmed to monitor flight of the target, however no feedback mechanism is in place in order to decipher whether the target is being monitored. Tracking systems are defined as devices that maintain alignment between target and measurement system. The tracking system can be either 'active' or 'inactive' whereby the real-time tracking system algorithm is switched 'on' or 'off' respectively.

### **1.3 Research aim and objectives**

The research aim of this thesis work is as follows:

*“To design, manufacture, develop, and demonstrate an optical based system that can objectively track a non-marked sports ball whilst measuring ball surface velocity in order to measure spin rate.”*

There are several methods of approaching the aim of this thesis. Therefore the following objectives must be answered in the quest to achieve the aim outlined above:

- To establish parameters for ball launch velocity, angle and spin rate for mainstream sports through analysis of literature and original experimentation.
- To review and critically evaluate existing technologies that researchers and OEMs are using to measure ball spin rate and launch conditions.
- To investigate the potential use of laser vibrometry for target ball surface velocity measurement.
- To design, manufacture, develop and demonstrate a novel prototype system that can measure ball launch characteristics in a non-contact and non-marking approach, showing consideration towards cost, accuracy, and functionality.
- To amalgamate the tracking device and the selected system for ball surface velocity measurement in order to carry out spin rate measurement of a ball with both translational and rotational velocity.

### **1.4 Summary of chapters**

This thesis is comprised of eight subsequent chapters. The chapters build up the knowledge base and testing acumen, in order to create the novel system introduced in Chapter 7. The summary of the subsequent chapters is as follows:

## Laser based tracking and spin measurement

Chapter 2 documents a literature review on optical engineering, introducing fundamentals of optics and leading up to complex scanning and tracking systems that have already been developed, either commercially or for research purposes.

Chapter 3 details current literature on mainstream sports rules governing the ball and general launch parameters. The importance of measuring launch and flight parameters are reported. Current technologies commercially available for these measurements are also reported.

Chapter 4 accounts typical errors associated with high speed video measurements of sports ball spin. This is investigated due to the popularity of the technique. It currently represents the single most common approach used to measure sports ball spin. The results show how easily errors are introduced into the measurement.

Chapter 5 reports player testing capabilities for soccer striking, in order to confirm previously reported launch parameters. For the first time the use of an automated system for soccer free kick measurement is reported. The core of this chapter compares some of the most advanced methods currently available to measure soccer ball launch characteristics.

Chapter 6 details single point vibrometry for ball velocity and spin measurement. Finite Element (FE) simulation is used to explore factors that affect the vibrometer spin rate measurement. A virtual vibrometer is created and validated.

Chapter 7 reports the novel laser tracking system (NLTS) that is designed, developed and tested. The hardware, software and concept of the system is reported in detail. Errors and further developments of the NLTS are reported.

Chapter 8 documents the combination of the NLTS and a single point vibrometer for tracking and spin measurement work. The two systems were combined successfully without compromising the operation of either device.

## Laser based tracking and spin measurement

Chapter 9 reports the conclusions of the work presented in this thesis. Future work is recommended, in order to develop the NLTS into a more functional device.

# 2 Literature review: Optical engineering

## 2.1 Chapter overview

This chapter introduces some fundamental principles involved in optics with particular regard to laser engineering. Main topics covered include laser optical engineering, laser Doppler vibrometry, dual and multiple beam vibrometry, scanning vibrometry and laser tracking. It is important that the information and data presented in this chapter is understood, to fully comprehend topics reported in succeeding chapters.

## 2.2 Fundamentals

Optics is a complex and wide ranging subject. This section introduces basic principles of light only. Should further knowledge of the subject be needed there are numerous reference books to consult, for example Daish (1971) and Hecht (1998).

### 2.2.1 Electromagnetic wave

Light is an electromagnetic wave, which is visible to the human eye in the approximate wavelength,  $\lambda$ , range between 400 to 700 nm generally referred to as visible light. The electromagnetic spectrum exists from gamma rays ( $\lambda \sim 10^{-2}$  to  $10^{-6}$  nm) to radio waves ( $\lambda \sim 0.001$  to 100 km), as shown in Figure 2-1.

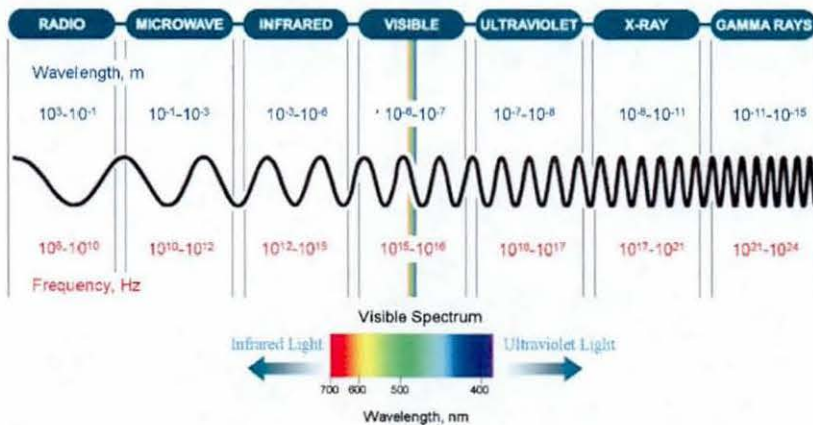


Figure 2-1: The light spectrum, adapted from (First Sight Vision 2004).



## Laser based tracking and spin measurement

Light waves consist of both electric and magnetic fields, which can be considered as oscillating perpendicular to each other. Two key equations associated with light, highlight the duality of light, whereby light consists of both particles and waves. In Equation 2-1, the speed of light,  $c$ , is equal to the frequency of light,  $f$ , multiplied by the wavelength of light,  $\lambda$ , illustrating the wave like behaviour of light. The particle like behaviour of light is demonstrated in Equation 2-2. The energy of light particles,  $E$ , equals Planck's constant,  $h$ , multiplied by the speed of light, divided by the wavelength of light.

$$c = f\lambda \quad \text{Equation 2-1}$$

$$E = \frac{hc}{\lambda} \quad \text{Equation 2-2}$$

The duality of light is commonly explained using Young's double slit experiment, whereby light penetrates a plate with two slits, the pattern of light observed at the target consists of light and dark stripes, shown in Figure 2-2. The observed pattern can only be explained if light acts as a transverse wave

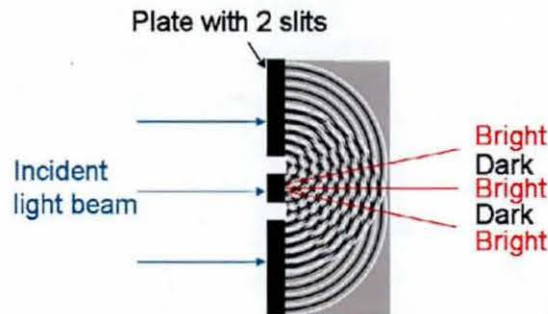


**Figure 2-2: Schematic of Young's double slit experiment.**

Coherence of light is important to understand in order to comprehend Young's double slit experiment. Coherence of light can be subdivided into temporal and spatial coherence. Temporal coherence is the ability of the light wave to maintain identical wavelength, direction and phase over time. The ability for the light wave to be identical at the bottom and top of the wave is spatial coherence thus keeping identical amplitude and wavelength in space. Coherence and interference (2.2.3) help explain Young's double slit experiment.

### 2.2.2 Propagation of light

Light can travel in three different formats, it can be transmitted, reflected or refracted. Light is transmitted through a vacuum at the speed of light,  $c$ ,  $3 \times 10^8 \text{ ms}^{-1}$ . Light propagation has been understood for a very long time, the basic principle was described by Huygens in the late 16<sup>th</sup> century (Huygens 1690), who stated that if the position of light is known then it is possible to calculate where it has moved to at a fixed time later.

When light is reflected there are two well understood laws that describe the event.

- The incident ray, the reflected ray and the normal to the surface at the point of incidence all lie in the same plane.
- The angle of incidence is equal to the angle of reflection.

Refraction is an important property of light propagation. Refraction is the change in direction of a wave due to a change in velocity. Typically all materials have a common stated refractive index, this is calculated using Equation 2-3, where  $\mu$  is the refractive index of a material.

$$\mu = \frac{\text{Speed of light in vacuum}}{\text{Speed of light in material}} \quad \text{Equation 2-3}$$

Light that enters a higher index medium bends towards the normal, thus light that enters a lower index medium bends away from the normal.

All objects can be classified into three groups according to how they behave when struck by light. A transparent object will transmit light, an opaque object will absorb light and reflective objects will reflect light. It must be noted however that no object can be perfectly transparent, opaque or reflective.

### 2.2.3 Interference

For the purpose of laser applications it is crucial to understand interference of light. The Young's double slit experiment explains this phenomenon, shown in Figure 2-2. This experiment shows that light waves interfere with each other, if two separate waves arrive at the same point in space, whereby they overlap, the two waves will

simply add or subtract from each other without permanently destroying each other. The resulting disturbance at each point in time is the algebraic sum of the individual constituent waves at that point in time and space. Post collision, the two waves will travel completely unaffected by the encounter. This principle is commonly known as the superposition principle, as illustrated in Figure 2-3.

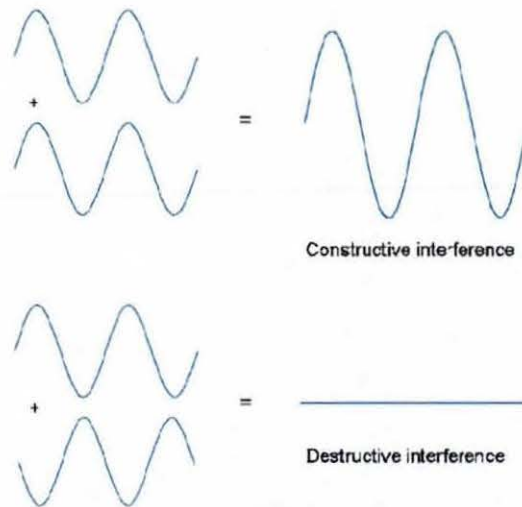


Figure 2-3: The superposition principle.

#### 2.2.4 Polarisation

Polarisation describes the possible orientations of an oscillatory process in a plane perpendicular to a transverse waves' path. In an electromagnetic wave the oscillating electric and magnetic fields are transverse to the direction of propagation, it is custom to assign the polarisation of the light wave in the same plane as the electric field and direction of propagating light.

Polarisation of light is a useful technique in order to separate or combine different components of light. Polarisation effects are significant in materials that are crystalline as they are electrically and optically anisotropic. Crystalline materials exhibit double refraction of light and are commonly known as birefringent materials, thus they possess two refractive indexes. These birefringent materials are often used to manipulate the polarisation of light in laser applications.

## 2.2.5 Lenses

A lens is an optical device with axial symmetry that transmits and refracts light, creating convergent or divergent light. Without doubt a lens is the most common optical device, currently being used to read this text.

Two basic lens designs are depicted in Figure 2-4. A biconvex lens is shown in (a) which converges light at a real focal distance,  $f_L$ . A biconcave lens shown in (b) causes the transmitted light to diverge, the focal distance,  $f_L$ , is said to be imaginary.

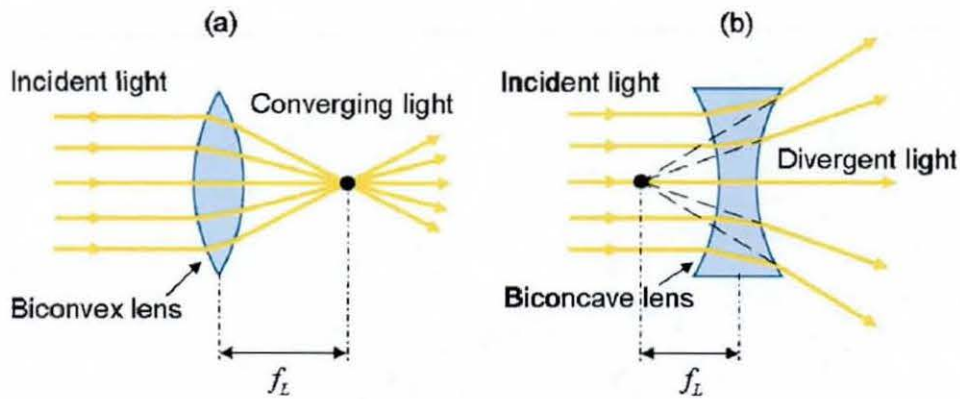


Figure 2-4: Simple lenses, (a) biconvex lens, (b) biconcave lens, adapted from (Precision Graphics 2000).

## 2.3 Laser optical engineering

### 2.3.1 Background

Maiman invented the ruby laser in 1960 and at the time researchers debated if it had any possible practical applications. The term 'a solution looking for a problem' was synonymous with the laser. The actual word laser was used as an acronym for 'light amplification by stimulated emission of light', this however gained such widespread use that it has become a noun in the common day dictionary.

Living in the 21<sup>st</sup> century it is inconceivable to avoid laser technology. Countless applications exist within a multitude of different sectors including medicine, military, automotive, construction, electrical, engineering, research, entertainment, information technology, law enforcement, retail and communications. Lasers are invaluable within many every day applications such as the bar code scanner, laser jet printers, reading

and writing CDs and DVDs, laser optical cables for television and internet and the list goes on. Within the sport industry laser range finders are popular amongst golfers in order to measure exact distances to specific markers.

Two common types of laser are reported, the pulsed laser and the continuous-wave (CW) laser. The difference is self explanatory however depending on the application required, one type of laser can ultimately be much more applicable.

Normal light, such as daylight or light from an electric bulb has been described as a 'broadband noise generator' meaning that light disperses randomly in all directions. It possesses coherence in the order of wavelengths and it has an inherently low brightness. Laser light is not limited by low brightness, recent advances have led to the maximal focused intensity of laser light to be in the range of  $10^{16} \text{ Wm}^{-2}$  which corresponds to a laser power in the petawatt ( $10^{15} \text{ W}$ ) class (Norby 2005). Lasers are reported in a huge variety of power levels. The power level indicates how much energy is released per unit of time, measured in watts and defined by Equation 2-4. One watt is defined as a rate of one Joule per second.

$$Power = \frac{\Delta Energy}{\Delta Time} \quad \text{Equation 2-4}$$

The laser has gained widespread usage because of the unique properties it possesses compared to normal light. The laser emits a collimated beam of light that possesses high spatial and temporal coherence, monochromaticity and potentially high brightness. It is important to understand these inherent properties and they are reported later in this section.

### **2.3.2 Laser operation**

Einstein (1917) was the first to hypothesise stimulated emission of an atom, which is the quantum principle that drives laser operation. This section will outline simplistically, principles that govern laser operation and design.

The process of creating laser light relies on a population inversion in the lasing medium. The lasing medium is the material used to create the light or photons. Achieving population inversion is complex, it is simplified to a three level process in

Figure 2-5. By exciting atoms from the ground state to a highly excited level atoms gain energy. Due to spontaneous emission these atoms will drop to a metastable level, still the atoms have more energy than in the ground state. Atoms remain excited at an atomic scale for a long duration at the metastable level (milli to micro seconds long). By introducing a stimulating emission wave to the atom at a metastable level, the atom releases energy as a photon. Imperatively the released photon has identical phase and direction as the stimulating wave. This process creates a cascade of photons.

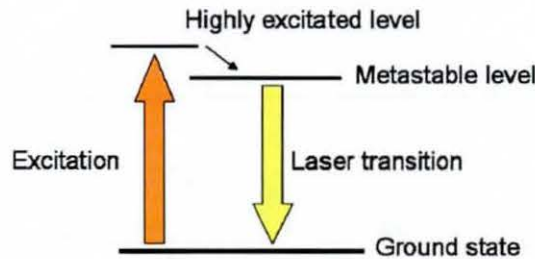


Figure 2-5: Three level population inversion.

In order for a laser to operate in CW mode it is paramount to keep the lasing material population inverted so that it is likely that a stimulating wave will hit an excited atom releasing energy rather than hitting an atom in the ground state and being absorbed. There are numerous methods of 'pumping' a lasing material maintaining the population inversion.

The general laser design in Figure 2-6 incorporates mirrors at both ends of the lasing material, this is common to all lasers because the more times light travels through the lasing material the more photons are emitted due to stimulated emission. This laser amplification is known as gain.

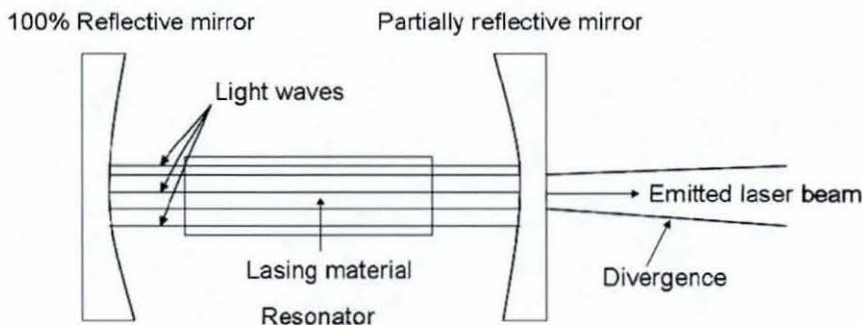


Figure 2-6: Basic laser design, Fabry-Perot interferometer.

Resonance is an important consideration in laser design. Due to the superposition principle of light it is important that the created light waves are amplified (constructive interference). In order to achieve amplification twice the cavity length,  $L$ , must be equal to an integer number,  $N$ , multiplied by the laser wavelength,  $\lambda$ , as shown in Equation 2-5.

$$N\lambda = 2L \qquad \text{Equation 2-5}$$

### 2.3.3 Collimation

Laser light can be highly collimated and this can be achieved due to the common laser design, see Figure 2-6. Light can only escape the laser cavity through a small transmitting part at the centre of one mirror, consequently because of this narrow emitting part, a very thin low diverging beam of light can escape. Due to diffraction effects between the laser light and the mirror, the laser beam will diverge upon leaving the cavity. Generally this diversion is very small and a common Helium-Neon (He-Ne) laser diversion is typically in the order of one milliradian.

### 2.3.4 Monochromaticity

Monochromaticity is a crucial property of laser light and this is the ability to exhibit a single wavelength (coherent) or realistically a very small range of wavelengths. The visible light spectrum has wavelengths in the range approximately 0.4 to 0.7  $\mu\text{m}$ , therefore consisting within a bandwidth of approximately 300 nm. There are numerous different filters but if a generic blue filter were used the bandwidth could be reduced to around 10 to 20 nm. To highlight the monochromaticity of laser light a typical bandwidth of less than 1 nm is readily ascertainable.

### 2.3.5 Coherence

The coherence of laser light is dependent on the monochromaticity and collimation of the light source. Laser coherence lengths up to several kilometres are feasible, standard flash bulbs generally emit light that is coherent in the order of millimetres.

### 2.3.6 Laser safety

The nature of laser light can make it extremely hazardous for human contact especially with the eye. As laser technology has evolved the guidelines for their operation has become more stringent. Globally laser operation is regulated by the International Electrotechnical Commission (IEC). The current classification system

## Laser based tracking and spin measurement

was introduced in 2002 and has been recently updated (IEC 2007). The system is categorized according to the damage the laser can inflict on exposed users, a summary of these classes is shown in Table 2-1.

With laser work the exposure or irradiance that an eye can see without potential harm is called the maximum permissible exposure (MPE) generally measured as an energy density. In order to work with eye-safe class 2 lasers the MPE was fixed at  $25.4 \text{ Wm}^{-2}$ .



**Table 2-1: Summary of IEC laser classes.**

Laser Class	Description
1	Eye-safe under all operating conditions.
1M	Eye-safe for all conditions except when viewed through magnifying optics, such as microscopes and binoculars.
2	For light in the visible spectrum, this class is safe for accidental viewing because the blink reflex will limit the exposure to no more than 0.25 seconds. Intention to suppress the blink reflex could cause damage to the eye. For lasers in this class and higher a clear warning label must be visible, as shown in Figure 2-7.
2M	For light in the visible spectrum, safe if not viewed through magnifying optics. Applies to laser beams with large diameter or divergence as long as light striking the pupil does not exceed the limits for class 2.
3R	Radiation is considered low risk, however potentially hazardous. CW lasers emitting between 1 and 5 mW generally fall into this class.
3B	Radiation is considered a risk, will cause damage if exposed to the eye directly. Protective eye wear is typically a must. A key switch and safety interlock are compulsory.
4	Radiation is considered high risk, all lasers above class 3B fall into this category. With direct viewing permanent eye damage is likely. Radiation can cut and burn skin, therefore it is a fire hazard. A key switch and safety interlock are compulsory.



**Figure 2-7: Warning label for class 2 to 4 lasers.**

## 2.4 Laser Doppler anemometry to laser Doppler vibrometry

The technique of laser Doppler vibrometry was used intensively for the work in this thesis. It was important to understand how this technique has evolved to its present stage in current optical engineering applications. The progression and principles of laser Doppler anemometry to laser Doppler vibrometry are reported.

### 2.4.1 Laser Doppler anemometry

The field of fluid dynamics was the first to benefit from the invention of the laser. The first reported work in this field was by Yeh and Cummins (1964), who observed localised fluid flow measurements. For their task the laser approach was unique because previously dyes had been injected into fluid flows to analyse flow patterns. At low speeds the dyes diffused in the fluid flow adding errors to actual fluid flow measurement. The laser allowed a novel non contact approach to the task.

The fluid flow velocity was measured using the Doppler effect principle. This effect relies upon the detection of the Doppler frequency shift in coherent light which occurs when it was reflected from a moving medium. Laser light was deflected by seeded particles travelling in the target fluid flow, as shown in Figure 2-8. The scattered light was detected by a photodetector at an angle ( $\theta$ ). This scattered light had an original frequency ( $f$ ) and an apparent change in phase ( $f_D$ ), Equation 2-6 is used to calculate the target velocity ( $U$ ).

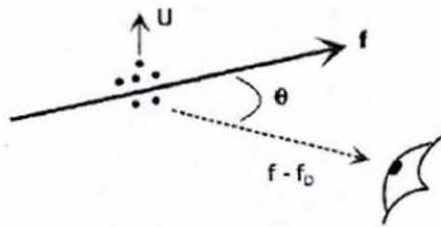


Figure 2-8: LDA set-up (Halliwell and Hargrave 2003).

$$f_D = \frac{2\mu|U|}{\lambda} \sin \frac{\theta}{2} \quad \text{Equation 2-6}$$

The application of lasers in fluid flow measurement is commonly referred to as laser Doppler anemometry (LDA). This is a common technique (Durst *et al.* 1981a, Tsai and Wu 1998) and has been extended to three dimensional fluid flow analysis

(Antoine and Simpson 1986). Both techniques have been developed into commercial products. There are numerous research papers and commercial products detailing many aspects of LDA, the basis for the majority of this work was published by Durst *et al.* (1981a).

#### 2.4.2 Laser Doppler vibrometry

The technique of LDA has been developed into solid mechanics which is referred to as laser Doppler vibrometry (LDV). This technique was analysed in depth in a publication by Drain (1980) who fully appreciated the capabilities of laser light. The premise of the technique relies on the detection of the Doppler shift in coherent light which occurs when it is scattered from a moving target, exactly as LDA relies on the Doppler shift.

LDV is a non-contact technique in which time resolved measurements can be outputted as surface velocity measurements. In contrast to LDA, generally the incident laser beam is directed towards the target surface and the Doppler shifted light is collected in direct backscatter, as shown in Figure 2-9. The velocity measurements obtained are in the direction of the incident laser beam only.

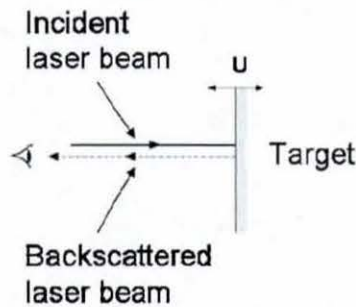


Figure 2-9: LDV set-up, adapted from (Halliwell and Hargrave 2003).

The technique allows the Doppler shift ( $f_D$ ) to be calculated using Equation 2-7. The on axis surface velocity of the target ( $U$ ) is measured in  $\text{ms}^{-1}$  and the angle between the incident laser beam and normal to the surface ( $\theta$ ) is measured in degrees. The refractive index of light in air is generally reported as one.

## Laser based tracking and spin measurement

$$f_D = \frac{2\mu|U|}{\lambda} \times \text{Sin}(\theta) \quad \text{Equation 2-7}$$

It is clear that if the angle of incidence is at  $90^\circ$  to the normal of the surface Equation 2-7 simplifies to Equation 2-8. Direct correlation between target velocity and Doppler shift is straightforward.

$$f_D = \frac{2\mu|U|}{\lambda} \quad \text{Equation 2-8}$$

A limitation in using LDV is the fact that light has a very high electromagnetic frequency  $\sim 1 \times 10^{15}$  Hz. Modern electronics can generally only process frequencies at maximum in the MHz range, therefore the coherence of laser light is utilised to overcome this. By introducing two light waves together constructive and destructive interference occurs, as documented in 2.2.3. There are two main approaches to this technique; heterodyne and homodyne techniques. Both techniques involve combining two light waves together at a photodetector. Homodyne interferometry relies on combining two light waves of the same frequency. Heterodyne interferometry however introduces a Doppler shift to one light wave, and the detector measures the phase difference between the two light waves. The main difference between the techniques is that the heterodyne technique is not dependent upon the intensity of the received light waves, which commonly fluctuates during dynamic measurements.

The heterodyne process was deemed superior and is the technique utilised in commercial vibrometers. The output at the photodetector using the heterodyne process is a beat frequency difference of the two light waves, as shown in Figure 2-10 by  $f_1 - f_2$ . Therefore a sinusoidal wave that has a frequency in the MHz range is achievable.

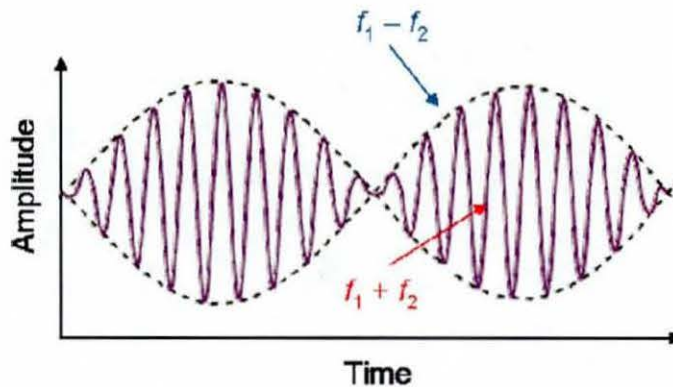


Figure 2-10: Heterodyne process, adapted from (Kurtus 2007).

Within literature the LDV has been highlighted as a powerful tool in measuring hot, light and rotating objects due to its non-intrusive nature (Pickering *et al.* 1986). Within sports engineering LDV has been used in modal analysis applications for golf (Hocknell *et al.* 1998a, Hocknell *et al.* 1998b, Roberts 2002), for soccer (Ronkainen and Harland 2006) and tennis (Barras 2006). Traditionally accelerometers have been used in modal analysis type applications within the sports engineering community (Thomas *et al.* 1995, Varoto and McConnell 1995, Knowles *et al.* 1996, Braunwart 1998, Wicks *et al.* 1999, Brooks *et al.* 2006). The main advantages of using a laser as opposed to an accelerometer approach are:-

- It avoids physical interaction between target and transducer.
- It removes the mass loading effect.
- It can achieve a very high spatial density of the measurement region.
- It enables speed and ease of carrying out the measurements.
- The transducer is very stable over time.

#### 2.4.2.1 The Michelson interferometer

Named after its inventor, the Michelson interferometer arrangement is widely used within LDV operation, the standard set-up is shown in Figure 2-11.

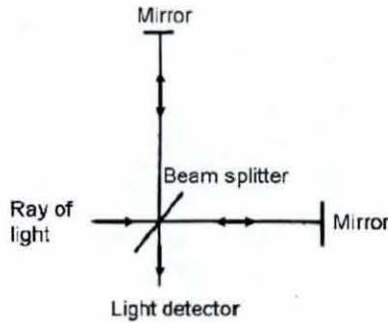


Figure 2-11: The Michelson interferometer, adapted from (Michelson 1887).

Using the original Michelson interferometer technique, directionality of the target movement was ambiguous. Therefore when introducing two light beams together in the heterodyne process it is essential to pre-shift the frequency of one of the beams. It has become convention to call the shifted laser light beam the reference beam and the laser light beam backscattered from the target, the target beam. The magnitude of the shifted reference beam determines the target velocity range that the system can demodulate. Measured positive or negative shift away from the reference frequency allows the target displacement direction and velocity to be ascertained.

#### 2.4.2.2 Frequency shifting devices

Literature has reported different methods for achieving a frequency shift in the reference beam, required to give the LDV technique directionality as well as velocity magnitude. The first such method was introduced by Oldengarm *et al.* (1973) where a rotating diffraction grating was used to shift the reference beam from 0.1 to 2.5 MHz. Soon after a rotating disc was utilised, as shown in Figure 2-12, to create the shift in a very simple and cheap method (Ballantyne *et al.* 1974), and copying this concept the first portable LDV was developed (Halliwell 1979). This design was used in the first commercial laser vibrometer manufactured by Bruel and Kjaer (B&K), type 3544.

## Laser based tracking and spin measurement

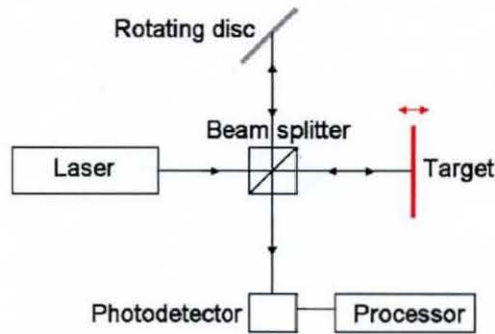


Figure 2-12: Basic schematic of portable LDV.

By changing the angle of incidence between the rotating disc and laser beam, altering the radial position at which the laser beam struck the rotating disc, and by modifying the rotation frequency of the rotating disc, the magnitude of the frequency shift could alter accordingly.

The Bragg cell frequency shift device was introduced by Buchave (1975) and is an opto-electronic system that enables large, stable and accurate frequency shifts. Initially the Bragg cell allowed 10 kHz to 50 MHz shifts, currently though 80 MHz and 120 MHz devices are commercially available. The Bragg cell is a comparatively expensive component, which most commercial LDVs utilise to introduce the shift in the reference beam. Figure 2-13 shows a basic schematic of the LDV set-up incorporating a Bragg cell frequency shift.

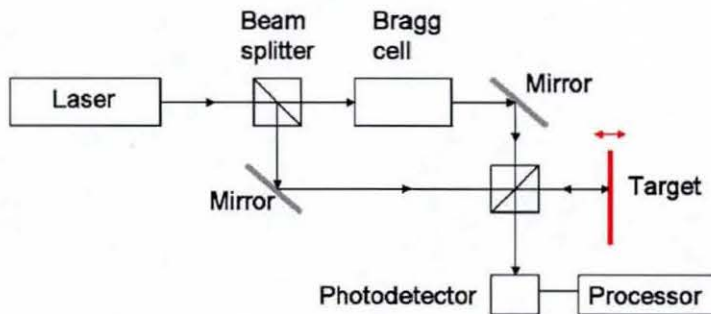


Figure 2-13: Basic schematic of LDV set-up with a Bragg cell frequency shift.

Other shift devices exist such as the piezoelectric element that was driven sinusoidally by Baker *et al.* (1990), this method was deemed to increase the complexity of the measured signal demodulation.

## **2.5 Dual and Multiple beam vibrometry**

This section is an extension to the foundations introduced for vibrometry in section 2.4. This section reports measurement of target velocity through all three translational and rotational degrees of freedom (DOF). These systems used at least two simultaneous laser measurement beams and allowed at least one translational DOF to be extracted, this can not be achieved using a single incident laser beam.

### **2.5.1 The cross beam vibrometer**

Dual beam vibrometry relies on exactly the same principles as single point vibrometry; however the introduction of an additional beam allows more than purely on-axis velocity measurement.

The dual beam vibrometer was first reported in the early 1980s by Durst *et al.* (1981a). A cross beam dual laser was used to measure tangential surface velocities of rotating shafts. The design of the cross beam vibrometer relied on the target being circular in cross section and the point of contact by the laser beams to differ less than 1 mm during rotation whilst the vibrometer was a fixed distance from the target. Solid body oscillations were indistinguishable from tangential target velocity components, adding to the limitations of the system.

### **2.5.2 The laser torsional vibrometer**

A novel development of the cross beam vibrometer was carried out by Halliwell *et al.* (1984) and Halliwell and Eastwood (1985). This technique was patented the following year (Halliwell 1986). Initially designed for torsional vibration measurement, the novelty was in the two incident laser beams being parallel to each other, as shown in Figure 2-14. This device was called the laser torsional vibrometer (LTV). Current commercial products available based on this principle are called rotational vibrometers.



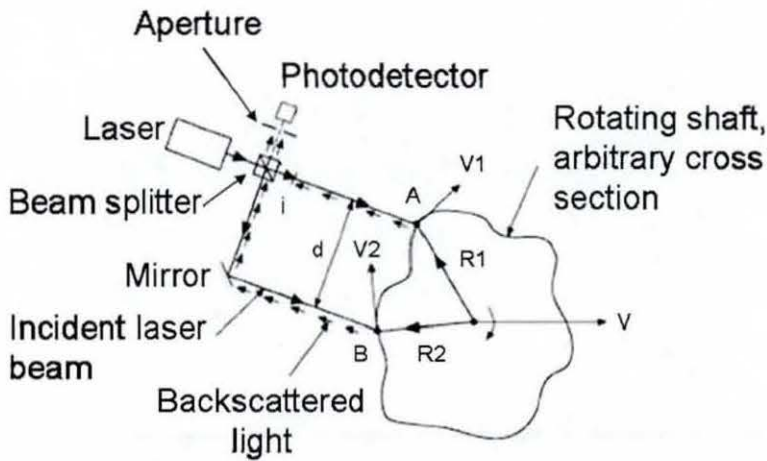


Figure 2-14: The laser torsional vibrometer (Halliwell *et al.* 1984).

The Doppler shift,  $f_D$ , can be calculated using Equation 2-9, where the target revolutions per second,  $N$ , is multiplied by the laser beam separation distance in metres,  $d$ .  $\alpha$  is the angle between the direction of incident laser beams and the direction of the spin axis, measured in degrees, as shown in Figure 2-15.  $\gamma$  is the angle between the plane of the cross section of the target and the plane of the incident laser beams, measured in degrees and shown in Figure 2-16.

$$f_D = \frac{(4\mu\pi)}{\lambda} Nd \times \sin(\alpha) \times \cos(\gamma) \quad \text{Equation 2-9}$$

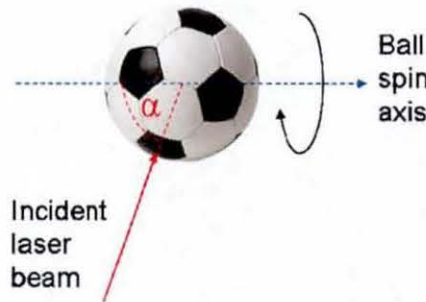


Figure 2-15: Plan view of target rotation.

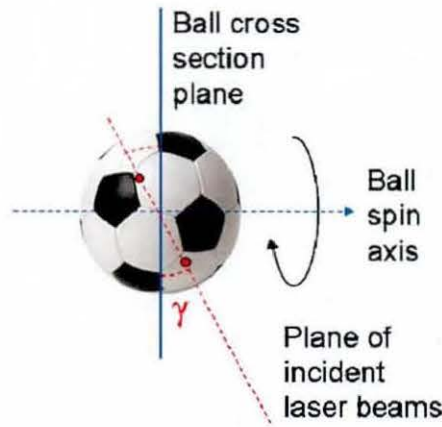


Figure 2-16: Front view of target rotation.

When the torsional vibrometer was aligned such that  $\alpha = 90^\circ$  and  $\gamma = 0^\circ$ , the Doppler shift could be calculated using Equation 2-10.

$$f_D = \frac{(4\mu\pi)}{\lambda} Nd \quad \text{Equation 2-10}$$

The laser torsional vibrometer was demonstrated to be insensitive to target or vibrometer solid body movements and could be used on arbitrary target shapes. Therefore one rotational DOF could be extracted. Two excellent review papers on the development of the LTV were written by its creator (Halliwell 1993 and 1996).

The current available commercial device allowed target revolutions per second (RPM) measurement from -7000 RPM to +11 000 RPM utilising a DC decoder (Polytec 2006). This spin rate measurement range meant that the decoder could measure a continuous Doppler shift from  $-2.93 \text{ ms}^{-1}$  to  $+4.61 \text{ ms}^{-1}$ . The reason for non symmetric directional discrimination was due to the inherent frequency shift in the reference laser beam at 40 MHz. The device also allowed dynamic angular velocity and vibration angle measurement utilising an AC decoder technique. B&K had a competing product that operated on exactly the same principles as the Polytec counterpart, the B&K type 2523 vibrometer could measure rotational speeds from 30 to 7200 RPM.

When a rotating target had angular lateral vibration whereby the target shaft rotation axis underwent a change in direction in time, it caused a change in angles  $\alpha$  and  $\gamma$ .

Observing Equation 2-9 it is clear that these changes influence the measured Doppler shift. Therefore the measured Doppler shift was unable to distinguish angular lateral vibration from genuine torsional vibration. Miles *et al.* (1996) created a set-up using two symmetrically placed laser torsional vibrometers pointing at the same location on the target as shown in Figure 2-17.

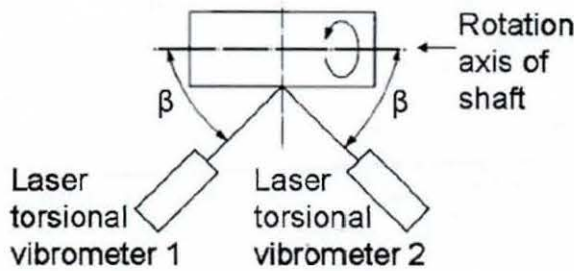


Figure 2-17: Torsional vibrometer test set-up, adapted from (Miles *et al.* 1996)

This set-up allowed unambiguous measurement of torsional vibration as well as simultaneous measurement of bending vibration. This was achieved by measuring the mean outputted value from both vibrometers as the rotational speed of the shaft and the fluctuating measured component provided the torsional vibration velocity. They concluded that the main factor causing angular lateral vibration was assumed to be shaft bending vibration. This initial work was extended to give comprehensive theory to account for the sensitivity of the LTV's measurements to shaft motion in all DOF (Miles *et al.* 1999).

The LTV relied on the target having a non-zero mean speed, to measure angular velocity. A system was developed whereby the two parallel beam system was incorporated, however a rotating diffraction grating was used to introduce a constant pre-shift between the incident laser beams. This system allowed local angular target velocity to be measured even if the target had zero mean speed of rotation (Halliwell *et al.* 1997). This system was designed with modal analysis applications in mind.

### 2.5.3 Other dual beam vibrometers

Trethewey *et al.* (1993) developed a system for dynamic measurements that was able to measure one translational DOF and two rotational DOF (pitch and roll) using two collimated light beams reflected from a planar target, shown in Figure 2-18. The set-

up required two position sensitive photodetectors so that each laser beam was analysed individually.

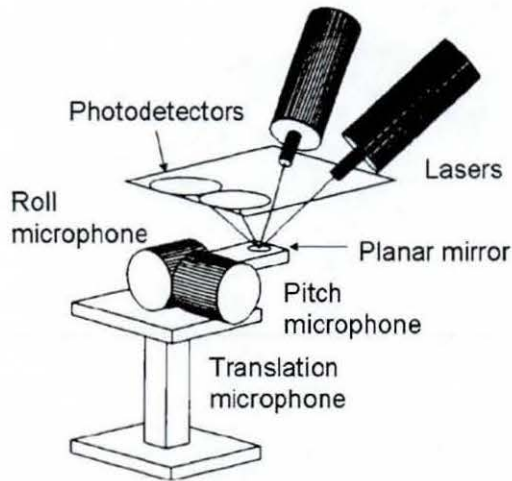


**Figure 2-18: Dual beam system, adapted from (Trethewey *et al.* 1993).**

A mathematical solution was formulated to output the 3D position and orientation of the target from the photodetector measurements. The main sources of error were the small differences between manufacturing specifications and finished machined geometries. Also a misalignment between the components was known to induce errors. It was essential that the surface was flat to compute correct 3D position and orientation of the target. The system only operated with relatively small target motions, limiting it to modal analysis type applications.

#### **2.5.4 Multiple beam vibrometers**

A development of the Trethewey *et al.* (1993) system was reported in a two part paper by Bokelberger *et al.* (1994a&b) whereby all three translational and three rotational vibrational DOF were measured. In the basic set-up the detectors are shown as  $D_1$ ,  $D_2$  and  $D_3$  and the laser vibrometers as shown as  $L_1$ ,  $L_2$  and  $L_3$ , see Figure 2-19, three laser beams were reflected off a tetrahedral target onto corresponding position sensitive photodetectors.

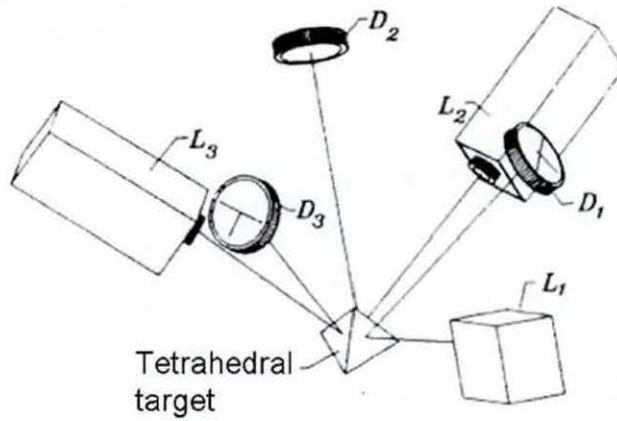


**Figure 2-19: Three beam system, adapted from (Bokelberger *et al.* 1994a).**

This system also suffered from small differences between the manufacturing specifications of the hardware and finished machined geometries, resulting in large errors. Another difficulty was encountered in the uncertainty associated with the 3D position and orientation of the lasers and photodetectors. This system was limited to flat targets and allowed only small rotational DOF and small translational displacements, which again lent itself to vibrational work only. The system relied on the tetrahedral target being mounted to the object under inspection, this attachment would not lend itself towards a non-contact approach pursued in this thesis work.

A novel device was manufactured and tested to measure three translational DOF of a submerged target cylinder (Vignola and Houston 1993). The system consisted of 6 beams, five external beams converged and struck the target object at one point in space, one beam was used exclusively as a reference beam in order to measure the out of plane target translation component. The set-up for the test is shown in Figure 2-20.

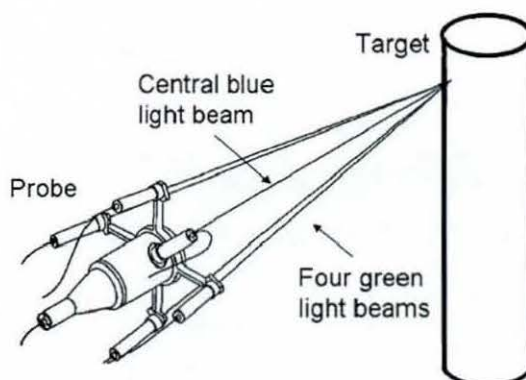


**Figure 2-20: Underwater measurement system, adapted from (Vignola and Houston 1993)**

In order to decipher the three translational DOF it was important to be able to decode each translational DOF individually. This posed difficulties since 5 beams struck the target at the same point in space. The authors overcame these difficulties using three different strategies. The first strategy involved using different wavelengths of light, four of the beams used green light at  $\lambda = 514.5 \text{ nm}$  and one of the lines used blue light at  $\lambda = 488 \text{ nm}$ . The second strategy introduced different frequency shifts to the light beams so that 1 MHz, 2 MHz and 3 MHz difference frequencies existed between the three translational DOF measurements. The third strategy distinguished the two in plane translational DOF by plane polarizing the light waves orthogonally. The three dimensional probe design employed different methods to demodulate the in plane and out of plane velocity components. Due to the converging laser beam design this method needed a fixed stand off distance to the target, which was seen as a major problem if anything but small movements were measured.

A recent and hugely important study described the comprehensive theory behind measuring all three translational and rotational DOF with any single or dual laser beam orientation (Bell and Rothberg 2000a). The study also utilised a multiple beam arrangement, which could be used to isolate in one single measurement the pitch and yaw vibration DOF, see Figure 2-21. This study was a development of previous work by Bell and Rothberg (2000b).

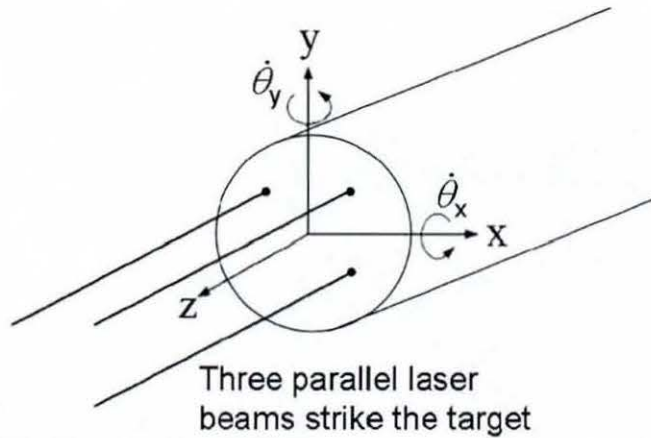


Figure 2-21: Parallel beam arrangement, adapted from (Bell and Rothberg 2000a).

## 2.6 Scanning and laser tracking

The techniques reported in this section have been developed predominantly for modal analysis type applications. For many engineering structures it is important to analyse the target under normal working conditions, for fans and propellers this means acquiring target velocity data whilst the target is rotating. The properties of laser light make it suitable for these applications.

This section reports techniques used to deflect the incident laser beam. Finally non-vibrometry type laser scanning and tracking are reported, since these types of techniques could be incorporated with LDV work being pursued in this thesis.

The work in this section is predominantly categorised into contributions by researchers at universities and companies because they have been the driving force behind the research and development within this field.

### 2.6.1 The scanning technique

The first researchers to introduce a shift in the direction of the incident laser beam placed an oscillating mirror in the optical path of the laser beam (Durst *et al.* 1981b, Sriram *et al.* 1990).

One mirror limited deflection to one dimension in the incident laser beam. Thus almost all reported scanning and tracking techniques utilise two mirrors, which are

aligned orthogonally to each other, as shown in Figure 2-22. This allows one mirror to scan the incident laser beam in the x-axis and the second to scan in the y-axis, this explains why the mirrors are generally referred to as the x and y-mirror.

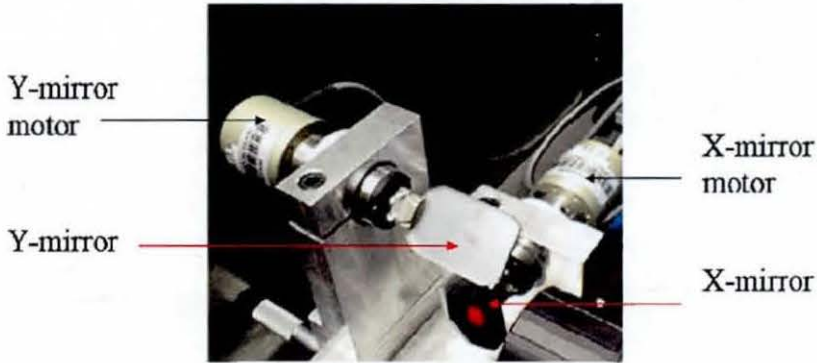


Figure 2-22: Scanning mirrors, adapted from (Halkon and Rothberg 2004)

Several manufacturers such as GSI Group, BFi Optilas, Cambridge Technology, Scanlab and Nutfield Technology have designed mirrors for deflecting incident laser beams, called galvanometers. A galvanometer or 'galvo' consisted of a mirror, rotation torque motor and a position sensitive detector. The main considerations to note regarding the speed of the mirrors was the torque to inertia ratio of the motor and mirror, as well as the stiffness to weight ratio of the mirror housing. The higher these two ratios, the quicker the potential drive speed of the mirrors. Generally galvanometer responses were stated in milliseconds in regards to a small step response ( $<1$  ms) or full step response time (1-3 ms), these were highly dependent upon the model and size of mirror aperture being utilised. The bandwidth at which the mirrors could be driven at was crucial regarding high speed scanning or tracking work, it was also worth considering that these mirrors possessed a natural resonant frequency, at which scanning would not be advised.

Galvanometers are mechanical systems. It was important to consider how the mirrors were driven, this is because wobble and timing jitter of the mirrors would significantly change the Doppler shift measured by the laser vibrometer. These factors mean that galvanometers were generally driven with sine and cosine waves for high speed applications, therefore the patterns shown in Figure 2-23 would utilise the bandwidth of the mirrors most efficiently. These were common lissajous patterns



which are described simply by sinusoidal waves, showing complex harmonic motion. "Lissajous patterns increase angular accuracy by using the natural inertia of the galvanometers to average out pointing noise" (Zeleny 2004).

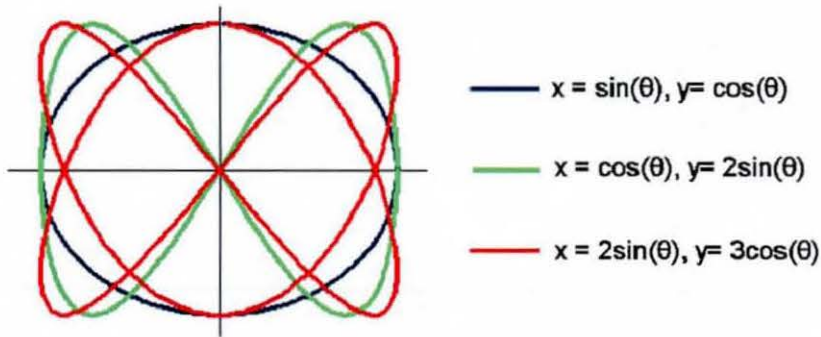


Figure 2-23: Complex harmonic motion.

## 2.6.2 Contributions by Imperial College London

The first reported work on scanning and tracking a target with a LDV was reported by Stanbridge *et al.* (1995). An Ometron LDV was used in combination with x and y-mirrors to direct the laser beam onto a rotating disc. A circular pattern was created on the disc by utilising two sinusoidal analogue inputs into the x and y-mirrors, as detailed in 2.6.1. Since the target disc incorporated a 1024 points per revolution decoder, the mirror inputs were synchronised with the disc rotation. This was the basic principle used for most scanning and tracking work.

Researchers at Imperial College extended their work to actually scan individual blades on rotating blisks (Stanbridge *et al.* 2002a). They also introduced a scanning path to avoid partially obscured parts of the target as well as straight line scans on moving belts (Stanbridge *et al.* 2002b).

Recent work has led to the development of a software platform for virtual and real vibration testing on stationary and rotating structures using SLDV (Di Maio and Ewins 2006). The real vibration testing could take one of three forms. Firstly a point could be tracked on a blade, secondly a line could be tracked along a blade and thirdly the most complicated technique, involved tracking an area of a blade whilst it was rotating. The area tracking operated in the range from 0 to 2400 RPM for the rotating target blade.

### 2.6.3 Contributions by Ancona University

The first work within the field of scanning and tracking investigated at Ancona University considered vibration measurement on blades of a naval propeller, in a very similar set-up to the initial work by Stanbridge *et al.* (1995). The propeller was however actually rotating in water. This was considered important since fluid-dynamic forces acting on the propeller vary randomly in time due to turbulence. This testing reflected in situ working parameters. This set-up meant that particular attention had to be paid to the refractive index of water since it affected the path travelled by the laser beam. A vibration map of the propeller was achieved at a maximum rotational speed of 540 RPM (Castellini and Santolini 1998).

A subsequent paper was published where the propeller was rotating through air and was excited acoustically (Castellini and Revel 1999). The modal shapes were extracted at propeller speeds up to 1680 RPM. It was concluded that to measure the vibration of the surface with high accuracy it was necessary to align the scanning head axis with the rotational axis, this method has since been adopted by almost all scanning modal analysis researchers. If alignment was not perfect, as shown in Figure 2-24, the distance between the SLDV and the target would change with sinusoidal shape at a frequency directly dependent upon the target spin rate, commonly referred to as pseudo-signal.

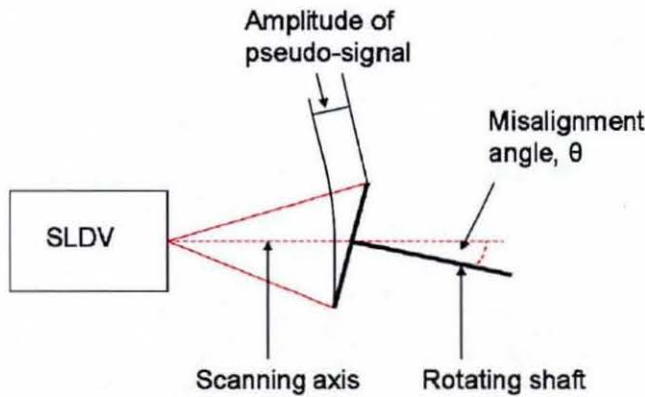


Figure 2-24: Misalignment between scan axis and rotating shaft axis, adapted from (Castellini and Paone 2000).

Research at Ancona had previously highlighted errors associated with SLDV. An in depth analysis of measurement uncertainty and laser spot positioning accuracy

## Laser based tracking and spin measurement

identifying the most critical elements in the measurement system was completed, suggesting optimisation strategies (Castellini and Paone 2000). The work concluded that the largest contributors to noise at the rotation frequency and its harmonics were:

- The kinematics of the mirrors.
- Misalignment between scanning axis and rotating shaft axis.
- Reflection of the laser beam on the mirrors whereby the reflected point was not on the axis of mirror rotation.
- The mirrors reflect all backscattered light, much of it hitting the photodetector, this included light that has travelled different distance to target and hit different points on the mirrors, inducing a broadband noise in the Doppler shift measured.
- Vibration of the body of the LDV due to the oscillation of the galvanometers.

The first reported work on tracking laser Doppler vibrometry (TLDV) whereby the target motion was not circular was reported by Castellini and Cupido (2001) and applied to tracking wind-screen wipers with either simple rotational motion or complex translational and rotational motion. The tracking was carried out by controlling the x and y-mirrors using signals received from a position transducer, which was directly connected to the moving target. The position transducer utilised wire potentiometers whose electric resistance was directly proportional to their extension.

The work compared a traditional accelerometer approach with the TLDV approach and found very similar vibrational behaviour. It was interesting to note from Figure 2-25, the vibrometer time history results showed a low frequency component in the measured target velocity. This phenomenon was accounted for due to varying laser path length to target.

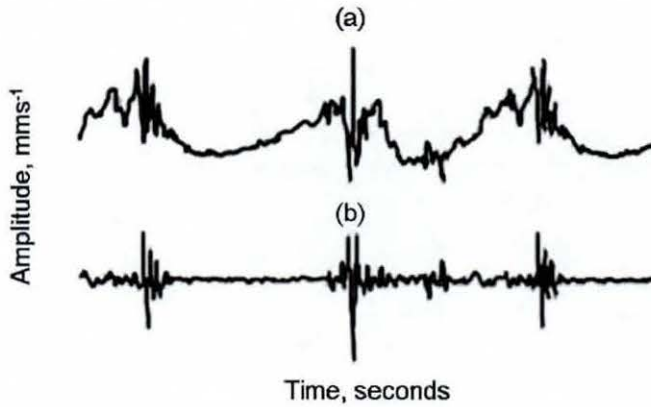


**Figure 2-25: Transducer time history, (a) for vibrometer, (b) for accelerometer, adapted from (Castellini and Cupido 2001).**

A relevant review paper on the capabilities of TLDV using encoders and position transducers was written looking specifically at vibration behaviour of automotive components. It highlighted the advantages in tracking work due to no relative motion between the laser beam and target (Castellini and Montanini 2002).

A novel image tracking laser Doppler vibrometer (iTLDV) was created in order to track a windscreen wiper with a retroreflective marker attached, as illustrated in Figure 2-26. The centre of the high speed video (HSV) camera field of view (FOV) was aligned with the single point laser beam. The FOV was defined as the object area imaged by the lens onto the camera sensor. Alignment was achieved using a laser line dielectric mirror in order to achieve identical optical axes for both HSV camera and laser beam at the target. During tracking the HSV analysed each frame and if the retroreflective marker moved in the FOV this was observed, and the galvanometers given a new driven voltage to realign the retroreflective target with the centre of the HSV camera FOV (Castellini and Tomasini 2002).

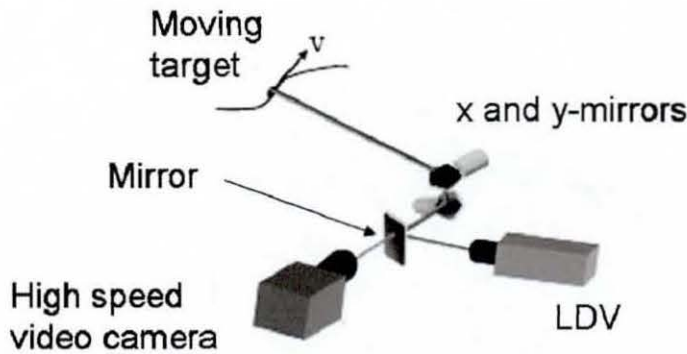


Figure 2-26: iTLDV set-up, adapted from (Castellini and Tomasini 2002).

A comprehensive analysis of this system was carried out by Castellini and Tomasini (2004), who concluded that the limiting factor in the tracking system was the CCD camera being used. It was able to record at 226 FPS, meaning the dynamic performance was directly linked to the camera frame rate. By increasing the camera frame rate, a higher maximum target velocity could be measured, whilst still being able to track the target.

#### 2.6.4 Contributions by Loughborough University

Initial work carried out at Loughborough University (LU) was aimed at creating a general analytical model for the velocity measured by a LDV (Bell 2001) on a rigid target at any angle of incidence. This work was applied to SLDV and published by Halkon and Rothberg (2002a&b). The analytical model clearly highlighted how a single point LDV could isolate the translational vibration sets, two in plane and one out of plane. It was not able however to isolate any of the rotational vibration sets. A conclusion was consistent with previous work, that one source of error was due to angular misalignments which resulted in an oscillating beam path length.

The laser beam path was altered by two orthogonal mirrors, which had a fixed stand off distance between each other. If equal sine and cosine amplitude drive functions were applied, the actual laser path at the target was not a circle but elliptical in profile. Therefore an elliptical scan trajectory correction was developed (Halkon and Rothberg 2002b).

A two part paper by Halkon *et al.* (2003) and Halkon and Rothberg (2003) extended the initial analytical model for the velocity measured by a LDV to flexible cross sections, many engineering components fall under this category. The initial paper provided the theoretical background for the measurements and the second paper reported the experimental validation. The work allowed the prediction of LDV output for any measurement set-up on any chosen target. The error introduced to the measurement by the relative motion of the x and y-mirrors was considered insignificant in relation to the misalignments between the scanning system and target rotation axis.

The classic scanning set-up was adapted by Halkon and Rothberg (2004), as shown in Figure 2-27. The novel application of this set-up was to actually carry out an area scan in real time of a rotating disc blade to measure the operational deflection shape (ODS). The set-up allowed tracking of a single point or a line scan on a particular blade, as shown in Figure 2-28. The authors called this a synchronised-SLDV system.

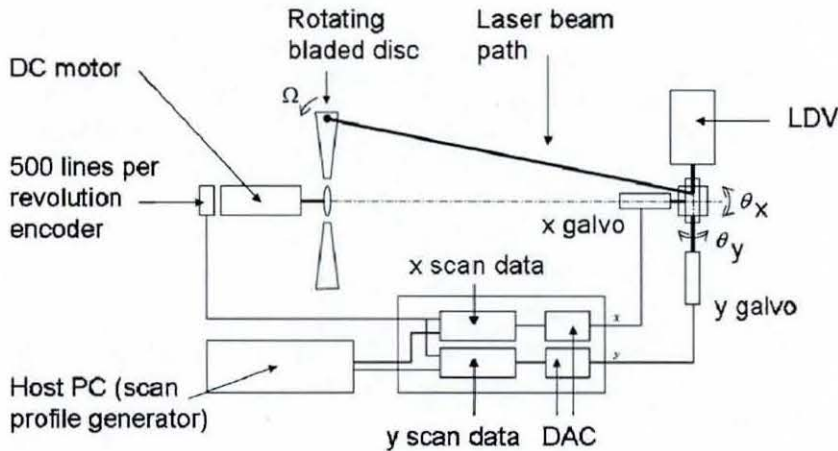


**Figure 2-27: Synchronised-SLDV system, adapted from (Halkon and Rothberg 2004)**

The system was able to track the rotating bladed disc up to 3000 RPM, the limiting factor in the system was the speed at which the galvanometers could scan the laser beam, the scanning bandwidth was limited at approximately 50 Hz.

## Laser based tracking and spin measurement

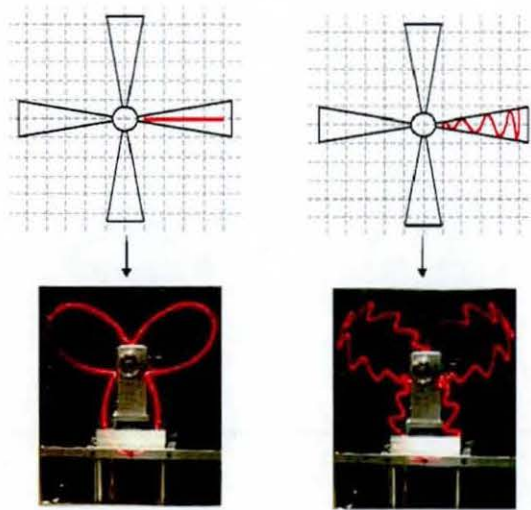


**Figure 2-28: Above – theoretical static line and area scan profile, Below – in situ real time tracking profile of target blade, adapted from (Halkon and Rothberg 2004)**

### 2.6.5 Contributions by Robert Bosch GmbH

Researchers at Robert Bosch Company have published two research projects based on the initial TLDV work at Ancona. The first paper tracked an arbitrarily moving window wiper-blade on a curved wind-screen and measured the ODS of the target (Dietzhausen *et al.* 2003). The novelty in this work lay in the open loop tracking architecture. Initially static control points of the target were recorded in a teaching phase, in tracking measurements the trajectory of the actual measurement points were interpolated, however a position sensitive sensor was used continuously to work out the base position of the wind-screen wiper. The ODS of the wind-screen wiper consisted of 78 measurement grid points.

Robert Bosch researchers applied this open loop tracking system to rotating fans. What differentiated this from other rotating target TLDV systems, was that the shape and orientation of the blades were irrelevant, since the teaching phase allowed enough control points from which all the actual measurement points could be interpolated. This testing method allowed arbitrary measurement grids to be measured at a maximum of 2500 RPM (Bendel 2004).

### 2.6.6 Contributions by Polytec GmbH

Polytec, a global player in the commercial laser vibrometry sector, have developed numerous optical metrology instruments. Their latest and most advanced product regarding three dimensional laser vibrometry, the PSV-400-3D was released in 2005, and is shown in Figure 2-29. This system contained three individual heads with scanning capability, allowing all three translational DOF to be extracted from analysis. A very useful add on tool was the geometry scan unit which could be attached onto the master scan head, this used the time of flight principle of light to calculate the distance to targets. The scan unit allowed 3D representation of vibration measurements.



Figure 2-29: PSV-400-3D system, three individual scanning heads.

The manufacturer claimed that the system was capable of recording measurements from targets between 0.4 to 100 m away. The laser beams were class 2 eye-safe operating at 633 nm (visible red light). The standard specification system could measure target velocity in the range 0.001 to 1  $\text{ms}^{-1}$  using an analogue decoder. The system used an intuitive software package for operation and visualisation purposes. Main drawbacks of the system included the fidelity and time required to calibrate the system and the retail price of £250k.

### 2.6.7 Laser based scanning and tracking systems.

This section provides an analysis of techniques which do not utilise laser vibrometry, however it was thought that the scanning and tracking techniques reported might be encapsulated into a LDV system.



## Laser based tracking and spin measurement

A laser system designed to track the motion of human gestures offered a novel tracking mechanism (Cassinelli *et al.* 2005). The system consisted of x and y-mirrors that shifted the laser beam in a circular pattern (driven by a 1:1 ratio of sine to cosine waves for driver input) towards a target. A photodiode was used to detect whether the laser beam struck the target, a binary result was achieved (1 = target struck, 0 = target missed). The circular pattern emitted consisted of a finite number of points. Once the circular scan had completed one full revolution the measured data was analysed to see whether the circular pattern needed to be translated in order to track the target, a schematic of this tracking protocol is shown in Figure 2-30.

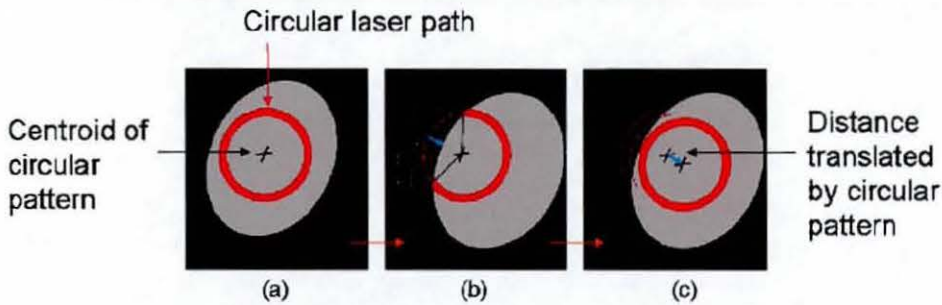


**Figure 2-30: Laser tracking protocol, (a) stationary target, (b) target moves, (c) laser pattern shifted to track target, adapted from (Cassinelli *et al.* 2005)**

The system was developed to allow a user with a natural non-contact approach of interacting with a computer or portable device (Perrin *et al.* 2003 & 2004). The system was stated to track target movements up to  $3 \text{ ms}^{-1}$ .

Laser based work has been undertaken for space applications where the 3D position and orientation of different structures and components was crucial (Blais *et al.* 2000 & 2001). Standard camera based approaches have encountered many difficulties due to the varying lighting conditions encountered in space. Laser based detection methods are not sensitive to noise from ambient light, therefore a laser scanning and tracking strategy has been initiated in order to measure target markers. The system developed consists of two high speed galvanometers that direct a laser beam in a lissajous pattern, as shown in Figure 2-31. A photo-avalanche diode based laser range finder was used to measure distance to target and an intensity measure of the laser beam at the target was recorded 256 times per each individual lissajous' pattern in

order to see whether the laser beam had struck the target or not, similar in approach to the human gesture recognition system.

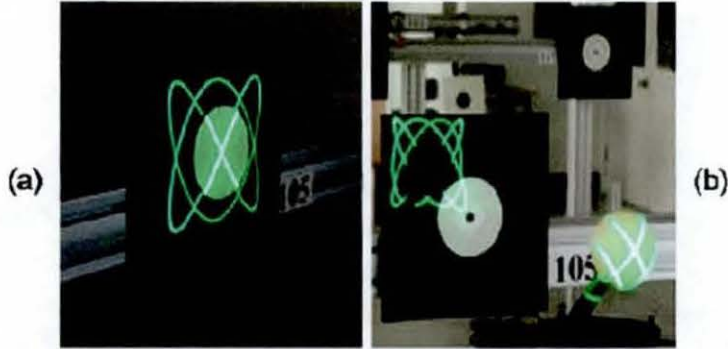


**Figure 2-31: (a) Lissajous pattern on flat target with 3:2 lissajous ratio, (b) lissajous pattern on sphere with 4:3 lissajous ratio (Blais *et al.* 2001b)**

Within robotics applications it is often important that the manipulator tool used has been accurately positioned and orientated in three dimensional space. Therefore laser interferometric based tracking has been researched (Shirinzadeh 1998). The highlighted system consisted of a laser beam being deflected by x and y-mirrors striking a target with a retroreflective marker. The reflected signal is measured using a lateral effect detector. The detector outputs x and y-axis signals, the x and y-galvanometers are adjusted accordingly in order to track the retroreflective marker. The system reported was able to track target motion at speeds up to  $0.5 \text{ ms}^{-1}$ .

## **2.7 Limitations with laser Doppler vibrometry**

This section aims to highlight limitations with LDV work. A common limitation with all laser work is the inherent phenomenon of speckle, which is reported in detail and its consequent effect on rotational targets, known as pseudo-vibrations. Other limitations such as signal demodulation and surface preparation are briefly explored.

### **2.7.1 Speckle phenomenon**

Since the advent of the laser the inherent speckle phenomenon has been observed. The early laser pioneers described speckle as “remarkable granular or peppery nature not present in ordinary light” (Rigden and Gordon 1962), “pattern of random dark and light spots” (Langmuir 1963) and “the illuminated area has sparkling appearance” (Oliver 1963).

Speckle is formed due to the coherence and monochromaticity of laser light and this explanation was suggested by the early observers of this phenomenon. Speckle occurs due to constructive and destructive interference of dephased yet coherent wavelets of light, resulting from striking an optically rough target, as shown in Figure 2-32. The result is a chaotic distribution in backscattered light at a target consisting of high and low intensities.

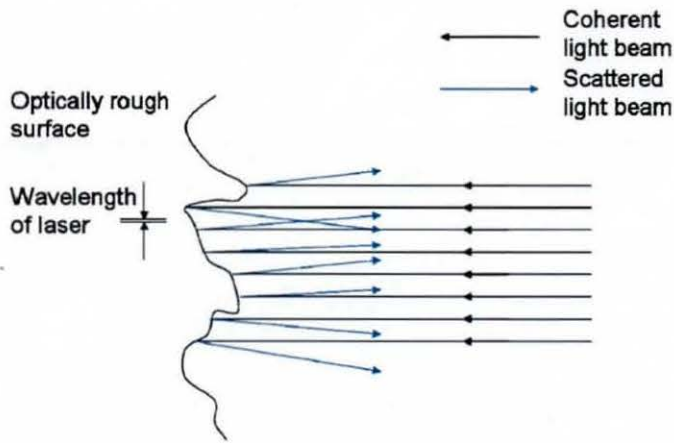


**Figure 2-32: Light striking an optically rough surface.**

Almost all targets of interest are optically rough, they all create a speckle pattern in reflected light. Retroreflective tape has been created with a target smoothness that is comparable with the wavelength of laser light. Due to most lasers consisting of a Gaussian profile laser beam, the backscattered light off a retroreflective target also appears Gaussian in light intensity distribution, as shown in Figure 2-33.

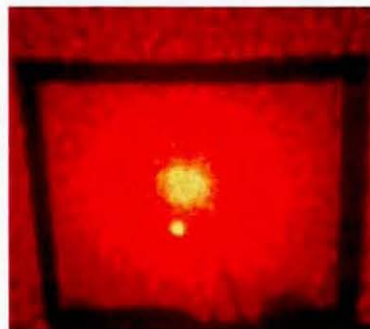


**Figure 2-33: Airy disc appearance of backscattered light from retroreflective target.**

The speckle phenomenon has been researched in depth (Takai *et al.* 1983, Rothberg and Halliwell 1993 & 1994, Rothberg and Halkon 2004) and has been reported to dominate all noise sources with LDV output (Rothberg 2006).

### **2.7.2 Pseudo-vibrations**

Pseudo-vibrations are directly linked to speckle pattern in targets that are tilting, rotating or have in plane motion. The speckle pattern introduces spectral peaks at the rotation frequency of the target and subsequent harmonics, which are hard to decipher from the actual target vibration information. Therefore pseudo-vibrations are generally periodic in nature with identical fundamental frequency as the target normal-to-surface velocity. This effect alone has been the subject of an entire journal paper (Rothberg *et al.* 1989), which concluded that careful interpretation of measurement data is required where genuine vibration data may be indistinguishable from pseudo-vibrations.

### **2.7.3 Noise-floor**

The noise-floor is a crucial parameter in laser measurements. The speckle effect dominates the noise-floor. If a laser is targeted at a static surface, the detector output varies with time in both amplitude and phase, this defines the noise-floor for the specific target. The difference between noise-floor measurement and target velocity measurement is known as the signal to noise ratio (SNR). Often the minimum resolvable signal level above the noise floor is stated as 3 decibels. A significant point to note is the noise-floor of the measurement system is directly dependent upon the measured target since each different target will exhibit a different speckle pattern.

### **2.7.4 Other issues**

The authors in 2.6.3 reported that alignment of the measurement system is important since a pseudo-signal could be induced if the optical measurement axis is not perfectly aligned with spin axis of the target. The target did not need to rotate to induce error in the measured target velocity, if target movement was not purely in the direction of the incident laser beam a reduced target velocity reading was achieved. Work has been carried out to determine SLDV 3D position and orientation with respect to a target coordinate system (Zeng *et al.* 1994). This investigation was able to obtain the relationship between input galvo voltages and the laser angle of incidence at target.

Optical arrangement within the LDV was crucial for measurement purposes. The output laser beam was generally not collimated and therefore had to be focused to targets at a specific stand off distance, in order to obtain maximal SNR. The colour and finish of the target surface was critical since traditionally laser vibrometers have only been used on retroreflective targets. A test carried out on a soccer ball illustrated how the colour, finish and angle of incidence could dramatically influence the SNR of the vibrometer, as shown in Figure 2-34. Within each image the SNR was stated numerically (0 = no signal and 20 = very strong SNR). Figure 2-34 (a) shows the strongest possible SNR when the laser beam struck perpendicular to the yellow ball surface. Figure 2-34 (d) shows no measured signal when the laser struck the black ball surface at an acute angle.

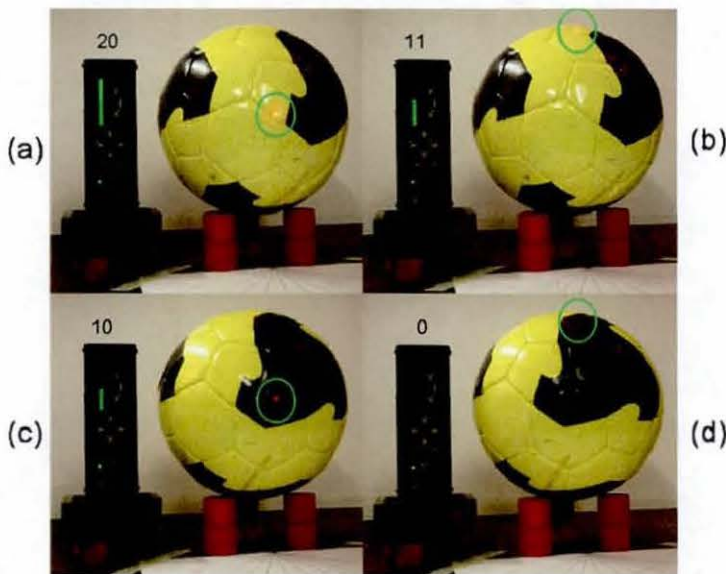


**Figure 2-34: SNR influenced by target colour, finish and angle of incidence**  
 (a) Laser incident perpendicular striking yellow surface – strongest SNR,  
 (b) Laser incident at acute angle striking yellow surface – strong SNR,  
 (c) Laser incident perpendicular striking black surface – strong SNR,  
 (d) Laser incident at acute angle striking black surface – no signal.

The optical system utilised in the LDV led to different noise issues in the measured target velocity. For example noise due to signal demodulation electronics was ever present, phase noise existed due to the bandwidth of the emitted laser beam (it was impossible to have a perfectly single wavelength laser beam) and thermal noise in the

measurement system existed from the detector and preamplifiers. LDV noise limitations were documented in detail by Johansmann *et al.* (2005).

## 2.8 Chapter summary

This chapter provided the reader with a basic understanding of all the main optical tools and techniques explored within this thesis. Optics fundamentals have been explored with particular emphasis regarding laser application. It has been concluded that the laser was deemed a vital tool because of its collimation, coherence and monochromatic characteristics providing the ability to carry out measurements with high resolution in a non-contact approach.

The development of LDA to LDV was reported where fluid flow measurements were extended to solid body target velocity measurements. Equation 2-8 highlighted the simplicity in measured Doppler shift in the direction of the incident laser beam, showing linear proportionality between measured Doppler shift and target velocity. In order to achieve directionality measurement in LDV work, the need for a reference beam that was shifted in frequency is implicit. Research demonstrated many different shifting devices, however the Bragg cell was highlighted as the most stable tool and this was reflected in commercial devices, almost all use this shifting method. Limitations with LDV were reported with particular attention given to the inherent property of speckle.

This chapter highlighted that translational DOF measurements could be isolated by utilising a single beam vibrometer. In order to isolate rotational DOF measurements, a multiple beam vibrometer arrangement must be utilised. The most useful rotational DOF device investigated was based on the torsional vibrometer technique, developed by Halliwell (1984), the flagship product being the Polytec 4000 series rotational vibrometer.

Multiple scanning and tracking LDV techniques were explored and they predominantly rely on two galvanometers to achieve the deflection in the incident laser beam. Non-vibrometry based scanning and tracking applications which utilise these x and y-mirrors to great effect were also reported.

## **3 Literature review: Sports engineering**

### **3.1 Chapter overview**

In order to develop a tracking and/or spin measurement system it is essential to know the likely launch parameters for the ball in question, these are reported for the chosen mainstream sports. Additionally these sports are introduced with specific reference to their respective governing bodies (GBs), and the rules they have specified for the fundamental implement, the ball.

Original equipment manufacturers (OEMs), GBs, athletes/coaches and the spectators/media all have varying interests in ball launch and flight characteristics measurement, these differing interests are reported in detail.

The core component of this chapter provides a review of reported methods and systems used for ball launch and flight measurement. Special attention is given to spin measurement. Techniques dating back to ancient Egypt through to modern day industrial applications are reported. Particular focus is given to spin measurement techniques with sport engineering application. At the close of this chapter a case study of Srixon, a global Japanese based golf brand, is carried out. The techniques employed to test and develop their equipment in a purpose built testing facility are identified.

### **3.2 Sports ball specifications**

The sports highlighted in this section have been selected to give a broad overview of the different balls commonly used in sport around the world. The different shape, size, weight, pressure, materials and construction of the balls, has been found to influence the launch and flight parameters of the ball. By combining knowledge of the specifications which have been laid down by the respective GBs, and knowing how

the sport balls are struck, a general picture of the launch and flight parameters could be established.

### **3.2.1 American football and rugby**

Professional American football is governed by the National Football League (NFL). Other governing bodies such as the National Collegiate Athletic Association and the Canadian Football League also exist, whose rules are similar to the NFL. The NFL rules regarding the football are specified as follows (NFL 2006):-

- Short circumference 527 to 540 mm.
- Long circumference 705 to 724 mm.
- Mass 397 to 425 grams.
- Pressure 89.6 kPa.
- Number of lace holes is 16.

A rugby ball is similar to an American football and the rules regarding the ball are specified by the International Rugby Board (IRB 2006):-

- The ball must be oval and made of four panels.
- Total length between 280 to 300 mm.
- Long circumference 740 to 770 mm.
- Short circumference 580 to 620 mm.
- Outer material must be leather or suitable synthetic material. This can be treated in order to be water resistant and easier to grip.
- Mass 410 to 460 grams.
- Air pressure at the start of play 65.5 to 68.9 kPa.

### **3.2.2 Baseball**

Many variations of this game exist around the globe; however Major League Baseball (MLB) is the professional baseball league in the United States, and is the richest



baseball league in the world. MLB specifies the following guidelines for the ball (MLB 2006):-

- The ball must be spherical and formed by a yarn around a small core of cork, rubber or similar material.
- The ball must be covered with two stripes of white horsehide or cowhide, tightly stitched together.
- Mass 149 to 262 grams.
- Circumference 22.9 to 23.5 cm.

Traditionally the two outer layers of leather are stitched together using red cotton thread using exactly 108 stitches and resemble an hour glass profile.

### **3.2.3 Golf**

Golf is governed by two bodies; (1) the Royal and Ancient Golf Club of St Andrews (R&A) who govern the sport worldwide, and (2) the United States Golf Association (USGA) who govern in the United States and Mexico. The golf authorities provide considerably more complex and numerous rules pertaining to equipment than the majority of other ball sports, and due to recent developments in material and manufacturing technology, they have set more stringent rules stating a maximum velocity and distance which the ball can travel through a standard test set-up (USGA 2006):-

- Mass less than 45.9 grams.
- Diameter more than 42.7 mm.
- The ball must possess spherical symmetry.
- Initial launch velocity must not exceed  $76.2 \text{ ms}^{-1}$ , with a 2% tolerance.
- Travel distance of ball must be less than 290 metres (317 yards), with a 2.7 metre (3 yard) tolerance.

### 3.2.4 Soccer

The worldwide governing body for soccer is the Fédération Internationale de Football Association (FIFA). Whilst the specifications for the ball is universally applicable in senior competitive soccer, two standards exist to identify “approved” balls – that satisfy the various criteria within tighter acceptable limits than “inspected” balls which satisfy less stringent requirements (FIFA 1996). The standards have been introduced to guarantee quality of the purchased soccer balls. Although the “approved” or “inspected” logo is generally displayed on the panels of conforming balls, it is ultimately the referee who must ensure that the soccer ball conforms to the following prior to kick off (FIFA 2006):-

- Mass 410 to 450 grams.
- Circumference 68.5 to 69.5 cm.
- The ball must be spherical.
- The ball must be made from leather or a suitable synthetic material.
- Air pressure at the start of play 8.2 to 14.6 kPa.

### 3.2.5 Tennis and table tennis

The International Tennis Federation (ITF) is the global governing body for tennis. ITF specifies the following rules regarding the ball (ITF 2006):-

- Outer surface to be uniform consisting of a fabric cover.
- White or yellow in colour, and seams to be stitchless.
- Mass 56 to 59.4 grams.
- Diameter 6.4 to 6.7 cm.

Depending on the playing surface there are permitted variations in rebound and deformation criteria for the ball.

The International Table Tennis Federation (ITTF) is the governing body for table tennis worldwide. Clear and strict regulations exist for the table tennis ball (ITTF 2003):-

- The ball must be spherical.
- Mass 2.7 grams.
- The ball must be 40 mm in diameter.
- Manufactured from celluloid or similar plastic.
- Ball must be white or orange in colour, and be matt.

### **3.3 Reported launch parameters**

Whilst the majority of ball specifications relate to static measurements, the dynamic characteristics of a particular ball are dependent upon a multitude of factors. For the purposes of this thesis research, it is not necessary to have detailed knowledge of these factors, however it is meaningful to appreciate general match play and maximum reported launch characteristics.

#### **3.3.1 American football and rugby**

American football has seen considerable research, dating back to Macmillan (1975) who reported average launch velocity of  $20 \text{ ms}^{-1}$  for a thrown football. This was subsequently confirmed by Watts and Moore (2003). The spin rate was first reported in the 1980s, with an average spin rate measured to be 600 RPM (Brancazio 1985). Brancazio also investigated the ideal launch angle for throwing the ball, and gave a range from  $40$  to  $60^\circ$  dependent on whether the player wanted to optimise flight for distance, or 'hang time'. A more recent study investigated 'college level' players at a reputable American college and reported a maximum spin rate for a quarter backs throw as 681 RPM (Holmes 2008).

The rugby ball has been specified to be generally slightly heavier and larger than the American football, however the techniques employed to throw the ball were found to be very different. Holmes (2008) reported an average spin rate of 426 RPM with a maximum spin rate of 554 RPM for thrown passes by elite players.

### 3.3.2 Baseball

Research in baseball dates back to 1959, where wind tunnel work was carried out on the ball. The tunnel was operated at a maximum velocity of  $45.7 \text{ ms}^{-1}$ , considered necessary to replicate maximal pitch speeds in baseball. The maximum ball spin rate was reported at 1800 RPM (Briggs 1959). These values have been confirmed by many researchers since, stating  $45 \text{ ms}^{-1}$  as maximum launch speed by the pitcher (Alaways and Hubbard 2001, Frohlich 1983) and stating 1800 RPM as a maximum spin rate (Mehta 1985).

A unique phenomena known as a 'knuckle ball' has been observed to cause peculiar characteristics of a baseball in flight. This phenomena was analysed in depth by Watts and Sawyer (1975). A knuckle ball involved the pitcher placing minimal spin on to the ball, almost none, which if executed properly resulted in the ball changing direction sharply in flight, consequently it was more difficult for the batter to predict the incoming flight path of the ball. A similar flight path taken by a soccer ball has recently been documented by Dart (2007). He observed free kicks taken by the Manchester United winger, Cristiano Ronaldo.

### 3.3.3 Golf

Cochran and Stobbs (1968) were the first to report launch velocities in golf stating a maximum velocity of  $61 \text{ ms}^{-1}$  for a professional hitting a driver shot. Wedge shots were reported with launch angle ranging from  $27$  to  $33^\circ$  with spin measurement from 7000 to 11000 RPM. Due to the action between the club and ball on impact, backspin is the predominant component of spin.

A comprehensive report on golf was carried out by Bearman and Harvey (1976) who used a wind tunnel to observe differences in lift and drag coefficients. From player testing, they reported driver shots with spin rates varying from 2000 to 4000 RPM, with a professional hitting the ball at an average spin rate of 3450 RPM, launch angle of  $6.1^\circ$  and a velocity at  $68.1 \text{ ms}^{-1}$ .

More recently it has been found that hitting a driver with 2800 to 3000 RPM and a launch angle from  $12$  to  $14^\circ$ , optimised ball flight distance. (Aldrich 2003). A similar

study by Smits and Ogg (2004) found maximum driver spin rates in the region 2000 to 3000 RPM, with a maximum ball velocity of  $79.2 \text{ ms}^{-1}$ .

In Japan a maximum launch velocity of  $80 \text{ ms}^{-1}$  was measured using a driver, and a maximum spin rate value of 10 000 RPM was reported, using a wedge shot. Where a golf robot was used, different launch conditions were reported to maximise either carry, or total distance travelled by the ball (Naruo and Mizota 2004).

The reported launch parameters through the years showed a clear trend in rising ball velocities. This was assumed to be due to a combination of two main factors; the advances in golf club/ball design, manufacture and materials, and the physiological strength gains amongst the professional players.

#### **3.3.4 Soccer**

The first recorded measurement of maximal velocity in soccer was stated as  $29.1 \text{ ms}^{-1}$  by Plagenhoef (1971), and all maximal reported velocities since have given similar values,  $32 \text{ ms}^{-1}$  (Carre 2004) and  $33.8 \text{ ms}^{-1}$  (Neilson *et al.* 2004a).

Analysis carried out at LU observed the free kick of a professional player, considered to be one of the best free kick takers in the world. The spin analysis carried out by Ireson (2001) concluded the soccer ball spin rate to be approximately 600 RPM. A soccer free kick generally involved striking the ball over or around the 'wall', and then ideally spinning away from the keeper, into the goal. The ball therefore had compound spin placed on it, and the spin axis was dependent upon the situation faced by the free kick taker. Further research at LU has predicted that the maximum spin rate possible within the game of soccer would be circa 1300 RPM, when a ball was struck at  $31.1 \text{ ms}^{-1}$  against a rounded cross-bar, with an offset between the respective centres, causing a non-normal rebound. This scenario was simulated using finite element analysis (FEA) and verified experimentally (Price 2005).

#### **3.3.5 Tennis and table tennis**

An extensive study was carried out at the US open in 1997, spin rates and velocities of tennis balls were analysed (Pallis 1998). Within tennis there is a very clear distinction

between the men's and women's game so these were analysed separately. Male forehand spin rates were measured to range from 833 to 3751 RPM whilst backhand spin rates ranged from 833 to 3333 RPM. Spin rates measured for professional women were slightly less, 600 to 3488 RPM for the forehand and 317 to 2413 RPM for the backhand. These numbers highlighted how the human body was able to generate different spin rates on the ball depending on the power and technique of the particular shot. Maximum ball velocity for the men was measured at  $56.4 \text{ ms}^{-1}$  and for women at  $42.2 \text{ ms}^{-1}$ .

For the spectator, table tennis arguably exhibits the most observable spin of any ball sport. Huge amounts of swerve, topspin or backspin are generated relatively easily, even by intermediate players. Tamaki *et al.* (2004) carried out an analysis on the topspin shot and found maximal spin rates for professional players to be approximately 5000 RPM and for beginners, approximately 3000 RPM. These high spin rates were principally a function of the low moments of inertia and low ball mass. These ball properties allow the ball trajectory to be readily influenced by relatively small aerodynamic forces.

### **3.4 Why measure launch and flight characteristics?**

It was important to comprehend the importance of measuring launch and flight characteristics of different sports balls. This section explains the rationale behind the reported investigation into launch and flight characteristics.

Sport ball OEMs must survive in a competitive market. In order to create better sports balls, manufacturers have continually looked into improving ball flight and impact characteristics. Their aim has been to make the ball fly further, quicker or truer whilst impacting more consistently. By providing manufacturers with the tools to measure these parameters, better understanding of launch and flight parameters could be achieved.

Athletes wish to maximise their performance and by measuring the launch and flight characteristics of a shot or kick, they could better understand how to optimise the trajectory of the ball. The ability for a coach to obtain real time or post processed

### Laser based tracking and spin measurement

objective feedback through such measurement, would permit the implementation of new coaching tips or strategies.

GBs are charged with running and regulating all aspects of their particular sport. By measuring launch and flight conditions they could set strict guidelines to limit performance. In golf the coefficient of restitution (COR) of the ball has been capped by the worldwide governing body. This was a preventative step in order to maintain the competitiveness of the sport, keeping the interest of the media and spectators, in the hope of attracting more money to the game. The ITTF made rule changes in 2000 in order to make the sport more appealing for television audiences, the ball diameter was changed from 38 to 40 mm in order to reduce the ball velocity through air, due to an increased drag force.

Spectators and media are interested in statistics of all games. Analysis is carried out in order to comprehend why one athlete or team is better than the other, and where the weaknesses and strengths of the athlete and team lie. By measuring and displaying launch and flight statistics to the spectators and media, interested parties are able to comprehend more about the sport they are following. For example at Wimbledon, a Doppler radar is used which measures the velocity of the ball being served. In golf, a system called Trackman (see 3.5.6) allows the television broadcasters to show comparison of spin rates, launch velocity and flight trajectories of players, during live tournaments, as shown in Figure 3-1.



Figure 3-1: Trackman data viewed on television, comparison of player's shots, adapted from (Trackman 2006).

### 3.5 Technologies for measuring sports balls

#### 3.5.1 Introduction

The measurement of the velocity and launch angle of a sports ball with moderate accuracy has been reported to be relatively straightforward. Therefore the measurement of spin rate is now given focus.

#### 3.5.2 General spin measurement

In modern day engineering, numerous methods have been developed for measuring spin rates of sports balls. The variety of methods and techniques available is a reflection of the varied needs and wide range of challenges faced by those concerned with the measurement of spin in sport. The differences in ball dimensions, orientation, velocity, spin rates and other launch conditions mean that it has not been possible to standardise measurement techniques.

Physical spin measurement devices date as far back as the ancient Egyptians, who used giant obelisks to measure the rotation of earth around its axis, in relation to the sun. These obelisks were developed into much smaller constructions, called the sun dial, which performed exactly the same task, whereby the time of day was measured using the shadow cast by the sun.



## Laser based tracking and spin measurement

In modern day engineering many different applications exist for spin measurement. Most engineering measurements involve the measurement of a rotating shaft, a very common application is the measurement of automotive engine crankshaft spin rate.

Traditionally, the spin rate of an engine motor on a test bed would have been measured using a shaft encoder whereby the crank shaft to angle resolution was  $1^\circ$  or  $0.1^\circ$  (Garner 2006). These shaft encoders were generally based on digital measurements where infrared emitters and detectors were used. This technique relied on counting pulse trains over a defined time period. Two main alternatives existed for this type of measurement, firstly an optoelectronic sensor component which emitted diode light that was reflected back to the sensor from a reflective target, and secondly a similar optoelectronic sensor component that emitted diode light which was interrupted by a target. Both of these techniques outputted a pulse train in a given time frame, which was elementary to convert into a spin rate value.

Two standard set-ups existed for measuring spin rate of car engines, during conventional driving conditions. The first set-up relied on the engine fly wheel having 'teeth', since these teeth were metallic, the Hall effect was used to generate a pulse train, relying on the magnetic properties of metal, therefore each time a tooth passed a magnetic encoder a pulse was outputted. The second set-up relied on an optical probe, whereby the number of pulses achieved per revolution was fixed. Using either method a pulse train was outputted, again these pulse trains were straightforward to convert into spin rate values.

The optical set-up detailed for engine spin rate measurements was commonly referred to as a tachometer. Tachometers have been utilised in many different applications such as blood flow, audio recording and as described in automotive measurement. Commonly a reflective marker was placed on the target shaft so that the laser light directed at the shaft would be reflected by the marker to provide a pulse that was recorded. A wide number of different manufacturers of laser tachometers were found, the spin rate range they were capable of measuring was dependent on the

manufacturer and model, as a rough guide the measurement range was vast, ranging from 6 to 99000 RPM.

The rotational vibrometer was developed to utilise the properties of laser light to measure target rotation spin rate repeatedly and accurately. This has previously been outlined in detail in section 2.5.2.

In lathes, milling machines and other workshop equipment, it could be decisive to cut at the correct spin rate (Rapp 2004). It was therefore important that the operational spin rate was known accurately. Often the lathes were calibrated using simple discs, shown in Figure 3-2. These discs were fixed rigidly to the end of the lathe shaft, utilising strobe lighting at a known frequency, certain discs would appear stationary if the lathe shaft was spinning at identical frequency to the strobe lighting. By fixing different discs onto the shaft, discrete spin rates of the shaft could be calibrated. Generally DC motors with a linear relationship between input voltage and spin rate were used meaning that the calibration procedure only needed to occur at a few values, before other spin rates could be extrapolated.

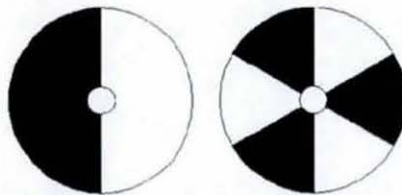


**Figure 3-2: Calibration disc used for spin rate measurement.**

Commonly the stroboscope has been used as a stand alone system to measure target spin rate (Morales *et al.* 2003). When the frequency at which the light was strobed, was known, and the target appeared stationary, the spin rate of the target could be calculated. The target would however appear stationary not only at its fundamental frequency, but also at harmonic multiples thereof.

Some objects with a metallic content could be measured using magnetometers (Acuna 2002), these allow the magnetic field strength and direction of the target to be measured, this has been widely reported for measuring spin rates of planets.

### **3.5.3 Spin measurement in controlled conditions**

Within sports engineering, traditional engineering methods have been adopted to achieve highly accurate measurements of sports ball spin under specific controlled conditions. A number of specialised techniques utilising stroboscopes (Bearman and Harvey 1976, Briggs 1959), a tachometer (Davies 1949) or encoders (Maccoll 1928, Carre *et al.* 2004,) have been developed. Whilst these methods have potential to provide traceable measurements, each requires either the spin axis of the ball to be constrained around a particular axis or the translational velocity of the ball to be zero. For these reasons, the application of these methods has largely been limited to laboratory based investigations.

In many situations however it would be desirable for the measurement of sports ball spin to occur in an arbitrary setting or match situation, without prior knowledge of the precise trajectory of the balls flight. Systems for ball launch and flight measurement are examined in the rest of this chapter.

### **3.5.4 High speed video camera measurement**

The HSV camera approach to spin measurement has been increasingly popular amongst researchers and industry. It now represents the single most common approach used to measure sports ball spin (Pallis 1998, Dignall *et al.* 2000, Ashcroft and Stronge 2002, Beasley and Camp 2002, Bao 2003, Goodwill *et al.* 2006, Nathan *et al.* 2006).

Spin measurement using HSV typically uses either CCD or CMOS camera technology to image the ball at different time intervals during its flight. Spin was determined by correlating the rotation of the ball through a given angle measured in a given time frame. The main camera parameters which determined the quality of the measurement were, capture rate in frames per second (FPS), shutter speed, the quality and dimensions of the lens and the resolution of the recorded picture.

By achieving a compromise between cost, complexity and speed, many investigators with access to HSV would utilise simple markings such as circumferential lines,

### Laser based tracking and spin measurement

shown in Figure 3-3, or dots (Gobush 1996&2005, Winfield 2002), as shown in Figure 3-4, to undertake quick and straightforward measurements.



Figure 3-3: Circumferential lines for spin measurement, adapted from (Cotton 2006).



Figure 3-4: Dots for spin measurement, adapted from (Alaways and Hubbard 2001).

For velocity and launch angle measurement, generally the ball centroid was marked and evaluated a number of frames apart. The launch angle was calculated using trigonometry and the velocity was calculated, whereby velocity equals distance divided by time.

The Hawkeye system (Hawkins and Sherry 2001) has been developed as a multi camera monitoring and estimation package, which operates at 120 FPS. The system has been used in cricket, tennis and snooker and is currently being developed for soccer, in an attempt to adjudicate on close decisions involving the ball crossing the

goal line (goal line technology). The system has also been used as an official line judge at the Wimbledon Grand Slam Tennis Championships (Harman 2007).

The system was commissioned to monitor the ball with a minimum of three gen-locked cameras. In each camera frame a search algorithm was carried out to locate the ball of interest, this operation was post processed and for cricket application reported to take approximately 30 seconds. The results were shown in visually aesthetic software, allowing a multitude of different results to be displayed. Powerful interpolation tools were used and 'filtered' ball trajectories were displayed, as shown in Figure 3-5. The manufacturer claimed that ball position in Tennis was located to 3 mm resolution, for line call decisions (Hawkins 2007).

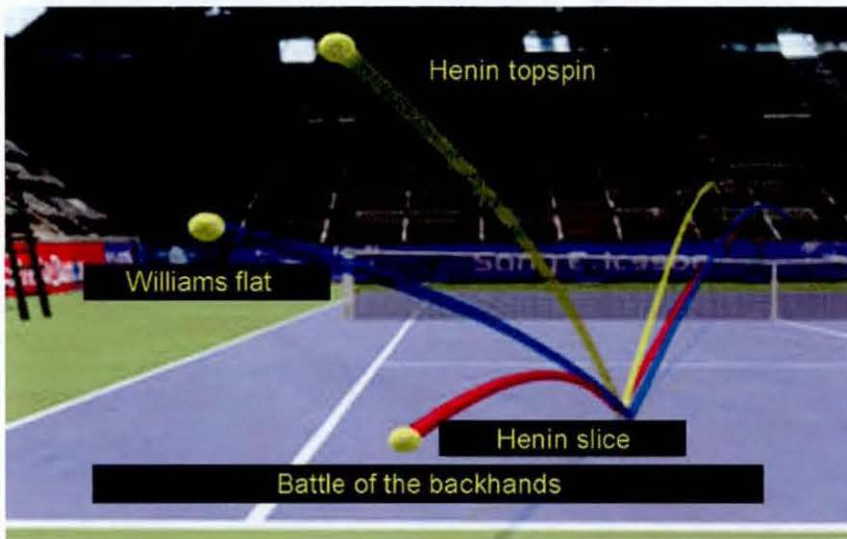
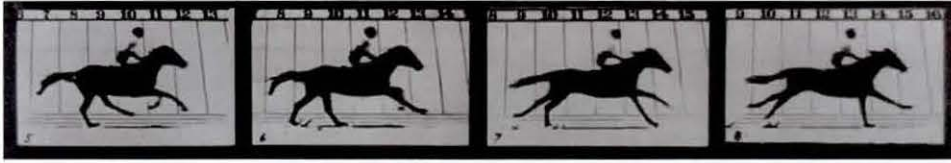


Figure 3-5: The Hawkeye system, Henin v Williams tennis backhand shots analysis (Hawkeye 2008).

The system reported was a monitoring device, without spin measurement capability. The installation cost for football was predicted to be circa £250 000 per ground.

### 3.5.5 Multi and long exposure camera measurement

The long exposure camera precedes HSV camera technology. The first experiments to measure changing or moving objects successfully, were carried out by Muybridge (1883) who was interested in animal movement. He used twelve separate but connected cameras to observe the locomotion of a horse, as shown in Figure 3-6.



**Figure 3-6: Animal locomotion, adapted from (Muybridge 1878).**

Within sports engineering, the long exposure camera technique has been utilised to measure high speed motion of a baseball, and a pitchers hand, during the pitching action (Theobalt *et al.* 2004). This technique required good contrast between the target and background, to permit ‘four digital’ stills cameras to take images of the hand and ball throughout the pitching action. Each camera had a resolution of five million pixels, yet represented a significantly cheaper option than HSV technology. The hand and ball images were recorded using a combination of strobe lighting and long exposure still images. The frequency at which the strobe lights were set, determined how many images of the target were present within one image. A visualisation of the ball and hand motions obtained by the experiment is shown in Figure 3-7.

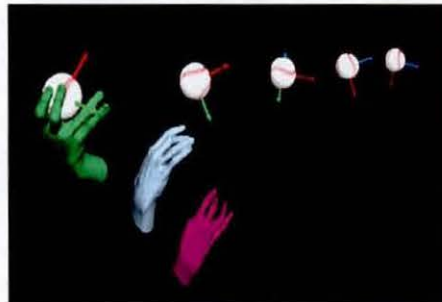


**Figure 3-7: Visualisation of baseball pitch, adapted from (Theobalt *et al.* 2004).**

### **3.5.6 Radar based techniques**

The first reported work using radar technology to measure sport ball spin was carried out by Tavares *et al.* (1998). A 2.54 cm (1 inch) diameter circle of thin metallic reflective tape was fixed onto a golf ball, and a ball launcher was used to fire different golf balls down range. An emitting and receiving radar device, was pointed in the flight path of the golf balls, and measured amplitude versus time. Spikes were measured every revolution, which corresponded to the point in time where the reflective tape was perpendicular to the radar device. Using Fourier analysis the mean

spin rate along with spin decay was extracted. The work reported an exponential decay curve for spin rate in relation to time after launch.

The technique proposed by Tavares *et al.* (1998), only allowed total spin rate to be calculated, therefore the spin axis could not be inferred. Mihran (2001) suggested using infrared radiation where a transmitter, receiver and appropriate demodulation allowed spin rate to be determined using the same principles as Tavares. However in order to decipher spin axis, Mihran suggested three areas of the target to be covered in reflective material, in a 'Z' shaped pattern. By careful analysis of the frequency spikes, the spin axis could be determined. It must be noted that this technique has not been used in any tests or in any commercial products, and the practicality of this technique has yet to be verified.

Currently most golf based OEMs use a system called Trackman (Tuxen 2005) to carry out flight path and launch condition measurements. The Trackman system was manufactured by a Danish company called Interactive Sports Games. The system originated from the military industry, utilising Doppler radar technology, emitting and receiving microwaves at 10.5 GHz, relying on the monopulse principle (Rhodes 1959).

Trackman has been demonstrated to be capable of measuring multiple parameters throughout the golf swing, ball launch and flight path. These parameters included club head speed, ball speed, ball x, y and z coordinates, vertical launch and landing angles and total spin rate. The system was developed to automatically align itself with the ground and was able to continuously measure launch and flight characteristics. Once triggered, the system would capture data, at 2000 Hz during the club swing, at 250 Hz during ball launch and at 55 Hz throughout the remainder of the ball flight. The Trackman system recorded a 'velocity spectrum'. Some of the key specifications are outlined as follows (ISG 2005):-

- Data visualised on the display, less than one second after impact.

### Laser based tracking and spin measurement

- It allowed measurements below  $\pm 13^\circ$  from the centre line (yaw angle), thus measurements achieved at  $\pm 45$  metres from centre line at a 200 metre stand off distance.
- Resolution of impact location at 200 metres to within  $1 \text{ m}^3$ .
- Measured ball flight data up to 350 metres.
- Measured all types of golf shot.
- Measured initial ball speeds from 10 to  $120 \text{ ms}^{-1}$ .
- Operated in temperatures from  $-5$  to  $+45^\circ\text{C}$ .
- The unit was waterproof and would measure data in rain, assuming rain direction was perpendicular to the ground.
- Monitored an individual ball in the driving range even if there were multiple balls in flight.
- Transmits at 10 mW, there was therefore no need for special transmitting licenses.

The spin measurement was dependent upon the measurement of Doppler shift. The system recorded a difference in the Doppler shift across the diameter of the golf ball. Therefore a ball spinning with higher angular velocity, would reflect a signal with a larger frequency shift across the ball, than a ball with slower angular velocity. The manufacturer claimed that generally spin rate was measured to an accuracy of  $\pm 10$  RPM. Without marking the ball, Trackman would generally measure spin rate from 0.1 second to 1 second post impact. The system assumed initially linear spin decay of the ball and related this back to initial launch spin rate. The SNR was the limiting factor in the system for measuring spin without any ball markings. In order to increase SNR of the system the ball was marked over a minimum of four dimples with a conductive metal. This allowed the system to measure the spin up to four seconds post impact, and often throughout the flight path. This increase in SNR by ball marking allowed a much better monitoring capability, due to an increase in the modulation index within the electronics.

Once the Trackman system was active no modifications were required to record successive shots. The initial set-up time for the device was under five minutes. The



## Laser based tracking and spin measurement

user interface was intuitive since it was specifically designed and based for PC software. The device is shown in Figure 3-8.

A number of disadvantages were considered with regards to Trackman. The spin rate measured was a total spin rate, thus axis of rotation was not measured, also the ball had to be marked to measure spin rate over the whole trajectory. The system algorithms were primarily designed for golf therefore to measure other sports balls was difficult, and it was predicted that the method for spin measurement may not be appropriate for non spherical balls.



Figure 3-8: The Trackman system, adapted from (Stachura 2006).

A very similar device to the Trackman system called 'Flightscope' has been developed by EDH of South Africa (Johnson and Foster 2003). This technology was also developed from military based monitoring applications. The technology relied on reflected microwaves being detected by three receivers to triangulate the position of the target in 3D space (identical to Trackman). 'Flightscope' measurement capabilities were similar to those of the Trackman system. However this system of measurement has so far not been widely adopted by golf manufacturers.

## Laser based tracking and spin measurement

EDH has however developed its technology for golf, cricket and tennis ball launch and flight path measurement. This has allowed integration of their products to a larger target market. Within tennis their 'RacquetRadar' product has been very successful and found in use at Wimbledon and other major events, as shown in Figure 3-9. All their products rely on the same fundamental measurement principles.

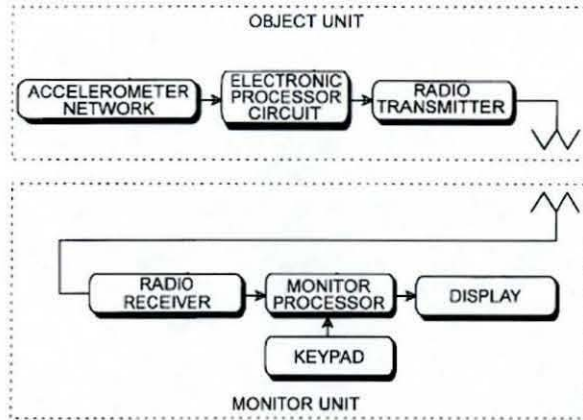


Figure 3-9: Visualisation of the measurements made at the Davis cup by RacquetRadar, adapted from (EDH 2006).

### 3.5.7 Devices in the ball

Embedding devices in to the ball in order to measure position or other parameters during flight has been a relatively recent development. Marinelli (2000) reported an accelerometer network, electronics processor unit and radio transmitter being located within the ball. This was linked to a receiver unit, that could process the transmitted data from the ball, a schematic of this process is shown in Figure 3-10. The principle of utilising an accelerometer network would allow the speed, spin rate and flight path of the ball to be measured.

### Laser based tracking and spin measurement



**Figure 3-10: Schematic of data acquisition and processing (Marinelli 2000).**

In 2003 an actual working prototype for measuring flight dynamics of a football was reported (Nowak 2003). The device consisted of accelerometers, which were able to measure acceleration components in two orthogonal directions, four chips were inserted inside a 'Nerf' American football, as shown in Figure 3-11. The system logged and stored data for ten seconds which was subsequently downloaded and analysed. The system was reported to measure axial and radial accelerations from which the wobble to spin ratio and spin rate of the ball were calculated, the results concurred with existing work by Brancazio (1985).

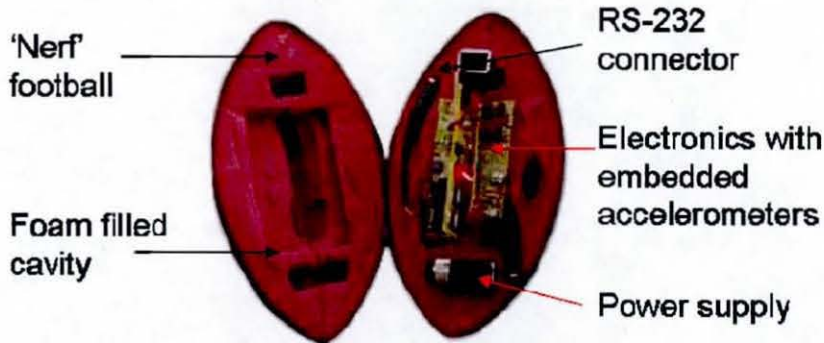


**Figure 3-11: Flight data recorder for a 'Nerf' football, adapted from (Nowak 2003).**

Observing Figure 3-11 it is clear that the electronics inside the 'Nerf' occupied a large percentage of the enclosed volume of the ball, thus likely to change the flight dynamics of the ball. The challenge remains, to implement such technology in a way that does not adversely affect the playing characteristics of the ball.

In 2001 Cairos Technologies AE, a German company reported high resolution methods for locating dynamic targets in 3D space. They published a patent (Hartmut *et al.* 2001) which was designed to monitor a soccer ball in real time using an embedded pulsed microwave transmitter, for use as goal line technology. The transmitter and electronics were located at the centre of the soccer ball and would transmit to a receiver outside the field of play. This technology has been tested in cooperation with adidas at the 2007 World Club Championships, hosted in Japan. Figure 3-12 shows the configuration of the electronics pod inside the Teamgeist II, a FIFA 'approved' match ball. Currently the results from this testing have not been released to the general public.



**Figure 3-12: Teamgeist II match ball (Soccer Ball World 2007).**

The Cairos technology was similar to other position monitoring devices (McReary *et al.* 2005), however three years ago Cairos released a patent (Walter 2005) in which they report technology that was capable of measuring pressure and three axis acceleration of the soccer ball. This technology would allow spin rate measurement and extraction of all the flight parameters of interest, presuming that this did not alter the flight dynamics of the ball, the cost of the system would be the main drawback.

### **3.5.8 Purpose built devices**

An image recognition system called Quinspin has been primarily developed for measuring soccer ball launch characteristics. The system was designed and manufactured by Sports Dynamics, a spin off company out of LU.

The system was initially designed with 32 coloured panels; five different panel colours were used so that the colour relationship between each panel to its neighbouring panels, was unique. It was described as a 'total surface marking scheme'

## Laser based tracking and spin measurement

by its creators (Neilson *et al.* 2004a). A camera allowed the ball to be visualised in 2D and through a genetic algorithm the 3D coordinates of the ball could be deciphered. By acquiring two sequential images of the ball, after launch, separated by a short time interval, the ball velocity, spin rate and launch angle were outputted. This initial system was described by Neilson *et al.* (2004a&b).

This system was modified in order to commercialise the product. The aesthetics of the coloured ball was a hindrance because professional players were not keen to strike and play with the ball. A limitation of the system was, the purpose built ball had to be used. This was not desirable for elite players, ideally they wish to train with the same ball that they play with on match days. The ball was modified, the coloured panels were removed and 50 points - 25 blue and 25 yellow – were marked on the ball in locations such that the distance and angle between each point was unique. The process of calculating the launch velocities remained similar to the original design. Two sequential images were acquired and comparison of the two images yielded the launch velocity, launch angle, spin axis and spin rate. The first image was acquired at a static ball position, the second image acquired shortly (6 ms) after impact.

The image analysis was originally carried out using Image Pro Plus software, the two images acquired were subtracted from each other, leaving disparate objects only, i.e. ideally two images of the soccer ball. Through a mathematical algorithm the two balls were compared against each other to measure spin and if a unique match was found, the value was outputted. The latest Quinspin system carried out a similar image analysis process, however it was run through open source software and programmed in C+, in order to reduce costs. In theory this measurement principle could be transferred to any sport ball measurement.

The final Quinspin system outputted the soccer ball velocity, launch angle, spin rate and spin axis displayed via a PC tablet, a video sequence of the player striking the ball, for the corresponding kick could also be displayed. The system is shown in Figure 3-13.



Figure 3-13: The Quinspin system (Quinspin 2006).

Tamaki *et al.* (2004) have reported a similar type of system to Quinspin for measuring table tennis spin rates. They acquired two sequential images of the ball which allowed the images to be registered with a known 3D model of the ball. The proposed method estimated the parameters of the transformation between the two images with known depth information. Images of the two acquired table tennis balls and the difference between the two images is shown in Figure 3-14. An iterative process was carried out in order to match the first image with the second image in order to estimate the spin rate of the ball. A further investigation would have to be carried out in order to verify that results produced by this measurement system were credible.



Figure 3-14: Difference between two acquired images, adapted from (Tamaki *et al.* 2004)

### 3.5.9 Case study: Srixon, golf science centre

Srixon has been reported as the fourth largest golf ball manufacturer worldwide (Srixon 2008). They inaugurated a dedicated golf testing facility in 1994 (Ihijima, Japan) with the aim of researching and developing advanced technological golf balls and clubs. In 2005 Srixon reported net sales of ¥8.3 billion world wide (Sumitomo 2006).

## Laser based tracking and spin measurement

The following is an in-depth case study to explore how spin measurement, velocity and launch angle are actually measured, how the results are displayed and analysed. The equipment in place at the testing facility are identified as well as the current limitations with the testing protocols. Potential for further research is highlighted.

Laser light gates were used, incorporating laser emitters and photoelectric receivers to measure golf club velocity prior to impact, measured at three locations. The ball velocity was measured using two locations post impact, from these two measurement points the azimuth angle of launch was measured. The vertical launch angle was measured by the ball cutting a laser beam grid at a fixed distance from the tee. These positions are shown in Figure 3-15.

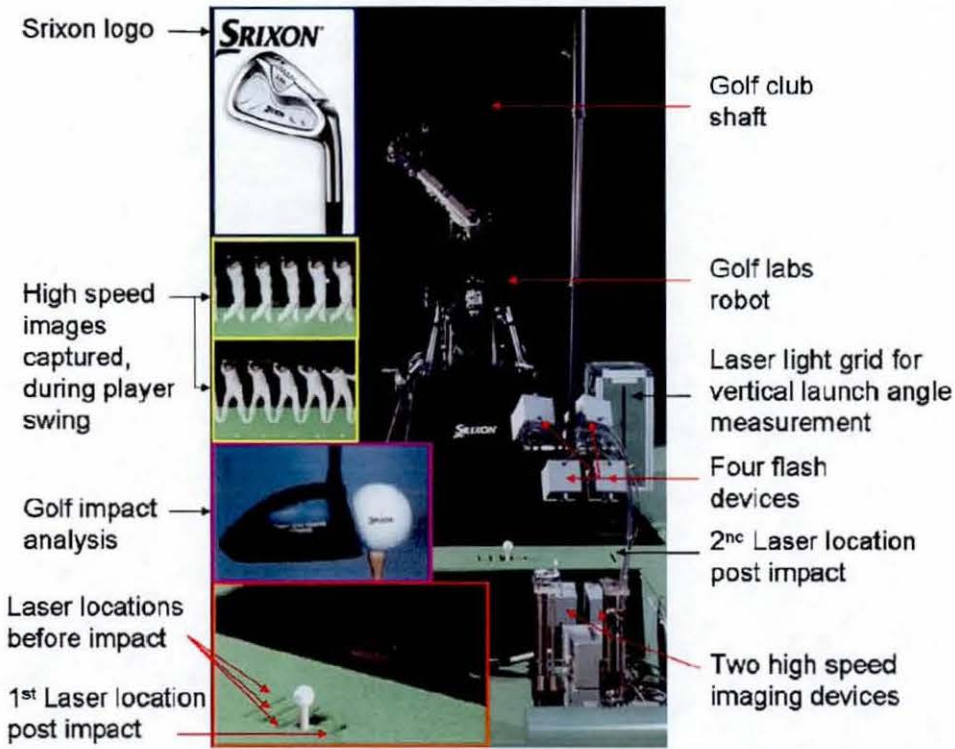


Figure 3-15: Overview of the Srixon golf testing facility, adapted from (Srixon 2003).

Srixon have developed a 3D spin measurement protocol which was thought to be a development of the patent by Gobush (1995). The golf ball was marked with 5 dots, and after impact two consecutive images were acquired by two separate high speed

## Laser based tracking and spin measurement

imaging devices. Each camera acquired an image in synchronisation with two flash lamps in order to achieve an image with high resolution and good contrast. The back spin analysis only required two of the dots to be in the FOV of the acquired images. Srixon claimed to be able to measure backspin with a confidence of  $\pm 50$  RPM. Utilising this system the ball had to be marked and pre-aligned, placed on the tee with the dots facing the cameras, this is a tiresome process and therefore the test engineers stated that they do not measure the spin rate of every shot.

The club face angle (open or shut) immediately prior to impact was determined using two distinct systems. The first system used three laser beam grids located within the hitting mat. The second system used two orthogonally located cameras focused on the tee position, which allowed image analysis techniques to decipher the club face angle.

Striking the ball onto a 274 metre (300 yard) driving range, allowed the flight path of the golf ball to be analysed. A golf ball has mass of approximately 45 grams. Therefore to fully appreciate ball carry and flight path wind conditions had to be accounted for. Srixon had installed five 3D wind velocity measurement systems along the length of the driving range, these reported the direction and strength of the wind conditions in real time. The flight of the ball was also measured using two cameras at opposing ends of the driving range, which performed an area scan to detect and measure the ball in flight. Srixon used two Trackman systems (see 3.5.6) in order to measure ball flight path in addition to other characteristics.

Srixon had two hitting bays from which to carry out their testing; the first was designed for the golf robot testing, as shown in Figure 3-15, and the second was designed for professional and amateur player testing. Each bay had a monitor which displayed the measured impact characteristics almost immediately post strike. The monitors were set-up to display the club head speed, initial golf ball velocity, vertical and azimuth angle of launch, back spin rate and side spin rate.



For player testing, Srixon obtained high speed video images of the player and club, from which the player and coach could qualitatively analyse the player's swing profile, as shown in Figure 3-14.

Other tests which were carried out at the testing facility included force measurements between clubface and ball on impact and additionally sound impact analysis, due to player perception being an influential part of golf club and ball design (Roberts 2002).

Overall Srixon have developed a comprehensive testing facility, however the main drawbacks are the measurement systems are disparate and fixed in place, the spin measurement is a time consuming process and the resolution and accuracy of the spin measurement is questioned.

### **3.6 Chapter summary**

This chapter has introduced the reader to sports ball specifications for mainstream sports enforced by their respective GBs. These specifications helped define commonly reported launch characteristics, particular attention was given to the spin rate measurement.

The importance of measuring launch conditions was emphasised from the viewpoint of the OEMs, GBs, athletes/coaches and media/spectators. It was discernible that all parties would gain valuable information from these measurements.

Highly accurate and traceable measurements for sport ball spin were reported, however these were generally not applicable to arbitrary measurement settings or match situations. Therefore spin measurement techniques which were more flexible to real life scenarios were investigated.

A review of the sports industry was carried out looking at multiple different techniques for measuring launch and flight parameters. The strengths and weaknesses of the investigated systems were outlined. The market leading product at the moment

## Laser based tracking and spin measurement

appeared to be the Trackman system. Systems that rely on placing devices inside the ball seem to be at the prototype stage, with huge potential if cost is kept low, and reliability and function can be proved. The Quinspin system provided a purpose built device for soccer ball measurement, which was the only reported system to calculate the spin axis of the ball.

The Srixon case study highlighted how much time and money OEMs are willing to sacrifice in order to measure launch parameters as accurately as possible. All launch conditions influence the flight of the ball, therefore greater accuracy of launch measurements will yield in a better estimate of ball flight. It is clear that there is no industry standard for sports ball measurement techniques, therefore justification exists for the work in this thesis in order to create a system that would allow extremely precise measurements of ball launch conditions.

## **4 Quantification of typical errors associated with high speed video measurements of sports ball spin**

### **4.1 Chapter overview**

The work reported in this Chapter assessed the accuracy of current ball spin measurements carried out using HSV technology and identified specific errors which may occur and suggested strategies for overcoming these errors.

Deliverables of this Chapter included the design and manufacture of an experimental instrumented 'spin rig' capable of spinning a ball at a known and controlled spin rate that could act as a benchmark for spin rate measurement. A clearly defined testing protocol was devised for spin error analysis and the 'spin rig' was used to output what was assumed to be the absolute value of spin rate. The outlined testing protocol aimed to mimic typical current HSV spin rate measurement methods and highlight likely errors. The testing protocol did not however account for all possible errors associated with HSV spin measurement, and therefore an additional section identified some other common causes for spin measurement error.

An objective of this thesis was to measure sports ball spin using a non-contact and non-marking approach. For the first reported work, a rotational vibrometer was employed in order to achieve this. The feasibility of using a laser based approach for sports ball spin measurement in the future was considered and discussed.

### **4.2 Test equipment**

#### **4.2.1 Experimental apparatus 'spin rig'**

It was important to identify the specifications for the successful operation of the 'spin rig'. It was essential that the 'spin rig' was designed so that most common sports balls could be attached to the rig. A prerequisite was the balls could be rotated up to realistic match play spin rates. For a soccer ball, the rig was required to rotate up to

600 RPM (Ireson 2001). For a golf ball the rig was required to mimic: (1) driver shots rotating between 2000 and 4000 RPM (Bearman and Harvey 1976) and (2) ideally replicate wedge shots achieving spin rates in the region of 10 000 RPM (Naruo and Mizota 2004). By designing the rig to operate for golf and soccer parameters, it allowed straightforward substitution of other sport balls.

Since the objective of this study was to analyse errors in measured spin rate, it was clear that the 'spin rig' had to provide an intrinsic measure of spin, which was as close to the true value as possible. The rig was instrumented with an encoder disc and electronics to measure and record the position with time, from which spin rate could be derived.

#### 4.2.1.1 Manufactured rig

The 'spin rig' is shown in Figure 4-1, which depicts the set-up for rotating soccer and golf balls.

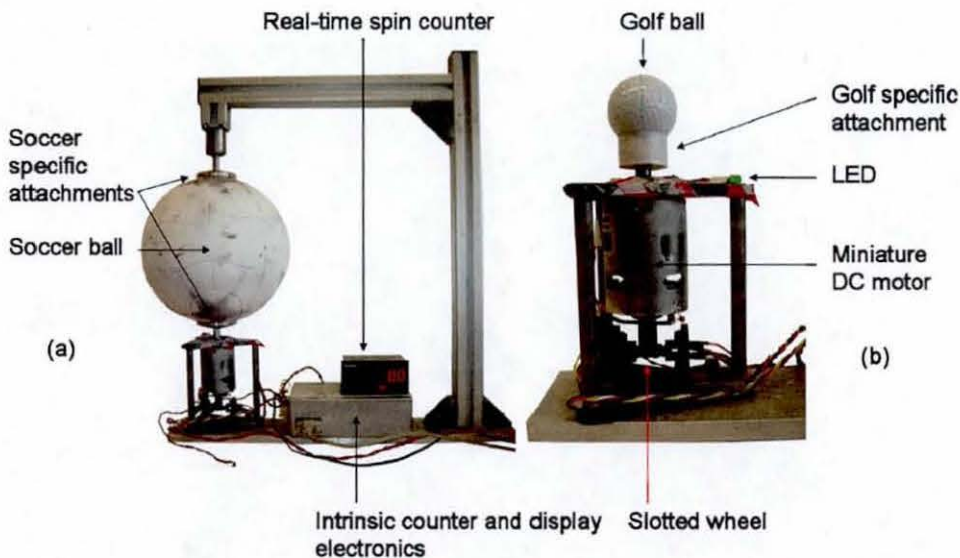


Figure 4-1: 'Spin rig' set-up, (a) for soccer (b) for golf.

For larger balls such as soccer balls, two diametrically opposite attachments were required to fix the ball permanently in position. This was to accommodate the inherent out of balance within soccer balls (Price *et al.* 2003). The attachment from above, was achieved using a single row of free running ball bearings.

The purpose of the 'spin rig' was to rotate the ball at a known spin rate. As shown in Figure 4-1, a miniature DC motor was used to rotate the chosen sports ball. The maximum motor spin rate with no load was specified at 9778 RPM. The rig was operated with a soccer ball at 750 RPM and subsequently a golf ball at 8000 RPM for a prolonged time period. The ability to replicate match specific spin rates for soccer and golf driver spin rates was confirmed. The motor used was extremely cost efficient and ideal for its front and rear shaft attachment. The measurement of spin was provided by a dedicated counting and display circuit, which is detailed below.

#### 4.2.1.2 Dedicated counter and display circuit

The rear shaft of the motor had a purpose built slotted wheel attached; this acted as an interruption between two emitting infrared diodes and Optoschmitt detectors. The buffer logic in the detectors read a high output when the optical path was clear, and a low output when the optical path was interrupted by the slotted wheel. A count input was recorded at 5 MHz by the data logger, whilst being able to detect whether the optical path was clear, or interrupted.

In order to achieve a high resolution measurement of spin rate the optical wheel included one slot, which was 10 mm long, and thirteen slots, which were 5 mm long. Two Optoschmitt detectors were aligned diametrically opposite. The first, detector A, measured only the 10 mm slot every revolution and the second, detector B, measured all slots on the wheel, achieving fourteen data set measurements per revolution. The slotted wheel arrangement is shown in Figure 4-2.

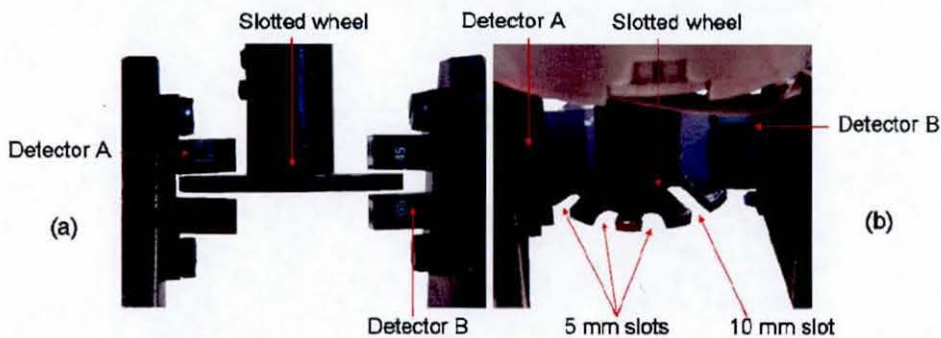


Figure 4-2: Slotted wheel attachment on motor shaft, (a) side view, (b) isometric view.

## Laser based tracking and spin measurement

The set-up allowed a known slot position (10 mm slot) on the disc to be identified from which all measurements were initiated; this was termed the 'index pulse'. For each individual revolution of the disc, the data logger outputted fourteen data sets, with a count number, to signify how long it had taken the disc to rotate between the rising edge of each slot; each count was taken 0.2  $\mu$ s apart. Detector A output was synchronised with an ultra bright light emitting diode (LED) so that in turn the LED was cyclically on/off for one full revolution. This function allowed synchronisation with external devices such as an HSV camera. To initially activate the synchronisation process the LED was on for two full revolutions of the motor shaft.

The data outputted by the dedicated counter and display circuit was transferred directly onto a PC via an RS-232 connector, and stored as a Microsoft Excel file. The software used to trigger the counter was a purpose built program operated in the Windows environment. This allowed direct control over the number of data sets recorded. The calibration for the 'spin rig' was achieved, by having detector A measurement (index pulse) occurring 10  $\mu$ s before detector B pulse measurement. Figure 4-3 displays calibration data for the 'spin rig'. Detector A displays a high measurement reading every revolution. Detector B displays a high measurement reading fourteen times per revolution. The LED pulse is high for the first two revolutions, thereafter cyclically low for a revolution then high for a revolution.

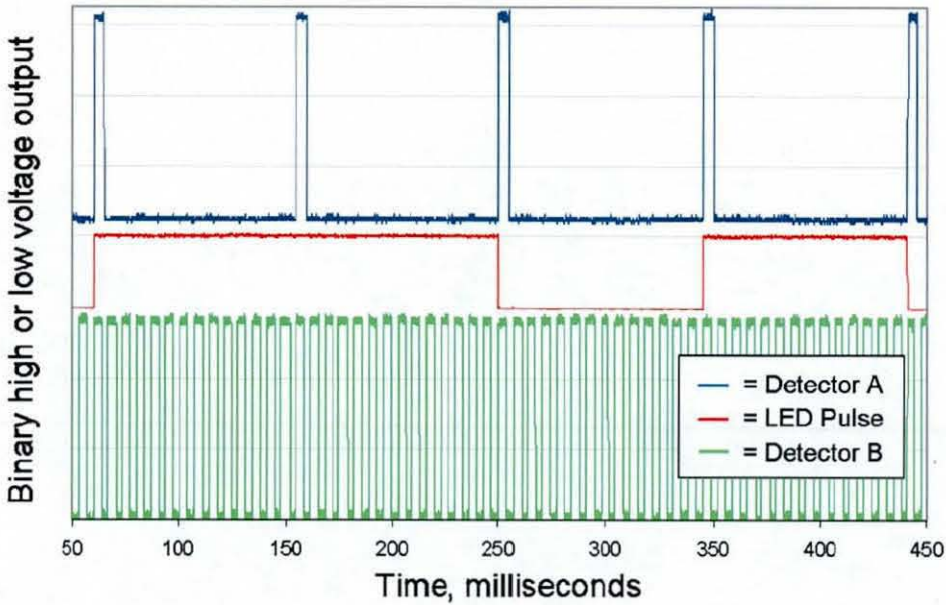


Figure 4-3: Calibration of 'spin rig' hardware, ball rotating at 600 RPM.

#### 4.2.1.3 Real time visual display

The purpose of the 'spin rig' was to rotate the ball at a known spin rate, however the dedicated counter and display circuit did not provide a real time visual display. A Codix 542 counter was linked to detector B, which counted fourteen pulses per revolution. The Codix counter operated at 20 kHz and updated the visual display every millisecond, providing the user with an approximate real time display of spin rate.

Both the Codix counter and dedicated counter and display spin rate values were compared against each other, as well as using an external Dynapar HT50 handheld tachometer to confirm that all devices were outputting the same, assumed to be very close to the true spin rate value. The manufacturer of the tachometer claimed measurement range from 30 to 30000 RPM, with resolution of 0.1 RPM and accuracy of  $\pm 0.01\%$ .

#### 4.2.1.4 Speed control

The 'spin rig' utilised a Como drills miniature DC motor (MFA/Comodrills, UK). This was controlled using a purpose built 12 volt pulse width modulation technique. A control dial allowed a relatively smooth ramp up to desired ball spin rate.

#### **4.2.2 HSV and Flightpath**

The camera used in this investigation was a Photron Fastcam Ultima APX camera with a Nikon 72 mm diameter zoom lens. The camera recorded greyscale images and was capable of operating at 10 000 FPS capturing a FOV with a  $1024 \times 256$  pixel region. The camera allowed several seconds of data to be stored in an on board memory. After measurement the data could be stored as a series of images, or as a video sequence. Due to the quantum efficiency of the camera sensor array, external lighting was required to achieve good quality images with a high shutter speed. Two fan cooled Unomat LX901GZ 1000 Watt halogen bulbs were used to achieve this.

The images captured from the HSV were analysed in software called Flightpath (Sumpter 1993), this program was purpose built for sports ball launch characteristics measurement. This program was considered to be typical of sports ball flight analysis tools.

This investigation involved the analysis of a non-translating, rotating target, therefore an intermediary image processing stage was carried out using ImageJ software (Rasband 2006). ImageJ is a powerful freeware Java based image processing and analysis package.

#### **4.2.3 Rotational vibrometer**

A Polytec 4000 series rotational vibrometer was used to record non-contact spin measurement of the target sport ball. This was believed to be a novel application for the rotational vibrometer. The specific principle behind the rotational vibrometer was reported in 2.5.2. A useful feature of the Polytec rotational vibrometer was that it indicated real time alignment between the spin axis and the incident laser beams. Where the plane of the incident laser beams was perpendicular to the target spin axis, and the spin axis was equidistant between the two laser beams, a green LED was lit.

The green LED displayed that a good quality spin rate measurement was being carried out. This indicated both reflected laser beams were measuring identical magnitude Doppler shifts, achieving a pure rotational velocity measurement. This allowed for a quick and simple confirmation, that alignment between the rotational vibrometer and the target had been achieved.



### **4.3 Testing protocol**

A testing protocol was established with relevance to the HSV measurement work cited in the literature review.

#### **4.3.1 Objective for HSV camera ball spin measurement**

The objective of this work was to investigate current HSV spin measurement techniques and highlight any errors which may arise regarding measurement and reporting of spin rate values. Factors anticipated to introduce errors in HSV spin measurement were, position of the ball in the camera FOV, radial lens distortion, and the angle between the camera axis and the ball spin axis.

In order to achieve the objective two independent measures of spin rate were acquired in addition to the intrinsic encoder and counter, which was assumed to output a true measure of spin rate.

#### **4.3.2 Methodology**

Due to the vast amount of published spin rate literature, the high spin rates achieved, the relatively small, lightweight ball involved, and golf dominating the sport equipment spend in the UK and USA, a golf ball was used as the basis for this investigation. This was because the additional top attachment required for soccer ball rotation, did not permit the HSV camera to be aligned co-axially with the ball spin rotation axis, whilst allowing for useful measurements.

The golf ball was marked with one circumferential line, passing through both poles of the ball. When the ball was viewed directly from above with the spin axis was co-axial with the camera axis the line appeared straight, as shown in Figure 4-4.



Figure 4-4: Plan view, circumferential line marking on golf ball.

The golf ball was rotated at approximately 2000 RPM, consistent with the spin present in a typical driver shot. Simultaneous measurements of spin rate were recorded using the three measurement systems. Each time the measurement systems were triggered, enough data were recorded to analyse ten separate revolutions of the ball.

The 'spin rig' and rotational vibrometer were fixed to provide a continuous measurement of spin rate, the focus of the investigation was to observe the effect of changing the position and orientation of the HSV camera. The basic testing set-up is shown in Figure 4-5.

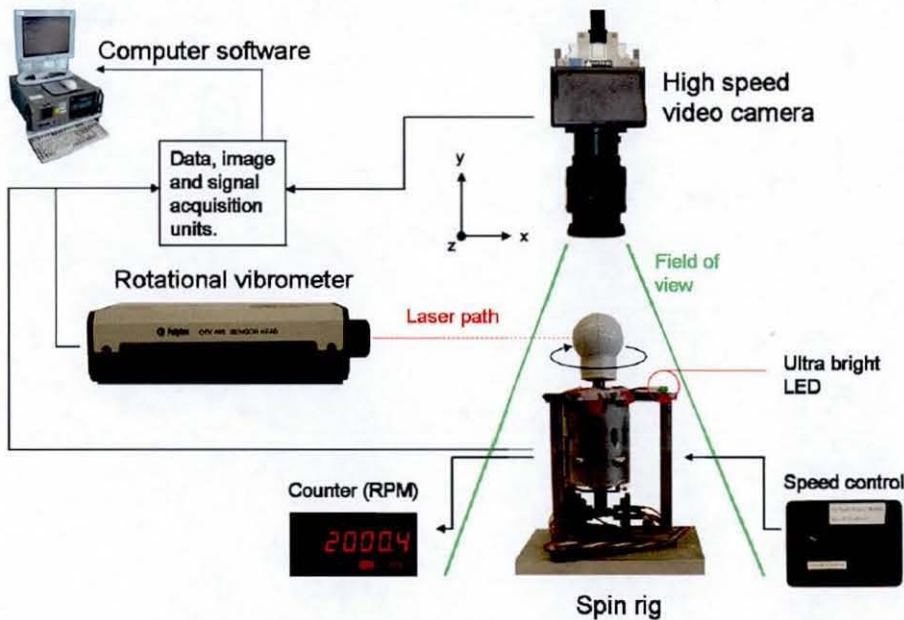


Figure 4-5: Basic testing set-up.

## Laser based tracking and spin measurement

Throughout testing, the Photron HSV camera was positioned  $129 \pm 5$  cm from the golf ball. The HSV camera measurements were synchronised with the dedicated counter and display circuit, by locating the flashing LED in the camera FOV. The video sequences acquired using the HSV camera were imported into ImageJ, and outputted as a golf ball collage image. Each collage consisted of four golf balls, imaged during the course of one revolution, spaced two milliseconds apart, so that consecutive ball positions were not overlaid. The collages were exported into Flightpath to calculate spin rate values. The analysis process involved superimposing a straight line as a chord between the visible ends of the circumferential line marking on the ball, as illustrated in Figure 4-6.



**Figure 4-6: Flightpath analysis of spin rate, using golf ball collage.**

The test was representative of a standard video analysis procedure previously carried out at LU to calculate golf ball spin rate, as shown in Figure 4-7. A Sensicam camera with a long exposure time was used in conjunction with three flashes from a stroboscopic light spaced 2 ms apart, in order to overlay three distinct golf balls in the captured image. This time period correlated to 500 FPS using a HSV camera set-up, thus all HSV testing was carried out at 500 FPS.

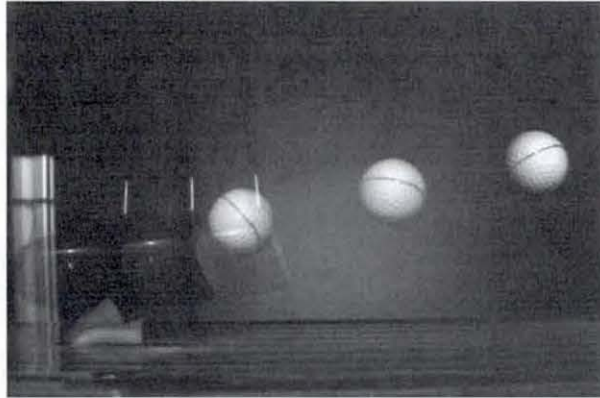


**Figure 4-7: Standard spin analysis technique, LU.**

In order to verify that the relative positions of the HSV camera, and 'spin rig', did not change during the course of each test, a CODA motion analysis system was used to monitor the 3D spatial coordinates of the HSV camera and 'spin rig'. Markers were attached to surfaces of each piece of equipment and the CODA system was used to record their 3D positions throughout the investigation. These 3D positions were used to make sure that the angle between camera axis and ball spin axis was within  $\pm 0.1^\circ$ .

As stated previously, the testing protocol focused on exploring the effect that changing the position and orientation of the HSV camera had on spin rate measurement. Three separate tests were carried out where the basic testing set-up depicted in Figure 4-5 was adjusted, by altering the HSV camera position.

#### **4.3.2.1 Test 1 – Effects of camera orientation**

The angle between the camera axis and golf ball spin axis was adjusted. The camera was rotated around the z-axis and then translated in the x and y-axis in order to maintain the ball in the centre of the camera FOV. A fixed stand off distance was maintained between the camera and the ball so that no perspective distortion was introduced into the measurements. Measurements were recorded at  $0^\circ$ ,  $5^\circ$ ,  $10^\circ$ ,  $15^\circ$  and  $30^\circ$  angles between the spin axis and camera axis (as shown in Figure 4-8) because it was anticipated these would yield differences in spin rate measurements. Forty individual revolutions were analysed at each position.

Laser based tracking and spin measurement

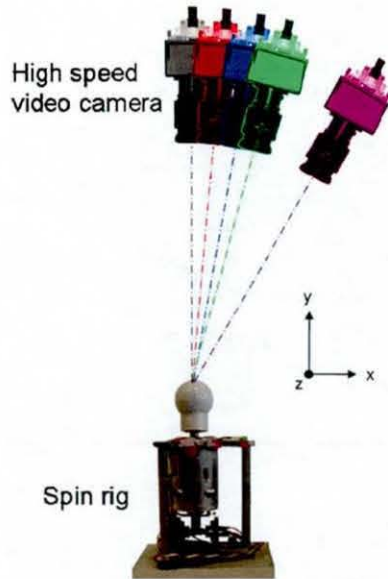


**Figure 4-8: Test 1 HSV camera angles, (black = 0°, red = 5°, blue = 10°, green = 15°, purple = 30°).**

The effect caused by the camera orientation in relation to the ball spin axis was simulated in CAD and shown in Figure 4-9. The camera angle was directly related to the rotation of the camera around the z-axis, as shown in Figure 4-8.

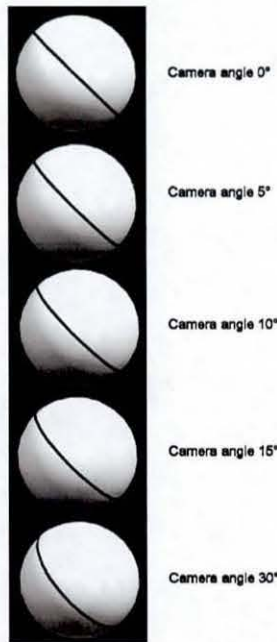


**Figure 4-9: CAD image of golf ball dependent upon the angle of the camera in relation to the ball spin axis.**

#### 4.3.2.2 Test 2 – Effects of radial lens distortion

To establish whether radial lens distortion affected the measured spin rate an arbitrary angle of  $5^\circ$  was maintained between the camera axis and ball spin axis, whilst the ball was displaced within the FOV of the camera. The ball was located at four different positions; position one being in the centre of the FOV through to position four at the very edge of the camera FOV, as shown in Figure 4-10. Ten individual revolutions were analysed at each position.

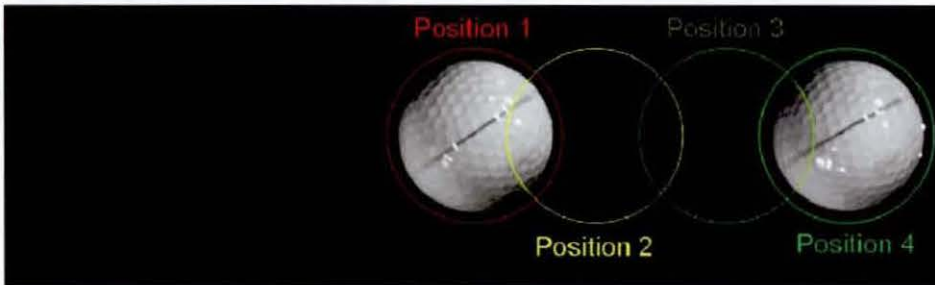


Figure 4-10: Four different golf ball locations in camera FOV (1024 × 256 pixels).

#### 4.3.2.3 Test 3 – Effects of camera orientation and radial lens distortion

In order to establish how the position of the ball within the camera FOV affected measured spin rate the ball position was fixed at the edge of the camera FOV (Test 2, Position 4), whilst the angle between the camera axis and the ball spin axis was adjusted to be  $0^\circ$ ,  $5^\circ$ ,  $10^\circ$ ,  $15^\circ$  and  $30^\circ$ , as shown in Figure 4-8. The camera was displaced in the x and y-axis to maintain a constant stand off distance to the golf ball. Again, ten individual revolutions were analysed at each angle.

#### 4.3.3 Statistical analysis

For brevity, the measurements recorded using the HSV camera and subsequently analysed are referred to as 'Flightpath' results. The measurements recorded from the 'spin rig' counter and display are referred to as 'counter' results, and the rotational vibrometer values are referred to as 'laser' results.

The collated final spin rate measurements were tested for normality (using a 1-sample Kolmogorov-Smirnov test); consequently parametric analyses were applied to all data. A one-way analysis of variance (ANOVA, Wagner 2007) was utilised to

indicate differences between the Flightpath, counter and laser spin rate data sets. Statistically critical values were set at 2 SD (95%) throughout the analysis.

#### 4.4 Results

All measurements were carried out simultaneously and the CODA positional markers were used to ensure the 'spin rig' and HSV camera were stationary ( $\pm 0.5 \times \pm 0.5 \times \pm 0.5$  mm) throughout each test.

##### 4.4.1 Test 1 – Effects of camera orientation

Forty repeated measurements of spin ( $n=40$ ) were taken for each camera angle position and the results plotted in Figure 4-11. The statistical analysis concluded that at all angles there was no significant difference between the laser and counter spin rate measurements. At a camera angle of  $0^\circ$  no significant difference was found between Flightpath and both the laser and counter measurements. However, at all other camera angles tested, a statistically significant difference between Flightpath and both the laser and counter spin rate measurements was found.

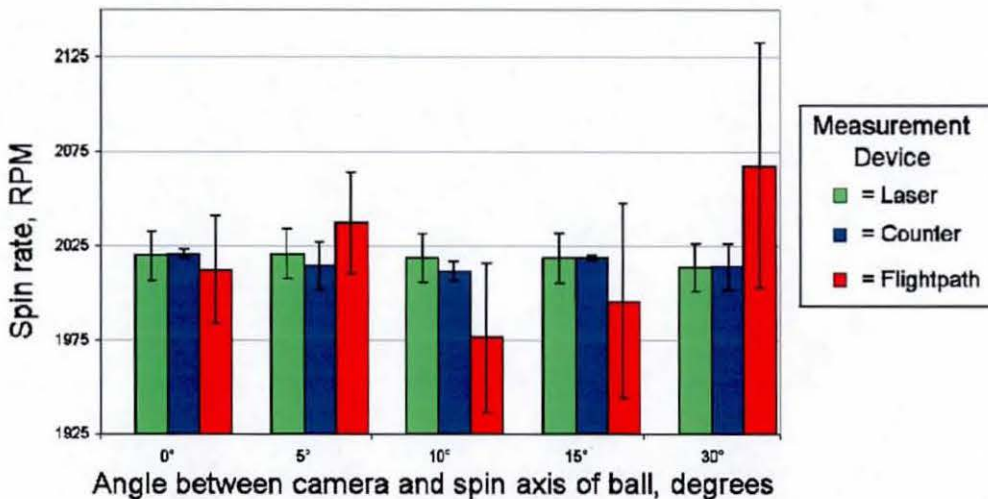


Figure 4-11: Test 1, Average spin rates showing  $\pm 1$  standard deviation.

The counter spin rate repeatability was found to be at best  $\pm 2.3$  RPM and at worst  $\pm 24.8$  RPM at the 95% confidence level. However the Flightpath repeatability was found to be at best  $\pm 54.4$  RPM and at worst  $\pm 129.6$  RPM at the 95% confidence level. The large contrast between the repeatability measures of the counter and

Flightpath demonstrate how much more repeatable the counter value is compared to the Flightpath spin rate value.

**4.4.2 Test 2 – Effects of radial lens distortion**

Ten repeated measurements (n=10) were taken at each of the four camera positions. The sample population was reduced from (n=40) due to experimental and analysis time constraints. The results were plotted in Figure 4-12. No significant differences were found between the laser and counter spin measurements at any position, however significant differences was found between Flightpath and both the laser and counter measurements at all positions.

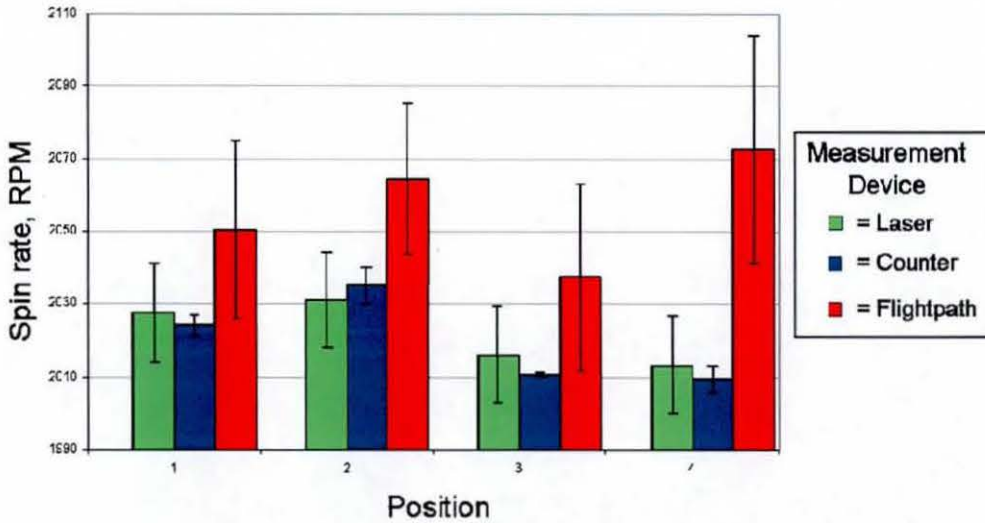


Figure 4-12: Test 2, Average spin rates showing ± 1 standard deviation.

The results in Figure 4-12 demonstrate the repeatability of the spin rate measurements of the three measurement systems. At worst the repeatability of the systems is ± 10 RPM, ± 27 RPM and ± 62.6 RPM at the 95% confidence level for the counter, laser and Flightpath systems respectively. The Flightpath repeatability is again shown to be far greater than for the other two measurement systems.

**4.4.3 Test 3 – Effects of camera orientation and radial lens distortion**

Ten repeated measurements (n=10) were taken for each camera position in test 3 and the results plotted in Figure 4-13. Statistically no significant difference was found between the laser and counter measurements at all positions. No significant difference was found between the Flightpath measurement and both the laser and



counter measurements at the 0° and 5° orientations, significant differences occurred in the remainder of the measurements.

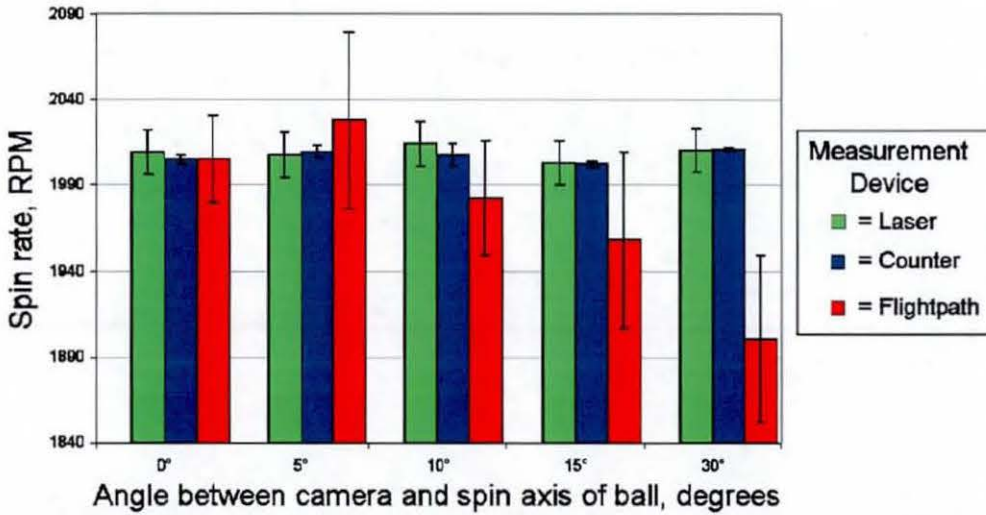


Figure 4-13: Test 3, Average spin rates showing  $\pm 1$  standard deviation.

The results in Figure 4-13 demonstrate the repeatability of the spin rate measurements of the three measurement systems. At worst the repeatability of the systems is  $\pm 13.2$  RPM,  $\pm 26.8$  RPM and  $\pm 103.4$  RPM at the 95% confidence level for the counter, laser and Flightpath systems respectively. The inability of the Flightpath system to provide repeatable and accurate measurements of spin is clearly highlighted.

#### 4.5 Discussion

Statistical analysis of each of the measurements revealed that when the spin axis was perpendicular to the camera axis, the spin rate measured by Flightpath was statistically similar to the counter and laser measurements. This provided confirmation of the capability of HSV to be a useful tool in sports ball spin measurement.

Statistically significant differences were found, however, between Flightpath measurements and laser and counter measurements, when changes were made in the angle of incidence between the camera axis and the ball spin axis and displacement of the ball from the centre of the FOV.

## Laser based tracking and spin measurement

Both tests 1 and 3 highlighted the critical influence of camera alignment, as significant differences, assumed due to errors, were found at all orientations of  $10^\circ$  or more to the spin axis. The most extreme scenario (maximum angle and displacement) resulted in a Flightpath measurement of  $1900 \text{ RPM} \pm 49$  at 1 standard deviation compared to a counter value of  $2011 \text{ RPM} \pm 0.7$  at 1 standard deviation. This represents a spin rate discrepancy of 5.5% and a dramatic increase in standard deviation by a factor of 70. The repeatability of the Flightpath measurements was proven to be poor for all three tests carried out in comparison to the laser and counter results. In the past there has been little or no recognition that change of conditions outlined above, significantly alters sports ball spin rate measurements.

It was interesting to note that there was a slight discrepancy in results with test 1 and 3. Test 1 concluded that when the difference between camera axis and spin axis was  $5^\circ$ , there was a significant difference between the Flightpath and laser/counter spin rate value, however test 3 reported no difference between the measurement systems at a  $5^\circ$  angle between camera axis and ball spin axis. It was thought that this discrepancy was caused by the effects of the radial lens distortion and the  $5^\circ$  angle between camera axis and ball spin axis cancelling each other out in test 3. The greater number of measurements recorded in test 1 ( $n=40$ ), by comparison to test 3 ( $n=10$ ), suggested that the results from test 1 were statistically more reliable.

The effect of imaging the ball away from the centre of the camera FOV in test 2 was shown to introduce errors due to 'radial lens distortion'. This distortion has been well reported in computer vision applications and compensation techniques have been developed to account for the effect (Zhang 1999&2000). However, such compensation methods have not typically been employed in sport ball spin measurement. Recently however Nathan *et al.* (2006) used ten HSV cameras to carry out spin measurement, adapting a very elaborate calibration scheme which was broadly based on the work carried out by Heikkila and Silven (1997). This scheme was used in order to calibrate the cameras and compensate for radial lens distortion, however the reliability of their spin measurement have not been evaluated or reported.

The findings of this study suggested that extreme care should be taken when using HSV based spin measurements. In practical situations, it is extremely likely that the spin of a sports ball would be accompanied by a translational velocity. Therefore for a stationary camera it would be inevitable that the ball would be imaged away from the centre of the FOV in at least one image of a multiple frame capture. To minimise this effect, the camera should be positioned practically as far away from the target as possible. In controlled laboratory investigations, careful pre-alignment of the camera with respect to the anticipated spin axis can minimise errors, however in many game scenarios, neither the trajectory nor the spin axis can be predicted. In these conditions, careful analysis should be carried out to establish appropriate uncertainties with measured spin rates.

No obvious relationship was observed between Flightpath spin measurements discrepancy and change in camera angle or position. It was hypothesised that the Flightpath measurements were dependent on the orientation of the ball at the start of the analysis, which was not controlled. The error introduced was therefore thought to vary in magnitude and direction.

Before conclusions were made based on this investigation, the validity of Flightpath for spin measurement was checked. A CAD image of two golf balls was inputted into Flightpath with known rotation ( $50^\circ$ ) between the balls, as shown in Figure 4-14. The theoretical time interval between the balls was set at 0.004167 seconds, corresponding to a spin rate of 1998.84 RPM. The balls were analysed in Flightpath ten times and a repeated value of 2002.67 RPM was obtained as the spin rate. This represented an error of 0.1% from the known spin rate, which was considered insignificant.

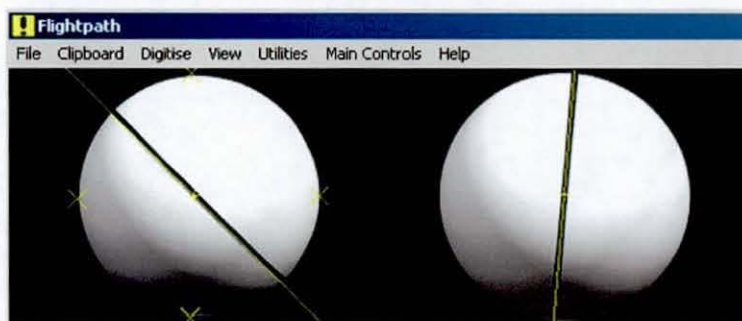


Figure 4-14: Flightpath analysis of CAD golf ball images.

## 4.6 Conclusions

The results of this study have highlighted the difficulties in accurately measuring sports ball spin rates using typical HSV analysis methods.

The ball spin axis relative to the camera FOV and radial lens distortion of the camera lens were found to significantly influence the measurements made using the HSV and Flightpath software. When the ball was positioned centrally within the FOV the HSV method was only found to provide accurate measurements when the spin axis was perpendicular to the camera axis. Due to the nature of sports ball spin measurement it is almost certain that this would not be the case in practice.

Since no significant difference was observed between the rotational vibrometer and the 'spin rig', further investigation to better establish the potential of laser based measurement methods for accurate non-contact spin measurement was justified.

## 4.7 Additional error sources

Given that the experimentation reported here represents a series of closely related set-ups, it is likely that not all possible sources of error were encountered. This section, therefore documents other possible causes of error and uncertainty in HSV camera spin rate measurement.

### 4.7.1 Frame rate of HSV camera

In certain spin rate measurement set-ups it was feasible to measure the ball for one complete revolution and then compute the spin rate. The testing in this investigation was carried out at 2000 RPM meaning that a complete revolution was completed in 30 ms. It was reasonable to estimate that a complete revolution could generally be identifiable to within  $\pm 1$  frame, which at 500 FPS (identical to this study) corresponded to an average uncertainty of  $\pm 134$  RPM in the measured value. Where the spin rate of the ball was increased or the camera frame rate decreased, this uncertainty in measured value would clearly increase accordingly.

Table 4-1 and Table 4-2 show the effect on measured spin rate resolution where one complete revolution was measured to  $\pm 1$  frame in the recorded video sequence, for

## Laser based tracking and spin measurement

soccer ball and golf ball spin rates. The predicted measured spin rate is given as an average uncertainty RPM value.

A clear trend was noticeable; as spin rate increased, the measurement resolution increased at a fixed frame rate. This result was expected, however the large calculated average uncertainties quite clearly show why spin rate measurements often show a large spread of results.

It should be noted however that some of the extremely large predicted average uncertainties would be most unlikely. For example a golf ball spinning at 6000 RPM with a camera working at 250 FPS, would only achieve 2.5 frames per revolution, therefore a worst case error would be to calculate the spin rate from the second or third frame, resulting in a spin measurement resolution of  $\pm 1250$  RPM. The spin measurement analyst would however be able to interpolate a much smaller resolution for the spin rate value. The main point to note from this predicted resolution is that measuring ball spin rates in the region of 6000 RPM is totally impractical using HSV operating at 250 FPS. Table 4-1 and Table 4-2 provide a quick and simple method of choosing an appropriate frame rate if the approximate spin rate of the ball is known.

**Table 4-1: Average uncertainty in soccer ball spin measurement dependant on HSV frame rate.**

HSV camera (FPS)	Soccer ball spin rate (RPM)		
	400	600	800
250	± 10.4 RPM	± 24 RPM	± 41.7 RPM
500	± 5.4 RPM	± 12 RPM	± 20.8 RPM
1000	± 2.7 RPM	± 6 RPM	± 10.7 RPM
2000	± 1.3 RPM	± 3 RPM	± 5.3 RPM
4000	± 0.7 RPM	± 1.5 RPM	± 2.7 RPM
6000	± 0.4 RPM	± 1 RPM	± 1.8 RPM
8000	± 0.3 RPM	± 0.8 RPM	± 1.3 RPM
10000	± 0.3 RPM	± 0.6 RPM	± 1.1 RPM

**Table 4-2: Average uncertainty in golf ball spin measurement dependant on HSV frame rate.**

HSV camera (FPS)	Golf ball spin rate (RPM)		
	2000	4000	6000
250	± 238.1 RPM	± 1000 RPM	± 1875 RPM
500	± 133.9 RPM	± 476.2 RPM	± 1250 RPM
1000	± 66.7 RPM	± 267.9 RPM	± 606.1 RPM
2000	± 33.3 RPM	± 133.5 RPM	± 300.8 RPM
4000	± 16.7 RPM	± 66.7 RPM	± 150 RPM
6000	± 11.1 RPM	± 44.4 RPM	± 100 RPM
8000	± 8.3 RPM	± 33.3 RPM	± 75 RPM
10000	± 6.7 RPM	± 26.7 RPM	± 60 RPM

In order to measure spin rate with small resolution it was recommended that the highest possible frame rate that is feasible is used whilst still being able to capture a good quality image for analysis.

#### **4.7.2 Error associated with dot monitoring spin measurement**

Within the sports engineering literature review section, several methods of monitoring the position of surface dots to measure spin have been cited. This section highlights a major flaw with dot monitoring for spin measurement and suggests that dot monitoring methods are susceptible to error. This section predicts likely underestimation of measured spin rate using dot monitoring methods.

For simplicity a soccer ball with one clearly visible black marker dot was monitored. Generally for spin measurement two images were taken whereby the dot on the ball was aligned with the centre of the ball in two separate images one revolution apart. Often these images were obtained at opposite sides of the camera FOV.

Figure 4-15 shows the general set-up for a dot monitoring methodology, whereby the soccer ball has completed one complete revolution in the camera FOV travelling from point 1 to 3. 1A, 2A and 3A show the soccer ball, viewed from above, travelling from left to right in the camera FOV. 1P, 2P and 3P show the soccer ball viewed from points q, x and t respectively. 1C, 2C and 3C show the image viewed by the camera. The essential point to note is that even though the HSV camera imaged the black dot on the ball in positions 1C and 3C in the centre of the ball, positions 1A and 3A actually show that the ball has completed more than one revolution during this time period.

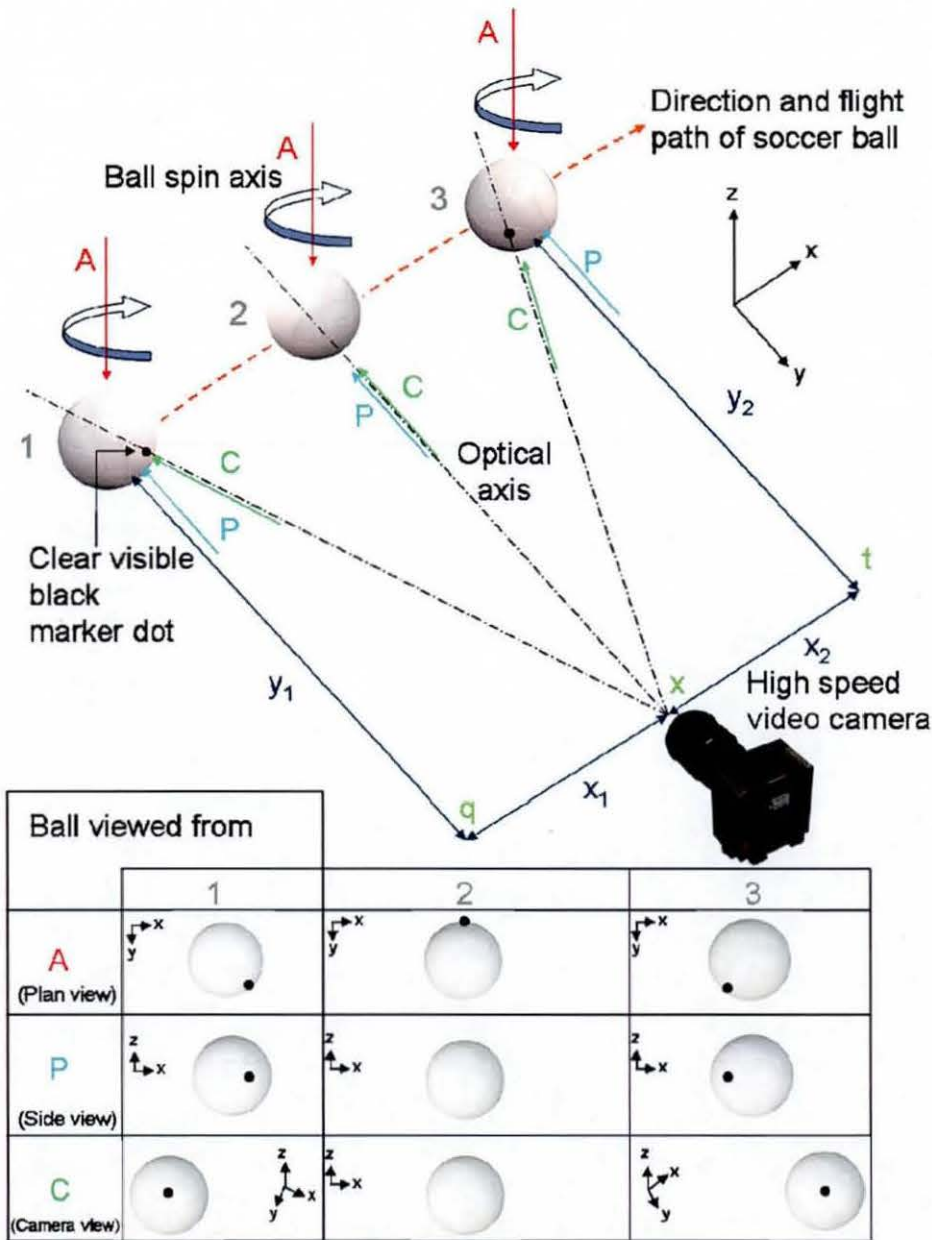


Figure 4-15: Spin measurement using dot monitoring method.

It was clear that the set-up for spin measurement in Figure 4-15 actually underestimated the spin rate of the soccer ball. The amount by which spin would have been underestimated was determined by the distances  $x_1$ ,  $x_2$ ,  $y_1$  and  $y_2$ .



### Laser based tracking and spin measurement

In order to find out how the measured spin rate was affected, several assumptions were made. The ball travelled in a perfect straight line, perpendicular to the camera axis. The stand off distance between camera and ball at 2B was two metres. It was assumed that the ball had rotated half a revolution when it reached point 2B. It was also assumed that the ball rotated at a fixed rate of 600 RPM travelling between point 1 and 3. Table 4-3 shows the calculated spin rates using the spin dot measurement process, for varying distances of  $x_1$  and  $x_2$ .

**Table 4-3: Predicted soccer ball spin rate values, depending on the distance  $x_1$  and  $x_2$ .**

Distance of $x_1$ and $x_2$ , metres	Calculated soccer ball spin rate, RPM
0.1	590.6
0.2	581.6
0.3	572.9
0.4	564.5
0.5	556.6
0.6	549.1
0.7	541.9
0.8	535.2
0.9	528.8
1	522.8
1.2	511.9
1.4	502.3
1.5	498.0
1.8	486.5
2	480.0

Table 4-3 shows how this error with HSV camera dot monitoring methodology, can induce a very large underestimation of the measured spin rate. The predicted 'worst case scenario', which was a feasible set-up, could underestimate the predicted spin rate by a significant 20%. This was a type B uncertainty (UKAS 1997), it was non-random in nature and all spin measurements carried out would induce this error. It

## Laser based tracking and spin measurement

should be noted though, sports ball flight paths and spin rates are not easily replicated, the error induced due to this process would almost certainly vary for each individual analysis.

Instead of constraining the  $y_1$  and  $y_2$  lengths, Table 4-4 shows the calculated soccer ball spin rates if the  $x_1$  and  $x_2$  lengths were fixed at 0.5 metres. The same assumptions were applied to the calculations as in Table 4-3. The calculations carried out for both Table 4-4 and Table 4-3 can be found in Appendix A.

The predicted worst case scenario again resulted in a underestimation by a significant 20% by a type B measurement uncertainty. In order to reduce this camera error, the ball would ideally be measured at the centre of the FOV, with the distance of  $y_1$  and  $y_2$  maximised and the distance of  $x_1$  and  $x_2$  minimised. These optimisations conflict with general spin dot measurement set-ups, however if an investigator is aware of this phenomenon and accounts for it, by following the analysis process in this section, the investigator should be able to indicate by how much the measured spin rate values underestimate the actual value.

**Table 4-4: Predicted soccer ball spin rate values, depending on the distance  $y_1$  and  $y_2$ .**

<b>Distance of <math>y_1</math> and <math>y_2</math>, metres</b>	<b>Calculated soccer ball spin rate, RPM</b>
0.5	480.0
1	522.8
1.5	544.3
2	556.6
2.5	564.5
3	570.0
3.5	574.1
4	577.2
4.5	579.6
5	581.6
5.5	583.2
6	584.5
6.5	585.7
7	586.7
7.5	587.6

#### **4.8 Chapter summary**

The 'spin rig' introduced to the reader in this Chapter has distinguished itself from other methods of imparting spin onto a ball. This is because the 'spin rig' was reported to spin soccer balls up to 750 RPM and golf balls up to 8000 RPM and by utilising an integrated encoder and counter it was able to display an accurate spin rate measurement of the ball. Therefore the usefulness of the 'spin rig' for further work was demonstrated.

The rotational vibrometer that was used for spin measurements was proven to output statistically similar results to the 'spin rig'. This highlighted the potential to record

## Laser based tracking and spin measurement

accurate measurements without the need to mark the target ball using a non-contact measurement instrument.

The HSV technology was shown to be an accurate tool only when the ball was imaged in the centre of the camera FOV and the ball spin axis was co-linear with the camera axis. In more realistic test scenarios, HSV spin rate measurements were shown to introduce large errors due to the ball being positioned away from the centre of the camera FOV and the spin axis not being perpendicular to the camera axis. Therefore the HSV was not advised when accurate spin measurements are required. The dot monitoring technique for spin rate measurement was also analysed and was shown to dramatically underestimate measured spin rate (up to 20%) for a standard measurement condition.

## **5** Launch parameter measurement

### **5.1 Chapter overview**

The purpose of this Chapter was to report a quantitative study on launch characteristics in soccer for the maximal velocity instep kick and the maximal driven kick, specifically measuring launch velocity, launch angle and spin rate values. The results from the testing protocol were also compared with previously reported launch characteristics. The objective of the player testing section was to identify the range of possible values for ball launch angle, velocity and spin rate, that any measurement system would be required to accommodate.

The results generated by an optical system used for the player testing raised some concerns regarding the validity of the results, and directly led to the work using a mechanical kicking simulator. The purpose of the mechanical kicking simulator testing was to compare the results achieved between three state of the art soccer launch measurement systems, which were measuring the launch conditions of identical kicks. The mechanical kicking simulator was used to achieve highly repeatable kicks and obviate issues associated with player testing such as fatigue and inconsistency. The objective of this study was to allow researchers and OEMs to choose the most accurate launch monitor for benchmark testing.

### **5.2 Player Testing**

#### **5.2.1 Previous work**

Numerous studies have been carried out on player kicking abilities, some of which were reported in 3.3.4. Roberts and Metcalfe (1968) used a mixture of professional and amateur players for their test protocol. Kicking velocities between 23 and 31 ms<sup>-1</sup> were reported. Based on imaging technology operating at 64 FPS. Another widely cited source was the work by Plagenhoef (1971) who used one ex-professional soccer player for his testing, reporting maximal strikes in the region of 24 to 28 ms<sup>-1</sup>.

By the 1980s HSV work at 500 FPS was practical; Asami and Nolte (1983) tested a mixture of professional and amateur players and recorded a maximal velocity instep kick at  $34 \text{ ms}^{-1}$  and average velocity at  $29.9 \text{ ms}^{-1}$ . Isokawa and Lees (1988) measured maximal instep velocities between 18 to  $22 \text{ ms}^{-1}$ . The low measured velocities were accounted due to the one step run up, in order to maintain a consistent kicking action. Their focus was on the approach angle and how this affected kinematic and kinetic data.

Tsaousidis and Zatsiorsky (1996) tested two amateur players and measured ball velocities in the range of 24 to  $26 \text{ ms}^{-1}$  for the toe kick/punt. This technique is exercised rarely by current professional players due to the unpredictability of the kick and the likelihood of pain or injury. Asai *et al.* (1998) tested three amateur players and measured velocities between 22 to  $27 \text{ ms}^{-1}$  for the instep kick. They operated the HSV camera at 4500 FPS and spin rates in the region of 400 to 600 RPM were reported.

Nunome *et al.* (2002) carried out a kinematic analysis of the instep and side foot kick, identifying significant differences. Reporting average velocities of 23.4 and  $28 \text{ ms}^{-1}$  for the side step and instep kick respectively. The most comprehensive reported player study to date testing professional players was carried out by Neilson (2003). This investigation is analysed in detail next. Carre *et al.* (2004) carried out analysis on the aerodynamics of a spinning soccer ball. To perform analysis they reported a range of 4.6 to  $32 \text{ ms}^{-1}$  in order to replicate match specific ball velocities.

#### **5.2.1.1 Comprehensive player testing study**

Neilson (2003) carried out a study on 25 professional players in the Senior English Football League, reporting ball velocity, launch angle and spin rate. The testing protocol involved achieving five 'good' strikes per player for a maximal power, instep and outstep kick. The players were told to maximise spin imparted to the ball for the instep and outstep swerve kick.

The hardware used for the test allowed recording at 500 FPS with a 1/1000 second shutter speed. The image consisted of vector graphics array (VGA 640 × 480) pixel

resolution and the camera was aligned perpendicular to the plane of ball travel. A composite image was created with two balls in view spaced 30 ms apart. To compute all launch characteristics the analysis technique using Flightpath, shown in Figure 4-6, was utilised. Table 5-1 and Table 5-2 display the testing results, the stated resolution of measurements were  $\pm 0.1 \text{ ms}^{-1}$  for velocity,  $\pm 0.3^\circ$  for launch angle and  $\pm 2.5 \text{ RPM}$  for spin rate.

**Table 5-1: Velocity measurements from player testing (Neilson 2003)**

<b>Kick type</b>	<b>Average velocity <math>\text{ms}^{-1}</math></b>	<b>Standard deviation</b>	<b>Maximum velocity, <math>\text{ms}^{-1}</math></b>	<b>Minimum velocity, <math>\text{ms}^{-1}</math></b>
Maximal power	27.05	2.23	33.1	20.72
Instep kick	23.52	2.31	28.91	18.06
Outstep kick	20.85	3.08	27.7	13.50

**Table 5-2: Spin rate measurements from player testing (Neilson 2003)**

<b>Kick type</b>	<b>Average spin rate, RPM</b>	<b>Standard deviation, RPS</b>	<b>Maximum spin rate, RPM</b>	<b>Minimum spin rate, RPM</b>
Instep kick	474.6	2.27	833.4	175.2
Outstep kick	472.2	2.46	833.4	156

The study reported clear indications of player kicking capabilities. The average body mass of the players tested was 76.04 kg and the average age of the players tested was 19.68 years.

Reilly *et al.* (2000) stated that the muscular strength of soccer players was linked to their position within the team, which would influence ball launch parameters. This claim was supported by muscular strength findings whereby midfielders exhibited the lowest strength out of the team. Midfielders and full backs however had the highest maximal oxygen intakes. The findings hypothesised that the differences in muscular strength was most likely due to the selection of specific type of player for a position, rather than development of strength as a result of playing in that position. Neilson did

not split the results according to position played, he did however report maximal kicks were achieved by goalkeepers which concurs with Reilly *et al.* (2000) findings.

Mathematically Plagenhoef (1971) calculated that the velocity of the ball,  $v_{ball}$ , was dependent upon the velocity of the foot,  $v_{foot}$ , the combined mass of the leg and foot,  $m_l$ , the coefficient of restitution (COR) and the mass of the ball,  $m_b$ , as shown in Equation 5-1.

$$v_{ball} = v_{foot} \left( \frac{(m_l) \times (1 + COR)}{(m_l + m_b)} \right) \quad \text{Equation 5-1}$$

A ball to foot velocity ratio of 1.2 was reported for a normal maximal instep kick. By analysis of Equation 5-1 it was assumed that larger average ball velocities could have been measured in Neilson's study if the average age of the players had been raised. As players mature usually muscle mass of the foot and leg increase, thus if maintaining technique - a rise in ball velocity would be inherent. Muscle has been reported as denser than fat by approximately 15% therefore a gain in muscle would increase the ball velocity by two different mechanisms; (1) increasing foot velocity due to increased strength and (2) increasing the mass of the foot and leg due to an increase in muscle mass. Currently no known investigations have related muscle strength to the age of soccer players. Reilly (2008) hypothesised however that strength and power should be maintained, if not improved, until retirement age (early 30s), suggesting increased ball velocity with age. It is argued that if professional players between 24 to 28 years had been tested by Neilson, a higher average velocity would have been measured.

Neilson concluded there was a need for an automated system to analyse soccer ball launch characteristics. This work directly led to the development of the optical system reported in 3.5.8.

### **5.2.2 Automated system for free kick measurement**

This section is the first to report player testing using an automated measurement system - the optical measurement system. In order to ascertain whether the use of an automated system was feasible, LU football players were tested during the course of



their training sessions. Additionally the spin axis of the struck soccer ball was calculated.

Two different kicks were investigated; (1) the maximal driven kick or straight kick and (2) the maximal velocity instep kick or swerve kick. The maximal driven kick was investigated in order to record and establish the maximum velocity that a soccer ball can be struck. This could be compared with other cited work. Nike (2007) reported that 69% of strikes on goal were taken using the instep swerve kick. The instep kick has been the predominant skill analysed by biomechanists for a free kick type set-up, and thus was also studied in this investigation.

Twenty three volunteers from the men's Loughborough University Football Club were chosen for this investigation. All the players were tested in two training sessions.

#### **5.2.2.1 Maximal driven kick**

The objective of this study was to get the player to strike the ball as hard as possible. In order to achieve this, players were told to strike the ball with a low trajectory of launch, a low spin rate, and aiming to strike the ball in a straight line, as shown in Figure 5-1. The kicking direction was reversed for left footed players, in order to avoid the standing foot being planted between the ball and the optical measurement system.

## Laser based tracking and spin measurement

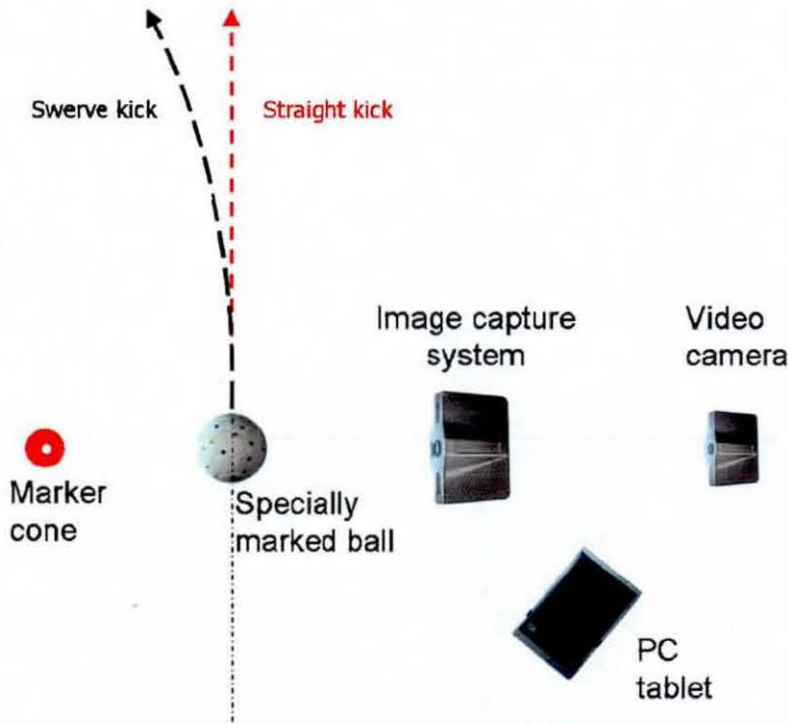


Figure 5-1: Plan view of straight and swerve kick set-ups.

Each player struck the ball at least twice in order to achieve two measurement results. The kicks were analysed automatically allowing direct feedback to the player after each strike. In past player testing protocols, only 'good' strikes were recorded for analysis, however the objective of this section was to define a range of possible velocities, launch angles and spin rates that a measurement system should record, thus 'poor' kicks were included.

### 5.2.2.2 Instep swerve kick

The objective of this study was to get the player to strike the ball as he would when taking a free kick on the edge of the box bending the ball over and/or around the wall, and past the goalkeeper, into the goal. This kick comprised of a combination of velocity and spin. In order for the ball trajectory to pass over players standing in the wall, the angle of launch was greater than for the maximal strike. The swerve kick set-up is shown in Figure 5-1. For a player to strike a free kick over the wall, at a distance of 9.1 metres from it, the launch angle must be above  $11.3^\circ$  based on the average height of a premiership footballer, 182 cm (Independent 2007). To make the free kick as realistic as possible players were asked to try and replicate this launch angle. Each

player took at least two strikes, so that a direct comparison with maximal strikes was possible.

### 5.2.2.3 Results and analysis from the player testing

The results from the two player tests carried out are summarised in Table 5-3.

**Table 5-3: Driven kick and swerve kick results from player testing.**

<b>Driven Kick</b>	<b>Velocity, ms<sup>-1</sup> (to 1.d.p)</b>	<b>Spin rate, RPM (to 1.d.p)</b>	<b>Angle of launch, ° (to 1.d.p)</b>
Average	31.6	629.3	7.9
Maximum	39.0	1335.7	18.4
Minimum	26.2	348.5	1.1
<b>Instep Kick</b>	<b>Velocity, ms<sup>-1</sup> (to 1.d.p)</b>	<b>Spin rate, RPM (to 1.d.p)</b>	<b>Angle of launch, ° (to 1.d.p)</b>
Average	27.7	714.7	12.7
Maximum	32.2	1281.9	25.8
Minimum	22.8	245.5	1.9

The maximum velocity measured was 39 ms<sup>-1</sup>. This was much greater than maximal velocities reported previously. Concerns were raised about the validity of the velocity results since the players tested were university level (amateur) players aged 18 to 21 years. Spin rates recorded, also appeared higher than expected, especially when the players were striking the ball maximally. A 'good' maximal strike was expected to produce minimal spin (<300 RPM). Two measurements reported spin rates above 1000 RPM, this was higher than expected, considering David Beckham has been reported to produce ~600 RPM spin on the ball (Ireson 2001). The optical system did however measure all three axis of spin (compound spin), rather than oblique spin measured with traditional techniques and this could account for larger spin rate measurements.

The average launch values for the two different types of kick, straight and swerve showed expected trends. The average velocity was less for the swerve kick than the

straight kick, whilst the spin rate observed was higher for the swerve kick than for the straight kick. These trends concur with the findings by Neilson (2003). The average angle of launch was  $4.8^\circ$  higher for the swerve kick than the driven kick, this was expected since the players were trying to kick the ball over the 'wall'.

The optical measurement system also produced results for the spin axis as well as the spin rate. As expected the soccer ball flight consisted of compound spin when struck with the instep. A large proportion of sidespin was recorded when trying to bend the ball over and/or around the wall.

### **5.3 Mechanical kicking simulator testing**

The results from the player testing were considered questionable since the validity of the optical system was under scrutiny. Therefore a further test was carried out in this section which utilised current top of the range technology to measure soccer ball launch characteristics. The optical, radar and HSV systems were operated simultaneously, the launch characteristics of 30 kicks representing a maximal velocity strike and 30 kicks representing a swerve pass were carried out. The kicks were carried out using a purpose built mechanical kicking simulator (Holmes *et al.* 2007) in order to obviate inconsistencies achieved with player testing. The results achieved using the optical system could be validated based on the work in this section.

#### **5.3.1 Equipment**

The kicking simulator was manufactured in 2007 at LU and capable of striking a soccer ball up to  $50 \text{ ms}^{-1}$  with a leg speed repeatability of  $\pm 0.032 \text{ ms}^{-1}$  at the 95% confidence level (Holmes 2008). Exactly the same optical measurement unit was used as for the player testing protocol reported in section 5.2.

The radar device was originally designed for golf, but recently the system was modified for soccer ball measurement. Using an identical principle of operation as was reported for golf in 3.5.6. The first soccer radar system was sold to adidas in 2006 and this unit was loaned for the duration of the testing. One advantageous feature of the radar device was that once testing commenced the system could be left in continuous acquisition mode. The Photron APX Ultima was the chosen HSV camera for testing.

### 5.3.2 Testing protocol

The set-up for the mechanical kicking simulator protocol is shown in Figure 5-2. The optical system was positioned perpendicular to the kicking direction at a stand off distance of 1.25 metres from the ball tee position at exactly the same height and co-linear with the kicking tee. The optical system required a ball with a specific surface pattern to be used. Five balls were used during testing, all inflated to 0.9 bar. For consistency the balls were placed identically onto the tee for all the straight and swerve kicks. To measure spin rate using the HSV camera, a circumferential line was placed identically onto all five balls. The camera was positioned perpendicular to the initial ball direction of travel placed 2 metres away from the ball plane of travel. This permitted a large FOV in which to carry out measurements of ball velocity, launch angle and spin rate.

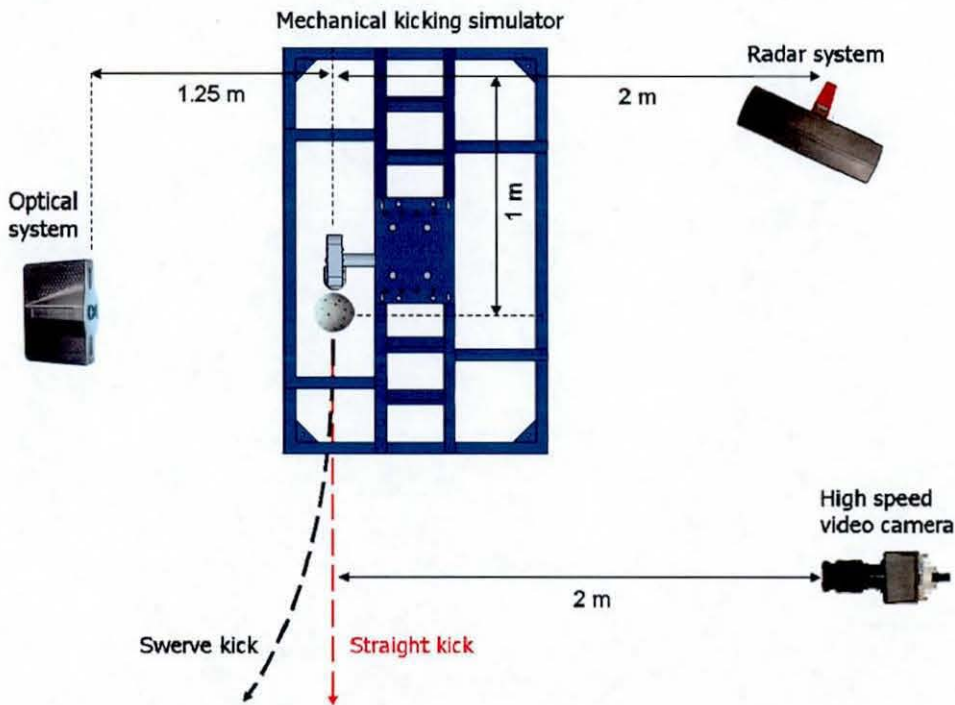


Figure 5-2: Plan view of mechanical kicking simulator testing set-up.

The radar system was positioned at the same height as the kicking tee and angled so that it could capture as much of the ball travel as possible, for both straight and curved kicks. The radar system was only initiated at the start of each different test since it acquired data continuously.

The kicking techniques employed in the player testing chapter, were mimicked in this investigation. The only difference was that the swerve pass was carried out for an outstep kick for a right footed player. This choice was for practical reasons as the guarding around the kicking simulator would have blocked the path of a ball simulating an instep kick.

The balls were struck at three different speeds for the maximal and swerve kicks. To replicate top of the range player kicking speeds the mechanical kicking simulator leg was swung at 16, 20 and 23 ms<sup>-1</sup> which upon impact achieved ball velocities in the range of 20 to 35 ms<sup>-1</sup>. To compare the three different measurement systems 10 tests were carried out for all kick scenarios, using two different kick types and three different ball velocities. The test protocol produced 60 valid results for each of the measurement systems, a valid result was obtained if each measurement system measured ball velocity, launch angle and spin rate. The reliability of each measurement system was recorded.

### **5.3.3 Results and Discussion**

The results for the mechanical kicking simulator testing are shown in Figure 5-5 and Figure 5-6. Figure 5-5 shows the launch angle and velocity results. The mean of the results were plotted on the bar graphs, displaying  $\pm 1$  standard deviation from the mean results. Figure 5-6 shows the spin rate measurement results for the testing protocol. All individually measured spin rate values were plotted on the scatter graphs. The results were analysed statistically using a one-way ANOVA test.

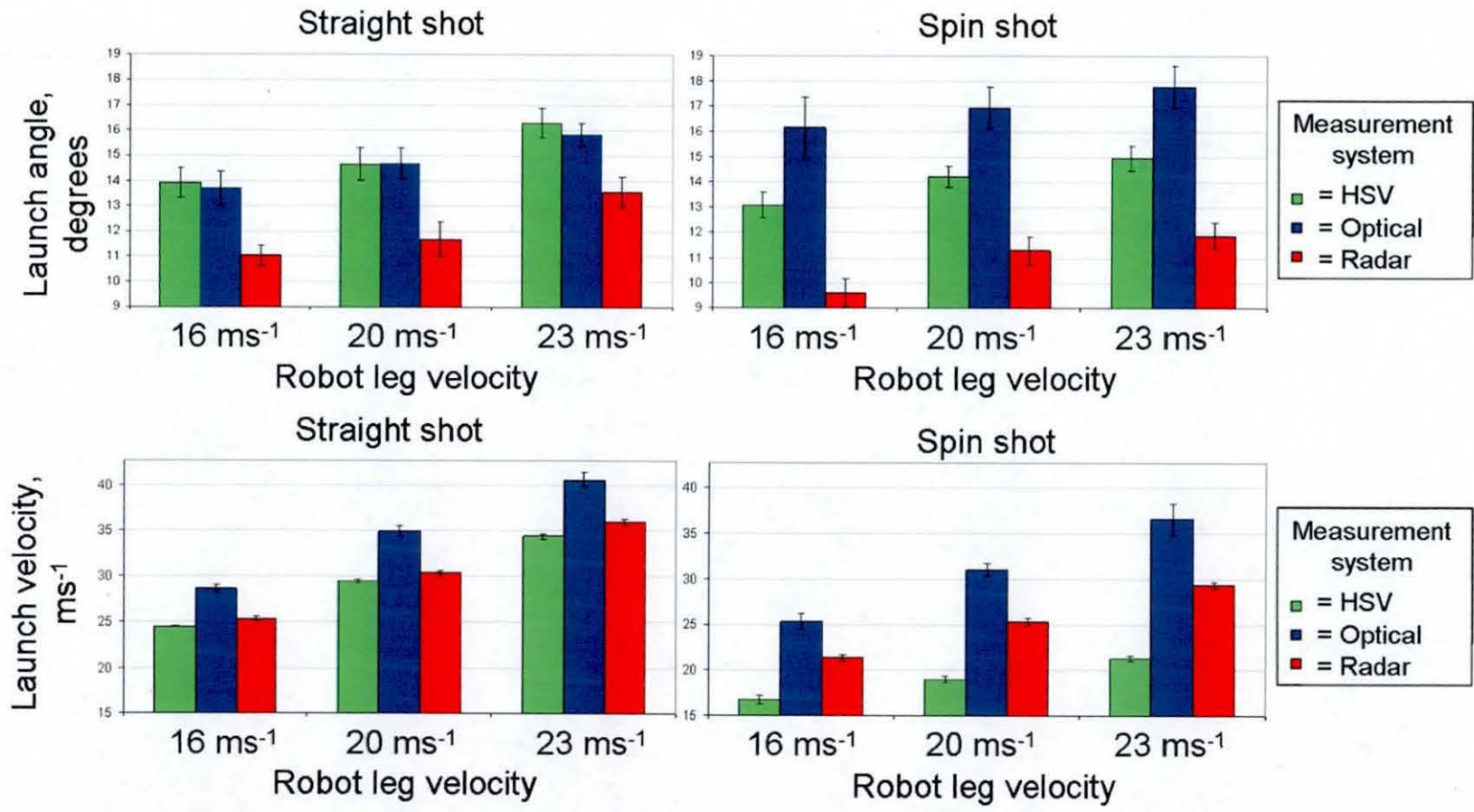


Figure 5-3: Launch velocity and launch angle measurements

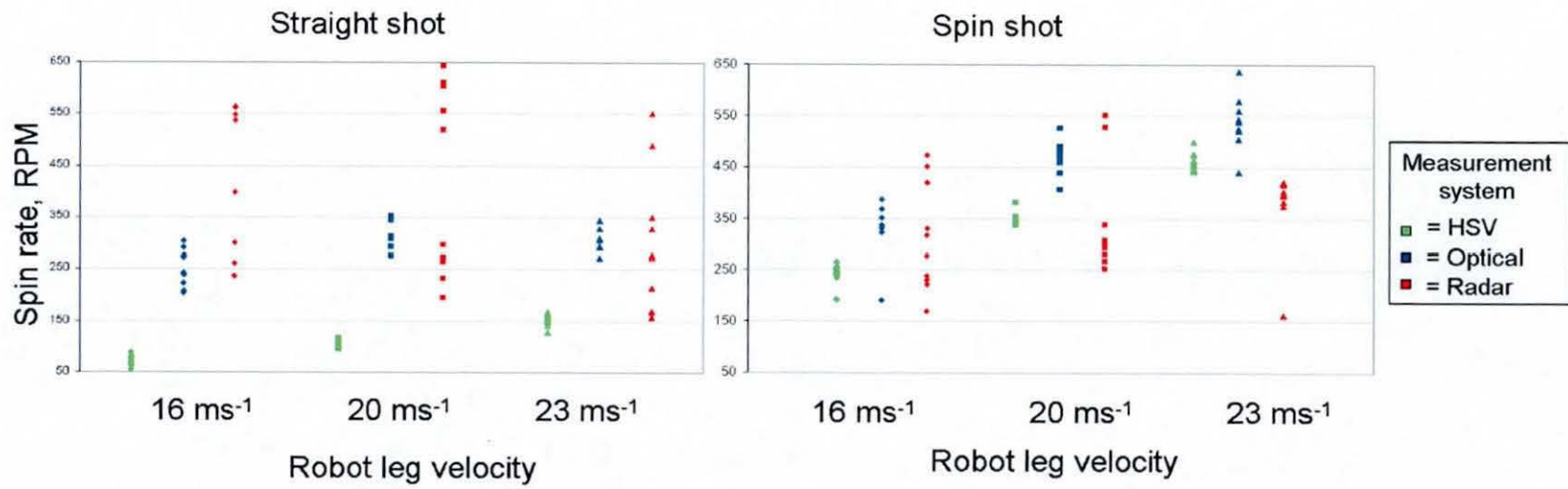


Figure 5-4: Spin rate measurements.



### 5.3.3.1 Launch velocity analysis

For straight shot analysis the radar measurements were found to have a slight velocity offset to the HSV results. This was assumed to be due to three different factors (1) the radar device measured three dimensional velocity and by analysing the HSV footage it was clear that the ball did not travel exactly in a plane perpendicular to the camera, as shown in Figure 5-5 (a), illustrated by the change in ball pixel diameter. (2) The radar device used undefined filtering algorithms and raw data were not used in calculations. (3) By scrutinising the radar results, the launch velocity was computed over the first 10 ms of ‘filtered’ data. The HSV launch velocity values were calculated over a 50 ms time period. These factors help explain the reasonably constant offset found between the radar and HSV velocity values in this experiment.

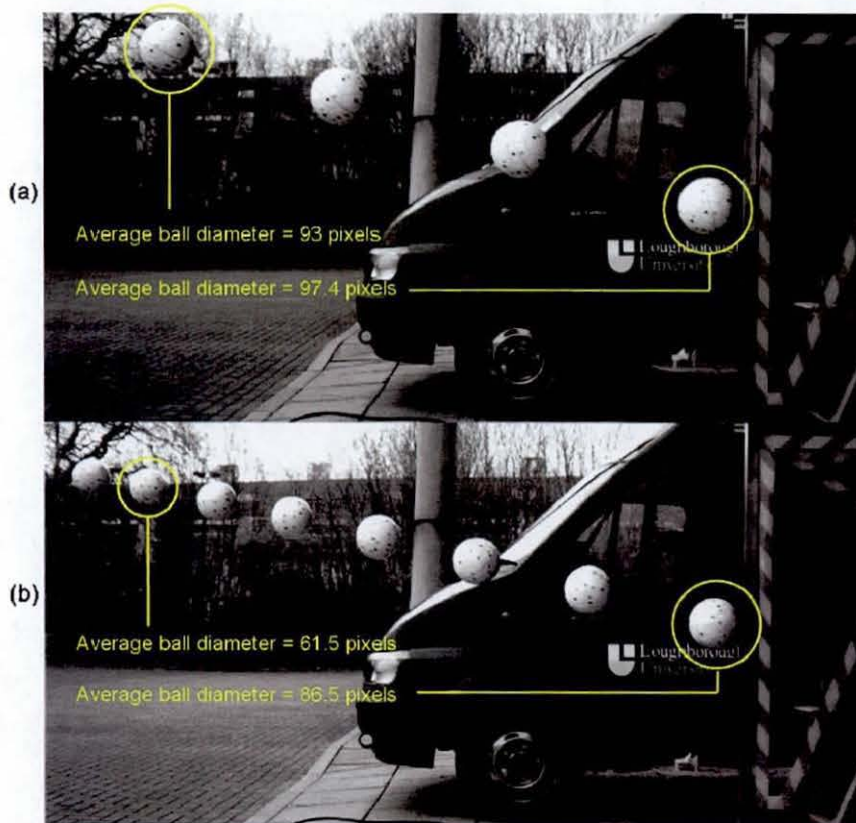


Figure 5-5: Composite images with balls spaced 20 ms apart, leg velocity at  $23 \text{ ms}^{-1}$ , (a) straight kick, (b) swerve kick.

The optical system outputted on average a 16% higher velocity value than the radar and HSV devices. The HSV and radar velocity values were consistently similar and

## Laser based tracking and spin measurement

the confidence in these results was deemed high due to the similar output and both systems having a smaller standard deviation in measured results than the optical system. Therefore it was concluded that the optical velocity values were overestimated. This was explained by the method by which the system operated.

Two images were used to calculate the velocity of the ball. The first image (static) was acquired when the ball was stationary, shown in Figure 5-6 (a&c). The second image (dynamic) was acquired when the ball was flying post impact, shown in Figure 5-6 (b&d) acquired 6 ms after launch (launch was measured using a sound trigger). The interval between the point of launch and the time at which the second image was acquired was critical in the velocity calculation.

If the ball was struck at  $30 \text{ ms}^{-1}$  and the dynamic image was taken two ball diameters after impact, underestimation by 1 ms in the time interval between images, would compute a launch velocity of  $32.1 \text{ ms}^{-1}$ , an error of 7%. This would be a large velocity measurement difference. General contact times between foot and ball have been measured in the order of 8 to 11 ms (Ronkainen 2004), and should such an error occur in the time interval estimation, it would prove catastrophic and invalidate the measurement accuracy. A time of flight delay is inherent between the ball being struck and the sound reaching the optical device. When the optical device is placed 1.25 metres from the ball, the time of flight delay would be 3.6 ms. It is unclear how this time of flight delay has been incorporated by the manufacturer into the calculations to work out the measured ball velocity.

Velocity measurement of the spin shot was harder to assess, since the HSV system of measurement and analysis certainly under predicted ball velocity. This was due to the ball travelling out of plane in the camera FOV, depicted in Figure 5-5 (b) by the large change in ball pixel diameter.

The radar velocity measurement of spin shots was thought to be the most accurate since the results possessed a low standard deviation and were much lower than the optical device results and much higher than the HSV results. The optical device

results were very similar to the straight kick results achieved by the HSV and radar devices. Therefore the optical device results were thought to be erroneous since the swerve kick velocities should be less than the straight kicks because the kicking leg energy was transferred on impact into linear as well as rotational energy, resulting in a smaller translational ball velocity. The radar results support this view, the average recorded results were 4, 5 and 6.6  $\text{ms}^{-1}$  lower for spin shots than the straight shots, for kicking simulator leg velocities of 16, 20 and 23  $\text{ms}^{-1}$  respectively.

#### 5.3.3.2 Launch angle analysis

Statistical corroboration revealed that agreement was found only between the HSV and optical systems for the straight kicks for launch angle measurement. A one-way ANOVA test was carried out showing a confidence level at 0.71, 0.99 and 0.19 for simulator leg velocities of 16, 20 and 23  $\text{ms}^{-1}$  respectively. Statistically all other comparisons were significantly different at the 95% confidence level. The radar device results were approximately 19% less than for the HSV and optical measurement systems for the straight shots. The  $\pm 1$  standard deviation plots demonstrate the similar repeatability for all three measurement systems for the straight shot. However for the spin shot the repeatability of the optical system is  $\pm 2.4^\circ$  at the 95% confidence level, which is noticeably larger than the repeatability of the HSV and radar system which were  $\pm 1^\circ$  and  $\pm 1.2^\circ$  at the 95% confidence level respectively. Therefore it was concluded that the optical system was unable to decipher launch angle as accurately when the ball was moving out of plane in the camera FOV.

HSV analysis of the curve kick yielded a lower launch angle than the optical system, assumed to be due to the ball travelling out of plane in the camera FOV. The tee position was slightly altered for the curve kick in order to allow the ball to travel a greater and more realistic distance before impacting the ground. The tee position was raised, thus the measured launch angle should have been higher for the curve kick than the straight kick. The optical device however showed that the ball travelled out of plane towards the camera and the capabilities of the software to handle this deviation were unknown, as shown in Figure 5-6 (c&d) by the increase in ball diameter. The optical system results did possess a larger launch angle in the spin shot kicks than the straight shot kicks, instilling confidence in the measured launch angle results.

Radar curve kick results showed a much lower launch angle than for the straight shots. These results were known to be erroneous due to two factors. Firstly the raised tee position should ensure a larger launch angle for the curve kick results. Secondly the radar device plots the flight of the ball in three dimensions, and allows an imaginary goal to be visualised, plotting the ball position at this stand off distance. Figure 5-7 displays these plots and concurs with the optical system results that the launch was greater for the curve kick results than the straight kick results, because the curve kick shots are plotted vertically higher than the counterpart straight shots. This conflict in the radar device results was accounted for by the device not detecting the ball until later in flight for the curve kicks. Analysis of the raw radar data showed the system did not detect spin shot kicks until the ball was approximately 2 metres post launch, straight shots were detected approximately 1 metre post launch.

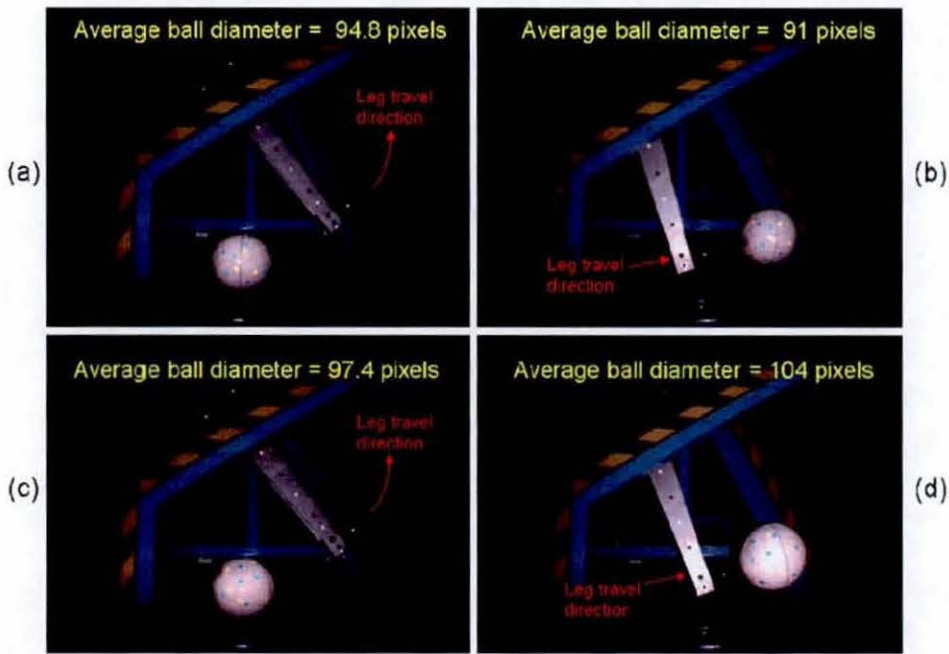


Figure 5-6: Optical device measurement images, (a) static image for straight kick, (b) dynamic image for straight kick (6 ms post launch), (c) static image for curve kick, (d) dynamic image for curve kick (6 ms post launch).



Figure 5-7: Radar device visual for balls striking an imaginary goal.

### 5.3.3.3 Spin rate analysis

Spin rate values in Figure 5-6 show how difficult it was to accurately measure spin, since all results had noticeable variation in measurement. Measurements of spin made using the radar device exhibited large standard deviations. For each of the different measurements it was found to be greater than 100 RPM. Within product literature the manufacturer has stated that the system would not be able to measure spin rates under 300 RPM, and from analysis of the swerve kick results it was concluded that spin rates up to ~ 450 RPM could not be measured accurately. Soccer ball spin rates have generally been reported up to 600 RPM, therefore the use of the radar device for spin rate analysis in soccer must be considered with caution.

The optical system was designed primarily for spin measurement. For straight shots the optical device results were ~ 200 RPM higher than the HSV spin rate values. Empirically during testing it was clear that the optical system results were erroneous. This was because by observation of the ball in flight and analysis of the HSV footage, it was clear that the ball possessed spin rate of less than 100 RPM. It was hypothesised that the interaction between the kicking simulator leg and ball during impact, rotated the ball slightly, and then post contact the ball departed with minimal spin for the straight shots. This was substantiated by closely scrutinising the images the optical device used to carry out the launch calculations. Due to the optical system

acquiring two images one before impact, shown in Figure 5-6 (a), and one after impact, shown in Figure 5-6 (b), any interaction causing a change in the orientation of the ball would have led to errors in spin rate measurement. By analysing the circumferential line around the ball it seemed evident that the ball was moved slightly obliquely during impact. Post impact HSV analysis showed that a small component of top spin was placed on the ball and almost zero oblique spin.

For the swerve shot a fixed offset of 100 RPM between the HSV and optical device results was found. Two main factors were assumed to produce this offset, (1) the same interaction between simulator leg and ball as for the straight shot, the ball was rotated on impact, this was less because the leg was striking the ball offset from the centre, causing mainly oblique side spin on the ball. (2) Due to the nature of the impact, back spin was placed onto the ball which was not measured by the HSV analysis.

**5.3.3.4 Reliability of the measurement systems**

In order to carry out testing it was useful to establish the reliability of each measurement tool in this practical experiment. Table 5-4 summarises how often each system captured all launch characteristics (velocity, angle and spin rate) throughout testing.

**Table 5-4: Success of measurement systems throughout testing.**

Type of kick	HSV	Optical	Radar
Straight kick	100 %	92.3 %	71.8 %
Swerve kick	96.8 %	95.1 %	75.6 %
Overall	98.4 %	93.7 %	73.7 %

The HSV camera only failed to record the launch once due to the manual trigger arrangement. Had an automated trigger system been used it was predicted that 100% reliability would have been achieved. The HSV system however required all data to be manually post processed.

The optical system was found to function consistently and struggled only with computing the launch spin rate. It should be noted that the reliability of the optical

system for the player testing work was not as good. On average the radar system outputted all launch characteristics ~75% of the time, like the optical device the radar device struggled only with the computing the launch spin rate.

### 5.3.4 Summary

The mechanical kicking simulator study highlighted the errors associated with ball launch parameter measurements. In all measurements the aim was to establish the true value. By analysing the work presented it is difficult to state with confidence what this true value was since predominantly all three systems showed variation in results.

The results obtained from this testing allowed the optical system to be calibrated for velocity and spin measurement. The launch angle measurement of the optical system was not altered since this was assumed to measure realistic values. The findings from this section suggested that the optical system would function more favourably if both images were acquired during flight. This was known to be the original configuration of the system, however due to the large possible variation in launch velocities, the camera would not be able to capture both images separately within the camera FOV at all velocities, using a fixed time delay between captures.

## 5.4 Chapter summary

The main objective of this chapter was to output a range of values that a soccer ball could exhibit when struck by amateur and professional players with a maximal driven kick and maximal velocity instep kick. All present and past work was summated to give the results displayed in Table 5-5.

**Table 5-5: Range of possible soccer free kick launch characteristics.**

Launch Characteristic	Range
Velocity, $\text{ms}^{-1}$	10 to 34 $\text{ms}^{-1}$
Launch angle, $^{\circ}$	1 to 30 $^{\circ}$
Spin rate, RPM	Almost zero to 1000 RPM

The player testing section highlighted the need to review current technology available to soccer OEMs for ball launch measurement since the optical system seemed to overestimate ball launch velocity. A comparison of three state of the art launch and

## Laser based tracking and spin measurement

flight measurement systems was carried out. The results showed that no system was able to measure all the launch characteristics successfully, therefore it was concluded that there was scope to develop a novel measurement system that would be able to carry out these measurements in an accurate and repeatable method. The testing reported in this Chapter definitely highlights the fidelity in spin rate measurement because this was found to be the most difficult variable to measure with accuracy.

The radar device tested was proven to be a very simple and intuitive tool to use, however currently for soccer ball spin measurement the device was found to lack the ability to measure spin rate accurately.

All three systems tested generally incurred systematic errors in measurements, therefore researchers and OEMs are recommended that if they are using one of these systems to recognise that although relative comparison between measurements can be carried out, the fidelity of the measured values is open to question.



## **6 Single point vibrometry for ball velocity and spin rate measurement**

### **6.1 Chapter overview**

A purpose of this Chapter was to analyse the suitability of golf and soccer launch characteristics for single point vibrometry measurement. It was important to explore other factors that were going to influence the vibrometry measurements. Therefore the influence of impact conditions and spin were reported in order to show how they would influence the vibrometer measurements.

Another purpose of this Chapter was to create a virtual vibrometer that allowed the simulation of an actual vibrometer. This would obviate large amounts of actual testing. However in order to validate the virtual vibrometer a series of tests were carried out and comparisons were carried out between the theoretical and practical measurements.

The potential of using a single beam vibrometer to extract on-axis linear velocity from a point on the surface of a target ball from which rotational velocity data can be derived is reported in this chapter.

The knowledge gained from Chapter 4 was expanded upon regarding laser measurement for sport ball spin and definitive direction was given to the laser work in this thesis.

### **6.2 Linear and angular velocity measurements within sport**

A single point vibrometer is known to measure the Doppler shift according to Equation 2-8. As previously discussed, to overcome directional ambiguity of the target, the Doppler shift must be contained within the initial Bragg cell shift in the vibrometer. The range of velocity values encountered for golf and soccer were

explored in order to satisfy that these values lie within current velocity measurement capabilities of vibrometers.

Figure 6-1 (a) depicts the Bragg cell Doppler shift required to measure the translational velocity of a golf ball, assuming that the vibrometer was positioned on-axis to the direction of travel. The minimum resolvable velocity value was required to be a positive measured frequency. The measurement wavelength of light was fixed at 633 nm.

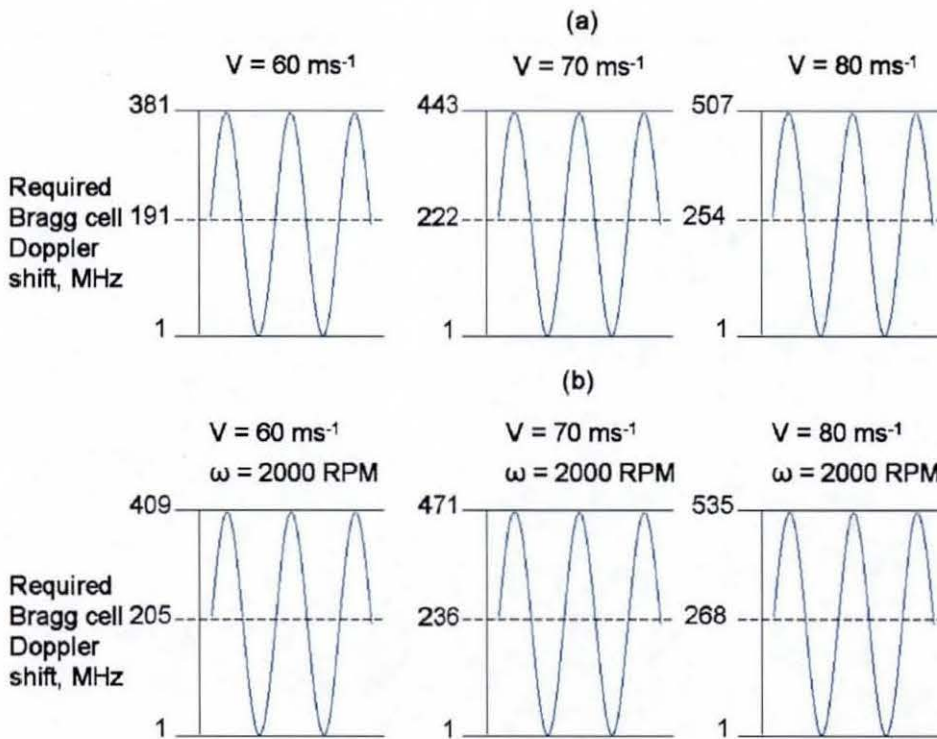


Figure 6-1: Bragg cell requirements for golf.

To achieve a better understanding of the Bragg cell shift required, the spin rate of the golf ball must also be incorporated within the calculations, see Figure 6-1 (b). At high golf ball velocities, 2000 RPM was considered a realistic spin rate (Smits and Ogg 2004). The maximum and minimum frequency shift values shown were based on the vibrometer striking the very edge of the ball at the 'equator'.

## Laser based tracking and spin measurement

Due to the large translational velocities and large spin rates, the Bragg cell shift required to achieve demodulation of the golf ball velocity was huge, in the order of 200 MHz. As reported previously, 120 MHz is the current maximum capability of commercially available Bragg cells, therefore measuring the ball on-axis to travel direction would not be feasible.

Hocknell (1998b) demonstrated that by measuring components of golf ball translational velocity, he was able to extrapolate the actual translational velocity of the ball using the set-up shown in Figure 6-2. The vibrometer velocity range of measurement was  $\pm 15 \text{ ms}^{-1}$ , by fixing angle  $\gamma$  at  $75^\circ$  he contained target velocity within the vibrometer measurement range.

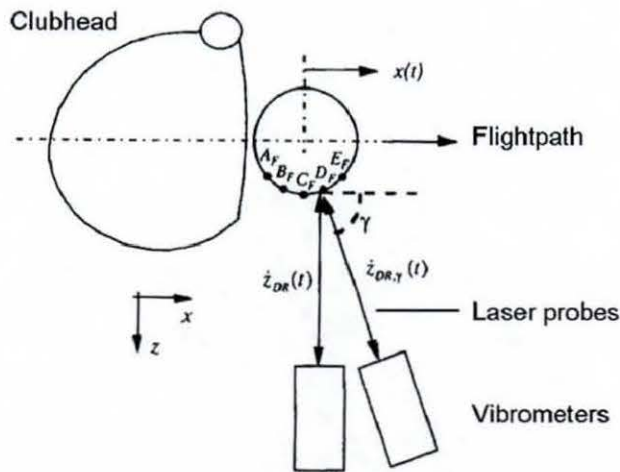


**Figure 6-2: Translational velocity measurement of a golf ball, Hocknell (1998b).**

When considering typical velocities and spin rates found in competitive soccer, the use of vibrometry is likely to be more appropriate, Figure 6-3 (a&b) show likely velocity values required for vibrometry measurements. The Bragg cell shift required for unambiguous target velocity is shown on the centre line in the Figures, and the vibrometer was pointed at the very edge of the soccer ball equator.

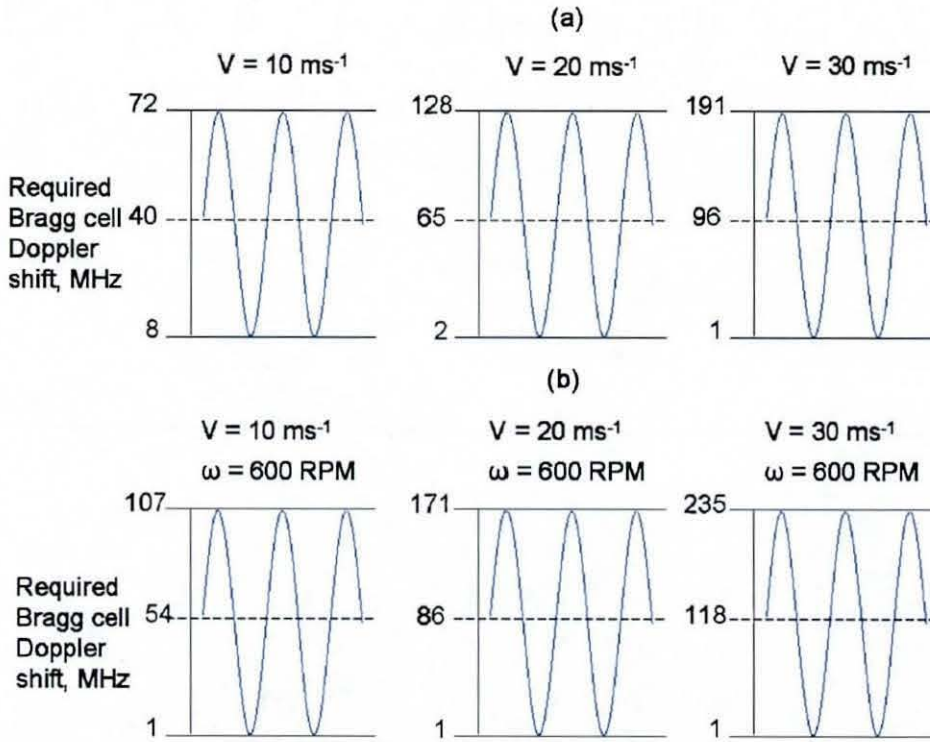


Figure 6-3: Bragg cell requirements for soccer.

The ‘worst’ case scenario shown with a translational velocity of  $30 \text{ ms}^{-1}$  and spin rate of 600 RPM would have required a Bragg cell frequency shift of 118 MHz. This shift is within current commercially available Bragg cell frequency shift capabilities.

### 6.3 Mathematical computer modelling of surface velocity

In order to identify the velocity range of points on the surface of a soccer ball in play, the ball was modelled in a finite element (FE) environment. Brief studies were undertaken to establish the oscillations of the surface during and after impact as well as the ball surface velocity due to spin. These studies utilised a ball model generated by Price (2005).

#### 6.3.1 Ball oscillations due to impact

Oscillations induced into the ball due to impacts were studied because they were considered likely to influence the vibrometer measurement. The vibrometer was known to be unable to distinguish between translational, rotational and oscillatory velocity components. Therefore a clear understanding of soccer ball oscillations and

how these would affect measured velocity was required. In order to simulate oscillations of a soccer ball kick, a FE model of a soccer ball impacting a rigid plate at a match realistic translational velocity ( $V_T$ ) was created and executed as shown in Figure 6-4.

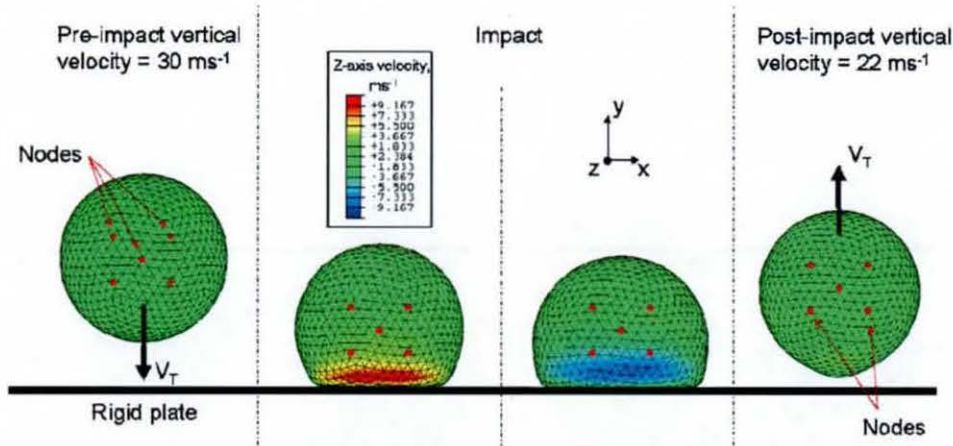
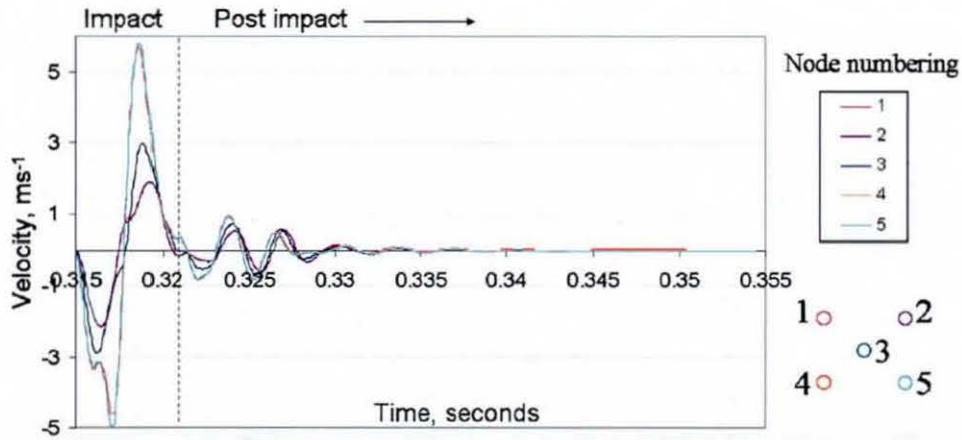


Figure 6-4: Soccer ball pre, during and post impact in FEA model, the contour plots of the balls are shown using z-axis velocity values.

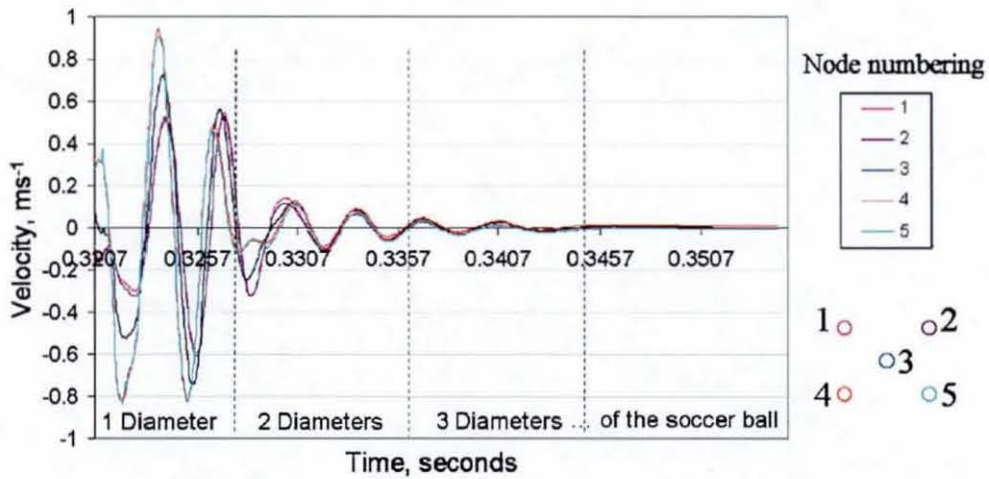
The soccer ball was translated in the y-axis only, out of plane velocity was measured in the z-axis. A measurement node was located centrally on the ball surface with four nodes placed equidistantly around it. These nodes were placed so that computed velocity values could be extracted from these nodes throughout the FEA stage.

Figure 6-5 shows the out of plane velocities for the measured nodes during and post impact. During impact, gross out of plane velocities were achieved due to longitudinal and tangential deformation of the soccer ball. For the purposes of ball launch measurement, it was the post impact velocities that were of relevance.



**Figure 6-5: Impact and post impact out of plane velocities ( $V_z$ ) measured at the nodes.**

Figure 6-6 shows post impact out of plane velocities for the five nodes on the ball. The post impact time was shown in relation to the equivalent number of ball diameters travelled by the ball. Large oscillation velocities were exhibited in the ball immediately post impact, although these were observed to have 'died' down after the ball has travelled approximately three ball diameters.



**Figure 6-6: Post impact out of plane velocities ( $V_z$ ) measured at the nodes.**

The velocity of the nodes were averaged over a 1.7 ms time duration which corresponded to approximately 4 cm of travel, three diameters post impact. The average velocity in the out of plane direction was calculated at  $0.00777 \text{ ms}^{-1}$  (to 3.s.f.). This was a small fraction compared to the measured post impact translational velocity of  $22 \text{ ms}^{-1}$ .

It was important to understand how the Polytec system outputted the measured velocity of a moving target. The Polytec OFV-323 system was able to demodulate measured velocity and output this as a voltage value as shown in Figure 6-7.

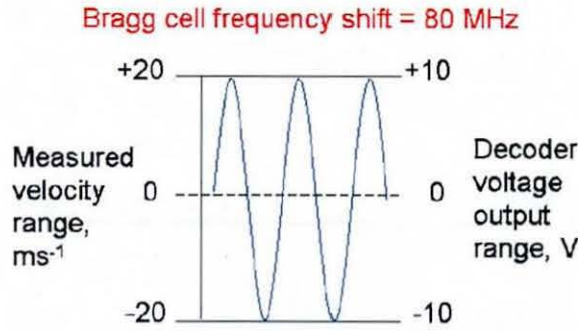


Figure 6-7: OFV-323 vibrometer range.

Due to the Bragg cell shift of 80 MHz, the measured velocity range was symmetrical, and as shown in Figure 6-7, it was  $\pm 20 \text{ ms}^{-1}$ .

It was important to be aware of the velocity difference measured where the spin rate had altered by 1 RPM. Table 6-1 shows the measured velocity recorded by the vibrometer for a 1 RPM difference. The difference in measured velocity was found to be independent of the spin rate.

Table 6-1: Spin rate versus measured vibrometer velocity.

Spin rate, RPM	Measured velocity at radius of 5 cm, $\text{ms}^{-1}$ (to 3.d.p)	Difference in measured velocity, $\text{ms}^{-1}$ (to 3.d.p)
100	0.524	0.005
101	0.529	
300	1.571	0.005
301	1.576	
600	3.142	0.005
601	3.147	

## Laser based tracking and spin measurement

The other factor to account for, was the perpendicular distance of the measurement point from the spin axis. Table 6-2 shows how the change in measurement point position affected the difference in measured velocity between a spin rate of 600 RPM and 601 RPM.

**Table 6-2: Dependence of radius on measured vibrometer velocities.**

Measurement point at radius, cm	Measured velocity at 600 RPM, ms <sup>-1</sup> (to 3.d.p)	Measured velocity at 601 RPM, ms <sup>-1</sup> (to 3.d.p)	Difference in measured velocity, ms <sup>-1</sup> (to 3.d.p)
1	0.628	0.629	0.001
2	1.257	1.259	0.002
3	1.885	1.888	0.003
4	2.513	2.517	0.004
5	3.142	3.147	0.005
6	3.770	3.776	0.006
7	4.398	4.405	0.007
8	5.027	5.035	0.008
9	5.655	5.664	0.009
10	6.283	6.293	0.010

The measured velocity value between a spin rate difference of 1 RPM at a radius of 5 cm was 0.005 ms<sup>-1</sup>, as shown in Table 6-2. This is less than the out of plane velocity of 0.00777 ms<sup>-1</sup> (to 3 significant figures) due to oscillations caused by ball impact, calculated after three ball diameters of ball travel. Therefore approximately 66 cm after impact the vibrometer should be able to distinguish motion from oscillation with a spin rate measurement resolution of  $\pm 1$  RPM. The Polytec decoder displayed 1 ms<sup>-1</sup> per 0.5 V, therefore in order to be able to measure spin rate with resolution of 1 RPM the decoder must be able to measure voltage to 2.5 mV resolution. However as Table 6-2 illustrates, the resolution of spin measurement was also dependent upon the radius at which measurement occurs. An oscillation of 0.00777 ms<sup>-1</sup> (to 3 s.f.) could therefore cause a  $\pm 1$  to 8 RPM resolution in spin measurement, if the radial measurement point was adjusted between 1 and 10 cm, away from the spin axis.



The soccer ball model used in the FEA model had isotropic material properties. In reality it was likely that the oscillations observed, occur and are constrained at the end of the ball where the impact occurs. This was predicted due to the stitching of the ball acting as a structural skeleton, as stated by (Ronkainen and Harland 2006). Therefore it was likely that the resolution stated for spin rate measurement due to oscillations, was a conservative estimation, when measuring the ball three diameters post impact.

### 6.3.2 Velocity contour map of a spinning soccer ball

An out of plane velocity contour map of a spinning ball was generated from the same FE model as used in 6.3.1. Although it was not necessary to use an FE simulator, this was used for convenience to simulate the rigid body motion of a spinning ball.

The ball model was given a rotational velocity about the z-axis, as shown in Figure 6-8.

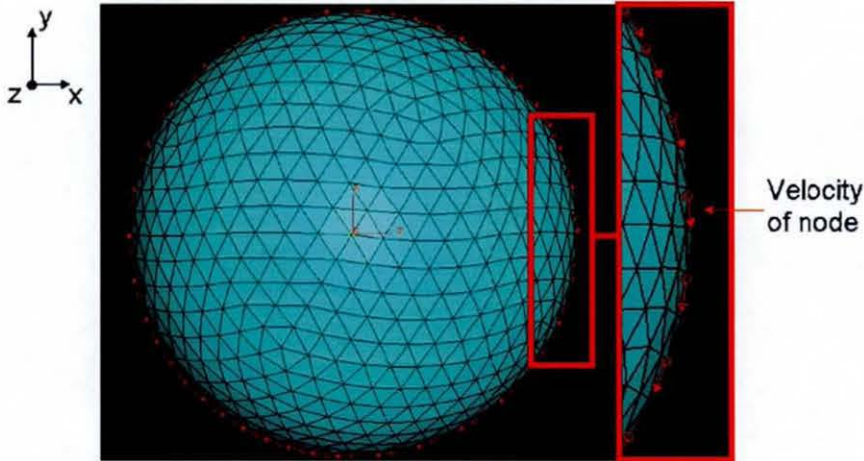


Figure 6-8: Spin loading scenario of FE soccer ball.

In order to simulate a typical spin rate achieved in a soccer game, the nodes were assigned velocity vectors equivalent to a rotational velocity of approximately 600 RPM. The resultant surface velocity plot is shown in Figure 6-9.

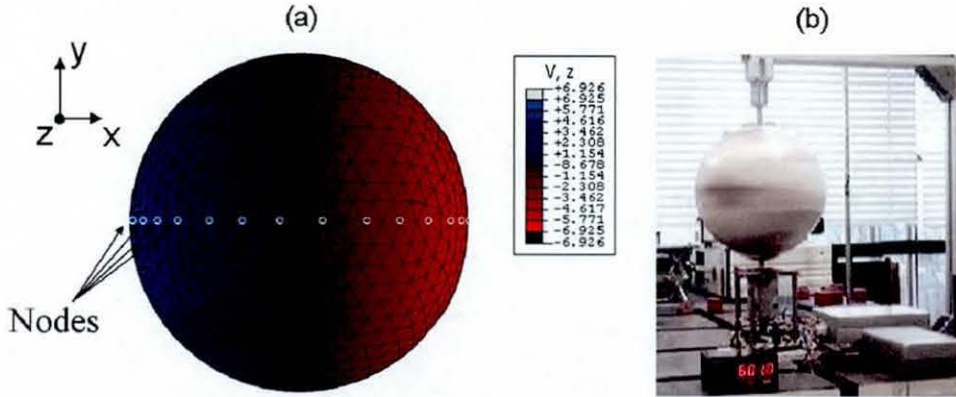


Figure 6-9: Soccer ball spinning at 601 RPM, (a) in the FE model, (b) on the 'spin rig'.

In order to deduce velocity values from the FE model, 14 equally separated nodes were monitored along the periphery of the ball for the duration of the simulation. The model ran for almost one entire revolution. The velocity ( $V_z$ ) for each node for the entirety of the simulation is shown in Figure 6-10. The 'noise' observed in the velocity output at the start of the simulation was due to the initial loading parameters. Each node exhibited sinusoidal behaviour with an amplitude of  $6.923 \text{ ms}^{-1}$ . The out of plane velocities corresponded to a spin rate of 601 RPM, calculated using Equation 6-1 whereby the radius of the ball was fixed at 11 cm.

$$V_z = \omega \times r = 2\pi \times \left( \frac{\text{RPM}}{60} \right) \times r \quad \text{Equation 6-1}$$

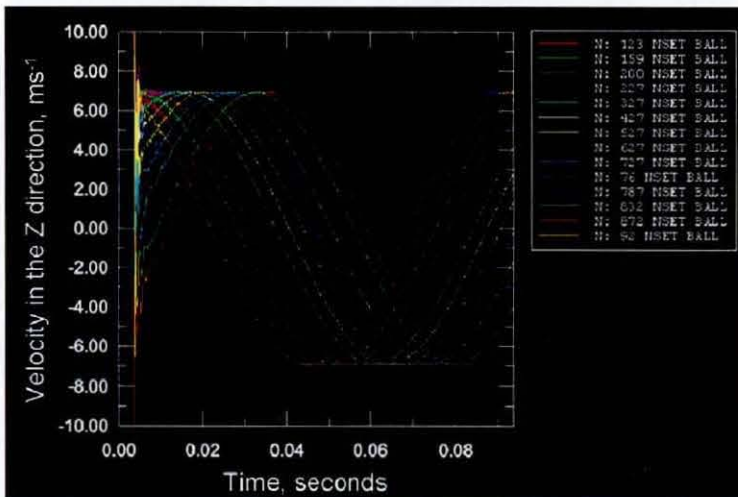


Figure 6-10: Velocity ( $V_z$ ) of the monitored nodes throughout the simulation.

The nodes monitored on the virtual ball were along the 'equator' with respect to the polar spin axis, however as the contour map of the ball shows in Figure 6-9, it is the radial distance away from the spin axis that defines the out of plane velocity, assuming constant spin rate. The FE model of the spinning ball was an excellent way of displaying the holistic velocity contour map of the ball due to the rotational velocity component, set in isolation from translational velocity. From Equation 6-1 it is evident that out of plane velocity can be measured at any position provided the perpendicular distance from the spin axis and the spin rate are known.

#### 6.4 Graphical user interface (GUI) for a virtual vibrometer

The work in 6.3.2 reported a ball with rotational velocity and zero translational velocity. Since the majority of ball sports involve translational and rotational components of ball motion, a linear velocity was also applied to the ball. Ideally the laser vibrometer point would have tracked the ball, however initially a static vibrometer set-up was modelled, to create a basis for further work.

This set-up was modelled in the Matlab environment. A GUI was designed so that the ball parameters could be adjusted accordingly. The initial set-up between the translational velocity ( $V_T$ ) and rotational velocity ( $V_R$ ) of the ball and the vibrometer are shown in Figure 6-11.

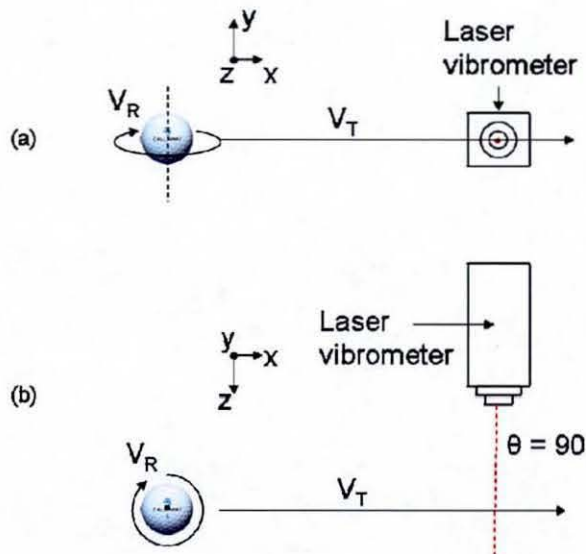


Figure 6-11: Matlab simulated vibrometer set-up, (a) side view, (b) plan view.

## Laser based tracking and spin measurement

The GUI allowed the velocity, spin rate, angle between laser beam and soccer ball direction of travel and the apparent diameter of the ball to be adjusted. The 'calculate' button executed the theoretical calculations in order to display in graphical form the measured velocity that would be recorded by the vibrometer, by plotting time versus measured velocity, as shown in Figure 6-12. The GUI allowed access to a 'virtual vibrometer', the script written for the model is found in Appendix B.

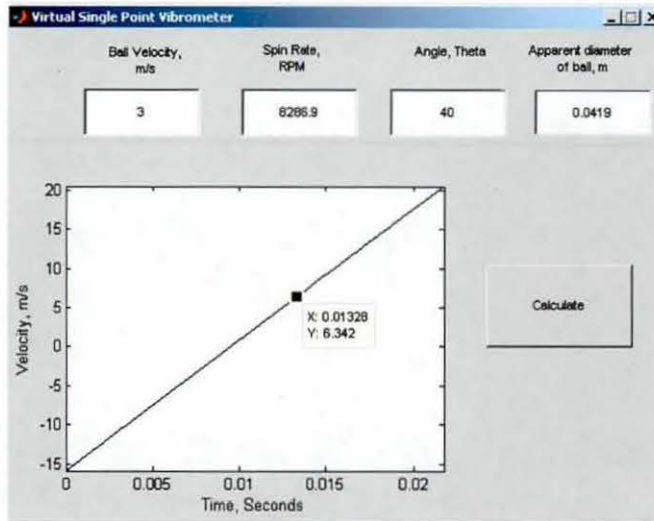


Figure 6-12: GUI for the 'virtual vibrometer'.

In order for the 'virtual vibrometer' to fully simulate an actual vibrometer the velocity measurement was insensitive to target shape. Therefore it was irrelevant whether a soccer ball was measured across a panel or within a stitched region between the panels, the velocity output of the vibrometer was not affected by the change in target shape, assuming that good SNR was retained.

## 6.5 Validation of 'virtual vibrometer'

### 6.5.1 Methodology

In order to validate the 'virtual vibrometer', initial theoretical values were inputted into the GUI model and a 'saw tooth' was outputted as the calculated measurement profile, whereby measurements before and after the ball struck the laser beam, read zero. During contact between laser and ball a line with constant gradient was observed, as shown in Figure 6-13. The sign of the initial velocity peak was

dependent upon the ball spin direction, the 'virtual vibrometer' initially assumed the ball spin to be away from the vibrometer.

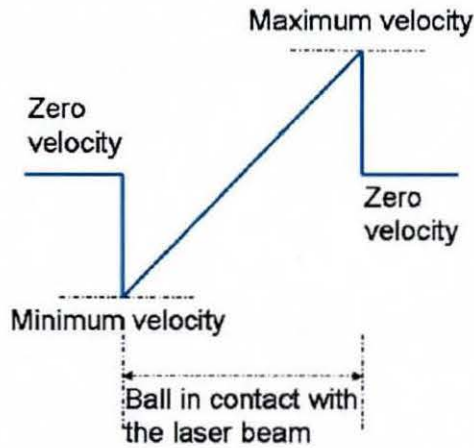


Figure 6-13: Predicted 'saw tooth' velocity profile using the virtual vibrometer.

To carry out the practical vibrometer test a linear actuator rig was utilised to achieve an adjustable translational velocity. To create a known angular velocity a 'Check-GO' golf spin device was used. Ideally the 'spin rig' reported in Chapter 4 would have been used, however the size, height, and cabling did not lend itself to being attached to the linear actuator rig.

The practical testing set-up was identical to the 'virtual vibrometer' set-up depicted in Figure 6-11. The golf ball was covered in retroreflective tape and was permanently mounted onto a runner. The runner was controlled by software to travel between 1 and  $5 \text{ ms}^{-1}$  over a 1.5 metre linear distance. Using an inbuilt position decoder in the linear actuator rig, the velocity of the runner was plotted versus displacement, measured at circa 85 Hz.

It was paramount that alignment between the vibrometer and the golf ball axis of travel was known. Also a marker dot was placed on the golf ball to ensure that every time the laser beam intersected the surface of the golf ball it was across the identical part of the ball, defined by the marker. The angle between vibrometer and golf ball axis of travel was altered whilst maintaining the identical measurement diameter across the ball.

## Laser based tracking and spin measurement

As the angle of the vibrometer was altered, the point at which the ball and laser came into contact changed along the runner path. Therefore in order to negate ramp up/down velocities of the runner the laser vibrometer was moved in the x-axis to maintain a fixed intersection point between the laser beam and ball.

The vibrometer velocity values were measured and recorded using SignalCalc software which captured data via an acquisition system. An internal trigger was set in the software so that measurements were taken without fail. Eight thousand samples were measured at approximately 12 kHz, which allowed pre, during and post contact measurement between the laser beam and ball.

Each time a test was carried out the velocity profile of the runner was stored so that a clear benchmark for golf ball speed existed. The testing was split into three phases and they are reported as follows.

### **6.5.1.1 Test 1**

Test 1 consisted of adjusting the angle of the vibrometer in relation to the golf ball travel direction as well as changing the translational speed of the golf ball. The vibrometer position was placed at four different angles to the ball travel direction at 105°, 90° and 75° depicted in Figure 6-14. The translational speed of the golf ball was adjusted to 1, 3 and 5 ms<sup>-1</sup>. Each test was repeated five times in order to obtain a clearer understanding of the repeatability capabilities of the vibrometer. A total of 60 tests were carried out.

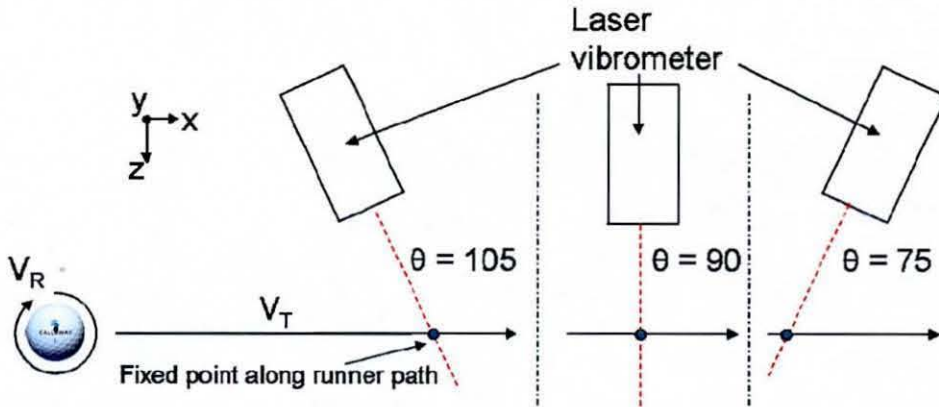


Figure 6-14: Plan view of test 1 set-up for velocity measurement.

The different vibrometer orientations shown in Figure 6-14 would achieve different peak measurement velocities due to the different components of linear and translational velocity present in the measurement. This is illustrated clearly in Figure 6-15.

#### 6.5.1.2 Test 2

The vibrometer was aligned on-axis to the golf ball direction of travel. The purpose of this test was two fold; (1) to confirm the validity of the stated velocities outputted by the linear actuator rig and (2) to procure an understanding for the velocity values measured when the laser beam was not focused on the target throughout measurement.

#### 6.5.1.3 Test 3

The angle ( $\theta$ ) was altered between  $90^\circ$  and  $40^\circ$  in  $10^\circ$  increments. The velocity of the runner was set at  $3 \text{ ms}^{-1}$  because the runner velocity was found to be stable at this speed. A successful measure was carried out at each test angle. Due to the shallower angle between the ball travel direction and the vibrometer, a much larger translational velocity component was present in the measurement.

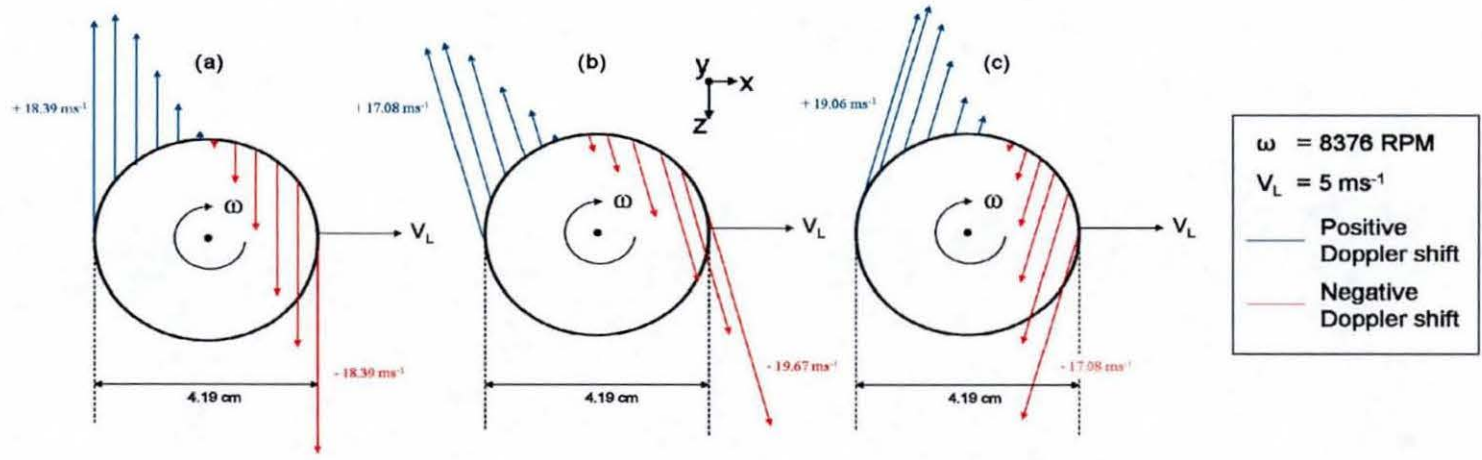


Figure 6-15: Theoretical vibrometer measurement (a)  $\theta = 90$ , (b)  $\theta = 105$ , (c)  $\theta = 75$ .



## 6.5.2 Experimental results

### 6.5.2.1 Test 1

Test 1 proved that it was possible to achieve 'saw tooth' velocity profile measurements from a golf ball with both rotational and translational velocity components. Table 6-3 shows a generic results table obtained from the measured velocity graphs.

**Table 6-3: Vibrometer at 90° to ball travelling at 1 ms<sup>-1</sup>.**

<b>Trial</b>	<b>Contact time between laser and ball, s</b>	<b>Minimum peak velocity, ms<sup>-1</sup></b>	<b>Maximum peak velocity, ms<sup>-1</sup></b>	<b>Modulus difference between maximum &amp; minimum velocities, ms<sup>-1</sup></b>	<b>Modulus average peak velocity, ms<sup>-1</sup></b>
1	0.0417	-17.25	17.38	0.13	17.32
2	0.0422	-18.36	18.35	-0.01	18.36
3	0.0418	-18.76	18.86	0.1	18.81
4	0.0419	-18.17	18.21	0.04	18.19
5	0.0421	-18.86	18.74	-0.12	18.8
<b>Average</b>	<b>0.0419</b>	<b>-18.28</b>	<b>18.31</b>	<b>0.028</b>	<b>18.30</b>

The raw 'saw tooth' profiles show that at the extreme angles of 75° and 105° the peak values measured higher for the positive and negative peaks respectively, as shown in Figure 6-16.

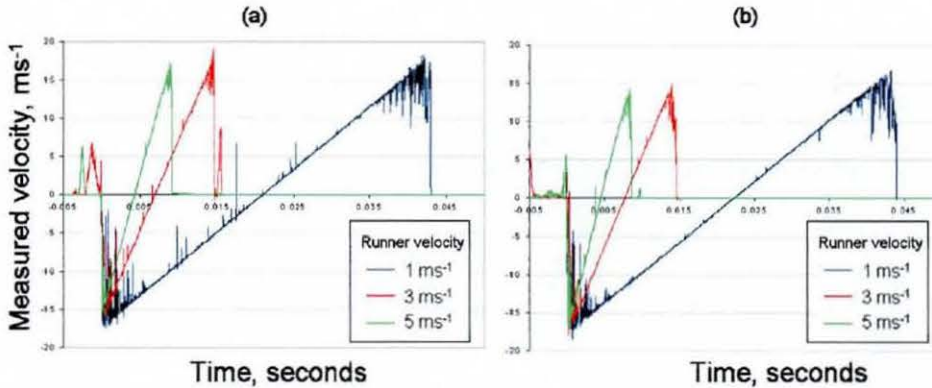


Figure 6-16: Saw tooth profiles, (a) at  $\theta = 75^\circ$ , (b) at  $\theta = 105^\circ$ .

It was important to observe the difference between the modulus of the peak values. This peak velocity modulus difference value, defines at which angle the vibrometer was positioned in relation to the ball travel axis. Unfortunately towards the edge of the ball the vibrometer exhibits poor SNR. The confidence in the identification of peak velocities was therefore difficult and estimates should be used as a guide rather than the definitive value. This method does not currently allow for accurate spin rate measurement, due to the loss of signal at the edge of the ball.

In summary, a constant velocity gradient was achieved in the measurements as expected, however currently there is no method by which to correlate the velocity value to a radial measurement point on the ball, this is why the edge of the ball is critical because the radius of the ball is fixed and therefore a strong SNR measurement across the diameter of the ball would allow for an accurate spin rate calculation.

#### 6.5.2.2 Test 2

The average results for displacement versus velocity are shown in Figure 6-17, which were outputted by the linear actuator position detector. At each runner velocity the test was repeated five times. It was evident that as the velocity was ramped up, the stability of the velocity over the duration of travel was compromised, a longer ramp up/down time was required. The runner velocity at  $5 \text{ ms}^{-1}$  induced larger oscillations in the outputted velocity and was the reason for fixing the runner velocity at  $3 \text{ ms}^{-1}$  for the work in test 3.

Laser based tracking and spin measurement

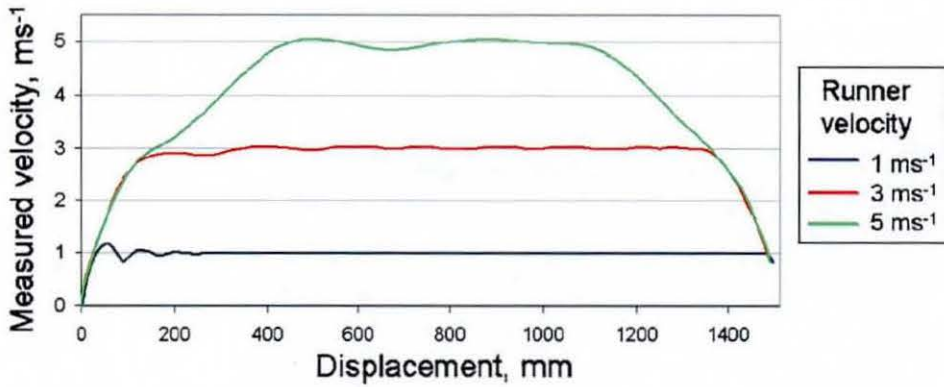


Figure 6-17: Average velocity versus displacement for linear actuator runner.

The corresponding vibrometer velocity measurements are shown in Figure 6-18, each repetition was plotted individually.

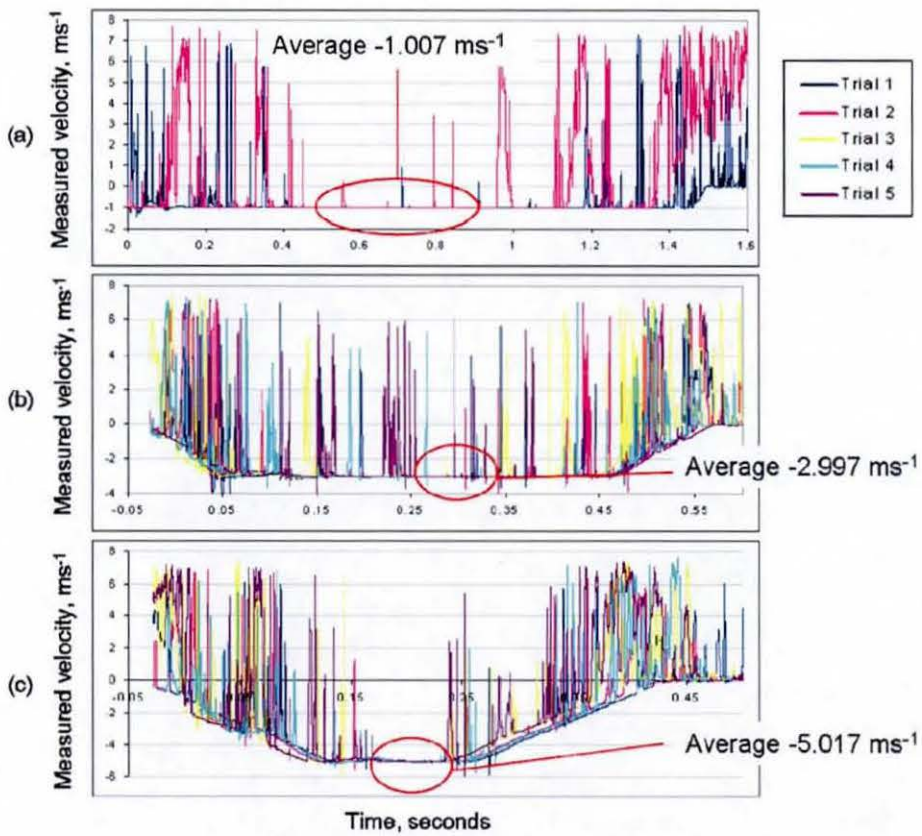


Figure 6-18: On-axis vibrometer velocity measurements to runner moving at, (a)  $1 \text{ ms}^{-1}$ , (b)  $3 \text{ ms}^{-1}$ , (c)  $5 \text{ ms}^{-1}$ .

## Laser based tracking and spin measurement

In each test the runner moved away from the vibrometer, therefore it was not possible to keep the laser focused throughout the complete measurement. The focus was set to optimum when the runner had travelled half of its travel length. By observing the graphs in Figure 6-18 it was clear that the region of fewest signal 'drop-outs' and consequently the best SNR was achieved approximately at 50% of the measurement duration. The SNR was at its weakest during the start and end of the measurement period.

The measured velocity 'spikes' were explained by signal drop out, because empirically it would have been obvious if the runner was actually dramatically adjusting its speed, as shown in Figure 6-18. Due to the nature of vibrometry velocity measurement tended towards infinity during instantaneous signal drop out.

The vibrometer measured on average 1.007, 2.997 and 5.017  $\text{ms}^{-1}$  for the constant maximum velocity of the runner when 1, 3 and 5  $\text{ms}^{-1}$  were outputted as the actuator velocities respectively. Negative Doppler shift was measured, due to the target movement being away from the vibrometer. Strong agreement was therefore found between the outputted linear actuator rig velocity and the measured vibrometer velocity.

### 6.5.2.3 Test 3

The results for Test 3 are depicted in Figure 6-19.

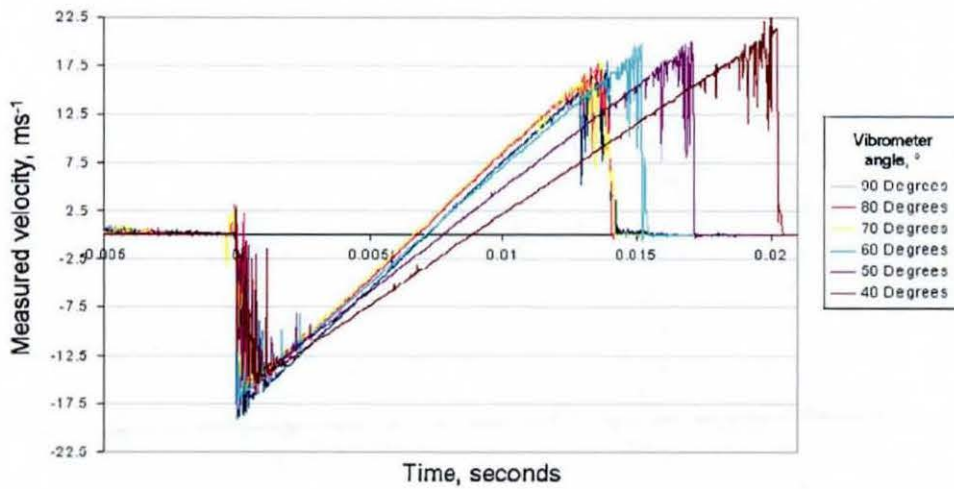


**Figure 6-19: Measured velocity ‘saw tooth’ profiles from  $\theta = 90^\circ$  to  $\theta = 40^\circ$ .**

The results highlight a constant pattern. As  $\theta$  was decreased, the measurement time period and the peak positive velocity values increased, whilst the peak negative velocity decreased. A very notable result from this testing was that when  $\theta$  was  $40^\circ$  the maximum velocity measured (excluding those due to signal drop out) was approximately  $21 \text{ ms}^{-1}$ . This was a significant result because the Polytec manual stated the upper limit for velocity measurement at  $+20 \text{ ms}^{-1}$ .

### 6.6 Comparison of virtual and actual vibrometer velocity measurements

The intersected golf ball diameter was measured to be 4.19 cm (to 2.d.p.). In test 1 the vibrometer was angled at  $90^\circ$  therefore direct correlation of the measurement time to the diameter of the ball was expected when the ball was travelling at  $1 \text{ ms}^{-1}$ . The actual average measurement time was 0.0419 seconds, this correlated perfectly to the virtual measurement time of 0.0419 seconds.

Using Equation 6-1 the virtual maximum and minimum velocity measurements were calculated as  $\pm 18.38 \text{ ms}^{-1}$ , with ball radius of 0.02095 metres and a spin rate of 8376 RPM. The spin rate was obtained through high speed video analysis of the ball spinning on the miniature rig. The miniature ‘spin rig’ was a commercial device sold for golfers to identify and mark the out of balance point of the golf ball. If the vibrometer was aligned perpendicularly, maximum and minimum vibrometer

## Laser based tracking and spin measurement

velocities would exhibit identical magnitude with opposite direction. For actual testing at  $90^\circ$  the average difference between maximum and minimum velocity values was found to be  $0.028 \text{ ms}^{-1}$ , which suggested slight misalignment. The angle ( $\theta$ ) between vibrometer and ball axis of travel was therefore predicted to be slightly below  $90^\circ$  incident angle.

The misalignment would cause a spin rate measurement uncertainty. There are two main factors that were predicted to affect the peak velocity values; (1) the laser spot was focused on the centre of the ball, therefore as the curvature of the ball increases towards the edge of the ball, the laser loses its focus, achieving poor SNR measurement resolution, (2) the ability for the spin device to maintain constant spin rate was questioned since the motor was cheap and not designed for high accuracy spin measurement applications.

The comparison of the virtual and actual vibrometer results showed some very clear differences. The virtual vibrometer exhibited a perfect 'saw tooth' graph whereas the actual vibrometer results showed that as the laser point moved towards the very edge of the ball a decrease in SNR was achieved. The virtual vibrometer achieved nominally higher peak velocity measurements than the actual vibrometer, mainly due to the aforementioned focusing issue. The laser was focused so that a good SNR was achieved during the central part of the ball. It is thought that the actual vibrometer did not achieve a measurement at the very edge of the ball, unlike the virtual vibrometer. Generally even though there were slight differences between the virtual and actual vibrometer results, the virtual vibrometer gave a good representation of the velocity measurements achieved by the actual vibrometer when  $\theta = 90^\circ$ , as shown in Figure 6-20. Where the gradient of both virtual and actual measurements are almost identical.

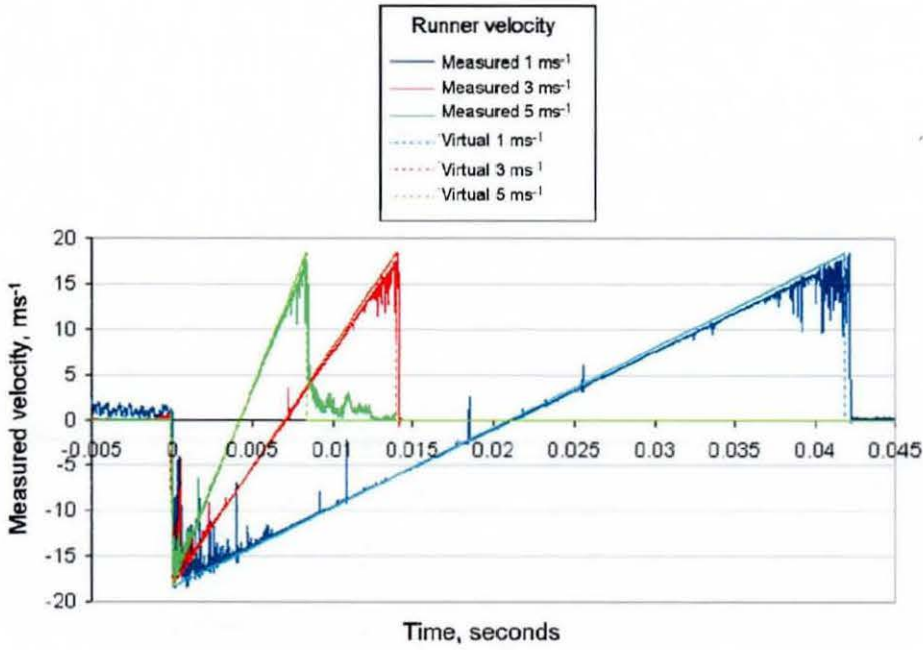


**Figure 6-20: Virtual and measured velocity ‘saw tooth’ profiles, vibrometer perpendicular to ball travel direction.**

As the angle  $\theta$  decreased from  $90^\circ$  towards  $40^\circ$ , test 3 results showed that discrepancies existed between the virtual and actual vibrometer velocity traces, as shown in Figure 6-21. Two main changes were observed as the angle  $\theta$  was reduced. The time period during measurement started to decrease for the actual measurement compared to the theoretical value, at  $\theta=40^\circ$  the measurement time was 1 ms less than the theoretical value. The initial negative peak velocity was less than the theoretical value for almost all the measured tests, thought to be accounted for by slight misalignments in the set-up.

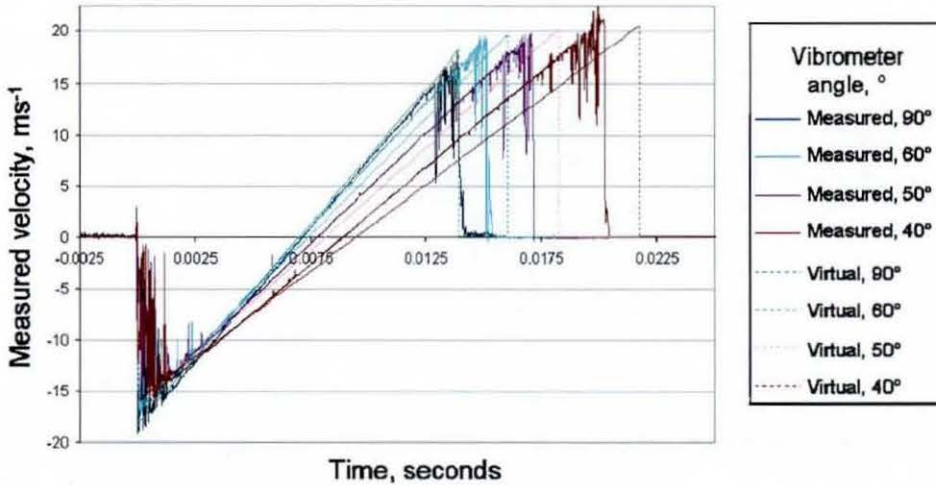


Figure 6-21: Virtual and actual velocity measurement comparison.

## 6.7 Chapter summary

The suitability of laser based measurements for soccer ball launch as opposed to golf ball launch measurement was reported due to the inability of current laser technology to measure the high velocities and spin rates produces in golf. Therefore soccer ball measurements were pursued for the remainder of this thesis.

Impact and spin simulations were both shown to influence vibrometer measurements. It was concluded that for soccer ball launch, measurements should only be initiated once the ball has travelled three ball diameters after impact, so that surface velocities due to oscillations have died down. Spin rate was shown to directly influence measured vibrometer readings and the velocity measured was related to the radial distance between the spin axis and laser measurement point and the magnitude of the spin.

A virtual vibrometer was created that allowed velocity output for adjustable translational and rotational ball conditions. Actual testing was carried out to validate the virtual vibrometer. When the vibrometer was positioned at 90° to the ball travel direction agreement was found between the virtual and actual vibrometer except at the start and end of the measurement duration. This was accounted due to the poor SNR of the actual vibrometer towards the edge of the ball. Therefore vibrometer



## Laser based tracking and spin measurement

measurements towards the edge of the ball were not advised in further work with current vibrometer technology.

# 7 Laser tracking

## 7.1 Chapter overview

The purpose of this Chapter was to design, manufacture and develop an optical system that can objectively track a non-marked soccer ball. The developed device was called the novel laser tracking system (NLTS) and demonstrated to operate successfully when the ball was moved by hand as well as using actual player testing. The use of the NLTS as a launch monitor was also demonstrated.

## 7.2 System Concept

The designs and systems described in chapter 2.6 were reviewed fully in order to aid brainstorming for the NLTS. The concept of the work by Castellini and Tomasini (2002) whereby a single point vibrometer and high speed camera were aligned to have an identical optical axis, was taken as a premise for this work. The tracking method was based on the concept used by Perrin *et al.* 2003 & 2004 whereby movement of the target within the FOV was monitored and mitigated through the repositioning of two orthogonal mirrors in a continuous feedback loop.

Within the sports industry no HSV tracking systems have been reported, therefore technology utilised in other industries was considered. A system called Trajectory Tracker (TT) developed by Specialised Imaging, was found to represent state of the art, within the military industry, costing ~£100k.

TT operated by incorporating HSV technology with a purpose built oval mirror which could be rotated at high velocities, through 100° of rotation, around a fixed axis. This allowed the imaged FOV to change in time.

TT has been demonstrated to be useful for military applications, by allowing missile visualisation throughout flight using a predictive monitoring system, in order to view

## Laser based tracking and spin measurement

and evaluate failure modes. The system was not considered suitable for sports applications because sports ball flight paths have been reported as parabolic in nature. TT allowed only linear movement paths to be monitored. The predictive monitoring meant that no onboard search algorithms were used in order to locate the missile of interest. Therefore the likely problem encountered with TT was that it had no method of adjusting to flight paths that were not predicted correctly.

The TT system provided a useful benchmark for current HSV monitoring systems, and was proven to predictably monitor soccer balls that were struck with a shallow launch angle, as shown in Figure 7-1. For the purposes of sports ball applications one scanning mirror was found to provide an unsatisfactory measurement envelope. In order to track an arbitrarily moving ball in real time, the system would benefit from a closed loop controller. Therefore feedback could be provided, in order to ensure the target was being tracked.

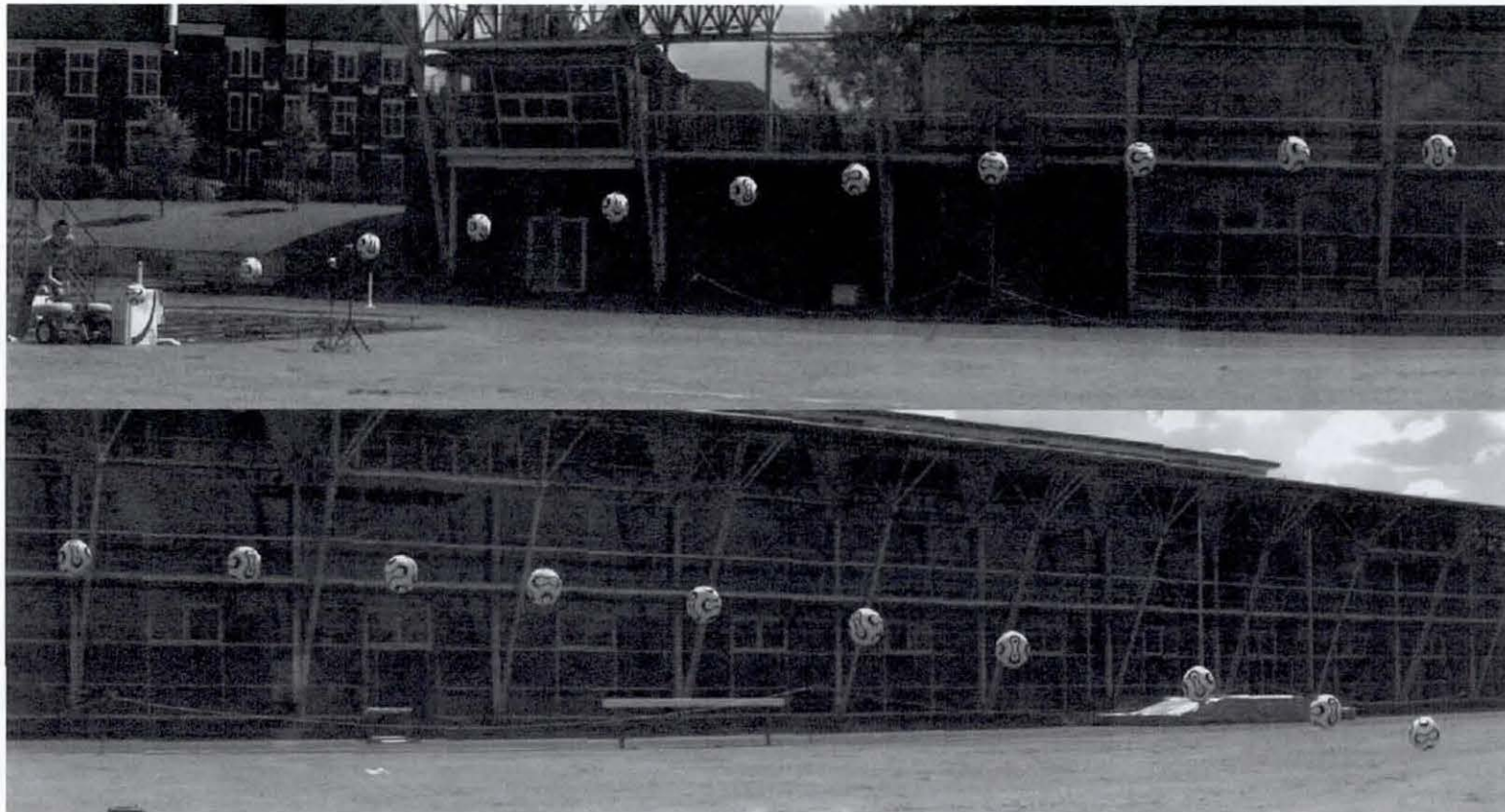


**Figure 7-1: Composite image of soccer ball in flight, using Trajectory Tracker (image resolution of  $1024 \times 1024$  pixels, captured at 1000 FPS and 1/1000 shutter speed).**

### 7.3 Hardware

In order to create the NLTS, careful attention was given to the implemented hardware. The system as a whole required that components complemented one another, therefore components were not selected in isolation. The core laser tracking system components are shown in Figure 7-2 and gives the reader a clear outline of the components selected for the NLTS.

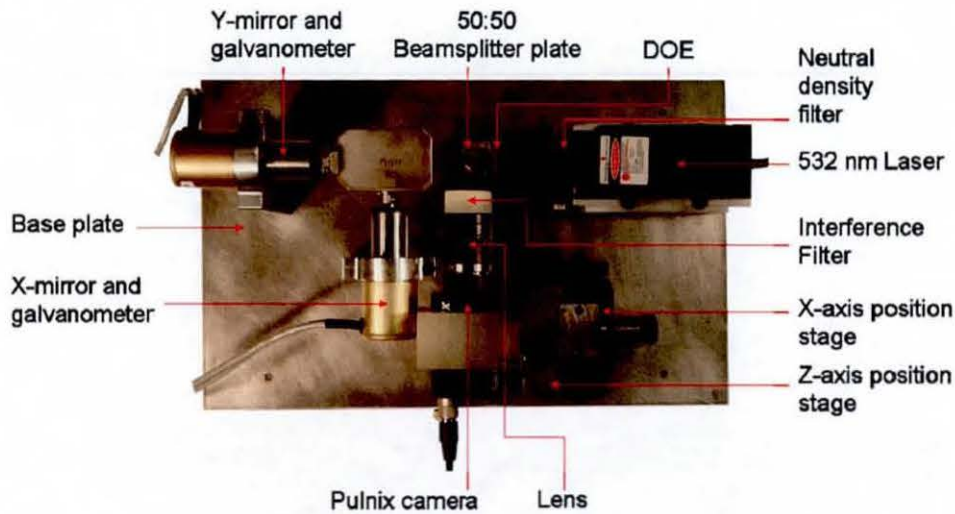


Figure 7-2: Plan view of core laser tracking system components.

The NLTS could have been created using other hardware choices; therefore justification for the selection of each component is given.

#### 7.3.1 Image Acquisition

##### 7.3.1.1 Camera

The chosen camera for the NLTS, following a critical thinking path, was the JAI Pulnix TM-6740GE. The first option regarding camera selection was whether to choose a monochrome or colour camera. Generally it has been reported that monochrome cameras have better SNR ratio, better contrast, increased resolution, reduced cost and do not suffer from chromatic aberration (Dougherty 2007). For the purpose of the NLTS the more monolithic the image transferred to the PC, the faster the image processing could be completed. Filtering techniques have advanced whereby isolation of single wavelengths of colour is deemed a basic task, therefore

## Laser based tracking and spin measurement

the need for a colour camera was not justified. All the research suggested that a monochrome camera was more beneficial than a colour counterpart.

The NLTS was designed to capture images of a rapidly moving target, therefore a progressive area scan camera was chosen, to prevent the combing effect, by capturing a full image in a single shot.

The camera interface was crucial for the selected camera. The PC used for the tracking system worked on a 32 bit PCI bus architecture, limiting maximum bandwidth for data transfer at  $132 \text{ Mbs}^{-1}$  (Wilson 2006). Several camera interfaces were considered such as Camera Link, USB, FireWire and Gigabit Ethernet (GigE), however recent trends indicated GigE connection was coming to the forefront of machine vision applications, so this was selected. GigE permitted the fastest connection, as shown in Table 7-1, without the need for a frame grabber card (Williamson 2006). The chosen Pulnix camera had a maximum data transfer rate of  $62 \text{ Mbs}^{-1}$ , well within the capacity of the PCI bus, leaving available transfer bandwidth, for updating the galvanometer controllers. The camera was set to output 8-bit data, which outputted pixels with 256 grey level values.

**Table 7-1: Bandwidth of typical machine vision interfaces, adapted from (Levis 2006).**

Interface	Bandwidth ( $\text{Mbs}^{-1}$ )
IEEE-1394a (FireWire)	50
IEEE-1394b (FireWire)	100
Camera Link	400
GigE	125
USB 2.0	60
PCI Bus	125
PCI-X Bus	4300

The technology available in the vision chip was either CCD or CMOS technology. The price for both technologies was found to be very similar. At present however CCD technology was reported as being far more sensitive than its CMOS counterpart,

therefore Wány (2007) maintains for machine vision applications, CCD imagers remain the detector of choice.

The resolution of the camera is critical and this is directly related to the frame rate at which the camera operates. A global review of GigE cameras was carried out in Vision Systems Design (Wilson 2007a). The ideal camera based on a high frame rate, combined with large pixel resolution, was the chosen Pulnix camera. The camera can record at VGA (640 horizontal  $\times$  480 vertical pixels) resolution, capturing at 200 FPS. Another decisive feature of the camera is the shutter capability. High shutter rate is required in order to view a target sports ball as close to static as possible, during flight. The Pulnix camera allowed a maximal electronic shutter rate of 1/64,000 of a second.

It was advantageous to obtain a camera with an onboard field programmable gate array (FPGA). This allowed the camera to have certain settings stored in 'hard' memory. The Pulnix camera allowed the shutter control, gain control, look up table (LUT) and scanning mode selection to be pre-programmed, using the FPGA. The scanning mode selection known as 'binning' allowed the camera to merge horizontal and/or vertical pixels together, before the image was transferred into the host PC. This permitted reduction in the central processing unit (CPU) requirement, providing the image processing task with a smaller image size, if required. Table 7-2 shows how using the same scan area, different images could be outputted by the camera, highlighting the value of the 'binning' function. The Pulnix camera could be set to operate in four different scan area modes, in combination with eight different binning modes.

Table 7-2: Pulnix camera 'binning' mode.

Binning mode	Scan area (A = 640 × 480 pixels)	Active pixels	Maximum camera frame rate, FPS	Image size, kilobytes
No binning	A	640 × 480	200	307.2
1 × 2	A	640 × 240	400	153.6
1 × 4	A	640 × 120	712	76.8
2 × 1	A	320 × 480	200	153.6
2 × 2	A	320 × 240	400	76.8
2 × 4	A	320 × 120	712	38.4
4 × 1	A	160 × 480	200	76.8
4 × 2	A	160 × 240	400	38.4
4 × 4	A	160 × 120	712	19.2

By analysing Table 7-2 it was possible to realise that the CCD sensor operates using a horizontal readout register, therefore the maximum frame rate of the camera was dependent upon the number of vertical pixels rather than the horizontal pixels. The actual setting chosen had to be a compromise between image resolution, the frame rate at which the system must operate, and the size of the inputted image for analysis. Therefore the binning mode, 2×2, was selected in order to output an image with resolution of 320 × 240 pixels. Important camera settings selected for the NLTS are shown in Appendix C.

The camera was packaged in a miniature rugged housing, weighing 194 grams. It was important for the camera to be compact so that it could be closely housed with other components. The sensor was 3.6 mm × 4.8 mm (1/3 inch) in size and each pixel was 7.4 × 7.4 μm in physical size.

### 7.3.1.2 Connector

Numerous network interface cards (NIC) existed that would allow data transfer between the camera and PC. The NIC selected was the Intel 82541PI because the Pulnix camera was specifically designed to interface with this card. This guaranteed transfer at the full potential of the GigE connection, at 125 Mbs<sup>-1</sup>.



### 7.3.1.3 Lens

The chosen lens for the laser tracking system was the c-mount Tamron 6.6 mm × 8.8 mm (2/3 inch) 25mm F/1.4 model. The lens permitted light onto the whole area of the camera sensor array. According to Equation 7-1 the 25 mm focal length of the camera allowed a FOV of 32.6 cm × 24.5 cm at a 170 cm stand off distance. The object size ( $O_s$ ), the working distance ( $W_D$ ), the focal length ( $f_L$ ) and the image sensor size ( $I_s$ ) were all measured in millimetres. This ensured that the camera FOV was small at the x and y-mirrors, 1.4 × 1.9 cm and 1.9 × 2.5 cm at their 10 and 13 cm stand off distances respectively. This allowed the camera to 'see' through the mirrors. The lens allowed manual adjustment of the focus and aperture, with locking screws to fix the settings.

$$O_s = \frac{W_D \times I_s}{f_L} \quad \text{Equation 7-1}$$

### 7.3.1.4 Interference filter

With previous work image processing tasks have been made difficult with changing background conditions, and having similar items in the FOV that the camera is trying to detect, e.g. multiple soccer balls in view.

Therefore in order to make this system adaptive to changing ambient and natural lighting conditions, an interference filter was positioned in front of the camera lens. The filter eliminated the intensity of unwanted light, allowing the image processing task to be carried out more effectively, based only on laser light. The interference filter was important since the Pulnix camera could image visible and infrared light in the range 375 to 1000 nm.

The interference filter simplified the image processing stage, since the camera only imaged the laser pattern, the visible image was monolithic in nature allowing for quick and simple image processing tasks, as shown in Figure 7-3.

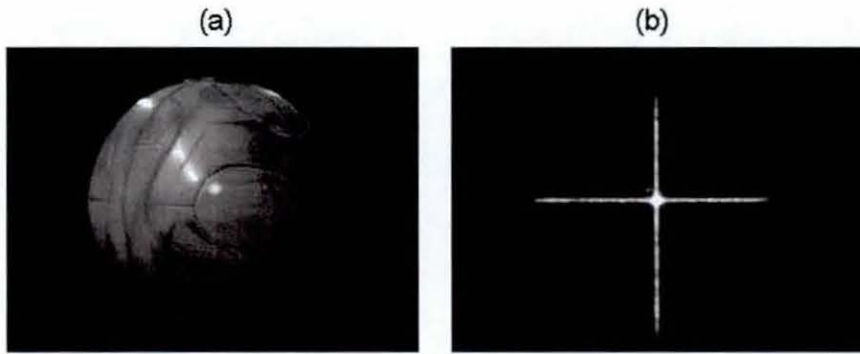


Figure 7-3: Pulnix camera snapshots,  
(a) standard image capture, (b) interference filter ( $\lambda = 530 \text{ nm}$ ) in front of lens.

### 7.3.2 Light source and alignment

#### 7.3.2.1 The laser

A 532 nm wavelength diode pumped solid state (DPSS) laser was selected to provide 300 mW of CW light. The NLTS set-up required the laser for illumination purposes only, therefore the lasers detailed in Chapter 2 were unnecessarily complex and expensive. The wavelength chosen for the laser was influenced by two main factors; (1) cost and (2) quantum efficiency. Quantum efficiency is defined as the percentage of photons hitting a photo reactive surface that will produce an electron-whole pair. Traditionally lasers have been manufactured at red wavelengths, due to the simplicity of making laser light at this wavelength, as a consequence of research and development the cheapest lasers found on the market, fall into this category. Observing Figure 7-4 it was noticeable that the quantum efficiency of the Pulnix camera was approximately half at red wavelengths, compared to blue and green wavelengths of light. Generally with CCD or CMOS cameras the quantum efficiency was reported as maximum at about 550 nm (Wilson 2007b).

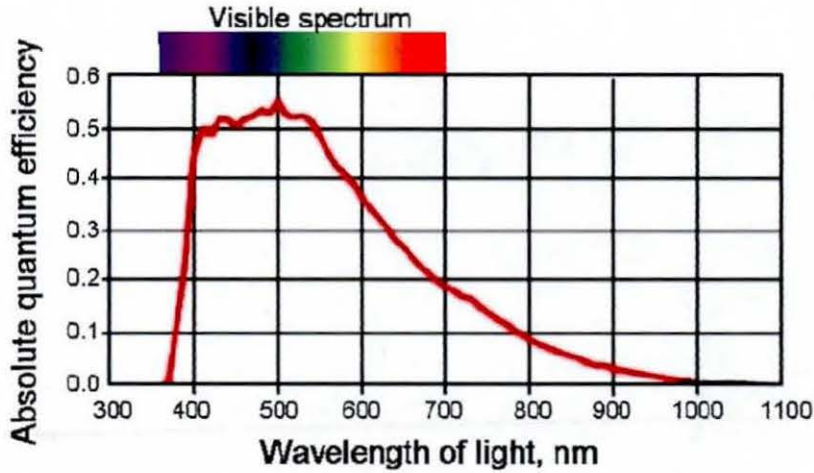


Figure 7-4: The absolute quantum efficiency of the Pulnix TM-6740GE camera.

Quantum efficiency at blue and green wavelengths was very similar for the Pulnix camera. With current laser technology, blue light can not be achieved via a cheap laser diode, since complex and expensive optics are required. Table 7-3 displays a cost comparison of identical power DPSS lasers, available through a UK supplier.

Table 7-3: Price comparison of equal power diode pumped laser sources (Scitec 2007).

Laser source	Cost, £
100 mW DPSS 660 nm (Red)	113
100 mW DPSS 532 nm (Green)	332
100 mW DPSS 473 nm (Blue)	1509

The chosen laser was comparably ‘cheap’, however it still possessed many of the desirable attributes associated with laser light. The laser had a good beam quality with a collimated beam diverging less than 1.5 milliradians, with beam diameter less than 1.5 mm. The laser was mounted within a completely self contained unit which was thermoelectrically cooled to allow the laser to work in CW mode at temperatures between 10 to 30°C. A pulsed system would require less energy to operate however synchronising the laser output with the image acquisition would have been problematic and required additional complication in the system design.

The output power stability of the laser source was critical because this directly influenced the irradiance of the laser beam. In order to keep the image processing consistent, it was imperative that the irradiance of the laser remained consistent throughout tracking. A power stability of within 5% of the set value was desired over a four hour period. As a general guide the more stable the laser power source, the higher the cost of the laser unit.

#### **7.3.2.2 Diffractive Optical Element (DOE)**

A DOE is a passive component which allows an input laser beam to be modified into a desired beam shape. The component redirects light to a set of pre defined positions working on the principle of diffraction. Complex illumination patterns could be generated, which in the past would have required complex optical set-ups, some of which were not readily available. Since the DOE relies on diffraction the component must be tuned to the input laser beam wavelength. DOEs require low maintenance and are highly efficient, Laser Optical Engineering claimed that their components have a diffraction efficiency of over 90% (LOE 2007a).

The industry for diffractive optical elements (DOE), also known as computer generated holograms, is a relatively new and specialist field. Worldwide there are few manufacturers and prices of these parts fluctuate greatly. Quotes for a single purpose built DOE ranged from £600 (LOE 2007b) up to £12 500 (DOC 2006).

A number of sample DOEs were purchased for the laser tracking application, since these were comparatively inexpensive and allowed the laser beam to be shaped into varying illumination patterns, as shown in Figure 7-5. The size of each diffractive optic was 10 × 10 mm. The diffractive optics were manufactured from acrylate, mounted on rectangular glass substrates. More powerful laser beams would have required the manufactured diffractive pattern to consist of silica rather than acrylate.

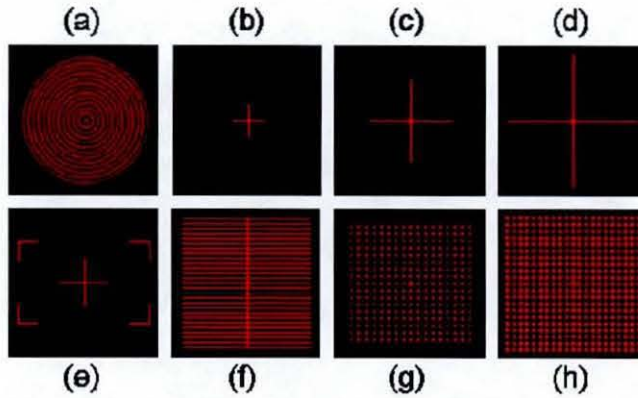


Figure 7-5: Purchased sample DOE illumination patterns.

The DOE chosen for the tracking application is shown in Figure 7-5 (c). The illuminated ‘cross’ pattern emitted light at a cone angle of  $30^\circ$ . The DOE was designed for an input laser beam of 630 nm wavelength, therefore the zero order was brighter and the illuminated projection angle was shallower than specified, using the chosen 532 nm wavelength laser. The zero order was defined as the central ‘bright’ component of the emerging illumination pattern.

### 7.3.2.3 Beam splitter and mirrors

In order to align the camera and laser both must be perpendicular to each other, facing the same mirror which is at a  $45^\circ$  angle to both camera and laser. A plate beamsplitter with a 50:50 ratio of reflected to transmitted light was used in the design. This was preferred to a cube beam splitter since it did not distort the camera FOV. The major drawback with the beamsplitter arrangement was that only  $\sim 25\%$  of the original laser light was detected at the camera sensor, due to the dual pass design. For the specified arrangement a  $90^\circ$  plate polarizing beamsplitter would allow  $\sim 50\%$  of the original plane polarized laser light to travel to the camera, as shown in Figure 7-6. This would have been achieved by passing the initially polarized light through the beamsplitter plate, and using the same plate to reflect  $\sim 50\%$  of the irradiance of the randomly polarized, backscattered light. However since the cost of a 2.54 cm (one inch) diameter  $90^\circ$  plate polarizer was circa £500, it was considered unjustifiable.

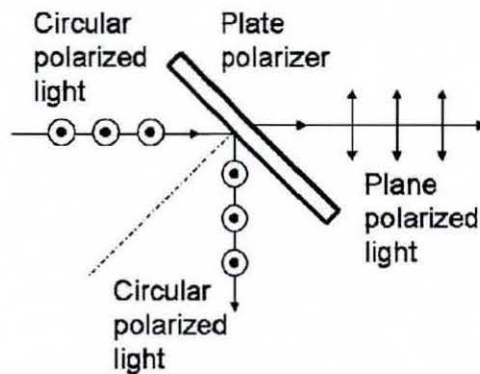


Figure 7-6: 90° plate polarizer.

Castellini and Tomasini (2002) used a dielectric mirror to align the camera and laser. Dielectric mirrors allow ultra high reflectivity over a narrow range of wavelengths, this would be ideal for efficient laser energy transfer at the mirror. This however would not allow the camera to image the desired bandwidth of light, because it would be reflected at the mirror away from the camera. Therefore the dielectric mirror was not suitable for the NLTS application.

### 7.3.3 The scanning system

A galvanometer based laser positioning system was reviewed in 2.6.4 allowing sub millisecond movements with microradian positioning accuracy. The 'galvo' consisted of three main components, the mirrors, the galvanometers and the servo controllers. This galvo set-up was chosen as the only dynamic part of the NLTS, this allowed the laser beam to be steered precisely towards the target. The galvo system was chosen because of the speed and accuracy with which the mirrors could be moved at a reasonable cost.

All three galvo components are documented in detail as well as the DAQ card used to drive the analogue input signal into the servo controllers.

#### 7.3.3.1 Mirrors

The mirrors were required to steer the laser and camera axis towards the ball being tracked, at high speed and resolution. The mirrors were also required to direct the entire laser illumination pattern projected from the DOE, therefore the larger the mirror aperture the greater the potential stand off distance between the DOE and the

scanning mirrors. The mirrors were chosen with a 30 mm clear aperture made from relatively inexpensive fused silica. Larger mirrors manufactured from beryllium were available, which provided a higher stiffness-to-weight ratio. These larger mirrors however were extremely expensive and therefore not considered for this application.

The profile of the mirrors was optimised by the manufacturer in order to provide a lower inertia for the system, allowing the mirrors to be manoeuvred at fast speeds. A notch filter was applied to the galvos in order to compensate for the natural resonant frequency of the mirrors. It was important that the mirrors were tuned as a pair for optimal operation.

There was a fixed stand off distance between the axes of rotation between the mirrors, the second mirror was designed and manufactured larger than the first. This was because the first mirror was capable of steering the laser beam at angles of up to  $\pm 20^\circ$ , therefore the FOV imaged by the camera and the projected laser illumination were able to strike the second mirror. The mirrors were simulated in a virtual environment in order to position the mirrors as close to each other as possible, without contacting each other, at the extreme angular positions. For the optimisation of the system it was important that the mirrors were placed physically as close as possible.

### **7.3.3.2 Galvanometers**

The galvanometer consisted of two parts; (1) the actuator that manipulated the mirror load and (2) a position detector that provided the mirror position to the galvo controllers. The galvanometer allowed a high torque transmittance to the mirrors whilst consuming a relatively small amount of power. The galvanometers chosen utilised a moving magnet actuator whereby the magnet was part of the rotor and the coil was part of the stator for driving the mirrors. The position detector was based on a radio frequency capacitive device which measured the position of the galvo actuator and mirror. The galvanometers provided low drift, noise reduction and linear dynamic performance.

### **7.3.3.3 Controllers**

Each galvanometer required a servo driver controller, which took the form of an efficient closed loop system that demodulated the position detector's current output

signal, performed a comparison between this signal and the commanded position signal and adjusted the actuator until the signals were unity.

The controllers purchased could be tuned for either speed or accuracy. The controllers chosen were tuned for speed due to the demands of the application and the fact that 20 micro radian resolution of mirror position could still be achieved. This selection provided a system that could carry out a large signal step (-3 V to +3 V) in 6.5 ms as opposed to 13 ms. Two choices existed for the speed tuned controllers; (1) Optimisation for small input signals, specifically designed for packaging type applications whereby text is printed onto labels, (2) Optimisation for large input signals. The laser tracking task observed transient events occurring across the system FOV, therefore the controllers were tuned for large input signal steps.

#### **7.3.3.4 DAQ card**

The selected card for the system was the DAQ-2501 series high performance analogue output multi-function card. The card was designed to work with a 32-bit PCI bus interface, allowing output at up to 1 MSs<sup>-1</sup> simultaneously for four analogue output channels, at 12 bit resolution. The output range was bipolar which was required to control the galvanometer mirrors, for a maximal output step (-10V to +10V) the settling time was stated as 3  $\mu$ s. This card possessed extra functions which were not required, however from a cost point of view it was considered the best card available to output the two required analogue channels. The card was connected to a screw terminal panel which allowed an interface for the analogue output channels.

The galvanometers required an input voltage between -3V to +3V, therefore a voltage conversion circuit was inserted between the DAQ card and the galvo servo controllers, to reduce the maximum card output range from -10 V to +10V to -3 V to + 3V.

#### **7.3.4 Operating system**

The NLTS was controlled through a PC. The PC was installed with 3.25 Gb of random access memory (RAM), consisted of a 2.8 GHz dual core Zeon processor, operating a 32 bit PCI bus functioning in the Windows XP environment.



## **7.4 Software**

The selection of software for the tracking system was influenced by current in-house availability and recommendations. The main criterion for the software was the ability to create a working real time image processing platform, which immediately made the use of Matlab and Image Pro Plus obsolete.

### **7.4.1 Common Vision Blox**

The software selected to perform the image processing was Common Vision Blox (CVB) developed by Stemmer Imaging. CVB was a modular software platform for development and implementation of image processing tasks with real-time capability. CVB supported a wide variety of standard cameras including the Pulnix TM-6740GE. CVB allowed all the image processing tools to be implemented as dynamically linked libraries (DLL), which allowed the integration with other software. CVB was designed to work on a variety of windows operating systems including Windows XP.

CVB allowed programming in two main types of environment. The chosen environment was a common high level language compiler. This allowed a wide variety of programming languages to be used.

### **7.4.2 Microsoft Visual Studio .NET**

The software used to run the CVB image processing tools was the 2003 version of Microsoft Visual Studio .NET. The .NET framework was designed for writing internet, web and windows applications. The framework allowed classes to be defined as language neutral, therefore most programming languages could be used. VB.NET was chosen as the language to write the code, since this was released in conjunction with and was able to use all the classes in the .NET framework.

The language neutrality of the .NET framework was achieved via a common languages specification. The framework was designed to work with DLL and therefore the CVB image processing tools could be effortlessly added into the VB.NET code. The .NET framework was designed to run efficiently in Windows, which allowed for a real time software platform.

### **7.4.3 Coyote Application**

The Coyote application software allowed integration between the Pulnix camera and the image processing algorithms. The software was an executable code based on DLL, which allowed for easy implementation into the VB.NET code.

The software acted as a bidirectional conversion device. It could grab image data from the camera and deliver control signals to the camera. The software allowed the camera connections to be set-up as well as configuring all the acquisition parameters of the camera. The onboard camera FPGA, was therefore programmed through the Coyote software.

## **7.5 System Design**

The design of the physical layout of the system was deemed very important, the design was to be in as small an envelope as possible and ideally the whole system should be encapsulated into one large scanning head.

### **7.5.1 The build**

The main components of the system were all placed on one base plate 40 × 25 cm in size, as shown previously in Figure 7-2.

The y-mirror, 50:50 beam splitter plate, the DOE, and the laser were all aligned parallel to the top of the base plate. The camera and 50:50 beam splitter plate were aligned parallel to the side of the base plate. The centre of the x-mirror was perpendicularly aligned from the base plate with the centre of the y-mirror.

In order for the camera to 'see' through the x and y-mirrors the camera could not be placed further than 10 cm in optical travel distance, from the x-mirror.

The DOE had a stated full pattern angle of 30° for red laser light ( $\lambda = 635$  nm). The pattern angle was measured at 25° using green laser light ( $\lambda = 532$  nm). Therefore in order to transmit the whole laser cross through the mirrors the stand off distance between the DOE and x-mirror had to be less than 6 cm. This was not physically possible with the set-up, shown in Figure 7-2, therefore the stand off distance was

fixed at 8.3 cm. This led to 'wasted' laser light, due to some laser light not striking the x and y-mirrors. The issue of 'wasted' laser light could have been resolved by creating a DOE that had a full pattern angle of  $\sim 17.5^\circ$ , which would have allowed all of the diverged 'cross' laser light to travel through the x and y-mirrors.

### **7.5.2 Alignment**

For the system to work effectively it was crucial that the camera and laser beam were perpendicular to each other, allowing the laser beam to be parallel and co-axial at the target to the camera axis, thus allowing both the camera and laser to have an identical optical axis at the target.

The initial setup time for aligning the system could take between 10 to 20 minutes, however once alignment was achieved, the camera was fixed into position. It was interesting to note with the aligned set-up, that the centre pixel of the camera did not correlate with the physical centre point of the camera lens.

### **7.5.3 Costs**

It was important to record the cost of each component used, in the NLTS build. If the system were to be developed into a commercial product the cost would become a vital factor. Table 7-4 shows the itemised cost of each component used. The total of £8.6k gives a clear indication of the outlay to provide the functioning prototype NLTS, however with further development it would be possible to reduce costs substantially. In contrast to improve system functionality some components such as the DOE would require further development time and money.

**Table 7-4: Itemised cost of the NLTS.**

Category	Item	Cost, £
Image acquisition	Pulnix TM-6740GE camera	1900
	Stabilised power supply	35
	Tamron 25mm lens	130
	GE desktop adapter card	62
	Interference filter ( $\lambda = 532$ nm)	61
Lighting and alignment	532 nm DPSS laser	332
	50:50 Beam splitter plate	27
	Disc magnets	10
	Neutral density filter	31
	Cross pattern DOE	32
	Metal base plate and fixings	145
Scanning system	×2 M3S galvanometers	1000
	×2 MiniSax servo drivers	640
	X and Y-mirrors	665
	Speed tune and notch filter	53
	± 15 V Power supply	350
	DAQ 2501 card	420
	Screw terminal panel	70
Operating system	3.25 GB Ram, 2.8 Ghz, PC	2000
Software	Common Vision Blox (Foundation)	650
<b>TOTAL :-</b>		<b>8613</b>

## 7.6 Soccer ball tracking application

This section reports the image processing algorithms required to make the system track in real-time, reporting two practical demonstrations of soccer ball tracking; (1) human moving the ball by hand and (2) soccer player carrying out different juggling

skills. The system was also programmed to act as a launch monitor, capable of measuring launch velocity and launch angle.

### 7.6.1 Image processing

The image processing was reliant on the laser and camera having an identical optical axis. The raw image captured by the camera, shown in Figure 7-7 (a&b), was transferred directly into the LUT algorithm whereby a fixed threshold value was used to create a binary image, as shown in Figure 7-7 (c&d). The LUT allowed predefined values stored in memory to be retrieved extremely quickly. The fixed threshold value was determined in a brief calibration stage, which occurred only once before testing commenced.

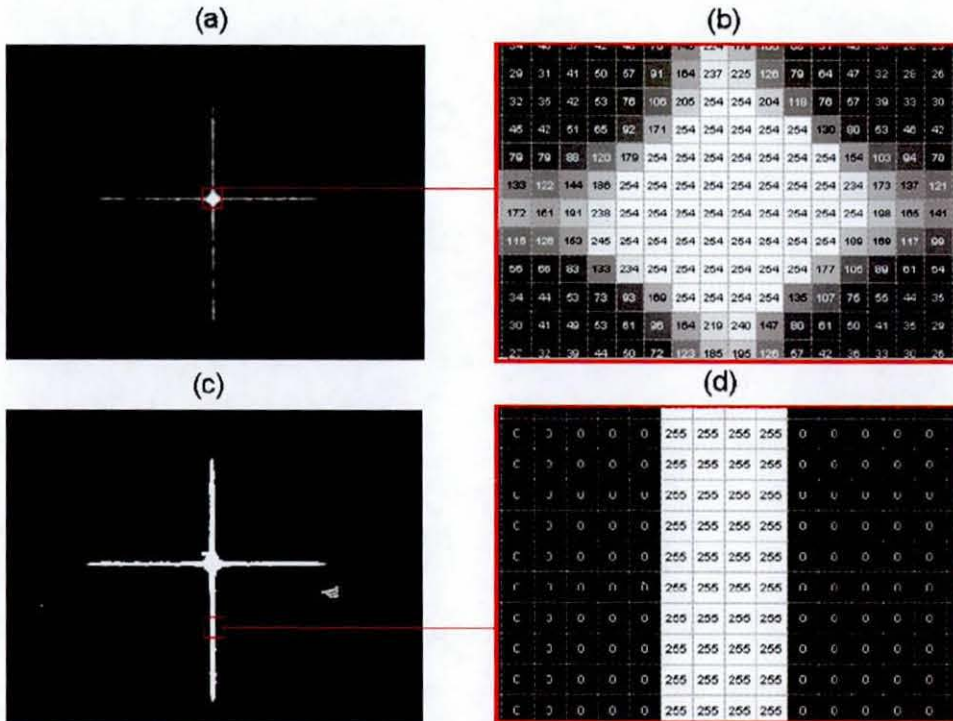


**Figure 7-7: Image processing,**  
 (a) raw acquired 8-bit image, (b) zoomed in section showing gray scale pixel values,  
 (c) processed image after LUT stage, (d) zoomed in section showing binary pixel values.

The binary image was transferred into a filtering algorithm, where a low pass filter was carried out on the image. This was carried out because the laser cross was slightly granular in appearance, due to the speckled nature of laser light passing through the DOE. Therefore the cross was filtered into a 'smooth' binary shape for further

analysis. The cross was then analysed in four individual 'edge' detect algorithms, where each line projecting out from the centre was analysed separately. The 'edge' detect algorithm was carried out along the long axis of each line, the intersection point of each line was therefore located and measured to sub-pixel accuracy. The four intersection points were defined as the intersection points between the arms of the cross and the perimeter of the ball. The midway points between the intersection points of the horizontal and vertical lines were calculated separately, the two midway points determined the centre point of the sphere in the horizontal and vertical direction.

When the measured centre point of the sphere was found not to coincide with the centre pixel of the camera, a voltage was applied to the galvo mirrors to re-position them, in order to re-align the centre point of the sphere with the centre point of the camera sensor array. A scale factor relating the voltage applied, to the angular motion of the mirrors and consequently the displacement in pixels was established. It was vital that the correct conversion scale factor was calculated between the measured pixel value to outputted voltage, this is documented further in Section 7.7.

In order for the system to operate in real time, all the logical events had to occur transiently in series. The system acquired an image, the image was then processed in the Visual Studio .NET environment, a voltage value was then outputted into the galvo mirrors, which were then positioned accordingly in a closed loop circuit. Only once the mirrors had been repositioned could the next image acquisition begin.

To summarise, a system has been developed whereby an 8-bit raw image was acquired by the camera, as shown in Figure 7-8 (a), the image was converted into a binary image, 'filtered' and then four 'edge' detect algorithms were used to extract four intersection points of the ball, as shown in Figure 7-8 (b). By taking the mid point of the horizontal intersection points and the vertical intersection points, the centre of the ball could be located, as shown in Figure 7-8 (c) where the red lines join and this information enabled realignment of the system.

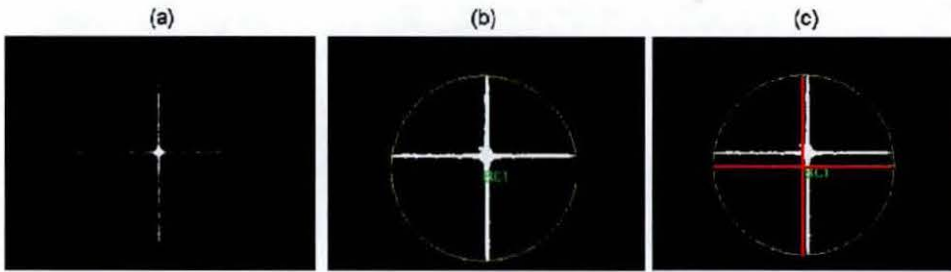


Figure 7-8: Summary of image processing , (a) raw 8-bit image, (b) 'edge' detect algorithm locates the edge of the ball, (c) the centre position of the ball is deduced.

### 7.6.2 Ball movement by hand

In order to prove that the system operated for soccer ball tracking, the NLTS was trialled in the laboratory environment whereby the target ball was moved by hand.

A soccer ball was positioned 1.7 m from the scanning mirrors. The laser cross was manually adjusted to strike the ball, and the laser tracking algorithm was set to 'track', the system was stated to be 'active'. The ball was moved in arbitrary directions maximally. Moving the ball physically as quickly as possible, the NLTS was able to track the ball. Using laser vibrometry to assess the velocity at which the human was able to move the target ball, a maximum velocity was measured at approximately  $3.6 \text{ ms}^{-1}$ .

The ball was moved in a plane perpendicular to the camera axis and the NLTS was able to track in an envelope 1.15 metres in width and 0.52 metres in height. If the NLTS was positioned so that the bench top did not block the laser path, the height of the measured envelope was predicted to be 1.04 m. The ball was also moved out of plane by  $\pm 0.5$  metres and the NLTS was able to keep track of the ball.

During testing the NLTS was able to track the ball at all times. The time required for the image processing and the update of the galvo servo controllers was less than 4 ms. This update speed was working at the limits of the current system capability. The initial programming was able to complete the image processing task in 15 ms, this still allowed the ball, moved by hand to be tracked, as shown in Figure 7-9. Figure 7-9

## Laser based tracking and spin measurement

(a&b) shows three snapshots of the NLTS 'active' where the laser cross tracked the soccer ball. The NLTS programming is found in Appendix D.

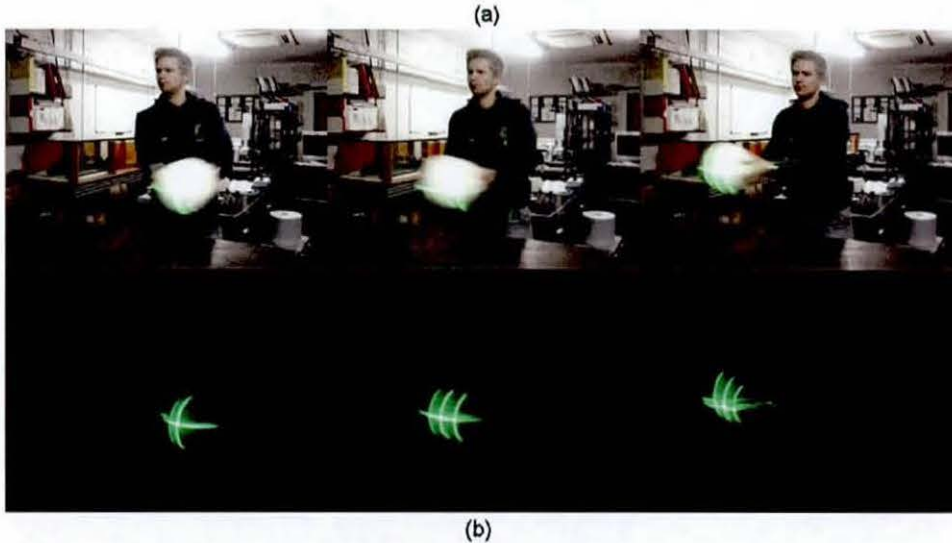


**Figure 7-9: Tracking a soccer ball, moved arbitrarily by hand, (a) lights on in laboratory, (b) lights off in laboratory.**

### 7.6.3 Player testing

This section reports the capability of the system to operate in a more realistic match/play situation, whereby a soccer player performed routine juggling skills.

The NLTS was proven to work extremely effectively, shown by observing Figure 7-10 to Figure 7-12, where the NLTS is displayed in action, tracking different soccer ball juggling skills. For purposes of recording camera footage, the player testing occurred in a dark room, in order for the laser cross to be displayed. However the NLTS system could operate successfully independent of the ambient and natural lighting conditions. During all testing the outputted laser beam complied with the level 2M laser safety classification (IEC 2007).

If anything blocked the view between the camera and the ball, the system would calculate the ball to be at the centre of the camera FOV, therefore the mirrors would remain fixed in space. Once the optical path was clear between the camera and ball, the system would regain tracking ability, assuming the centre of the cross still struck



## Laser based tracking and spin measurement

the ball. In practice this would mean that a momentary loss of the ball by the NLTS would not cause the tracking to stop.

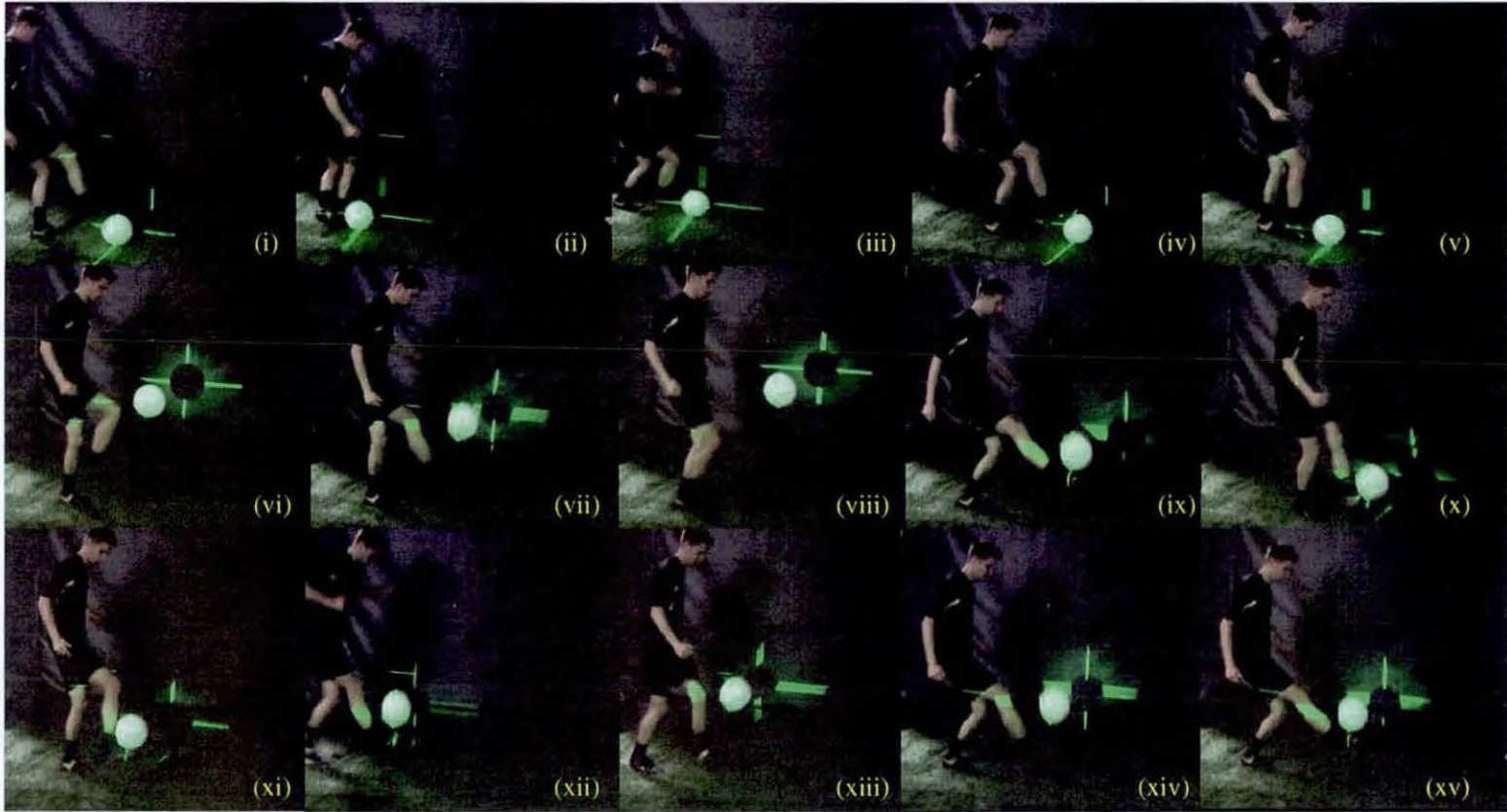


Figure 7-10: Player testing, juggling.

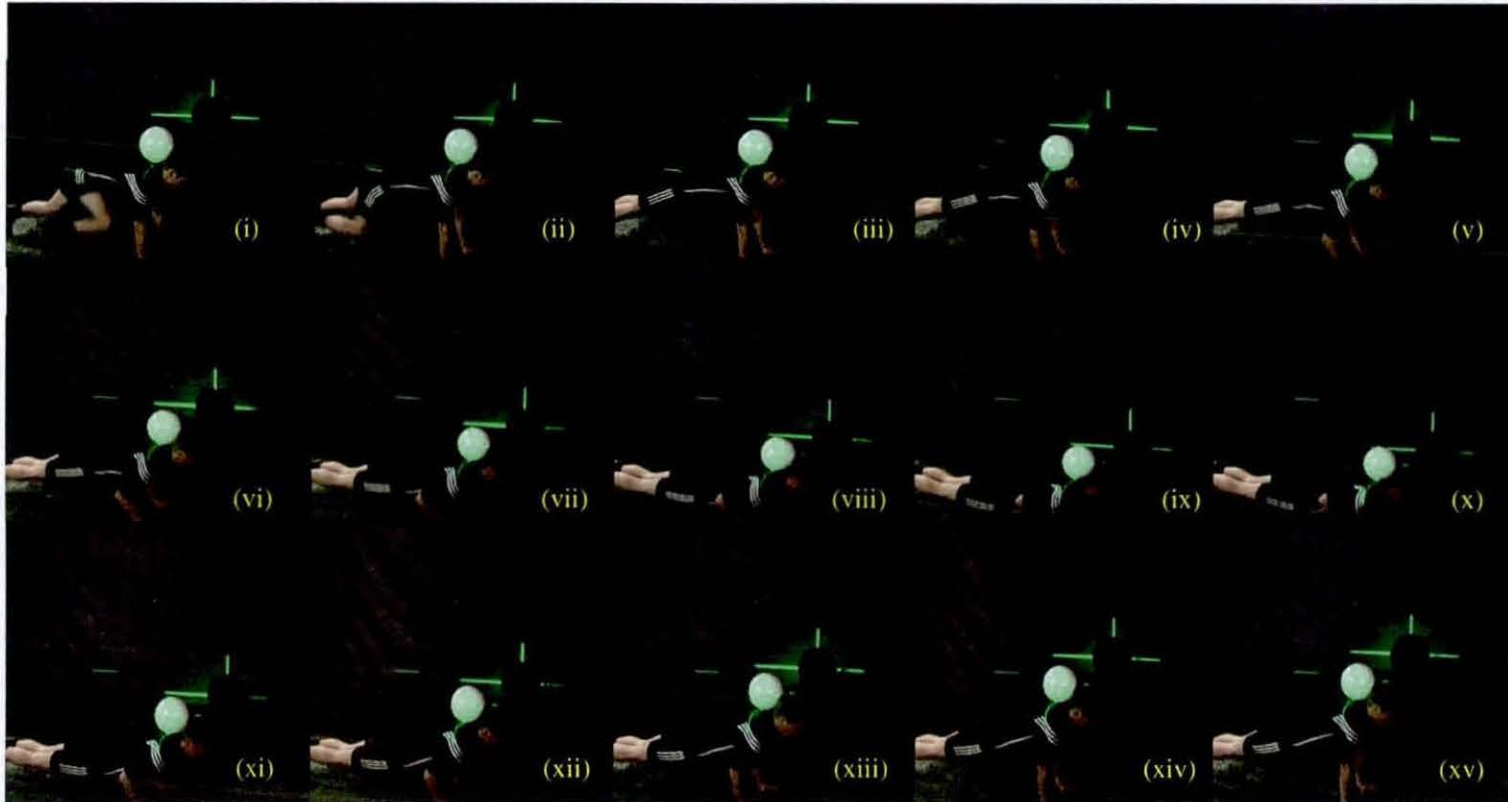
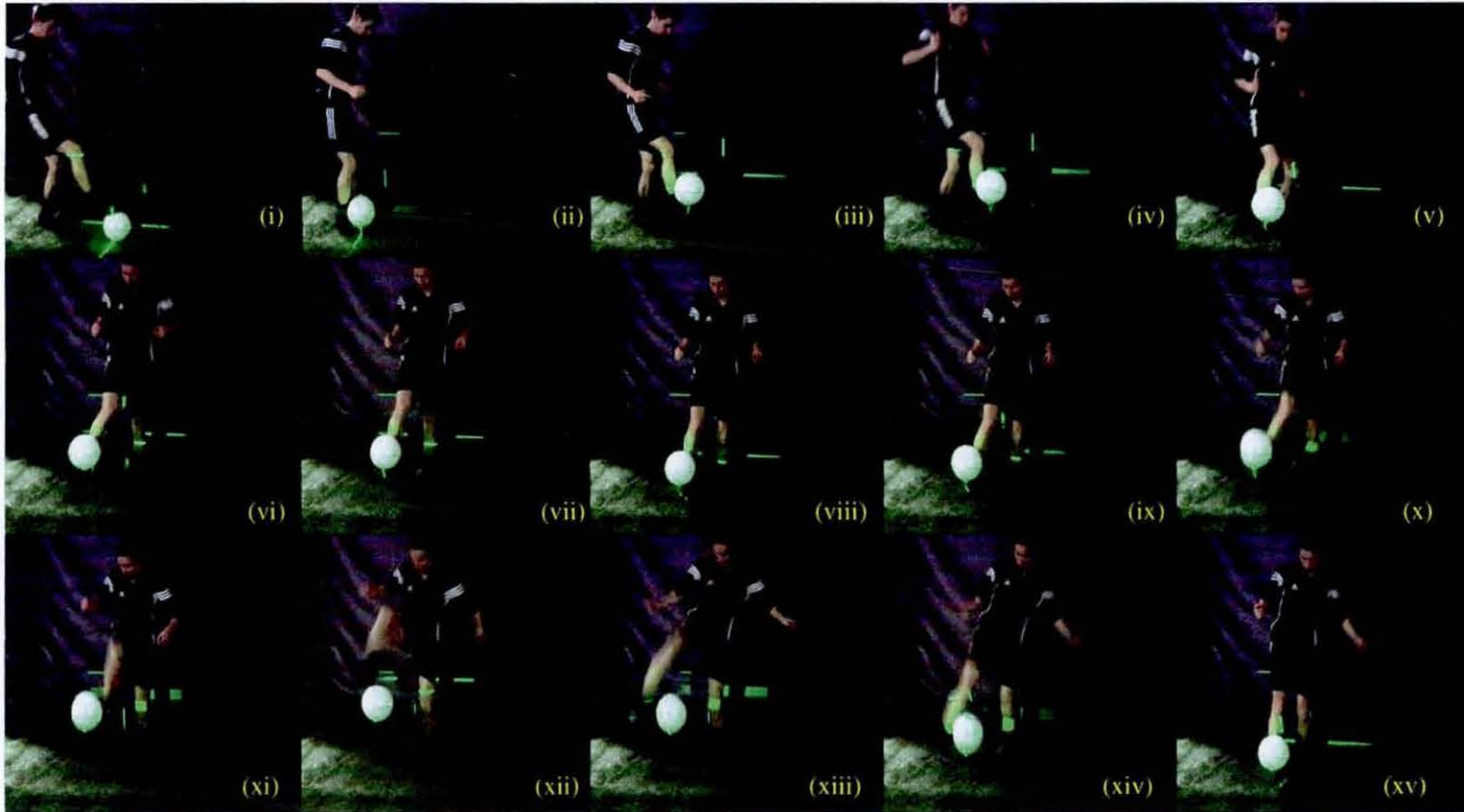


Figure 7-11: Player testing, press-up.



Laser based tracking and spin measurement

Figure 7-12: Player testing, 'round the world'.

#### 7.6.4 Soccer ball launch monitor

Given the demonstrated capability of the system to track a ball in space with time, it followed that information about the launch of a ball could be gathered. The velocity and launch angle of the ball could be outputted, in a similar approach to the Quinspin system.

In order to function as a launch monitor, modifications were made to the VB.NET code. The code was reconfigured such that the initial ball position was to the left of the system FOV. The laser cross was positioned on the ball and the tracking initiated. The tracking system would wait indefinitely for the ball to be kicked, as shown in Figure 7-13 (a). Once the ball was kicked and measured to have moved more than half a ball diameter in the horizontal axis by the NLTS, as shown in Figure 7-13 (b), the system was programmed to record each x and y-mirror voltage. The mirror voltages were recorded for each step until the ball approached the edge of the system FOV. Once the x-axis voltage decreased below  $-4$  V the tracking was stopped, as shown in Figure 7-13 (c). All the recorded x and y-mirror voltages were analysed in order to output the average launch velocity and launch angle, throughout the recording phase. The system presumed that the ball travelled perpendicular to the NLTS, therefore 2D launch measurements were computed.



Figure 7-13: Laser tracking, launch monitor in action.

The calculated launch parameters for the strike in Figure 7-13, are shown in Figure 7-14 and these were displayed via the tracking software, immediately after the tracking was stopped. The programmed code for the launch monitor is shown in Appendix E.

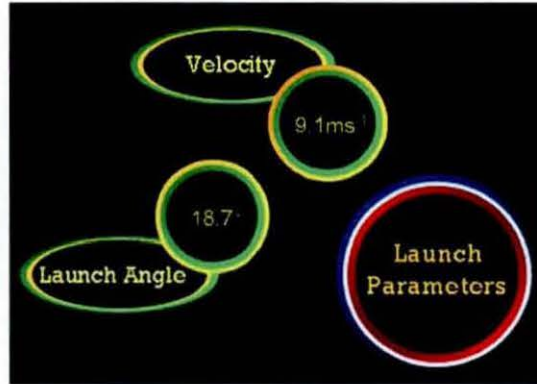


Figure 7-14: Calculated launch parameters.

## 7.7 Tracking calibration

One of the most important factors of the NLTS was the scale factor that was used to relate the required pixel displacement with the voltage applied to the galvo mirrors. It was important to achieve the correct scale factor, if the scale factor was too large, the system would fail to remain fixed on the centre of a static ball, causing a circular laser saccade around the centre of the ball. If the scale factor was too small, the maximum target velocity that the system could track would be reduced.

### 7.7.1 Fixed scale factor

The fixed scale factor was straightforward to compute. A cylindrical block exactly 9.6 cm in diameter was placed 1.7 metres from the camera, in the centre of the laser tracking system FOV. Five images were acquired of the block positioned horizontally and vertically. Each image was analysed in Image Pro Plus and the diameter of the block in pixels was measured, as shown in Figure 7-15.

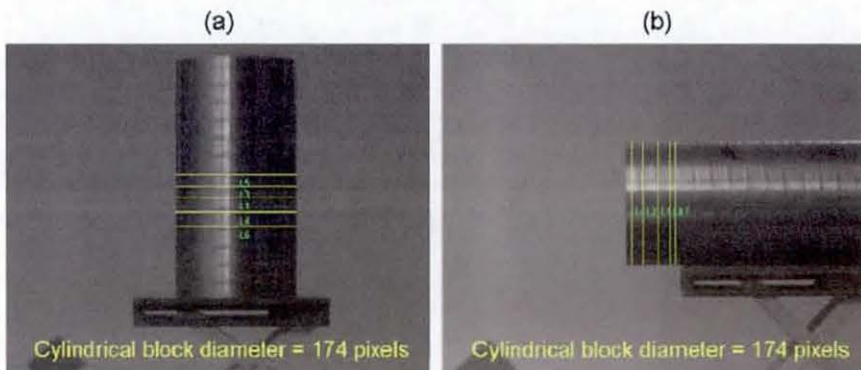
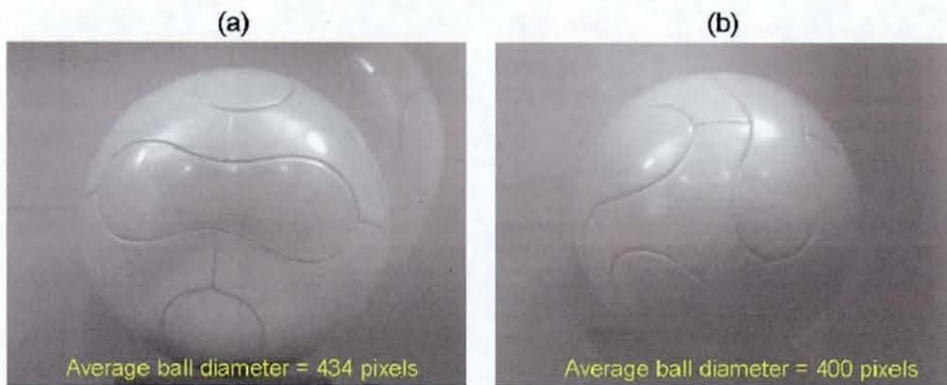


Figure 7-15: Scale factor calibration, (a) horizontally, (b) vertically.

Using the results obtained from the calibration images, it was straightforward to calculate 1 pixel to be equal to 0.0552 cm (to 3 s.f.). From further testing it was noticeable that the mirrors were able to adjust the laser beam more horizontally than vertically. This was due to the fixed offset distance between the x and y-mirror. Therefore at the fixed stand off distance of 1.7 metres the scale factor for the x-mirror was calculated at 1 pixel = 0.00369 volts (to 3 s.f.) and for the y-mirror 1 pixel = 0.00461 volts (to 3 s.f.). The calculation for these scale factors can be found in Appendix F.

### 7.7.2 Adaptive scale factor

The NLTS used a camera to 'see' the FOV, therefore the stand off distance between the camera and target was important. If the ball was translated in a plane perpendicular to the camera axis, the stand off distance between the ball and camera would change. The smallest stand off distance was achieved when the ball was in the centre of the system FOV, consequently the largest stand off distance was observed when the ball was in the corners of the NLTS FOV. This change in size of the FOV, as shown in Figure 7-16, directly affected the scale factor used to convert between pixels and voltage in order to realign the NLTS.



**Figure 7-16: Change in FOV size due to stand off distance, (a) x and y-mirror voltage values (0,0), (b) x and y-mirror voltage values (4,-4).**

With the ball in the centre of the NLTS FOV at a 1.7 m stand off distance, Figure 7-17 gives an indication of how the scale factor could be adjusted in order to track the ball with better realignment accuracy.

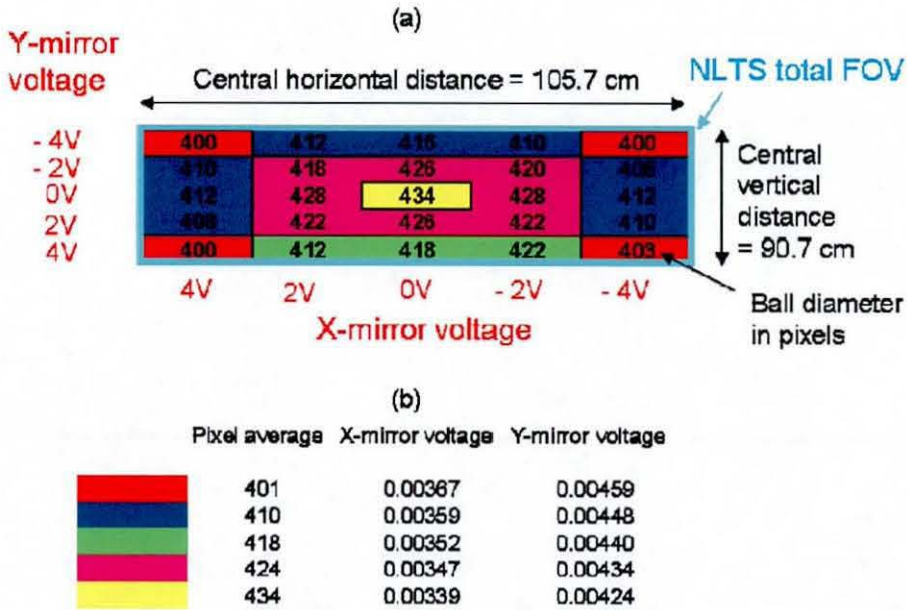


Figure 7-17: Adaptive scale factor, (a) changing diameter of the ball in the system FOV, (b) Calculated x and y-mirror voltage scale factor when the need to realign by one pixel.

As the soccer ball moved to the edge of the system FOV, a larger area was imaged by the camera. Therefore when realignment of the system was required by one pixel at the edge of the FOV, the voltage value change was less than when realignment was required by one pixel, in the centre of the system FOV. The adaptive scale factor was envisaged to operate with five different values as shown in Figure 7-17 (b). This adaptive scale factor was dependent upon the stand off distance when the x and y-mirror voltages were 0 volts, therefore if this stand off distance was altered, the adaptive scale factors would also need to be changed.

## 7.8 Sources of error

The development of the NLTS reported in this chapter was seen as a good advancement in laser tracking methods, however the system did have some limitations which are reported.

The scale factor used to convert the measured centre point of the ball in pixels to the voltage required to drive the galvo mirrors, was a critical part of how successfully the NLTS was able to track the target. The work reported in 7.7.2 demonstrated that an adaptive scale factor was required for a more accurate tracking strategy.



## Laser based tracking and spin measurement

The NLTS has been demonstrated to track the ball within a volume of  $1.15 \times 1.04 \times 1$  metres and tracking was achieved even when the ball displaced out of plane. However currently the NLTS has no method of verifying the stand off distance to the ball. By measuring three edge points in the camera FOV, as shown in Figure 7-18, whereby two fixed edge points were selected and the third edge point is shown as a red dot, the edge of the ball can be extrapolated. This could be achieved using a 'Hough' transform, to predict the ball diameter, which would enable the stand off distance to be derived.

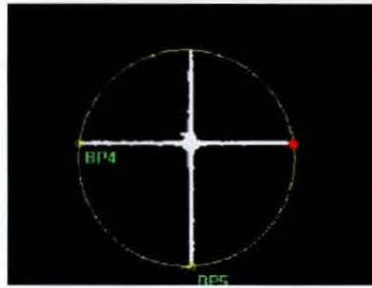


**Figure 7-18: The 'Hough' transform, to locate the edge of the soccer ball.**

The work in 2.7.4 showed how the spherical profile of the ball influenced the amount of laser light backscattered in the direction of the incidence beam. Stronger laser backscatter was apparent at the centre of the ball, by comparison to the edge of the ball, where the vital intersection points were acquired. This was only a minor obstacle, however when the ball was moved to the edge of the laser system FOV, the very edge point backscattered a different light intensity value than the very edge point of the ball at the centre of the laser system FOV. This was a limitation of the NLTS, therefore the threshold value used for the LUT processing task was chosen carefully. To limit this issue an adaptive threshold value could have been incorporated, the main drawback to this would be that drastically more (>2.5) CPU time would be required to analyse the acquired images.

An assumption in the tracking principle was that the camera and laser had the same optical axis when striking the target. If any misalignments occurred due to the system being knocked, or attachments loosening, the tracking accuracy would have been

compromised. Therefore it was important to carry out the calibration protocol before carrying out any testing.

When the system was used with a soccer ball with graphics, that had large contrast between them, e.g. black and white, as present with the adidas 'Teamgeist' ball, difficulties arose. The reason for this was, when the black marking was at the edge of the ball the system would not detect this as an intersection point, the system therefore misconstrued the centre point of the ball. However only slightly erratic tracking of the 'Teamgeist' ball was demonstrated with the player testing.

## **7.9 Further developments**

Most of the points outlined in 7.8 which contributed to error sources, could be improved upon and therefore would allow scope for further development of the NLTS. However five key parameters have been highlighted that would allow the prototype NLTS to be developed into a more functional system.

### **7.9.1 FOV of the NLTS**

The only moving components of the NLTS were the x and y-mirrors. The system FOV was directly limited by the range of the mirrors,  $\pm 20^\circ$ . It would be reasonably straightforward to mount the base plate onto a rotary stage, this would allow a more suitable tracking envelope for the system, since soccer free kicks possess high horizontal motion and a much smaller component of vertical motion. The rotary stage would provide whole field pointing capability (in a similar method to the TT system), and the x and y-mirrors would provide the existing fine tracking function. The rotary stage could be quickly implemented, offering a large increase in functionality, however the stage was estimated to increase the cost of the NLTS by ~£200.

### **7.9.2 Image processing stage**

The main limiting factor for the real-time tracking system capability was the image analysis processing time. At present the processing occurred in 4 ms, it was foreseeable that by operating on a 'real time' PC or dedicated image processing card this operating time could be reduced. This reduction in image processing time is foreseen to be large so that the 'bottleneck' in the NLTS would be directly related to the maximum frame rate of the Pulnix camera, 712 FPS. The functionality of the

NLTS would be improved due to larger target velocities being tracked. The cost of the image processing stage would be unlikely to change, however significant time would have to be spent on the new programming required for the image processing, if a dedicated image processing card were used.

### **7.9.3 The DOE**

The DOE used in the NLTS functioned because it emitted a laser 'cross' pattern onto the ball, however the limitation with the DOE was that it was not purpose built for the application. By using a purpose built DOE the light intensity at the zero order could have been dramatically reduced, currently it was predicted to be at approximately 80% of the total light intensity. Therefore the DOE would be designed to operate with laser light at 532 nm wavelength. The laser pattern angle could have been modified to fit the system exactly, allowing all the laser light to travel through the x and y-mirrors. An initial purpose built DOE was estimated to cost approximately £3k. It was estimated that obtaining the desired DOE would take 3 months to develop, therefore purchasing the correct DOE would be a time consuming and expensive process. However purchasing the purpose built DOE was recommended due to the functionality improvements gained.

### **7.9.4 System automation**

Each time tracking was initiated, the centre of the laser cross was manually positioned onto the ball. In order to improve the NLTS, it was important that the tracking system could locate the ball in the FOV automatically.

It was foreseen that this could be achieved by having a cheap, ~£20 web camera pointing out of the NLTS. By capturing a snapshot of the FOV, this image could be analysed using a 'Hough' transform, to identify a circle outline of the ball. As long as only one circle was located in the FOV, it would be straightforward to locate the ball and output matching x and y-mirror coordinate values. Presuming that the realignment led to the centre of the laser cross striking the ball, the NLTS would initiate tracking successfully.

### 7.9.5 Non-spherical target tracking application

The NLTS was demonstrated to operate successfully when tracking spherical objects. However users may require that other shapes are tracked. This was not foreseen to be a problem, as long as good contrast existed between the target and the background.

For tracking non-spherical targets, the code was already created, found in Appendix G. The image processing algorithm would have to be adjusted as follows. The 'edge' detection stage would be replaced with a 'blob' (Binary Large Object) analysis stage.

A different DOE would have to be selected for the 'blob' analysis application. However after preliminary testing it was predicted that the 'blob' analysis stage would take longer than the 'edge' detection stage, therefore the maximum velocity of tracking would be slower than with the present system.

### 7.10 Chapter summary

A completely novel laser tracking system (NLTS) was designed, developed and demonstrated to track non-marked soccer balls. Implemented hardware and software choices were accurately outlined, for the successful operation of the device. The concept behind the NLTS strategy was clearly explained and a promotional image of the prototype system is shown in Figure 7-19.

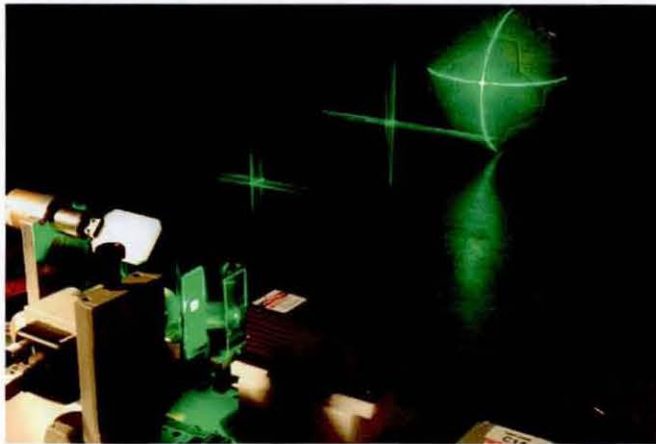


Figure 7-19: The novel laser tracking system (NLTS).

## Laser based tracking and spin measurement

This NLTS was reported to track faster than any other similar laser based device. At present the system was reported to track targets up to approximately  $10 \text{ ms}^{-1}$ . Other tracking systems were reviewed and the NLTS was found to be the only 'active' HSV sports ball tracking system. The prototype system was proven to work inside regardless of lighting conditions. The cost of buying the components to assemble the prototype device was £8.6k.

Demonstration of the NLTS was carried out with soccer ball application, although it was envisaged that the current technique could be applied to any spherical object or sports ball. The principle was foreseen as valuable for other applications, such as automotive or military tracking tasks.

## **8** Laser based spin measurement system

### **8.1 Chapter overview**

In order to carry out laser based surface velocity measurements different scan strategies were implemented for spin rate measurement.

The objective of this Chapter was to allow surface velocity measurement of the target ball in order to measure spin rate of the ball whilst using the NLTS to track the target ball. The amalgamation of a single point vibrometer and the NLTS for surface velocity measurement allowed spin rate measurement of a ball moving with both translational and rotational velocity.

### **8.2 Testing protocol**

For the purposes of the testing carried out at the beginning of this section, the 'spin rig' reported in Chapter 4 was used to rotate a soccer ball with known spin rate around a fixed axis.

#### **8.2.1 Selected laser vibrometer**

The laser vibrometry work reported so far was carried out using the Polytec single point vibrometer. Before carrying out any further testing a review of current commercial vibrometers was carried out, ensuring that testing was carried out with the most suitable vibrometer. The three main systems that were considered for this were the 'Polytec' OFV-302 vibrometer, the 'Ometron' VH-300 and the 'Metrolaser' Vibromet 500V single point vibrometer. The strengths and weaknesses of each system with regard to this application were highlighted in Table 8-1.

**Table 8-1: Comparison of commercial single point vibrometers.**

<b>System</b>	<b>Strengths</b>	<b>Weaknesses</b>
Polytec	<ul style="list-style-type: none"> <li>- High velocity measurement range, <math>\pm 20 \text{ ms}^{-1}</math>.</li> <li>- Measurement distance, more than 5 metres.</li> <li>- Eye-safe laser operation.</li> </ul>	<ul style="list-style-type: none"> <li>- Average SNR (no signal striking black surface at any distance).</li> <li>- Adjustable focus.</li> <li>- Bulky system, built into two units; measurement head and controller.</li> </ul>
Ometron	<ul style="list-style-type: none"> <li>- Excellent SNR (good signal striking black surface at 3 metre stand off distance).</li> <li>- Compact system, built into one unit.</li> <li>- Measurement distance up to 100 metres.</li> <li>- Eye-safe laser operation.</li> </ul>	<ul style="list-style-type: none"> <li>- Low velocity measurement range <math>\pm 0.42 \text{ ms}^{-1}</math>.</li> <li>- Adjustable focus.</li> </ul>
Metrolaser	<ul style="list-style-type: none"> <li>- Collimated beam, no need to focus the emitted infrared beam (stand off distance 1 cm to 5 metres).</li> <li>- Compact system, built into one unit.</li> </ul>	<ul style="list-style-type: none"> <li>- Low velocity measurement range <math>\pm 1 \text{ ms}^{-1}</math>.</li> <li>-Not eye-safe, class 2 laser at <math>\lambda = 650 \text{ nm}</math> (visible) for pointing, class 3B laser at <math>\lambda = 780 \text{ nm}</math> (infrared) for measurement.</li> </ul>

The Polytec single point vibrometer was selected because it allowed eye-safe operation at large stand off distances whilst being able to measure a large range of target velocity values. The main drawback with this system was that the surface of the soccer ball had to be covered in retroreflective tape in order to measure adequate SNR. The Ometron system suffered due to its minimal velocity measurement range, and the suitability of the Metrolaser for future player testing was out of the question, due to the device operating outside eye-safety levels.

For the purposes of sports ball measurement a combination of the current available commercial single point vibrometers, would have provided a more satisfactory measurement device.

### **8.2.2 Line scan work and results**

The work in this section involved the laser beam path being scanned horizontally across a rotating ball, in a plane perpendicular to the ball spin axis, as shown in Figure 8-1 (a). A script was written in Visual Studio to allow the line scan length and number of measurement points to be adjusted. The scan line length was set at approximately 16 cm so that measurements were not taken at the edge of the ball, since previous testing had shown, this resulted in 'poor' SNR. The single point laser vibrometer beam was steered using the x and y-mirrors which were removed from the NLTS, the mirrors were positioned so that their zero position (0,0 Volts) guided the laser beam to the centre of the target ball. The stand off distance between the ball and the scanning mirrors was fixed at 1.7 metres.

Three different tests were carried out; the scan line length was fixed and the number of measurement points along the scan line were altered. The 'spin rig' maintained a spin rate of approximately 600 RPM throughout the testing protocol. The number of measurement points chosen, were 60, 120 and 180. For each distinct number of measurement points, the line scan was repeated eight times, measurements were taken over a one second duration, and each one second measurement was repeated ten times (10 trials were carried out).



Laser based tracking and spin measurement

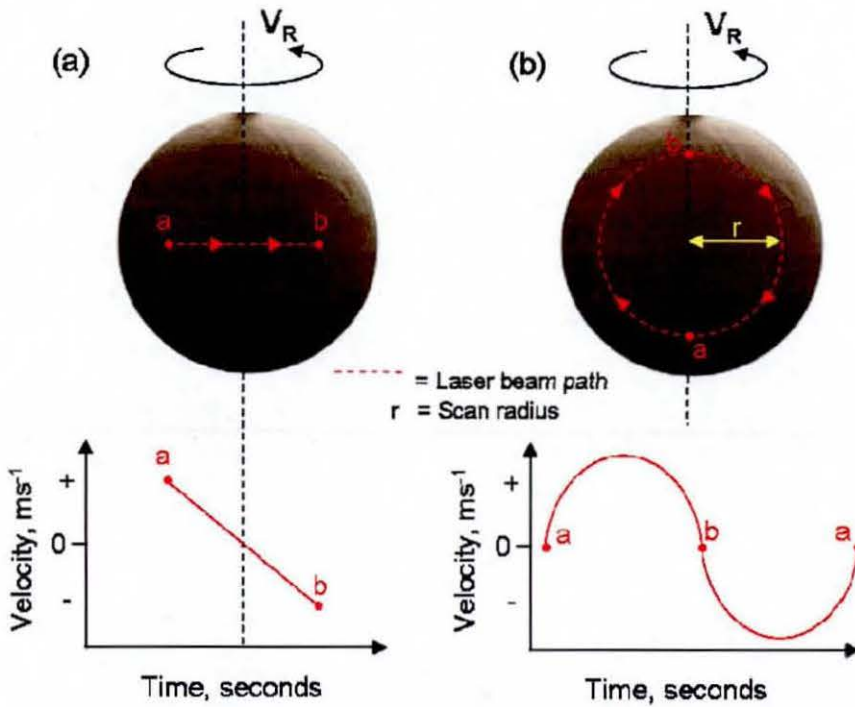
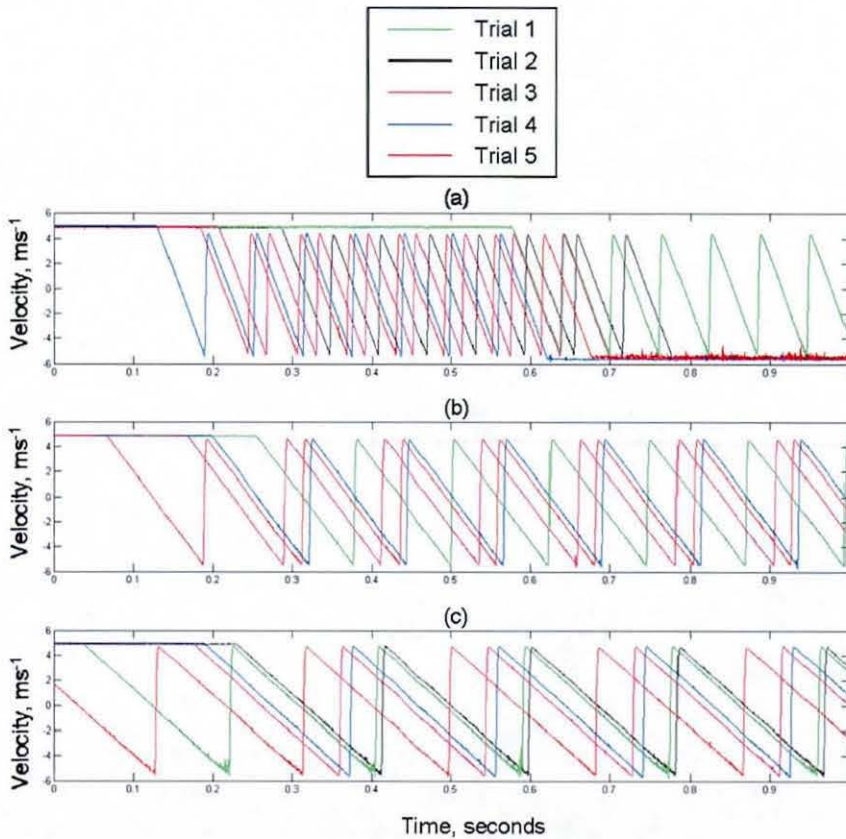


Figure 8-1: Scanning strategy, (a) line scan, (b) circular scan.

The graphed results from the line scan study are shown in Figure 8-2. The results show that the vibrometer could measure repeatable ‘saw tooth’ velocity profiles. As the number of measurement points along the scan line increased the gradient of the measured velocity reduced accordingly.

Equation 6-1 defines that in order to be able to compute a spin rate value from the velocity values measured using the line scan work, the radial distance of the laser beam from the ball spin axis and the laser beam angle of incidence at the soccer ball must be known. Therefore after each line scan measurement the radial distance from the spin axis was measured to point a and b, which were the start and end point of each individual line scan. It was these end points of the line scan that were used to compute the spin rate of the ball. The laser beam angle of incidence was presumed to be 90° in all calculations.

## Laser based tracking and spin measurement



**Figure 8-2: Line scan velocity measurements,  
(a) 60 scan points, (b) 120 scan points, (c) 180 scan points.**

Figure 8-3 shows for each line scan trial the spin rate outputted by the 'spin rig', called the counter value and showing the standard deviation of the measurement throughout the one second measurement period. Using the average maximum and minimum velocity measurements (measured at point a and b) the vibrometer velocity readings were computed into a spin rate value. Therefore for each trial, two calculated spin rate values were outputted, known as the laser values which were plotted against the corresponding counter spin rate value.

### Laser based tracking and spin measurement

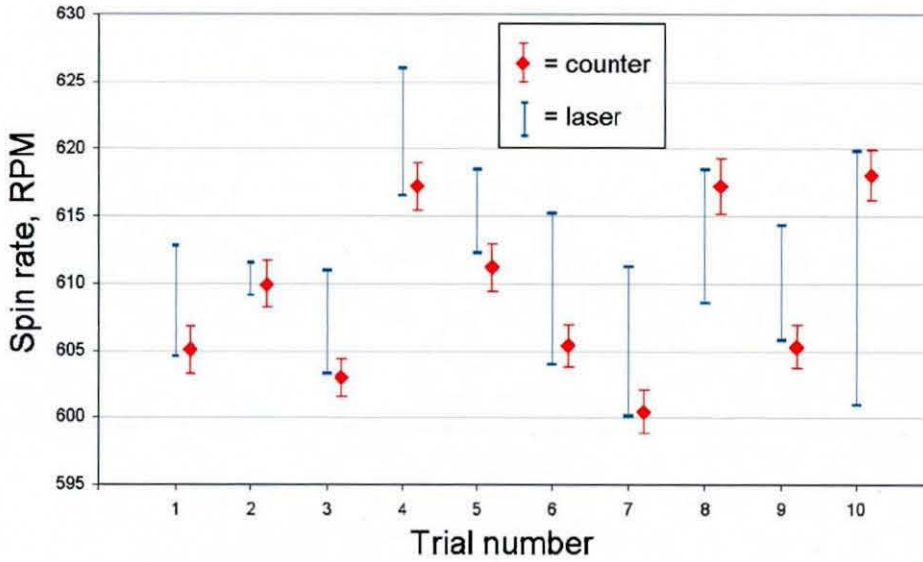


Figure 8-3: Line scan results, 60 measurement points along the line.

Extremely good qualitative agreement was achieved between the counter and laser values in Figure 8-3. The difference between the counter and laser values was less than 3% in all trials carried out.

The results for each trial were plotted in Figure 8-4 for the line scan measurements with 120 scan points.

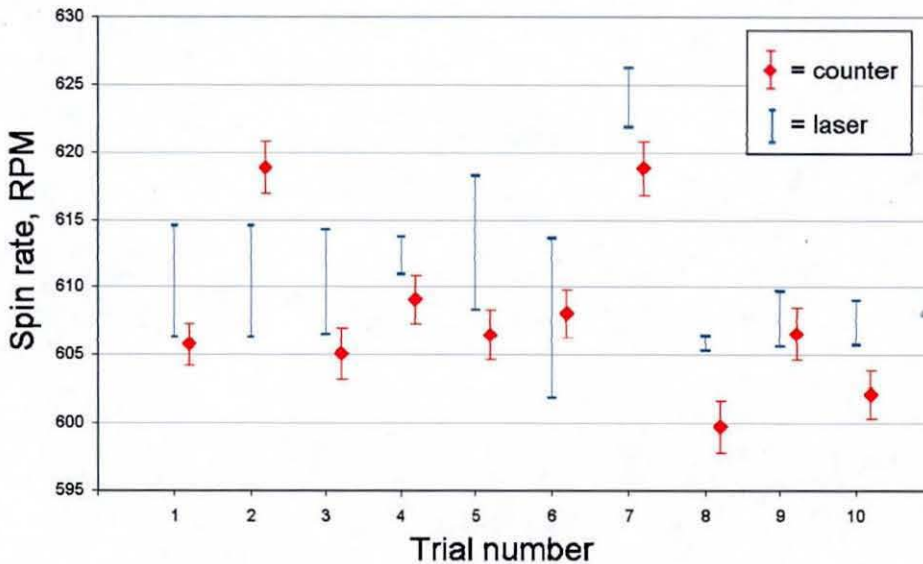


Figure 8-4: Line scan results, 120 measurement points along the line.

## Laser based tracking and spin measurement

The qualitative agreement between the counter and laser spin rate results was good as shown in Figure 8-3, especially since the difference between counter and laser spin rate values was less than 2.1% in all trials. Trial 8 showed a spurious data value since the outputted laser values were almost identical in spin rate. This was accounted due to extremely strong SNR at the start and end of each line scan throughout trial 8, which was not achieved in the other trials.

The results for each trial were plotted in Figure 8-5 for the line scan measurements with 180 scan points. The qualitative agreement between the counter and laser spin rate results was excellent and the difference between the counter and laser spin rate values was less than 2.5% in all trials. Trial 7 showed a spurious data value even though an extremely good qualitative match was found between the counter and laser spin rate value. It was accounted for by the laser measuring extremely strong SNR at the start and end of each line scan throughout trial 7.

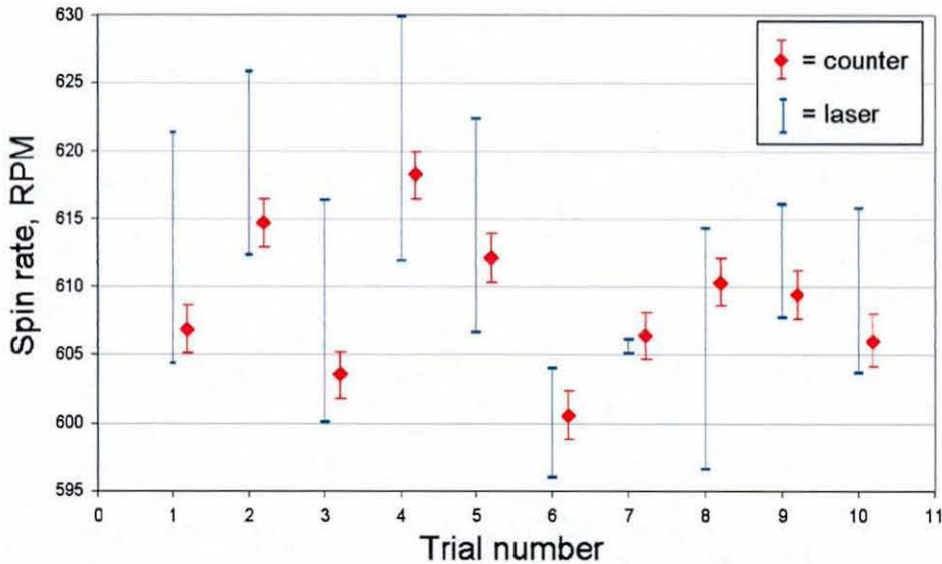


Figure 8-5: Line scan results, 180 measurement points along the line.

The repeatability of the counter spin rate measurement for all line scan results was between  $\pm 2.8$  and 4 RPM at the 95% confidence level. Therefore this difference was considered insignificant in influencing the laser spin rate measurements.

The results from the line scan testing were extremely positive, suggesting that laser vibrometry allowed a useful, accurate non-contact approach to sports ball spin measurement of a ball with no translational velocity.

### **8.2.3 Circular scan work and results**

In order to assess the ability of the vibrometer to measure velocity from an arbitrary position on a spinning ball, a circular scan was employed, as shown in Figure 8-1 (b). Three different tests were carried out whereby the scan radius was altered. At each scan radius, five repeats/trials were carried out. The spin rate of the 'spin rig' was set to approximately 600 RPM and each individual measurement was sampled over two seconds. The single point vibrometer beam was again steered using the x and y-mirrors taken from the NLTS, with a stand off distance of 1.7 metres between the scanning mirrors and the target ball.

The velocity recorded by the circularly scanned vibrometer laser beam at 3 radii with time is depicted in Figure 8-6. The larger the scan radius the larger the maximum measured velocity by the vibrometer, due to the increased radial distance between the measurement point and the spin axis. The circular scan profile was programmed such that the time to carry out the 360° circular saccade was identical in all tests.

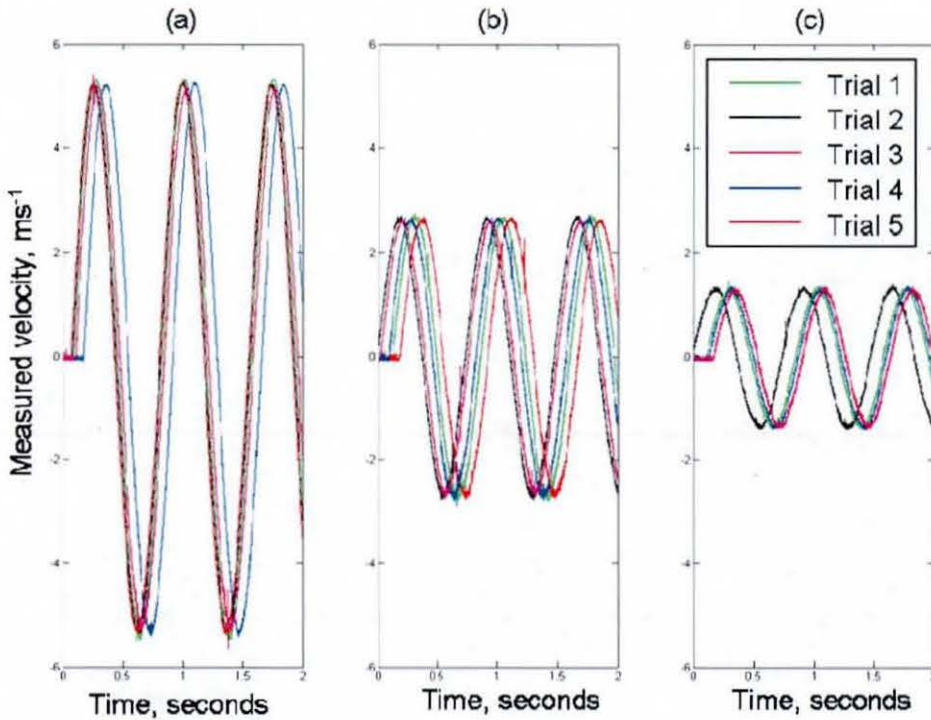


**Figure 8-6: Circular scan velocity measurements, (a) scan radius 8 cm, (b) scan radius 4 cm, (c) scan radius 2cm.**

In a similar approach to the line scan work, the spin rate of the ball could be calculated by measuring the radial distance from the maximal positive and maximal negative surface velocity measurement points to the centre of the ball. The laser beam angle of incidence was assumed to be  $90^\circ$ .

The calculated spin rate of the ball for the circular scan work and the counter spin rate results are depicted in Figure 8-7. The repeatability of the counter spin rate measurement for all circular scan results was between  $\pm 3.3$  and  $4.6$  RPM at the 95% confidence level. Therefore this difference was considered insignificant in influencing the laser spin rate measurements.

## Laser based tracking and spin measurement

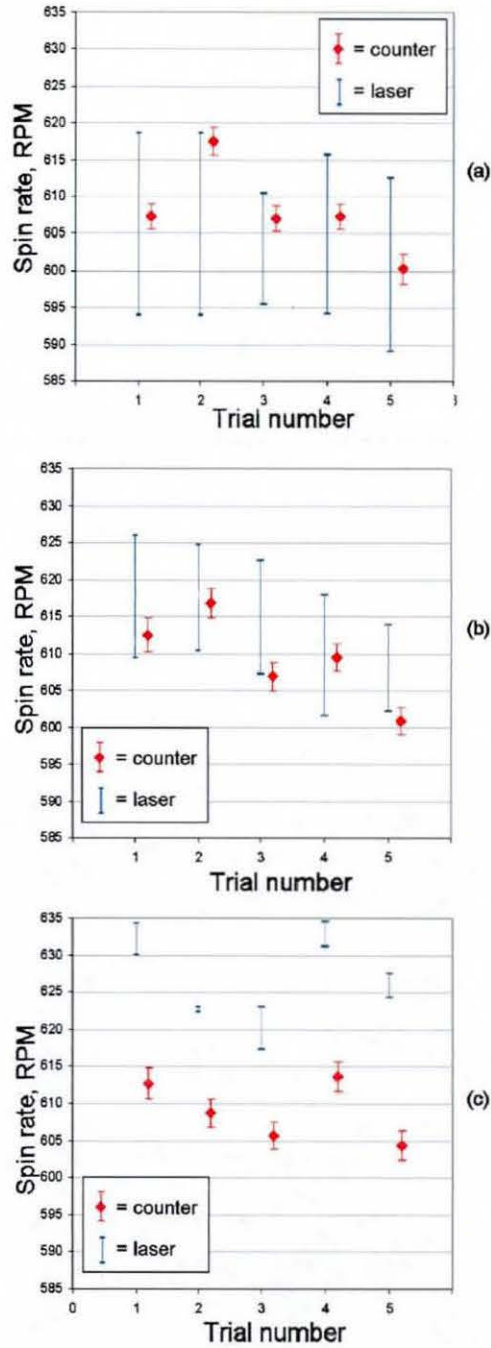
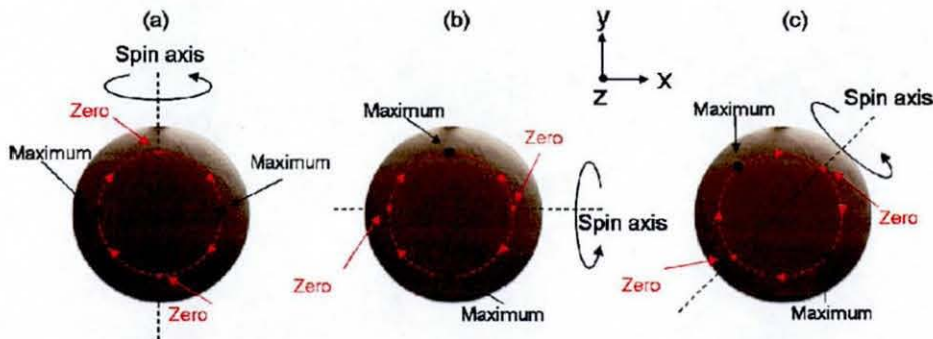


Figure 8-7: Circular scan spin rate results, (a) scan radius 8 cm, (b) scan radius 4 cm (c) scan radius 2 cm.

Good qualitative agreement was achieved between the laser and counter measurements since the difference between the counter and laser spin rate values was

less than 4% in all trials. This results was not as good as for the line scan work, however by observing Figure 8-7 (c) it was noticeable that a non-random type B measurement error was present in all trials, which would increase the difference between the counter and laser spin rate values. This error was most likely due to an optical alignment issue or an over estimation of the radial measurement distance. Trial 2 also demonstrates an extremely small range of spin rate measurement by the laser which is obviously desired, however the result is spurious compared to the other trials. This results is thought to be accounted due to extremely strong SNR at the maximal velocity readings, therefore no signal drop out was occurring.

The circular scan technique is however much more powerful than the line scan technique. This is depicted in Figure 8-8 (a-c) using the knowledge that the spin axis in a plane can be calculated by observing where on the circular scan line the maximum and zero velocity values are measured. The spin axis in the x-y plane will always be perpendicular to a straight line drawn between the maximum positive and negative measured velocity values.



**Figure 8-8: Spin axis definition using circular scan technique,  
zero = zero surface velocity value along the laser scan path,  
maximum = maximum positive and negative surface velocity along the laser scan path.**

The results from the circular scan testing were encouraging suggesting that laser vibrometry allowed a useful, extremely accurate non-contact approach to ball spin measurement of a ball with no translational velocity. The technique was found to be more functional than the line scan technique, because the spin axis of the ball in the x-y plane could be defined.



### 8.2.4 NLTS combined with single point vibrometry

The laser vibrometer was introduced into the NLTS to allow concurrent surface velocity measurement and tracking. The laser vibrometer beam was directed to travel parallel to the illumination laser beam, utilising a small mirror ( $4 \times 4$  mm) positioned at  $45^\circ$  to the original laser vibrometer axis, from which it was reflected by the two scanning mirrors in the same way as the illuminating laser 'cross' beam. This permitted the laser vibrometer to be incorporated without affecting the NLTS performance. This set-up, as shown in Figure 8-9, worked successfully when an offset existed between the illumination laser beam and the vibrometer laser beam, therefore the mirror introducing the vibrometer laser beam into the tracking system did not interfere with the existing NLTS system.

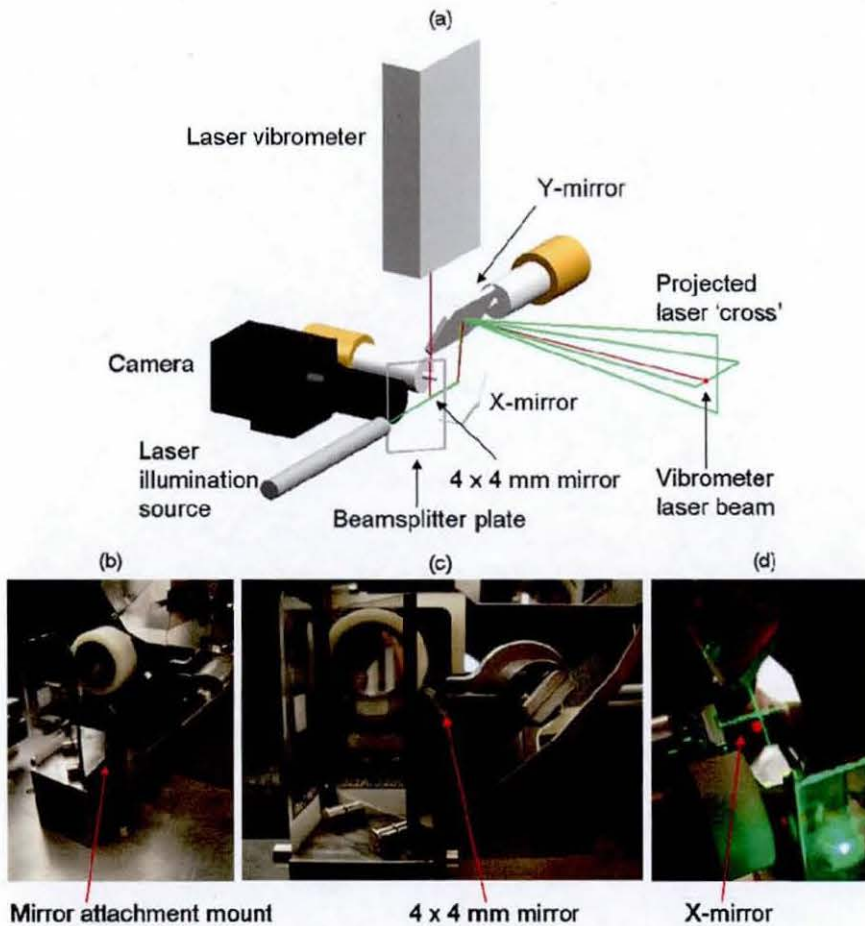


**Figure 8-9: Combination of NLTS and single point vibrometer set-up, (a) 3D schematic (b) isometric view of mirror attachment, (c) side view of mirror attachment, (d) juxtaposition of vibrometer and illumination laser beams.**

### Laser based tracking and spin measurement

Once the laser vibrometer was successfully incorporated, measurements were carried out in order to decipher whether accurate spin measurements could still be derived. The stand off distance between the ball and the scanning mirrors was fixed at 1.7 metres and the zero position of the mirrors (0,0 Volts) was set so that the centre of the laser cross struck the centre of the target ball.

The laser vibrometer was used to carry out measurements from the ball spinning at approximately 400, 500 and 600 RPM, firstly with the NLTS and vibrometer beams statically centred on the ball, however the system was 'inactive'. Subsequently the NLTS was set to 'actively' track. All laser vibrometer measurements were carried out over a one second time duration and each measurement condition was repeated 10 times. The measurements carried out using the laser vibrometer and the 'spin rig' counter were averaged for each measurement, in order to determine the average measured spin rate value.

By analysing the results, shown in Figure 8-10, it was clear that the real-time ball tracking system added 'noise' to the measurement. This was attributed to the fact that the mirrors were known to exhibit small oscillations when tracking a static ball.

## Laser based tracking and spin measurement

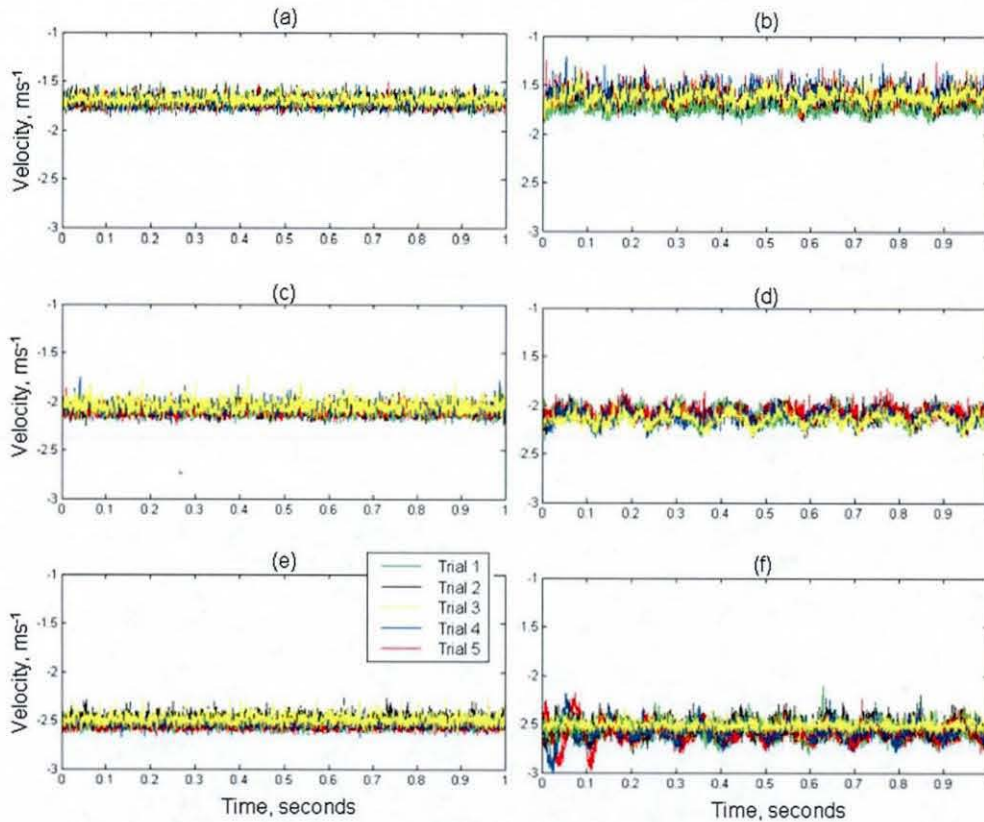


**Figure 8-10: Vibrometer measurements,**  
(a) spin rate 400 RPM, tracking 'inactive', (b) spin rate 400 RPM tracking 'active',  
(c) spin rate 500 RPM, tracking 'inactive', (d) spin rate 500 RPM, tracking 'active',  
(e) spin rate 600 RPM, tracking 'inactive', (f) spin rate 600 RPM, tracking 'active'.

Using Equation 6-1 the spin rate of the ball was calculated from the results plotted in Figure 8-10. The laser beam angle of incidence was assumed to be 90° and the radial measurements point between the spin axis and laser beam point at the ball was measured after each trial. The counter value was averaged over the entire one second measurement duration. The calculated spin rates are shown in Figure 8-11, where the average laser value is plotted for both 'active' and 'inactive' tracking strategies. The counter spin rate values are also shown for both 'active and 'inactive' conditions with the standard deviation shown.

### Laser based tracking and spin measurement

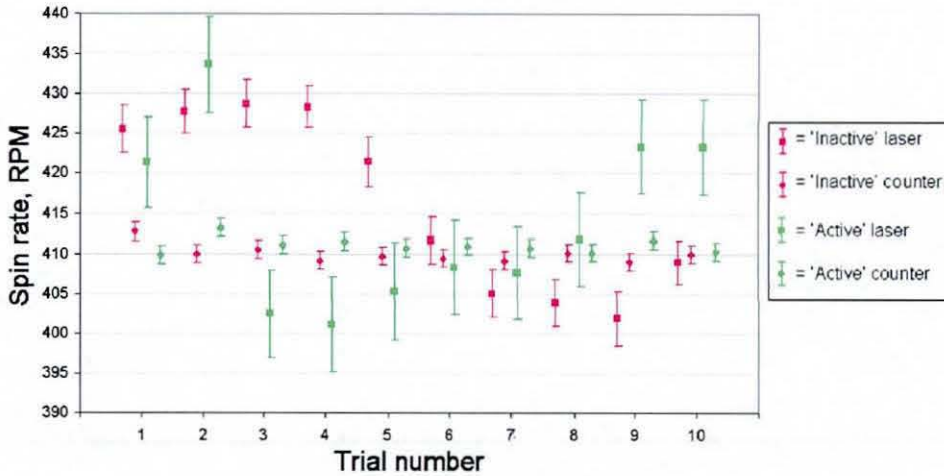


Figure 8-11: Spin rate values for 'active' and 'inactive' tracking at ~400 RPM.

The percentage difference between the counter and laser measurements was less than 5% for all trials. There appeared to be no significant difference between the 'active' and 'inactive' tracking strategies regarding the average computed spin rate.

Figure 8-12 and Figure 8-13 show the results for the testing at ~500 and ~600 RPM, respectively. Similar results were obtained as at the ~400 RPM spin rate, which was encouraging since 600 RPM is a match specific spin rate encountered in competitive soccer (Ireson 2001). The percentage difference between the counter and laser measurements was less than 5% for all trials

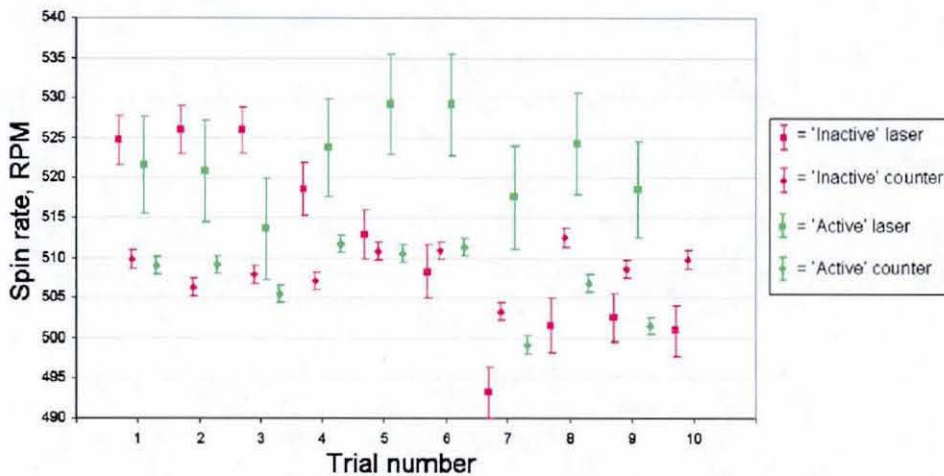
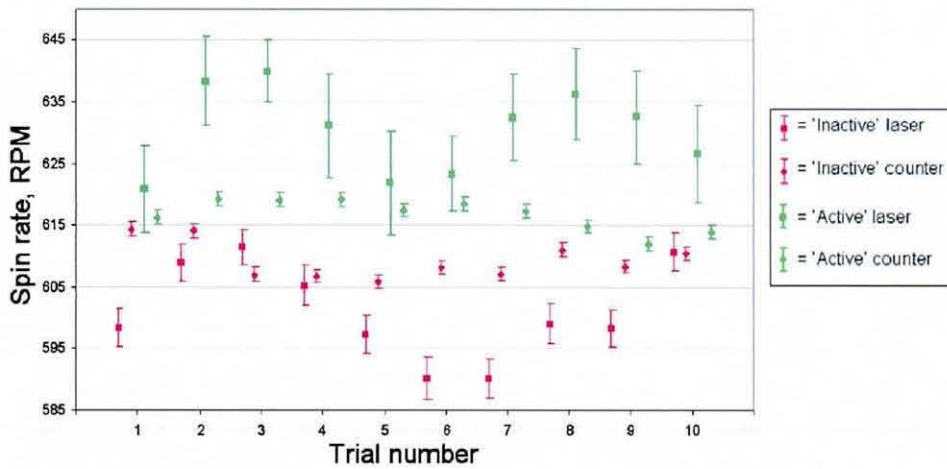


Figure 8-12: Spin rate values for 'active' and 'inactive' tracking at ~500 RPM.

## Laser based tracking and spin measurement



**Figure 8-13: Spin rate values for 'active' and 'inactive' tracking at ~600 RPM.**

The testing that combined the vibrometer and NLTS allowed concurrent and highly accurate spin rate measurement of a ball that was spinning with no translational velocity.

Figure 8-10 shows that noise is added into the measurement system when the NLTS is 'actively' tracking the target ball. Therefore the repeatability values as shown in Figure 8-11 to Figure 8-13 by the 'active' laser is between  $\pm 10$  and 12.2 RPM at the 95% confidence level for all measurements. This is greater than the repeatability values for the corresponding measurements using the 'inactive' laser measurements for all measurements, which range between  $\pm 5.2$  and 6.8 RPM at the 95% confidence level.

An interesting phenomenon is observed in Figure 8-11 through to Figure 8-13. Sinusoidal behaviour was found in the laser measurement results for both the 'active' and 'inactive' condition, which was not reflected in the respective counter spin rate values. The exact reason for this was not known, however this phenomenon was possibly attributed to a slightly changing spin axis of the ball within the 'spin rig' due to the ramp up/down of the spin rig between trials. Temperature changes were not considered because the ten trials were carried out within a 20 minute period. To fully comprehend why this phenomenon occurred further work would have to be carried out.

### 8.2.5 Pendulum rig study

A pendulum rig was designed and manufactured that allowed a FIFA 'approved' ball to be rotated as well as translated simultaneously. The spin rate and position of the ball in space were recorded by an encoder and potentiometer attached to the pendulum arm and pendulum fulcrum respectively, as illustrated in Figure 8-14. When the ball was manually moved, the ball was subject to a restoring force due to gravity, it therefore acted as a simple pendulum, causing translational velocity of the ball.

A motor and encoder were placed in series allowing rotation of the ball, a low inertia 5 volt DC servo motor was used. The motor was able to output 14 Ncm continuous torque and spin up to 1600 RPM, which fulfilled the spin rate range achieved in competitive soccer. A Hengstler 12 bit absolute shaft encoder was connected in series with the motor, outputting 64 pulses per revolution (PPR). The encoder output was directly connected into a Hameg 3 GHz programmable counter, in order to display the spin rate of the ball. The mode selected for the counter was 'RPM' which allowed input between 1 to 65535 PPR, the update time was fixed at 330 ms.

A wire wound potentiometer was attached onto the rig so that the angular position of the pendulum arm could be deciphered. The device outputted 5 volts for 360° of shaft rotation. The potentiometer system provided a linear output in relation to the angle of rotation. A brief calibration stage was carried out, 1° of rotation of the pendulum arm corresponded to a change of 0.0244 volts (to 3.s.f).

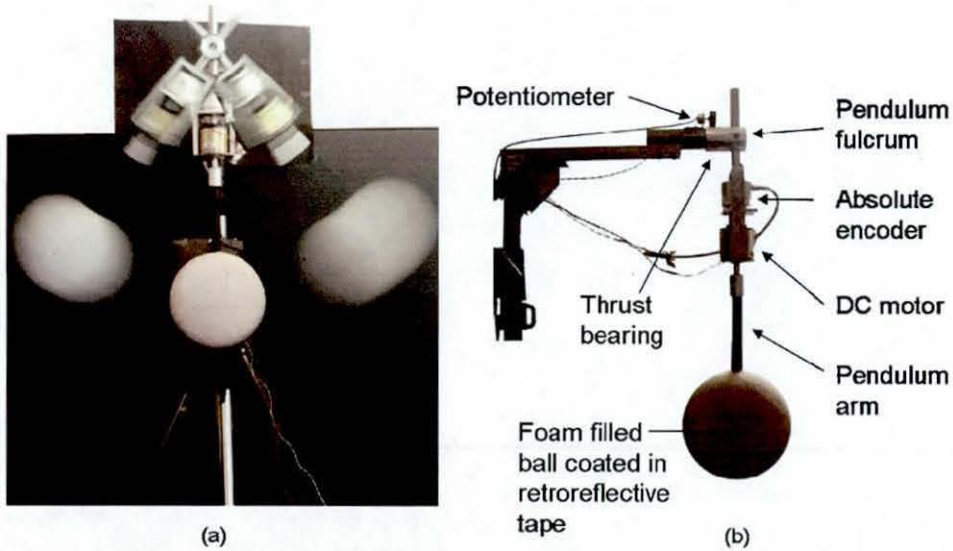


**Figure 8-14: Pendulum rig, (a) composite image of the rig in 'action', (b) side view of the rig components.**

The NLTS system as well as the single point vibrometer were set-up so that when the tracking system was at its zero position (0,0 Volts) the laser cross struck the centre of the foam filled ball coated in retroreflective tape. Throughout the testing reported in this section, the NLTS was 'active'. As the ball swung on the pendulum arm, it was tracked and its surface velocity was measured by the vibrometer.

For testing, the pendulum arm was rotated  $+50^\circ$  (counter clockwise) from the zero (vertical) position. Once the ball was released, signal acquisition was triggered and set to record for two seconds at 8.192 kHz, acquiring both the single point vibrometer velocity and the voltage output of the potentiometer system, which was converted into the angle of the pendulum arm. Ten repeats of this protocol were carried out.

The stand off distance between the NLTS and the soccer ball at zero position, was fixed at 170 cm, the pendulum rig was positioned so that the translational motion of the ball was perpendicular to the NLTS. The spin rate of the ball was fixed at approximately 200 RPM throughout testing, since higher spin rates were found to cause greater out of balance forces, leading to unstable operation of the pendulum rig. A presumption of the testing was that the distance between centre of the illuminating

'cross' and the point of incidence of the vibrometer beam remained constant in the horizontal axis. The test set-up is shown in Figure 8-15.

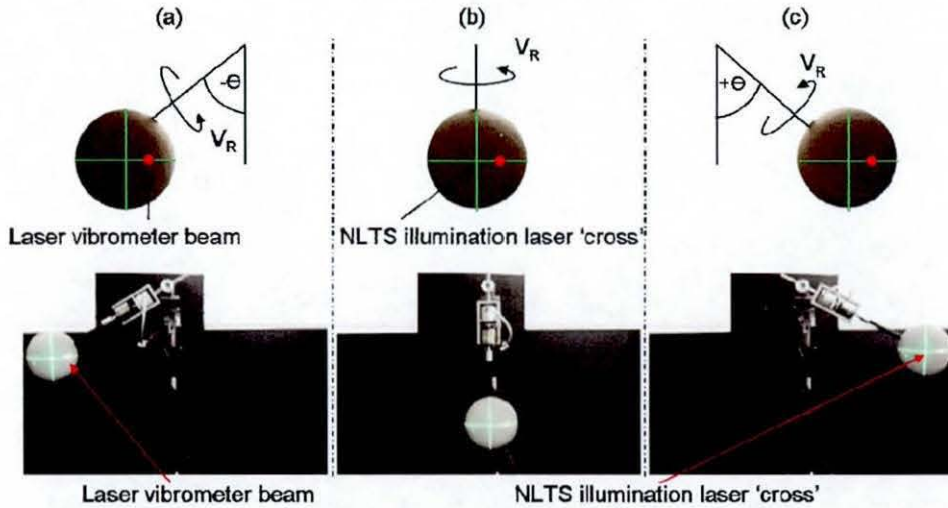


**Figure 8-15: The laser vibrometer and projected NLTS 'cross' on the ball, (a) clockwise negative rotation, (b) zero position, (c) counter clockwise positive rotation.**

Considerable noise was observed in the single point vibrometer measurement, therefore a 10 Hz low pass filter was applied to all the results of outputted vibrometer velocity. The results for two trial measurements are shown in Figure 8-16. The black line indicates the angle of the pendulum arm versus time, the magenta line indicates the 'raw' vibrometer velocity readings versus time and the red line indicates the 'filtered' vibrometer velocity readings.



## Laser based tracking and spin measurement

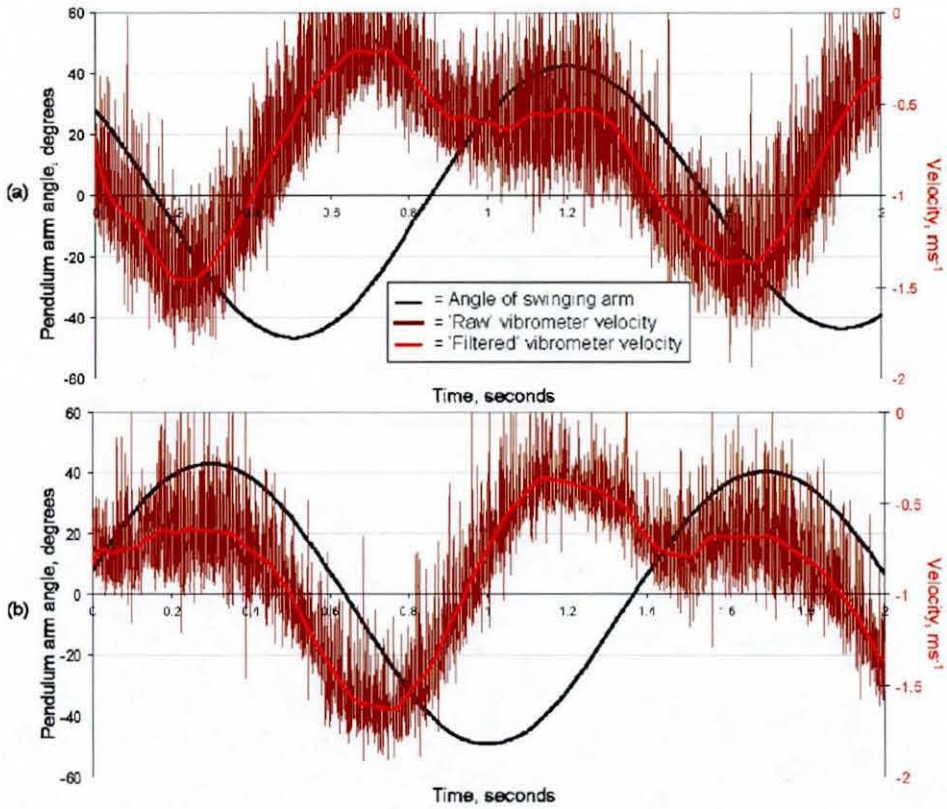


**Figure 8-16: Pendulum rig results, including the 'raw' vibrometer readings, (a) trial 1, (b) trial 10.**

The results for all ten trials showed consistent patterns between the measured vibrometer velocities and the measured pendulum arm angles. Two further trials were plotted in Figure 8-17 to show this. The 'raw' vibrometer measurements were omitted for clarity.

Laser based tracking and spin measurement

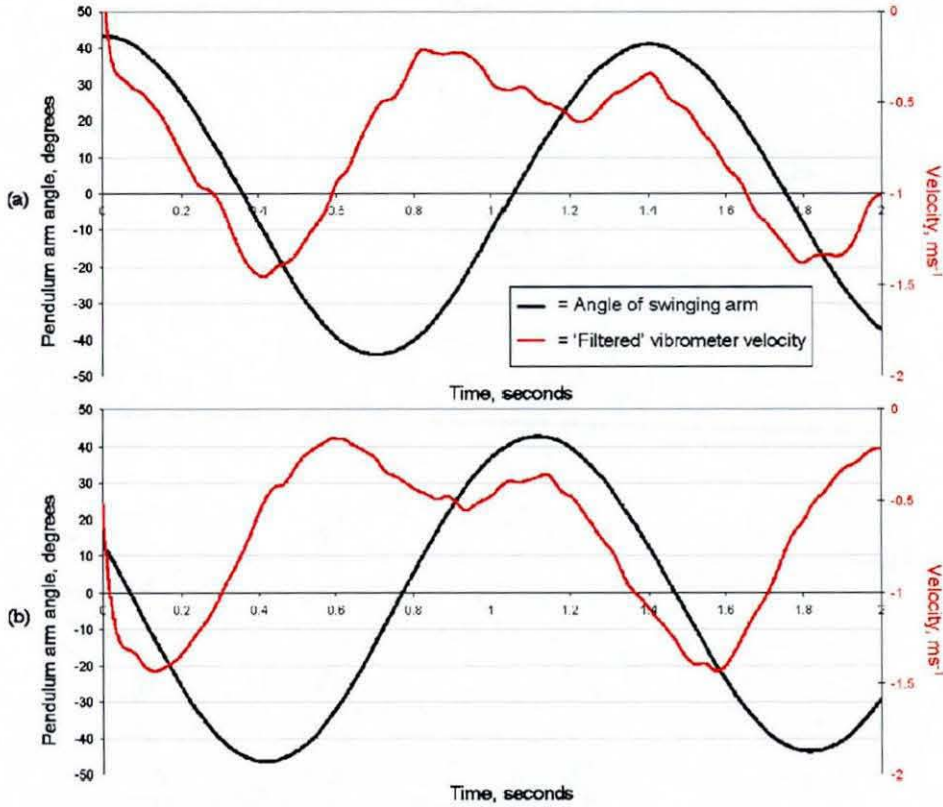


Figure 8-17: Pendulum rig results, showing 'filtered' results, (a) trial 7, (b) trial 8.

In both Figure 8-16 and Figure 8-17 data saddle trends are shown for the laser measurements which does not agree with the consistent sinusoidal results achieved for the pendulum arm angle. The reason for these consistent data saddle trends is due to the asymmetric position of the laser point to the right of the centre of the illumination laser cross. When the ball swings from position (a) to (b) in Figure 8-15 the radial distance between the laser point and the spin axis decreases due to the lag in the NLTS re-aligning itself with the centre of the ball. Therefore when the ball swings from position (c) to (b) in Figure 8-15 the radial distance between the laser point and the spin axis increases due to the lag in the NLTS re-aligning itself with the centre of the ball.

Using the information gained from the vibrometer testing, Equation 6-1 was expanded into Equation 8-1, where the pendulum arm shaft angle ( $S_A$ ) and the vertical vibrometer laser beam angle of incidence ( $V_A$ ) must be known in order to compute the

## Laser based tracking and spin measurement

radial perpendicular distance ( $r$ ) between the laser beam measurement point and the spin axis of the ball. The presumption was that the vibrometer velocity and the spin rate of the ball were known. The horizontal vibrometer laser beam angle of incidence was always fixed perpendicular to the spin axis.

$$v = 2\pi \times (r \times \sin(90 - S_A)) \times \left( \frac{RPM}{60} \right) \times \cos(V_A) \quad \text{Equation 8-1}$$

The vertical vibrometer angle of incidence,  $V_A$ , was measured between 0 and 6.6° throughout testing, therefore at worst the spin rate was influenced by ~1.5 RPM at a ball spin rate of 200 RPM. This was considered negligible, therefore for further calculations  $V_A$  was fixed at 0.

For trial 1, the spin rate was measured at 207 RPM, the maximum magnitude of velocity was measured to be 1.46 ms<sup>-1</sup>, which occurred at a shaft angle of 16.76°, the calculated radial measurement distance for this measurement point was calculated to be 7 cm (to 1.d.p.).

For trial 10, the spin rate was measured at 212 RPM, the maximum magnitude of velocity was measured to be 1.63 ms<sup>-1</sup>, which occurred at a shaft angle of 25.17°, the calculated radial measurement distance for this measurement point was calculated to be 8.1 cm (to 1.d.p.).

By observing Figure 8-16 (a&b) it is noticeable that the ball had greater momentum in trial 10 than in trial 1 shown by the larger pendulum arm angle reached. Therefore the larger radial measurement distance in trial 10 was justified due to the ball travelling faster than in trial 1.

All the information required to calculate the radial measurement distance of the laser beam from the spin axis was recorded in this test protocol. Therefore the radial distance could be computed for the entire duration of the measurement. These calculated values are shown in Figure 8-18, plotted alongside the measured vibrometer velocity values.

## Laser based tracking and spin measurement

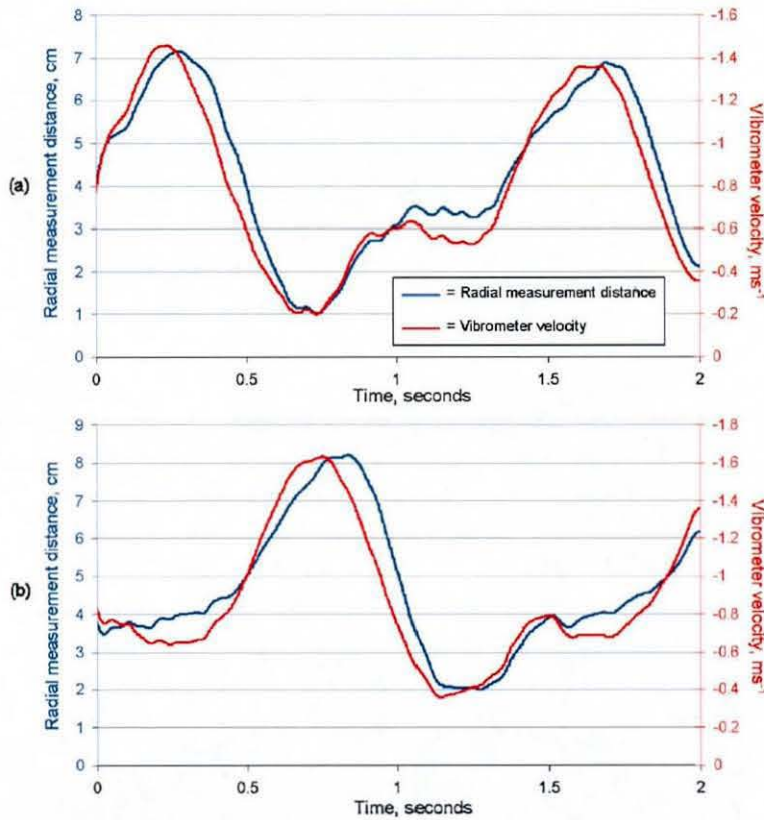


**Figure 8-18: Radial measurement distance plotted alongside vibrometer measurements, (a) trial 1, (b) trial 10.**

By examining Figure 8-18 it was noticeable that the maximal radial measurement distance was achieved immediately after the vibrometer measured the largest velocity magnitude. This result was consistent in all measurements and was accounted for by the fact that there was a delay in the NLTS between measuring target movement and repositioning the mirrors to realign with the target. The larger the ball velocity, the longer it took for the NLTS to realign with the centre of the ball.

The overall purpose of the introduction of the single point vibrometer into the NLTS was to achieve spin rate measurements of a target ball spinning. Analysis of Equation 8-1 highlighted that in the present state of the system the spin rate value could not be extracted when the ball had angular and linear velocity because the system has no method by which to measure the radial distance between laser beam and the ball spin axis.

### 8.3 Sources of error

Equation 8-2 identifies the variables that affect the computed spin rate of the ball. The vibrometer provides a measure of the surface velocity in  $\text{ms}^{-1}$ , therefore the other two variables that would influence spin rate are the radial distance between the laser beam at ball surface and the spin axis of the ball and the laser beam angle of incidence in the vertical direction.

$$RPM = \frac{60v}{2\pi \times r \times \sin(\theta)} \quad \text{Equation 8-2}$$

A three dimensional graph was plotted in Figure 8-19, showing the effect of angle of incidence and the radial measurement point perpendicularly away from the spin axis had on the measured spin rate value. A horizontal plate was plotted at exactly 600 RPM, by observing Figure 8-19 (b) it was clear that by altering the angle of incidence and the radial measurements point the same spin rate measurement could be achieved. Figure 8-19 (c) shows when the radial measurement distance was altered how this influenced the measured spin rate. By observing the vertical line in the graph it displays that by measuring the radial distance at 25 mm from the spin axis a different spin rate value could be measured dependent on the laser angle of incidence. Figure 8-19 (d) shows how measurements away from  $90^\circ$  incident angle do not measure the correct spin rate of the ball, the spin rate would be under estimated because the total component of spin would not be measured.

The effect of angle of incidence on the spin rate measurement was found to be minimal compared to the effect of the radial distance from the spin axis. A  $20^\circ$  error in angle of incidence estimation yielded an error of  $\pm 18$  RPM in the measurement spin rate, however a 5 mm error in radial distance yielded an error of  $\pm 60$  RPM in spin rate measurement. These magnitudes of error could occur and every effort must be made therefore to minimise the error in radial distance measurement, since this would cause significant errors. A 1 mm error in radial distance would cause a spin rate error of  $\pm 12$  RPM. This influence is significant and must be accounted for in all measurements.

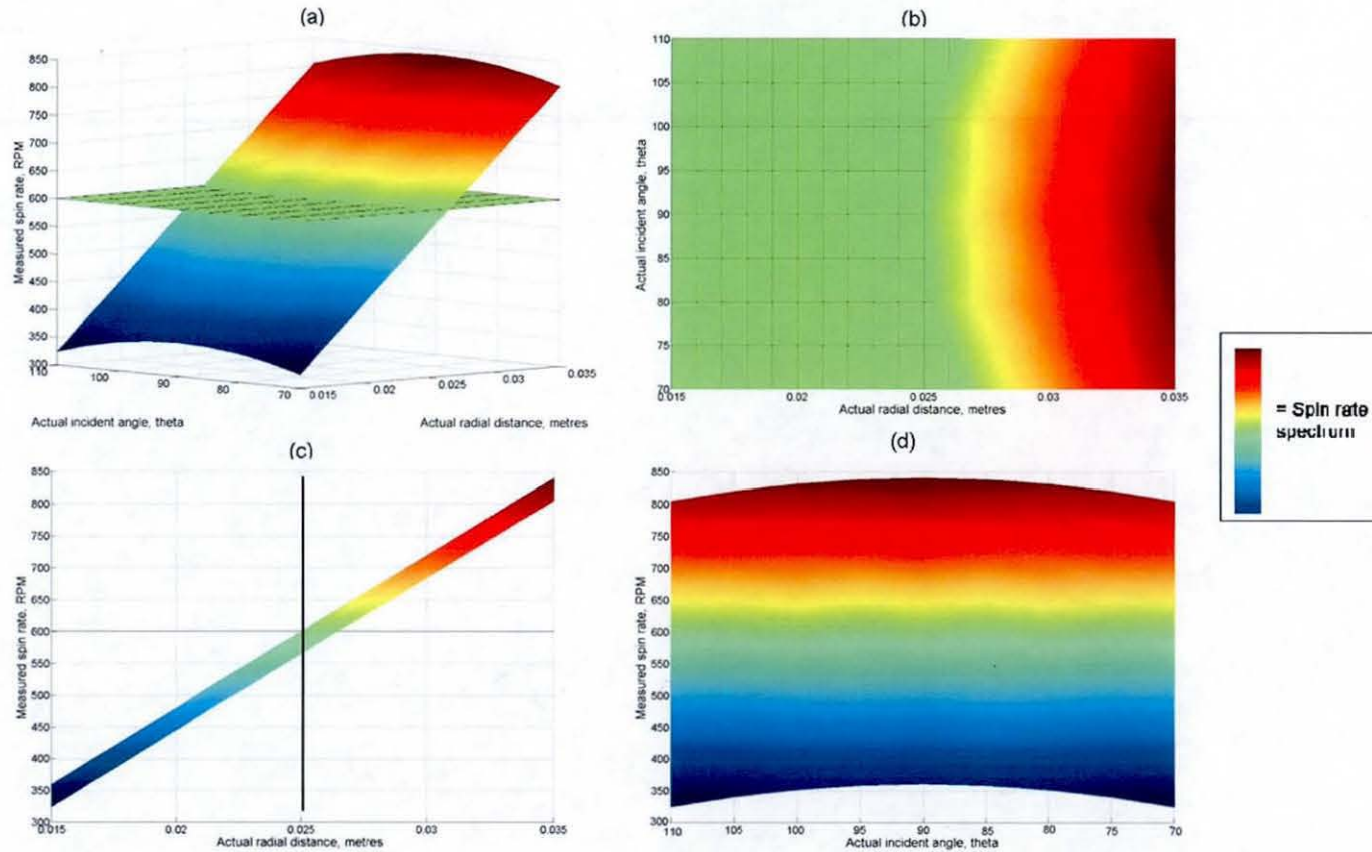


Figure 8-19: Sources of error, (a) isometric view of errors, (b) plan view, angle of incidence to achieve 600 RPM, (c) side view – change in radial distance (d) front view, change in angle of incidence.

#### **8.4 Chapter summary**

The Polytec system was selected as the most suitable commercial single point vibrometer for the surface velocity measurements reported in this Chapter. The main drawback with this vibrometer was that the target ball had to be covered in retroreflective tape in order to measure strong SNR.

Line scan and circular scan strategies were implemented for surface velocity measurement using the single point vibrometer in combination the scanning x and y-mirrors. The circular scan strategy was proven to be more desirable because it allowed the spin axis of the ball to be derived in a given plane.

The amalgamation of the single point vibrometer and the NLTS was carried out successfully. Surface velocity measurements were carried out on a ball with no translational velocity but discrete amounts of rotational velocity. The spin rate measurements were concluded to be highly accurate since the difference between the spin rates of the laser vibrometer and the 'spin rig' was found to be less than 5% for all measurements.

Further work with the single point vibrometer and the NLTS led to the first reported continuous measurement of surface velocity using a single point vibrometer on a ball with both translational and rotational velocity. The results showed that further work was required to achieve accurate spin rate measurement capability with the set-up.

Error in radial measurement distance between the spin axis and the laser measurement point was shown to dominate the error induced into vibrometry based spin rate measurement.

## 9 Conclusions and recommendations for future work

### 9.1 Conclusions

The research in this thesis has successfully reported the design, manufacture and development of an optical based system that has been demonstrated to track a non-marked sports ball. Work has been reported whereby a single point vibrometer has recorded surface velocity measurements from a spinning and translating ball.

The need for this research was established from a review of literature in the area of ball spin measurement needs, current state of the art measurement systems and previous optics research with particular focus on vibrometry and tracking applications.

Difficulties in accurately measuring sports ball spin using HSV camera technology have been identified. Errors in spin measurements made using camera based methods are likely to result from radial lens distortion and the orientation of the spin axis in relation to the camera axis. Analysis of these factors showed how errors of up to 5.5% could be introduced into the spin rate measurement. With careful attention given to the testing conditions the influence of these factors could be minimised, however in real measurement scenarios these factors were shown to be difficult to control.

Analysis of three state of the art soccer ball launch measurement systems reported for the first time, showed how the devices gave statistically different results for almost all launch variables measured. The Doppler radar system tested was found to have the most potential as a soccer ball launch and flight monitor, although it was not shown to be reliable when measuring ball spin.

The technical requirements of a soccer specific ball launch measurement device were established from published literature and additional player testing. The ranges of



## Laser based tracking and spin measurement

parameters for a maximal velocity instep kick were found to be; velocity between 10 to 34  $\text{ms}^{-1}$ , launch angle between 1 to 30° and spin rate measurement between 0 to 1000 RPM.

The application of single point laser Doppler vibrometry to record surface velocity measurements from spinning soccer balls was shown to offer significant potential. Current vibrometry capabilities were concluded to be more suitable for soccer ball application rather than golf, due to the extremely high velocities and spin rates observed in golf. FE simulations predicted that in order to record a surface velocity measurement that was representative of the translational and rotational velocity only, measurements should not occur within the first three diameters of travel after impact, since surface oscillations would influence the measurement.

A novel laser tracking system (NLTS) was developed to allow real-time tracking of a soccer ball. A need in the sports industry had been identified for an accurate, repeatable, non-contact and non-marking approach for sports ball launch parameter measurement. The NLTS combined the latest optical engineering, laser engineering, electronics and image processing hardware and software to operate on a real-time platform in order to track the target soccer ball up to circa 10  $\text{ms}^{-1}$ . Therefore the NLTS was demonstrated to work faster than previously reported systems of its kind. Significant potential exists in order to increase the speed with which the system can track as computer processor speeds increase.

A component of the research aim was to develop methods that did not require reference markers to be placed on the ball being tracked. This was met with the NLTS. Since the method of operation of the NLTS involved tracking the position of the ball with every time increment in order to update the mirrors, this information could be saved to provide a record of the balls flight path. Consequently, the NLTS was demonstrated to be capable of acting as a launch monitor, calculating and displaying the soccer ball launch angle and velocity.

Initial work carried out with the single point vibrometer and the NLTS measuring the spin rate of a ball with angular but no translational velocity was extremely successful, all spin rate values exhibited agreement within 5% of the spin rate values outputted by the 'spin rig' counter which, were assumed to be extremely close to the true value of the ball spin rate. Currently however for vibrometer measurements the target had to be covered in retroreflective tape, therefore this would require further work to make the technique extremely useful to OEMs and researchers.

The integration of a single point vibrometer within the NLTS was demonstrated to yield the first reported continuous measurement of surface velocity from a single point on a spinning and translating ball's surface. In order to correlate the measured surface velocity into a spin rate value knowledge of the laser beam angle of incidence and the perpendicular distance between the laser beam point and the spin axis was required. An error analysis of these two variables showed the fidelity in computing the spin rate value was reliant on achieving a precise measure of the perpendicular distance between spin axis and laser beam, because an error of 1 mm in this distance caused an error of  $\pm 12$  RPM in the spin rate output.

## **9.2 Recommendations for future work**

Work reported in Chapter 4 and 5 compared different measurement systems and statistically the results were analysed using a one-way ANOVA. This was considered to output a good representation of the mean and repeatability of the measurements. It is however suggested that future statistical work carrying out similar comparisons utilised the paired t-test to ensure that a difference analysis is carried out rather than simply observing the mean values.

The mechanical kicking simulator was used to achieve consistent ball launch conditions reported in Chapter 5. Three different state of the art measurement systems were used to measure these ball launch conditions and statistically different results were recorded for almost all launch conditions. Therefore a set-up that would record the true launch conditions for at least launch velocity and launch angle should be created maybe utilising a series of light gates.

## Laser based tracking and spin measurement

A significant initial contribution has been made towards creating a laser based tracking and spin measurement device for sports applications. Considerable potential exists to develop the current system further. The next stage of work would be to address the areas in which the system could be made to function better than in the prototype device, these improvements are classed into short, medium and long term targets.

The current functionality of the NLTS could be improved by short term developments of the existing set-up. The NLTS was currently set to operate in the Windows environment on a top of the range PC for circa 2004. With rapid advances in computer technology the NLTS could be made to function more quickly by simply using the latest PC. However making the image processing part of the NLTS operate on specifically designed digital signal processing (DSP) boards or field programmable gate arrays (FPGAs) would allow for even faster image processing and update speeds, making the real-time component of the system even quicker, ultimately allowing the NLTS to track faster moving targets.

The DOE used in the system was a crucial component for the functionality of the NLTS. In order to optimise the optical efficiency of the system and achieve a better distribution of light, reducing the amount of light projected in the zero order of the beam a custom designed DOE would be required.

Although in the current design, the initial identification of the ball position was made manually, to automate this process an inexpensive option was suggested. By using a web camera the ball could be located in the system FOV, by using simple image processing techniques the galvo mirrors could be steered towards the ball.

The single point vibrometer combined with the NLTS outputted surface velocity readings of a ball with both angular and translational velocity. It was ascertained that in order to output accurate spin rate measurements the perpendicular distance between the laser beam and the spin axis had to be accurately recorded. This was not possible with the current NLTS set-up. Therefore a medium term solution would be to insert an

## Laser based tracking and spin measurement

additional system that could output this measurement distance in real-time working alongside the current NLTS.

Ideally, measurements would be taken throughout the flight of a soccer ball, perhaps up to 30 metres for a free kick. In order to increase the current system FOV the base plate that housed the core system components could be placed onto a rotary stage. This would permit large angular movements, whilst still allowing the galvo mirrors to steer the laser pattern precisely onto the target soccer ball.

In order to realign and track the target ball the image processing stage relied on detecting all four intersection points, which were found on the edge of the ball in the processed image. Currently with large movements of the target ball, one or two of these intersection points did not necessarily correlate with the edge of the ball, because the whole ball was not imaged by the camera. By enlarging the FOV imaged by the camera this issue would be overcome, this would allow faster and more accurate tracking of the target ball.

One single point vibrometer was used in most surface velocity measurements. The theory outlined in the optical literature review stated that in order to achieve spin rate around two axes of rotation in a single measurement, three laser beams would be required. It is therefore suggested that in the long term a three beam laser vibrometer system be combined with the NLTS. The vibrometer itself could be designed specifically for the sports ball application. The main design modifications would involve developing a vibrometer with a larger velocity measurement range, a collimated beam output and an increase in measured SNR from diffuse targets.

The spin axis of the ball in a given plane could be extracted and the magnitude of surface velocities by the circular scan work carried out using one single point vibrometer. Therefore a radically different approach is suggested to achieving three dimensional spin rate than by purely increasing the number of single point vibrometers. By combination of the current tracking strategy and a single point vibrometer measurement beam that performs a circular or similar scan profile whilst

## Laser based tracking and spin measurement

being projected onto the ball through the scanning mirrors, could allow the three dimensional spin rate and spin axis of the ball to be calculated if the measurements were carried out over a longer time duration. This method would involve two sets of tracking mirrors working together which would demand an intricate physical set-up.

The research has proven that velocity measurements can be taken from specific points on the surface of translating and spinning balls. Whatever strategies are employed in the future to better discriminate between the different contributing velocity components, this work has demonstrated the potential of laser measurement to be a useful tool.

The recommendations for future work suggested short, medium and long term strategies for improving the current prototype NLTS. The work in this thesis has reported a significant contribution to the first stage of a multistage optical approach to achieving a device that can measure launch velocity, launch angle, spin rate and spin axis.

## Appendix A

Example calculation for Table 4-3.

$y_1$  and  $y_2 = 2$  metres, spin rate of the ball = 600 RPM.

When  $x_1$  and  $x_2 = 0.1$  metres

Angle,  $\theta = \text{ATAN}(0.1/2) = 2.86^\circ$

Angle,  $\theta \times 2 = 5.72^\circ$

Total angle rotated by the ball =  $5.72^\circ + 360^\circ = 365.72^\circ$

The ball is rotating at 600 RPM, thus = 10 RPS, thus ball rotating  $3600^\circ$  in 1 second,  $1^\circ$  in 0.000478 seconds.

Time for ball to complete the measured rotation =  $365.72^\circ \times 0.000278 \text{ s} = 0.102 \text{ s}$

The calculated RPS of the ball =  $1/0.102 = 9.84 \text{ RPS}$

The calculated spin rate =  $9.84 \times 60 = \underline{590.6 \text{ RPM}}$

Example calculation for Table 4-4.

$x_1$  and  $x_2 = 0.5$  metres, spin rate of the ball = 600 RPM

When  $y_1$  and  $y_2 = 0.5$  metres

Angle,  $\theta = \text{ATAN}(0.5/0.5) = 45^\circ$

Angle,  $\theta \times 2 = 90^\circ$

Total angle rotated by the ball =  $90^\circ + 360^\circ = 450^\circ$

The ball is rotating at 600 RPM, thus = 10 RPS, thus ball rotating  $3600^\circ$  in 1 second,  $1^\circ$  in 0.000478 seconds.

Time for ball to complete the measured rotation =  $450^\circ \times 0.000278 \text{ s} = 0.125 \text{ s}$

The calculated RPS of the ball =  $1/0.125 = 8 \text{ RPS}$

The calculated spin rate =  $8 \times 60 = \underline{480 \text{ RPM}}$

## Appendix B

The code written in the Matlab script for the 'virtual vibrometer' GUI. Text in black and blue are command lines. Green text is annotations to go with the command lines.

```
function varargout = Saw_Tooth_velocityProfile_14arp07(varargin)
% SAW_TOOTH_VELOCITYPROFILE_14ARP07 M-file for
% Saw_Tooth_velocityProfile_14arp07.fig
%     SAW_TOOTH_VELOCITYPROFILE_14ARP07, by itself, creates a new
%     SAW_TOOTH_VELOCITYPROFILE_14ARP07 or raises the existing
%     singleton*.
%
%     H = SAW_TOOTH_VELOCITYPROFILE_14ARP07 returns the handle to a
%     new SAW_TOOTH_VELOCITYPROFILE_14ARP07 or the handle to
%     the existing singleton*.
%
%     SAW_TOOTH_VELOCITYPROFILE_14ARP07('CALLBACK',hObject,eventData,handle
%     s,...) calls the local
%     function named CALLBACK in SAW_TOOTH_VELOCITYPROFILE_14ARP07.M
%     with the given input arguments.
%
%     SAW_TOOTH_VELOCITYPROFILE_14ARP07('Property','Value',...)
%     creates a new SAW_TOOTH_VELOCITYPROFILE_14ARP07 or raises the
%     existing singleton*. Starting from the left, property value
%     pairs are
%     applied to the GUI before
%     Saw_Tooth_velocityProfile_14arp07_OpeningFunction gets called. An
%     unrecognized property name or invalid value makes property
%     application
%     stop. All inputs are passed to
%     Saw_Tooth_velocityProfile_14arp07_OpeningFcn via varargin.
%
%     *See GUI Options on GUIDE's Tools menu. Choose "GUI allows
%     only one
%     instance to run (singleton)".
%
% See also: GUIDE, GUIDATA, GUIHANDLES

% Edit the above text to modify the response to help
% Saw_Tooth_velocityProfile_14arp07

% Last Modified by GUIDE v2.5 08-Sep-2006 15:12:59

% Begin initialization code - DO NOT EDIT
gui_Singleton = 1;
gui_State = struct('gui_Name',       mfilename, ...
                  'gui_Singleton',  gui_Singleton, ...
```

## Laser based tracking and spin measurement

```
        'gui_OpeningFcn',
@Saw_Tooth_velocityProfile_14arp07_OpeningFcn, ...
        'gui_OutputFcn',
@Saw_Tooth_velocityProfile_14arp07_OutputFcn, ...
        'gui_LayoutFcn', [] , ...
        'gui_Callback', []);
if nargin && ischar(varargin{1})
    gui_State.gui_Callback = str2func(varargin{1});
end

if nargin
    [varargout{1:nargout}] = gui_mainfcn(gui_State, varargin{:});
else
    gui_mainfcn(gui_State, varargin{:});
end
% End initialization code - DO NOT EDIT

% --- Executes just before Saw_Tooth_velocityProfile_14arp07 is made
% visible.
function Saw_Tooth_velocityProfile_14arp07_OpeningFcn(hObject,
 eventdata, handles, varargin)
% This function has no output args, see OutputFcn.
% hObject    handle to figure
% eventdata  reserved - to be defined in a future version of MATLAB
% handles    structure with handles and user data (see GUIDATA)
% varargin   command line arguments to
Saw_Tooth_velocityProfile_14arp07 (see VARARGIN)

% Choose default command line output for
Saw_Tooth_velocityProfile_14arp07
handles.output = hObject;

% Update handles structure
guidata(hObject, handles);

% UIWAIT makes Saw_Tooth_velocityProfile_14arp07 wait for user
% response (see UIRESUME)
% uiwait(handles.figure1);

% ball1 = linspace(0,180,50);
% handles.ball1 = ball1;
% guidata(hObject,handles);
set(handles.figure1, 'Name','Virtual Single Point Vibrometer'); %
name for the graph

% --- Outputs from this function are returned to the command line.
function varargout =
Saw_Tooth_velocityProfile_14arp07_OutputFcn(hObject, eventdata,
handles)
% varargout  cell array for returning output args (see VARARGOUT);
% hObject    handle to figure
```



## Laser based tracking and spin measurement

```
% eventdata reserved - to be defined in a future version of MATLAB
% handles structure with handles and user data (see GUIDATA)

% Get default command line output from handles structure
varargout{1} = handles.output;

% --- Executes on button press in calculate.
function calculate_Callback(hObject, eventdata, handles)
% hObject handle to calculate (see GCBO)
% eventdata reserved - to be defined in a future version of MATLAB
% handles structure with handles and user data (see GUIDATA)

if (str2double(get(handles.ang, 'String')) == 0);
    time = 50; % if the vibrometer is on-axis to the ball travel,
time would be infinite in reality set at 50s arbitrarily
else
    time = (handles.dial)/(handles.bv1*(sin(deg2rad(handles.ang1))));
% time it takes for laser velocity measurement
end

rads1 = linspace(-(handles.dial/2),(handles.dial/2),500); % 500
linearly placed points along the ball are measured
% rads1 = abs(rads);

% if (str2double(get(handles.dia, 'String')) == 0.22);
% ball1 = linspace(90,-90,500);
% else
% ball1 = linspace(+acosd((handles.dial/2)/0.11),-
acosd((handles.dial/2)/0.11),500);
% end

for i = 1:500;
    mv(i) = (((handles.bv1) * (cos(deg2rad(handles.ang1))))+...
    ((rads1(i))*2*pi*((handles.rpm1)/60)*sin(deg2rad(90)))); %
dont really need sin(deg2rad(90)) in the equation
% First line of calculations is translational velocity component that
laser
% measures
% Second line is rotational velocity component that vibrometer
measures
end

axes(handles.graph1);
format long;
% % offset = 0
% if (str2double(get(handles.dia, 'String')) == 0.22);
%     offset = 0
% else
```

## Laser based tracking and spin measurement

```
constant = (0.22/(handles.bv1*cos(deg2rad(handles.ang1))))/2; %
setting constant from which measurements start
constant2 =
(handles.dial/(handles.bv1*cos(deg2rad(handles.ang1))))/2;
offset = constant-constant2;

x = linspace(0,time,500); % x values set equally apart for the whole
time duration of laser measurement

mv1 = mv % unnessecary step
plot(x,mv1,'k-');
xlabel('Time, Seconds');
ylabel('Velocity, m/s');
axis([0 max(time) min(mv1) max(mv1)]);
hold on
datacursormode;

function bv_Callback(hObject, eventdata, handles)
% hObject    handle to bv (see GCBO)
% eventdata  reserved - to be defined in a future version of MATLAB
% handles    structure with handles and user data (see GUIDATA)

% Hints: get(hObject,'String') returns contents of bv as text
%        str2double(get(hObject,'String')) returns contents of bv as
a double

bv1 = str2double(get(hObject,'string'));
if isnan(bv1)
    set(hObject,'String',0);
    errorDlg('input has to be a number you idiot','Error');
end
handles.bv1 = bv1;
guidata(hObject,handles)

% --- Executes during object creation, after setting all properties.
function bv_CreateFcn(hObject, eventdata, handles)
% hObject    handle to bv (see GCBO)
% eventdata  reserved - to be defined in a future version of MATLAB
% handles    empty - handles not created until after all CreateFcns
called

% Hint: edit controls usually have a white background on Windows.
%        See ISPC and COMPUTER.
if ispc && isequal(get(hObject,'BackgroundColor'),
get(0,'defaultUicontrolBackgroundColor'))
    set(hObject,'BackgroundColor','white');
end

function rpm_Callback(hObject, eventdata, handles)
```

## Laser based tracking and spin measurement

```
% hObject    handle to rpm (see GCBO)
% eventdata  reserved - to be defined in a future version of MATLAB
% handles     structure with handles and user data (see GUIDATA)

% Hints: get(hObject,'String') returns contents of rpm as text
%         str2double(get(hObject,'String')) returns contents of rpm as
a double

rpml = str2double(get(hObject,'string'));
if isnan(rpml)
    set(hObject,'String',0);
    errordlg('input has to be a number you idiot','Error');
end
handles.rpml = rpml;
guidata(hObject,handles)

% --- Executes during object creation, after setting all properties.
function rpm_CreateFcn(hObject, eventdata, handles)
% hObject    handle to rpm (see GCBO)
% eventdata  reserved - to be defined in a future version of MATLAB
% handles     empty - handles not created until after all CreateFcns
called

% Hint: edit controls usually have a white background on Windows.
%         See ISPC and COMPUTER.
if ispc && isequal(get(hObject,'BackgroundColor'),
get(0,'defaultUicontrolBackgroundColor'))
    set(hObject,'BackgroundColor','white');
end

function ang_Callback(hObject, eventdata, handles)
% hObject    handle to ang (see GCBO)
% eventdata  reserved - to be defined in a future version of MATLAB
% handles     structure with handles and user data (see GUIDATA)

% Hints: get(hObject,'String') returns contents of ang as text
%         str2double(get(hObject,'String')) returns contents of ang as
a double

ang1 = str2double(get(hObject,'string'));
if isnan(ang1)
    set(hObject,'String',0);
    errordlg('input has to be a number you idiot','Error');
end
handles.ang1 = ang1;
guidata(hObject,handles)

% --- Executes during object creation, after setting all properties.
function ang_CreateFcn(hObject, eventdata, handles)
% hObject    handle to ang (see GCBO)
```

## Laser based tracking and spin measurement

```
% eventdata reserved - to be defined in a future version of MATLAB
% handles empty - handles not created until after all CreateFcns
called

% Hint: edit controls usually have a white background on Windows.
% See ISPC and COMPUTER.
if ispc && isequal(get(hObject,'BackgroundColor'),
get(0,'defaultUicontrolBackgroundColor'))
    set(hObject,'BackgroundColor','white');
end

function dia_Callback(hObject, eventdata, handles)
% hObject handle to dia (see GCBO)
% eventdata reserved - to be defined in a future version of MATLAB
% handles structure with handles and user data (see GUIDATA)

% Hints: get(hObject,'String') returns contents of dia as text
% str2double(get(hObject,'String')) returns contents of dia as
a double

dial = str2double(get(hObject,'string'));
if isnan(dial)
    set(hObject,'String',0);
    errordlg('input has to be a number','Error');
end
handles.dial = dial;
guidata(hObject,handles);

% --- Executes during object creation, after setting all properties.
function dia_CreateFcn(hObject, eventdata, handles)
% hObject handle to dia (see GCBO)
% eventdata reserved - to be defined in a future version of MATLAB
% handles empty - handles not created until after all CreateFcns
called

% Hint: edit controls usually have a white background on Windows.
% See ISPC and COMPUTER.
if ispc && isequal(get(hObject,'BackgroundColor'),
get(0,'defaultUicontrolBackgroundColor'))
    set(hObject,'BackgroundColor','white');
end
```

## Appendix C

Pulnix TM-6740GE settings for testing in Chapter 7.

- PIXEL TYPE
- Greyscale
  - 8 bits
  - Tap quantity, 2
  - 2 taps, interleaved
- DEVICE FEATURES -
- Pulse Generator 0
  - Width, 718 ( 718 + 17 = 180 FPS)
  - Delay, 17 (1/8000 shutter speed)
  - Granularity, 250
  - Periodic, true
  - Triggered on rising edge
- CAMERA SOFTWARE
- Exposure
  - Mode, Async
  - Shutter speed, 9
  
  - Gain settings
  - 5.94 dB (lowest setting)
  - 5.94 dB
  
  - Scan modes
  - A, 640 × 480 (full resolution)
  - Binning, 2 × 2, pixel output 320 × 240
  
  - LUT, positive, linear selection
  - X1 = 11, X2 = 40, Y1 = 1, Y2 = 225

## Appendix D

Code for NLTS software.

```

*****
'
'          NOVEL LASER TRACKING SYSTEM CODE
'
' Program : Soccer ball laser tracking - Full code
' Author  : J A Ronkainen
' Date    : November 2007
'
'
*****

' declarations section

Private DoGrab2 As Short
Private timer As Integer
Private GrabMode As String
Private TimeMS As Double

Private PixelX As Single
Private VoltageX1 As Single
Private VoltageX2 As Single

Private Pixely As Single
Private VoltageY1 As Single
Private VoltageY2 As Single

Private m_blaunch As Boolean
Private m_btrack As Boolean
Private m_iXZero As Integer
Private m_iYZero As Integer
Private i As Integer
Private xx(255), yy(255) As Single
Private LaunchX As Single

Private card As Short
Private cont As Integer

Private Sub Form1_Load(ByVal sender As System.Object, ByVal e As
System.EventArgs) Handles MyBase.Load

    card = D2K_Register_Card(DAQ_2501, 0)
    D2K_AO_CH_Config(card, -1, DAQ2K_DA_BiPolar,
DAQ2K_DA_Int_REF, 10) ' initial card config, -1 sets all 4 AO chans,
int ref = 10, want bipolar output
    m_iXZero = 159
    m_iYZero = 119

    Picture_one.Image =
System.Drawing.Image.FromFile("C:\vbfiles\Pictures\JR.jpeg")
    Picture_two.Image =
System.Drawing.Image.FromFile("C:\vbfiles\Pictures\JR2.jpg")

```

## Laser based tracking and spin measurement

```
'Set left edge detect values
Edge_left.X0 = 0
Edge_left.X1 = 0
Edge_left.X2 = 159
Edge_left.Y0 = 119
Edge_left.Y1 = 119
Edge_left.Y2 = 119

'set right edge detect values
Edge_Right.X0 = 319
Edge_Right.X1 = 319
Edge_Right.X2 = 159
Edge_Right.Y0 = 119
Edge_Right.Y1 = 119
Edge_Right.Y2 = 119

'set top edge detect values
Edge_Top.X0 = 159
Edge_Top.X1 = 159
Edge_Top.X2 = 159
Edge_Top.Y0 = 0
Edge_Top.Y1 = 0
Edge_Top.Y2 = 119

'Set bottom edge values
Edge_bottom.X0 = 159
Edge_bottom.X1 = 159
Edge_bottom.X2 = 159
Edge_bottom.Y0 = 239
Edge_bottom.Y1 = 239
Edge_bottom.Y2 = 119

' Do the following snap,imager2to2, lut *3, edge *3, Filter
*3, this is so that images are ready to track
'snap
cvImage.Snap()
cvDisplay.Image = cvImage.Image
cvDisplay.Refresh()

'image 1 to 2
cvDisplay2.Image = cvDisplay.Image
cvDisplay2.Refresh()

'Edge, LUT, and filter *3
Filter.ImageIn = cvDisplay2.Image
Filter.Execute()
Filter.ImageIn = cvDisplay2.Image
Filter.Execute()
Filter.ImageIn = cvDisplay2.Image
Filter.Execute()

Lut.ImageIn = cvDisplay2.Image
Lut.Execute()
Lut.ImageIn = cvDisplay2.Image
Lut.Execute()
Lut.ImageIn = cvDisplay2.Image
Lut.Execute()

Edge_left.Image = cvDisplay2.Image
```

## Laser based tracking and spin measurement

```
Edge_left.Execute()
Edge_left.Image = cvDisplay2.Image
Edge_left.Execute()

Edge_Right.Image = cvDisplay2.Image
Edge_Right.Execute()
Edge_Right.Image = cvDisplay2.Image
Edge_Right.Execute()

Edge_Top.Image = cvDisplay2.Image
Edge_Top.Execute()
Edge_Top.Image = cvDisplay2.Image
Edge_Top.Execute()

Edge_bottom.Image = cvDisplay2.Image
Edge_bottom.Execute()
Edge_bottom.Image = cvDisplay2.Image
Edge_bottom.Execute()

End Sub

Private Sub cvImage_ImageSnaped(ByVal sender As Object, ByVal e
As System.EventArgs) Handles cvImage.ImageSnaped
    Dim timer As Integer
    TWCreate(timer)
    TWStartStopWatch(timer, 0)

    'cvDisplay.Image = cvImage.Image
    If m_btrack = True Then
        processImage()
    End If

    cvDisplay.Refresh()

End Sub

Private Sub CheckBox_Grab_CheckStateChanged(ByVal sender As
Object, ByVal e As System.EventArgs) Handles
CheckBox_Grab.CheckStateChanged
    cvImage.Grab = CheckBox_Grab.CheckState
    cvDisplay.Image = cvImage.Image
End Sub

Private Sub button_track_Click(ByVal sender As System.Object,
ByVal e As System.EventArgs) Handles button_track.Click

    Lut.LUTIndex = 1
    Lut.LUTLevel = Textbox_ThresholdValue.Text

    If m_btrack = False Then
        m_btrack = True
        button_track.Text() = " Stop Tracking "
    Else
        m_btrack = False
        button_track.Text() = " Start Tracking "
    End If

End Sub

Public Sub processImage()
```



## Laser based tracking and spin measurement

```
'LUT
Lut.ImageIn = cvImage.Image
Lut.Execute()

'Filter
Filter.ImageIn = Lut.ImageOut
Filter.Execute()

Dim xcoord(1) As Single
Dim ycoord(3) As Single

'do Edge
'Edge_left.Image = Lut.ImageOut
Edge_left.Image = Filter.ImageOut
Edge_left.Execute()
xcoord(0) = Edge_left.PX

'Edge_Right.Image = Lut.ImageOut()
Edge_Right.Image = Filter.ImageOut()
Edge_Right.Execute()
xcoord(1) = Edge_Right.PX
If xcoord(1) = 0 Then
    xcoord(1) = 320
End If

'Edge_Top.Image = Lut.ImageOut
Edge_Top.Image = Filter.ImageOut
Edge_Top.Execute()
ycoord(2) = Edge_Top.PY

'Edge_bottom.Image = Lut.ImageOut
Edge_bottom.Image = Filter.ImageOut
Edge_bottom.Execute()
ycoord(3) = Edge_bottom.PY
If ycoord(3) = 0 Then
    ycoord(3) = 240
End If

PixelX = (xcoord(0) + xcoord(1)) / 2
PixelY = (ycoord(2) + ycoord(3)) / 2

'update X-mirror voltage
VoltageX1 = (PixelX - m_iXZero)
VoltageX1 = VoltageX1 * 0.003693439

'update Y-Mirror voltage
VoltageY1 = (PixelY - m_iYZero)
VoltageY1 = VoltageY1 * 0.004610918

' change x-mirror position
VoltageX2 = (VoltageX2 + VoltageX1)
D2K_AO_Group_Set-up(card, DA_Group_A, 1, 0)
D2K_AO_Group_VUpdate(card, DA_Group_A, VoltageX2)

'change y-mirror position
VoltageY2 = (VoltageY2 + VoltageY1)
D2K_AO_Group_Set-up(card, DA_Group_A, 1, 1)
D2K_AO_Group_VUpdate(card, DA_Group_A, VoltageY2)
'End If
End Sub
```

## Laser based tracking and spin measurement

```
Private Sub Button_Snap_Click(ByVal sender As System.Object,
ByVal e As System.EventArgs) Handles Button_Snap.Click
    'stop grabbing
    cvImage.Grab = False
    'uncheck the checkbox_grab
    CheckBox_Grab.Checked = False
    'snap the image
    cvImage.Snap()
    cvDisplay.Image = cvImage.Image
    cvDisplay.Refresh()
End Sub

Private Sub Button_Load_Click(ByVal sender As System.Object,
ByVal e As System.EventArgs) Handles Button_Load.Click
    cvImage.LoadImageByDialog()
    cvDisplay.Image = cvImage.Image
    cvDisplay.Refresh()
End Sub

Private Sub Button_SaveDisplay1_Click(ByVal sender As
System.Object, ByVal e As System.EventArgs) Handles
Button_SaveDisplay1.Click
    cvDisplay.SaveImageByDialog()
End Sub

Private Sub Button_Savedisplay2_Click(ByVal sender As
System.Object, ByVal e As System.EventArgs) Handles
Button_Savedisplay2.Click
    cvDisplay2.SaveImageByDialog()
End Sub

Private Sub Button1_Click(ByVal sender As System.Object, ByVal e
As System.EventArgs) Handles Button_saveLut.Click
    cvDisplay.Image = Lut.ImageOut
    cvDisplay.SaveImageByDialog()
End Sub

Private Sub Button_SaveFilter_Click(ByVal sender As
System.Object, ByVal e As System.EventArgs) Handles
Button_SaveFilter.Click
    cvDisplay2.RemoveAllLabels()
End Sub

Private Sub button_Filter_Click(ByVal sender As System.Object,
ByVal e As System.EventArgs) Handles button_Filter.Click
    Dim TimeMS As Double
    Dim Timer As Integer
    TWCreate(Timer)
    TWStartStopWatch(Timer, 0)
    Filter.ImageIn = cvDisplay2.Image
    Filter.Execute()

    TWReadStopWatch(Timer, 0, TimeMS)
    cvDisplay2.StatusUserText = "Processing Time : " +
FormatNumber(TimeMS, 3) + " ms "

    cvDisplay2.Image = Filter.ImageOut
    cvDisplay2.Refresh()
End Sub
```

## Laser based tracking and spin measurement

```
Private Sub TrackBar_Voltage_Scroll(ByVal sender As
System.Object, ByVal e As System.EventArgs) Handles
TrackBar_VoltageX.Scroll
    Text_ScrollX.Text() = TrackBar_VoltageX.Value
    'Dim voltages As Double
    'voltage = text_voltage.Text()
End Sub

Private Sub Button_Daq_Click(ByVal sender As System.Object, ByVal
e As System.EventArgs) Handles Button_Daq.Click
    card = D2K_Register_Card(DAQ_2501, 0)
    D2K_AO_CH_Config(card, -1, DAQ2K_DA_BiPolar,
DAQ2K_DA_Int_REF, 10) ' initial card config, -1 sets all 4 AO chans,
int ref = 10, want bipolar output
End Sub

Private Sub button_freezedaq_Click(ByVal sender As System.Object,
ByVal e As System.EventArgs) Handles button_freezedaq.Click
    D2K_Release_Card(0) ' to stop the card outputting voltage
readings
End Sub

Private Sub TrackBar_VoltageY_Scroll(ByVal sender As
System.Object, ByVal e As System.EventArgs) Handles
TrackBar_VoltageY.Scroll
    Text_ScrollY.Text() = TrackBar_VoltageY.Value
End Sub

Private Sub Button1_Click_1(ByVal sender As System.Object, ByVal
e As System.EventArgs) Handles Button1.Click
    G2Freeze(cvImage.Image, True)
    Button_Snap.Enabled = True
    CheckBox_Grab.Enabled = True
End Sub

Private Sub Button2_Click(ByVal sender As System.Object, ByVal e
As System.EventArgs) Handles Button2.Click
    cvDisplay2.Image = cvDisplay.Image
    cvDisplay2.Refresh()
End Sub

Private Sub CheckBox_STOP_CheckedChanged(ByVal sender As
System.Object, ByVal e As System.EventArgs) Handles
CheckBox_STOP.CheckedChanged
    DoGrab2 = False
    G2Freeze(cvImage.Image, True)
    Button_Snap.Enabled = True
    CheckBox_Grab.Enabled = True
End Sub

Private Sub Button_Edge_Click(ByVal sender As System.Object,
ByVal e As System.EventArgs) Handles Button_Edge.Click

    Dim xcoord(3) As Double
    Dim ycoord(3) As Double

    'do Edge
    Edge_left.Image = cvDisplay2.Image
    Edge_left.Execute()
```

## Laser based tracking and spin measurement

```

xcoord(0) = Edge_left.PX
ycoord(0) = Edge_left.PY

Edge_Right.Image = cvDisplay2.Image
Edge_Right.Execute()
xcoord(1) = Edge_Right.PX
ycoord(1) = Edge_Right.PY
If xcoord(1) = 0 Then
    xcoord(1) = 320
End If

Edge_Top.Image = cvDisplay2.Image
Edge_Top.Execute()
xcoord(2) = Edge_Top.PX
ycoord(2) = Edge_Top.PY

Edge_bottom.Image = cvDisplay2.Image
Edge_bottom.Execute()
xcoord(3) = Edge_bottom.PX
ycoord(3) = Edge_bottom.PY
If ycoord(3) = 0 Then
    ycoord(3) = 240
End If

cvDisplay2.RemoveAllLabels()
cvDisplay2.AddLabel("C", False, RGB(128, 0, 0), 1, xcoord(0),
ycoord(0))
cvDisplay2.AddLabel("C", False, RGB(128, 0, 0), 1, xcoord(1),
ycoord(1))
cvDisplay2.AddLabel("C", False, RGB(128, 0, 0), 1, xcoord(2),
ycoord(2))
cvDisplay2.AddLabel("C", False, RGB(128, 0, 0), 1, xcoord(3),
ycoord(3))

PixelX = (xcoord(0) + xcoord(1)) / 2
PixelY = (ycoord(2) + ycoord(3)) / 2
Text_UpdateX.Text() = PixelX
Text_UpdateY.Text() = PixelY

cvDisplay2.AddLabel("XY", False, RGB(0, 255, 0), 1, PixelX,
PixelY)
End Sub

Private Sub Text_ScrollX_TextChanged(ByVal sender As
System.Object, ByVal e As System.EventArgs) Handles
Text_ScrollX.TextChanged
    Dim ScrollX_voltage As Single

    ScrollX_voltage = Text_ScrollX.Text

    D2K_AO_Group_Set-up(card, DA_Group_A, 1, 0) ' last integer
decides which channel voltage is outputted from ( 0 to 3)
'wNumChan as short, decides how many channels are in this
group ( want one group for x mirror and one group for y mirror)
D2K_AO_Group_VUpdate(card, DA_Group_A, ScrollX_voltage)
VoltageX2 = ScrollX_voltage
End Sub

```

## Laser based tracking and spin measurement

```
Private Sub Text_ScrollY_TextChanged(ByVal sender As
System.Object, ByVal e As System.EventArgs) Handles
Text_ScrollY.TextChanged
    Dim ScrollY_voltage As Single
    ScrollY_voltage = Text_ScrollY.Text

    D2K_AO_Group_Set-up(card, DA_Group_A, 1, 1) ' last integer
decides which channel voltage is outputted from ( 0 to 3)
'wNumChan as short, decides how many channels are in this
group ( want one group for x mirror and one group for y mirror)
D2K_AO_Group_VUpdate(card, DA_Group_A, ScrollY_voltage)
VoltageY2 = ScrollY_voltage
End Sub

Private Sub Textbox_XZero_TextChanged(ByVal sender As
System.Object, ByVal e As System.EventArgs) Handles
Textbox_XZero.TextChanged
    m_iXZero = Textbox_XZero.Text
End Sub

Private Sub TextBox_YZero_TextChanged(ByVal sender As
System.Object, ByVal e As System.EventArgs) Handles
TextBox_YZero.TextChanged
    m_iYZero = TextBox_YZero.Text
End Sub

Private Sub Button_Calibrate_Click(ByVal sender As System.Object,
ByVal e As System.EventArgs) Handles Button_Calibrate.Click

    Dim jar As DialogResult = MessageBox.Show(" Before proceeding
make sure laser centre spot is at (159,119), would you like to
proceed?", "Calibration", MessageBoxButtons.YesNoCancel,
MessageBoxIcon.Question, MessageBoxDefaultButton.Button1,
MessageBoxOptions.RightAlign)
    If jar = DialogResult.Yes Then
        processCalibration()
    Else
        End If
End Sub

Public Sub processCalibration()
    Form2.Show()
End Sub
End Class
```

## Appendix E

The code written specifically for the launch monitor.

```

*****
'
'          NOVEL LASER TRACKING SYSTEM CODE
'
' Program   :   Soccer ball laser tracking - Launch Monitor Code
' Author    :   J A Ronkainen
' Date     :   December 2007
'
*****

Private m_blaunch As Boolean
Private m_btrack As Boolean
Private m_iXZero As Integer
Private m_iYZero As Integer
Private i As Integer
Private xx(255), yy(255) As Single
Private LaunchX As Single

Private VX1(1000), VY2(1000) As Single
Private PL(1000), PT(1000), PR(1000), PB(1000) As Single

Private Sub cvImage_ImageSnaped(ByVal sender As Object, ByVal e
As System.EventArgs) Handles cvImage.ImageSnaped
    Dim timer As Integer
    TWCreate(timer)
    TWStartStopWatch(timer, 0)

    'cvDisplay.Image = cvImage.Image
    If m_btrack = True Then
        processImage()
    End If

    If m_blaunch = True Then
        processLaunch()
    End If

    cvDisplay.Refresh()
    FormatNumber(TimeMS, 3) + " ms "
End Sub

Public Sub processLaunch()
    'If m_blaunch = True Then

    Dim xstart As Single

    ' track until the ball has moved half a diameter approx 11cm
= 0.822 V
    xstart = LaunchX - 0.822

    ' this loop will track forever if ball doesn't move

```

## Laser based tracking and spin measurement

```
If VoltageX2 > xstart Then
  'LUT
  Lut.ImageIn = cvImage.Image
  Lut.Execute()

  'Filter
  Filter.ImageIn = Lut.ImageOut
  Filter.Execute()

  Dim xcoord(1) As Single
  Dim ycoord(3) As Single

  'do Edge
  'Edge_left.Image = Lut.ImageOut
  Edge_left.Image = Filter.ImageOut
  Edge_left.Execute()
  xcoord(0) = Edge_left.PX

  'Edge_Right.Image = Lut.ImageOut()
  Edge_Right.Image = Filter.ImageOut()
  Edge_Right.Execute()
  xcoord(1) = Edge_Right.PX
  If xcoord(1) = 0 Then
    xcoord(1) = 320
  End If

  'Edge_Top.Image = Lut.ImageOut
  Edge_Top.Image = Filter.ImageOut
  Edge_Top.Execute()
  ycoord(2) = Edge_Top.PY

  'Edge_bottom.Image = Lut.ImageOut
  Edge_bottom.Image = Filter.ImageOut
  Edge_bottom.Execute()
  ycoord(3) = Edge_bottom.PY
  If ycoord(3) = 0 Then
    ycoord(3) = 240
  End If

  PixelX = (xcoord(0) + xcoord(1)) / 2
  PixelY = (ycoord(2) + ycoord(3)) / 2

  'update X-mirror voltage
  VoltageX1 = (PixelX - m_iXZero)
  'VoltageX1 = VoltageX1 * 0.003693439
  VoltageX1 = VoltageX1 * 0.003693439
  'VoltageX1 = VoltageX1 * 0.008

  'update Y-Mirror voltage
  VoltageY1 = (PixelY - m_iYZero)
  VoltageY1 = VoltageY1 * 0.004610918
  'VoltageY1 = VoltageY1 * 0.009

  ' change x-mirror position
  VoltageX2 = (VoltageX2 + VoltageX1)
  D2K_AO_Group_Set-up(card, DA_Group_A, 1, 0)
  D2K_AO_Group_VUpdate(card, DA_Group_A, VoltageX2)

  'change y-mirror position
  VoltageY2 = (VoltageY2 + VoltageY1)
```

## Laser based tracking and spin measurement

```
D2K_AO_Group_Set-up(card, DA_Group_A, 1, 1)
D2K_AO_Group_VUpdate(card, DA_Group_A, VoltageY2)
End If

If VoltageX2 < xstart Then
    processLaunch3()
End If
End Sub

Public Sub processLaunch3()

    'LUT
    Lut.ImageIn = cvImage.Image
    Lut.Execute()

    'Filter
    Filter.ImageIn = Lut.ImageOut
    Filter.Execute()

    Dim xcoord(1) As Single
    Dim ycoord(3) As Single

    'do Edge
    'Edge_left.Image = Lut.ImageOut
    Edge_left.Image = Filter.ImageOut
    Edge_left.Execute()
    xcoord(0) = Edge_left.PX

    'Edge_Right.Image = Lut.ImageOut()
    Edge_Right.Image = Filter.ImageOut()
    Edge_Right.Execute()
    xcoord(1) = Edge_Right.PX
    If xcoord(1) = 0 Then
        xcoord(1) = 320
    End If

    'Edge_Top.Image = Lut.ImageOut
    Edge_Top.Image = Filter.ImageOut
    Edge_Top.Execute()
    ycoord(2) = Edge_Top.PY

    'Edge_bottom.Image = Lut.ImageOut
    Edge_bottom.Image = Filter.ImageOut
    Edge_bottom.Execute()
    ycoord(3) = Edge_bottom.PY
    If ycoord(3) = 0 Then
        ycoord(3) = 240
    End If

    PixelX = (xcoord(0) + xcoord(1)) / 2
    PixelY = (ycoord(2) + ycoord(3)) / 2

    'update X-mirror voltage
    VoltageX1 = (PixelX - m_iXZero)
    'VoltageX1 = VoltageX1 * 0.003693439
    VoltageX1 = VoltageX1 * 0.003693439

    'update Y-Mirror voltage
    VoltageY1 = (PixelY - m_iYZero)
    VoltageY1 = VoltageY1 * 0.004610918
```



## Laser based tracking and spin measurement

```
'VoltageY1 = VoltageY1 * 0.009

' change x-mirror position
VoltageX2 = (VoltageX2 + VoltageX1)
D2K_AO_Group_Set-up(card, DA_Group_A, 1, 0)
D2K_AO_Group_VUpdate(card, DA_Group_A, VoltageX2)

'change y-mirror position
VoltageY2 = (VoltageY2 + VoltageY1)
D2K_AO_Group_Set-up(card, DA_Group_A, 1, 1)
D2K_AO_Group_VUpdate(card, DA_Group_A, VoltageY2)

xx(i) = VoltageX2
yy(i) = VoltageY2
i = i + 1

If VoltageX2 < -4 Then
  'stop grabbing
  cvImage.Grab = False
  'uncheck the checkbox_grab
  CheckBox_Grab.Checked = False
  'snap the image
  cvImage.Snap()
  cvDisplay.Image = cvImage.Image
  cvDisplay.Refresh()

  D2K_Release_Card(0) 'to stop the DAQ card outputting
voltage readings

Dim XVoltIni, XVoltFin, YVoltIni, YVoltFin As Single
Dim TimeInt, Vel, LAngle As Single
Dim XVoltDif, YVoltDif As Single
Dim XVoltDist, YvoltDist, hyp As Double
Dim q, zzt As Integer

' decide whether i = odd or even , i mod 2 = 0, number is
even
' if i = 1 number is odd
If i Mod 2 = 0 Then
  i = i
Else
  i = i - 1
End If
q = i / 2

For zzt = 0 To q - 1
  XVoltIni = XVoltIni + xx(zzt)
  YVoltIni = YVoltIni + yy(zzt)
Next

For zzt = q To i
  XVoltFin = XVoltFin + xx(zzt)
  YVoltFin = YVoltFin + yy(zzt)
Next

XVoltIni = XVoltIni / q
YVoltIni = YVoltIni / q
XVoltFin = XVoltFin / q
YVoltFin = YVoltFin / q
```

## Laser based tracking and spin measurement

```

TimeInt = (1 / 180) * q

' X Initial start point must be more than 2V
' Y Initial start point is irrelevant
XVoltDif = XVoltIni - XVoltFin
YVoltDif = YVoltIni - YVoltFin

XVoltDist = XVoltDif * 0.14937925      ' 1 volt =
0.14937925 m in distance
YvoltDist = YVoltDif * 0.119656      ' 1 Volt = 0.119656 m
in distance

hyp = System.Math.Sqrt((XVoltDist ^ 2) + (YvoltDist ^ 2))
Vel = hyp / TimeInt

LAngle = System.Math.Acos(XVoltDist / hyp)
LAngle = LAngle * 57.2958

Label_Velocity.Text() = FormatNumber(Vel, 1) & " m/s"
Label_LAngle.Text() = FormatNumber(LAngle, 1)

MessageBox.Show("Congratulations on a Succesful Launch ",
"Launch")
'MessageBox.Show(q, " q Value ")
'MessageBox.Show(YVoltIni, "YVoltIni")
'MessageBox.Show(YVoltFin, "YVoltFin")
'MessageBox.Show(hyp, "hypotenuse m")
'MessageBox.Show(XVoltDist, "x volt dist")
End If
End Sub

Private Sub Button_Launch_Click(ByVal sender As System.Object,
ByVal e As System.EventArgs) Handles Button_Launch.Click

' Make Bottom half of screen invisible
GroupBox2.Visible = False
Label5.Visible = False
TrackBar_VoltageX.Visible = False
TrackBar_VoltageY.Visible = False
Label16.Visible = False
Text_ScrollX.Visible = False
Text_ScrollY.Visible = False
Label17.Visible = False
Button_Daq.Visible = False
button_freezedaq.Visible = False
GroupBox3.Visible = False
Label19.Visible = False
Label20.Visible = False
Textbox_XZero.Visible = False
TextBox_YZero.Visible = False
button_track.Visible = False
Picture_one.Visible = False
Label6.Visible = False

button_launch2.Visible = True
Label_Velocity.Visible = True
Label_LAngle.Visible = True
Button_Tracking.Visible = True
Label_Velocity.Text = 0
Label_LAngle.Text = 0

```

## Laser based tracking and spin measurement

```
LaunchX = VoltageX2
Picture_three.Visible = True
Picture_three.Image =
System.Drawing.Image.FromFile("C:\vbfiles\Pictures\Picture_three.jpg"
)
Label_Velocity.Text() = 0 & " m/s"
End Sub

Private Sub button_launch2_Click(ByVal sender As System.Object,
ByVal e As System.EventArgs) Handles button_launch2.Click
If m_blaunch = False Then
m_blaunch = True
button_launch2.Text() = " Stop Launch Measurement "
Else
m_blaunch = False
button_launch2.Text() = " Measure Launch "
End If
End Sub

Private Sub Button_Tracking_Click(ByVal sender As System.Object,
ByVal e As System.EventArgs) Handles Button_Tracking.Click
'make launch buttons dissappear
button_launch2.Visible = False
Label_Velocity.Visible = False
Label_LAngle.Visible = False
Button_Tracking.Visible = False
Picture_three.Visible = False

' Make Bottom half of screen visible
GroupBox2.Visible = True
Label5.Visible = True
TrackBar_VoltageX.Visible = True
TrackBar_VoltageY.Visible = True
Label16.Visible = True
Text_ScrollX.Visible = True
Text_ScrollY.Visible = True
Label17.Visible = True
Button_Daq.Visible = True
button_freezedaq.Visible = True
GroupBox3.Visible = True
Label19.Visible = True
Label20.Visible = True
Textbox_XZero.Visible = True
Textbox_YZero.Visible = True
button_track.Visible = True
Picture_one.Visible = True
Label6.Visible = True

If VoltageX2 < 0.001 Then
'need to fire DAQ card again
card = D2K_Register_Card(DAQ_2501, 0)
D2K_AO_CH_Config(card, -1, DAQ2K_DA_BiPolar,
DAQ2K_DA_Int_REF, 10) ' initial card config, -1 sets all 4 AO chans,
int ref = 10, want bipolar output
End If
End Sub
End Class
```

## Appendix F

Calculations for the pixel to voltage conversion in section 7.7.1.

Basic measurements:

Diameter of cylinder = 9.6 cm

Diameter of cylinder measured in pixels = 174 pixels

Diameter of cylinder identical in vertical and horizontal axis

1 Pixel = Distance in cm / Distance pixels =  $9.6 / 174 = \underline{0.05517244 \text{ cm}}$

Measurement of laser pattern at 170 cm stand off distance:

Horizontal distance of measurement area at 170 cm stand off distance = 119.5 cm

Vertical distance of measurement area at 170 cm stand off distance = 95.7 cm

Galvo mirrors controlled manually:

119.5 cm =  $\pm 4\text{V}$  in galvo mirrors

95.7 cm =  $\pm 4\text{V}$  in galvo mirrors

X and Y-mirrors required separate control due to stand off distance between mirrors:

X-mirror Volts/cm = N° of Volts / Distance in cm =  $8 \text{ V} / 119.5 = \underline{0.066943592 \text{ V/cm}}$

Y-mirror Volts/cm = N° of Volts / Distance in cm =  $8 \text{ V} / 95.7 = \underline{0.083572891 \text{ V/cm}}$

Computed Voltage change per pixel:

X-mirror, Volts/cm  $\times$  pixel/cm =  $0.066943592 \times 0.05517244 = \underline{0.00369344 \text{ V}}$

Y-mirror, Volts/cm  $\times$  pixel/cm =  $0.083572891 \times 0.05517244 = \underline{0.004610918 \text{ V}}$

## Appendix G

Code for 'blob' analysis, other code to run program found in Appendix C.

```

*****
'
'          NOVEL LASER TRACKING SYSTEM CODE
'
' Program   :   Soccer ball laser tracking - BLOB ANALYSIS
' Author    :   J A Ronkainen
' Date      :   September 2007
'
*****

Public Sub processImage()
    If m_btrack = True Then

        Dim timer As Integer
        TWCreate(timer)
        TWStartStopWatch(timer, 0)

        cvDisplay.Image = cvImage.Image
        cvDisplay.Refresh()

        'LUT
        Lut.ImageIn = cvDisplay.Image
        Lut.Execute()

        'Filter
        Filter.ImageIn = Lut.ImageOut
        Filter.Execute()

        cvDisplay2.Image() = Filter.ImageOut
        cvDisplay2.Refresh()

        'Fblob
        Fblob.Image = Filter.ImageOut
        Fblob.Execute()

        Dim bc, totalx, totaly, totaldiv As Single

        For bc = 0 To Fblob.BlobCount - 1
            Fblob.BlobIndex = bc
            totalx = totalx +(Fblob.BlobCenterX * Fblob.BlobSize)
            totaly = totaly +(Fblob.BlobCenterY * Fblob.BlobSize)
            totaldiv = totaldiv + Fblob.BlobSize
        Next

        PixelX = (totalx / totaldiv)
        PixelY = (totaly / totaldiv)

        Text_UpdateX.Text() = PixelX
        Text_UpdateY.Text() = PixelY
    End Sub

```

## Laser based tracking and spin measurement

```
'update X-mirror voltage
VoltageX1 = (PixelX - m_iXZero)
If VoltageX1 < 0 Then
    VoltageX1 = VoltageX1 * 0.0087190557
Else
    VoltageX1 = VoltageX1 * 0.0080215313
End If

'update Y-Mirror voltage
VoltageY1 = (PixelY - m_iYZero)
If VoltageY1 < 0 Then
    VoltageY1 = VoltageY1 * 0.0096332065
Else
    VoltageY1 = VoltageY1 * 0.0099944531
End If

'change x-mirror position
VoltageX2 = (VoltageX2 + VoltageX1)

D2K_AO_Group_Set-up(card, DA_Group_A, 1, 0)
D2K_AO_Group_VUpdate(card, DA_Group_A, VoltageX2)

'change y-mirror position
VoltageY2 = (VoltageY2 + VoltageY1)

D2K_AO_Group_Set-up(card, DA_Group_A, 1, 1)
D2K_AO_Group_VUpdate(card, DA_Group_A, VoltageY2)

'read watch
TWReadStopWatch(timer, 0, TimeMS)
cvDisplay2.StatusUserText = "Processing Time : " +
FormatNumber(TimeMS, 3) + " ms "
    End If
End Sub
End Class
```

## References

- Acuna, M., H., 2002. Space based magnetometers. *Review of Scientific Instruments*, **73**, 11, pp. 3717-36.
- Alaways, L., W., and Hubbard, M., 2001. Experimental determination of baseball spin and lift. *Journal of Sports Sciences*, **19**, (5), pp. 349-58.
- Aldrich, D., 2003. Laser surface modifications in golf clubs. *Advanced Materials and Processes*, **161**, September, pp. 38-40.
- Antoine, M., M., and Simpson, R., L., 1986. A rapidly scanning three velocity component laser Doppler anemometer. *Journal of Physics part E: Scientific Instruments*, **19**, pp. 853-8.
- Asai, T., Akatsuka, T., and Haake, S., 1998. The physics of football. *Physics World*, **11**, 6, pp. 25-7.
- Asami, T., and Nolte, V., 1983. Analysis of powerful ball kicking. *Biomechanics VIII-B*, Champaign, IL: Human Kinetics publishers.
- Ashcroft, A., D., and Stronge, W., J., 2002. Putting spin on a tennis ball: friction between tennis ball and racket string-bed. *4<sup>th</sup> International Conference of Sport*, Kyoto, Japan, pp. 185-91.
- Baker, J., R., Laming, R., I., Wilmschurst, T., H., and Halliwell, N., A., 1990. A new, high sensitivity laser vibrometer. *Optics and Laser Technology*, **22**, 4, pp. 241-4.
- Ballantyne, A., Blackmore, C., S., and Rizzo, J., E., 1974. Frequency shifting for laser anemometers by scattering. *Optics and Laser Technology*, **6**, August, pp. 170-3.
- Bao, L., 2003. Relation between frictional characteristics and strings' ability to make a tennis ball spin, *Textile Research Journal*, **73**, (7), pp. 570-74.
- Barras, D., E., 2006. The feasibility of sports grips customisation using rapid manufacturing methodologies. *PhD Thesis*, Loughborough University.
- Bearman, P., W., and Harvey, J., K., 1976. Golf ball aerodynamics, *Aeronautical Quarterly*, May, pp. 112-22.

- Beasley, D., and Camp, T., 2002. Effects of dimple design on the aerodynamic performance of a golf ball. *Science and golf IV: Proceedings of the World Scientific Congress on Golf*, St Andrews, Scotland, pp. 329-38.
- Bell, J., R., and Rothberg, S., 2000a. Rotational vibration measurements using laser Doppler vibrometry: comprehensive theory and practical application. *Journal of Sound and Vibration*, **238**, 4, pp. 673-690.
- Bell, J., R., and Rothberg, S., 2000b. Laser vibrometers and contacting transducers, target rotation and six degree-of-freedom vibration: What do we really measure? *Journal of Sound and Vibration*, **237**, 2, pp. 245-61.
- Bell, J., R., 2001. Application of laser Doppler velocimetry to rotor vibration measurement. *PhD Thesis*, Loughborough University.
- Bendel, K., 2004. Measuring ODS of fans with a SLDV. *Sixth International Conference on Vibration Measurements by Laser Techniques*, Ancona, Italy, pp. 292-7.
- Blais, F., Beraldin, J., Cournoyer, L., Christie, I., and Serafini, R., 2000. Integration of a tracking laser range camera with photogrammetry based space vision system. *SPIE Proceedings*, Orlando, Florida, **4025**, NRC 43650.
- Blais, F., Beraldin, J., El-Hakim, S., F., and Cournoyer, L., 2001. Real-time geometrical tracking and pose estimation using laser triangulation and photogrammetry. *Proceedings of the Third International Conference on 3D Digital Imaging and Modelling*, Ottawa, Canada, 28<sup>th</sup> June, pp. 1-9.
- Bokelberger, E., H., Sommer, H., J., and Trethewey, M., W., 1994a. A six degree of freedom laser vibrometer, part I: theoretical development. *Journal of Sound and Vibration*, **178**, 5, pp. 643-54.
- Bokelberger, E., H., Sommer, H., J., and Trethewey, M., W., 1994b. A six degree of freedom laser vibrometer, part II: experimental validation. *Journal of Sound and Vibration*, **178**, 5, pp. 655-67.
- Brancazio, P., J., 1985. The physics of kicking a football. *The Physics Teacher*, **23**, pp. 403-7.
- Braunwart, P., R., 1998. Experimental and analytical examination of golf club dynamics. *MSc*, Virginia Polytechnic Institution, December, 11<sup>th</sup>, pp. 60.
- Briggs, L., 1959. Effect of spin and speed on the lateral deflection (curve) of a baseball; and the Magnus effect for smooth spheres. *American Journal of Physics*, **27**, pp. 589-96.



## Laser based tracking and spin measurement

- Brooks, R., Mather, J., S., and Knowles, S., 2006. The influence of impact vibration modes and frequencies on cricket bat performance. *Special Issue Paper, Proceedings of the IMechE, Part L, Journal of Materials: Design and Applications*, **220**, 4, pp. 237-48.
- Buchave, P., 1975. Laser Doppler velocimeter with variable optical frequency shift. *Optics and Laser Technology*, **7**, February, pp. 11-6.
- Carre, M., J., Asai, T., Akatsuka, T., and Haake, S., J., 2002. The curve kick of a football II: flight through the air. *Sports Engineering*, **5**, 4, pp.193-200.
- Carre, M., Goodwill, S., Haake, S., Hanna, R., and Wilms, J., 2004. Understanding the aerodynamics of a spinning soccer ball. *The Engineering of Sport*, **5**, pp. 70-6.
- Cassinelli, A., Perrin, S., and Ishikawa, M., 2005. Smart laser-scanner for 3D human-machine interface, ACM SIGHI, *International Conference on Human Factors in Computing Systems*, Portland, USA, pp. 33-5.
- Castellini, P., and Santolini, C., 1998. Vibration measurements on blades of a naval propeller rotating in water with tracking laser vibrometer. *Measurement*, **24**, pp.43-54.
- Castellini, P., and Revel, G., 1999. Tracking laser vibrometer measurements for estimation of excitation level in rotating structures. *IMAC*, Kissimmee, Florida, USA, pp. 1005-11.
- Castellini, P., and Paone, N., 2000. Development of the tracking laser vibrometer: performance and uncertainty analysis. *Review of Scientific Instruments*, **71**, 12, pp. 4639-47.
- Castellini, P., and Cupido, E., 2001. Vibration measurements on wind-screen wipers by TLDV. *IMAC*, Kissimmee, Florida, USA, pp. 457-63.
- Castellini, P., and Montanini, R., 2002. Automotive components vibration measurements by tracking LDV: advances in signal processing. *Institute of Physics Publishing, Measurement Science and Technology*, **13**, pp.1266-79.
- Castellini, P., and Tomasini, E., 2002. Novel image tracking LDV for application on automotive field. *IMAC*, pp. 1004-8.
- Castellini, P., and Tomasini, E., 2004. Image-based tracking LDV. *Review of Scientific Instruments*, **75**, 1, January, pp.222-32.
- Cochran, A., J., and Stobbs, J., 1968. The search for the perfect swing. Triumph books, Chicago, ISBN 1-57243-109-1

Cotton, R., T., 2006. Unpublished spin rate work in cooperation with adidas, Testing spin rate on the adidas fevernova world cup 2002 soccer ball.

Daish, C., 1971. Light. English universities press, ISBN 0340115904.

Dart, T., 2007. Why Ronaldo holds the trumps in goalkeepers guessing game. *The Times, Sport*. Friday, December, 21<sup>st</sup>, pp. 99.

Davies, J., 1949. The aerodynamics of golf balls. *Journal of Applied Physics*, **20**, (9), September, pp. 821-8.

Dietzhausen, H., Bendel, K., and Scelles, N., 2003. Tracking scanning LDV: extending laser vibrometry to arbitrarily moving objects. *IMAC*, Kissimmee, Florida, USA, pp. 168-74.

Dignall, R., J., Haake, S., J., and Chadwick, S., G., 2000. Modelling of an oblique tennis ball impact on a court surface. *3<sup>rd</sup> International Conference of Sport*, Sydney, Australia, pp. 185-92.

Di Maio, D., and Ewins, D., J., 2006. Caizer Nymesis, a new software platform for virtual and actual vibration testing on rotating structures using continuously scanning LDV technique. *Seventh International Conference on Vibration and Measurements by Laser Techniques*, Ancona, Italy, pp. 27-32.

DOC, Digital Optics Corporation., 2006. Quote for purpose built DOE. Personal communication with Brandi Ramsey, Sales support engineer, 20<sup>th</sup> November 2006.

Dougherty, J., 2007. Using filters in colour inspection. *Vision Systems Design*, June, pp. 33-38.

Drain, L., E., 1980. The laser Doppler technique. John Wiley & Sons, ISBN 0471276278.

Durst, F., Melling, A., and Whitelaw, J., H., 1981a. Principles and practice of laser-Doppler anemometry. London academic press, ISBN 0122252608.

Durst, F., Lehman, B., and Tropea, C., 1981b. Laser-doppler system for rapid scanning of flow fields. *Review of Scientific Instruments*, **52**, 11, November, pp. 1676-81.

EDH, 2006. EDH sport homepage, EDH RacquetRadar product, internet website, <http://www.edhsport.com/>, accessed 12<sup>th</sup> December 2006.

Einstein, A., 1917. Zur Quantentheorie der Strahlung. *Physikalische Zeitschrift*, **18**, pp. 121-8.

## Laser based tracking and spin measurement

- FIFA, Federation Internationale de Football Association, 1996. The denominations programme, Magazette, Thursday, 15<sup>th</sup>, February, www.Fifa.com, accessed 14<sup>th</sup> april 2008.
- FIFA, Federation Internationale de Football Association, 2006. Laws of the game, Law 2, the ball, fifa.com, accessed 15<sup>th</sup> January 2008.
- First sight vision, 2004. Vision elements 'the machine vision handbook', vision components 2004/2005, catalogue.
- Frohlich, C., 1983. Aerodynamic drag crisis and its possible effect on the flight of baseballs. *American Journal of Physics*, **52**, (4), pp. 325-34.
- Garner, C., P., 2006. Spin rates. Personal communication with professor of applied thermodynamics, email 9<sup>th</sup> of November.
- Gobush, W., 1996. Friction coefficient of golf balls. *The Engineering of Sport* (Rotterdam), pp. 193-4.
- Gobush, W., 1995. Monitoring systems to measure and display flight characteristics of moving sports object, *United States patent*, 5,471,383, patented 28<sup>th</sup> November.
- Gobush, W., 2005. Multishutter club-ball analyser, *United States patent application* 20050054456.
- Goodwill, S., Douglas, J., Miller, S., and Haake, S., 2006. Measuring ball spin off a tennis racket. *The Engineering of Sport*, **6**, *Developments for sports*, (1), pp. 379-84.
- Halkon ,B., and Rothberg, S., 2002a. Comprehensive velocity sensitivity model for scanning and tracking LDV on rotating structures. *Fifth International Conference on Vibration Measurements by Laser Techniques*, Ancona, Italy, pp. 9-21.
- Halkon, B., and Rotherg, S., 2002b. Comprehensive velocity sensitivity model for scanning and tracking laser vibrometry. *IMAC*, Los Angeles, California, USA, pp. 1166-70.
- Halkon, B., Frizzel, S., R., and Rothberg, S., 2003. Vibration measurements using continuous scanning LDV: theoretical velocity sensitivity analysis with application. *Institute of Physics Publishing, Measurement Science and Technology*, **14**, pp.382-393.
- Halkon, B., and Rothberg, S., 2003. Vibration measurements using continuous SLDV: velocity sensitivity model experimental validation. *Institute of Physics Publishing, Measurement Science and Technology*, **14**, pp. 773-83.

## Laser based tracking and spin measurement

Halkon, B., and Rothberg, S., 2004. Synchronised SLDV. *Sixth International Conference on Vibration Measurements by Laser Techniques*, pp. 260-71.

Halliwell, N., and Hargrave, G., 2003. Optical engineering: diagnostic for industrial applications. *Proceedings of Institute of Mechanical Engineers Part C: Journal of Mechanical Engineering Science*, **217**, pp. 597-617.

Halliwell, N., A., 1979. Laser Doppler measurement of vibrating surfaces: a portable instrument. *Journal of Sound and Vibration*, **62**, 2, pp. 312-5.

Halliwell, N., A., 1986. Measurement of oscillatory and vibrational motion. *United States patent*, 4601590, July 22<sup>nd</sup>, pp.1-17.

Halliwell, N., A., 1993. Laser vibrometry, Chapter 6 in *Optical methods in engineering*, author: Williams, D., C., pp. 179-211, ISBN 0412396408.

Halliwell, N., A., 1996. The laser torsional vibrometer: a step forward in rotating machinery diagnostics. *Journal of Sound and Vibration*, **190**, 3, pp. 399-418.

Halliwell, N., A., and Eastwood, P., G., 1985. The laser torsional vibrometer, *Journal of Sound and Vibration*, **101**, 3, pp. 446-9.

Halliwell, N., A., Hocknell, A., and Rothberg, S., 1997. On the measurement of angular vibration displacements: a laser tiltmeter. *Journal of Sound and Vibration*, **208**, 3, pp. 497-500.

Halliwell, N., A., Pickering, C., J., and Eastwood, P., G., 1984. The laser torsional vibrometer: a new instrument. *Journal of Sound and Vibration*, **93**, 4, pp. 588-92.

Harman, N., 2007. Hawkeye to have final say at Wimbledon. *The Times*, 24<sup>th</sup> May.

Hartmut, B., Roland, S., Walter, E., and Udo, K., 2001. Device for detecting the position and/or movement of objects and/or living things. *World Wide patent*, WO0166201, patented September 13<sup>th</sup>.

Hawkeye., 2008. Tennis. Website <http://www.hawkeyeinnovations.co.uk>. accessed 6<sup>th</sup> February 2008.

Hawkins, P., and Sherry, D., 2001. Video processor systems for ball tracking in ball games. *World wide patent*, WO01/41884A1, International patent classification A63B71/06, 14<sup>th</sup> June.

Hawkins, P., 2007. (Quoted from) Hawkeye creator defends his system after Federers volley, *The Times*, article written by Pavia, W., 10<sup>th</sup> July.

Hecht, E., 1998. Optics. Addison Wesley Longman Inc, 3<sup>rd</sup> edition, ISBN 0201304252.

Heikkila, J., and Silven, O., 1997. A four step camera calibration procedure with implicit image correction. *Proceedings of CVPR, IEEE*, pp. 1106-12.

Hocknell, A., Mitchell, S., Jones, R., and Rothberg, S., 1998a. Hollow golf club head modal characteristics: determination and impact applications. *Experimental Mechanics*. **38**, 2, June, pp. 140-6.

Hocknell, A., Jones, R., and Rothberg, S., 1998b. Remote vibration measurements: compensation of waveform distortion due to whole body translations. *The Journal of Sound and Vibration*. **214**, 2, pp. 285-307.

Holmes, C., E., Jones, R., Harland, A., and Ward, D., 2007. Development of a mechanical kicking simulator. *Journal of Sports Science and Medicine*, **10**, pp. 44-5.

Holmes, C., E., 2008. Advanced modelling of ovoid balls. *PhD thesis*, Loughborough University, pp. 71-87.

Huygens, C., 1690. *Traite de la lumiere*. Dover – New York press.

IEC, International Electrotechnical Commission., 2007. International Standard, Safety of laser products – Part 1: Equipment classification and equipment. Edition 2.0, March, ISBN: 2-8318-9085-3.

Independent., 2007. Today's top twenty: Average height of premier league squads (2007 – 2008). October 26<sup>th</sup>.

IRB, International rugby board, 2006. Playing charter, as framed by the international rugby board. irb.com, accessed 15<sup>th</sup> December 2006.

Ireson, G., 2001. Beckham as physicist? *Institute of Physics Publishing, Physics Education, Special Feature: Physics in Sport*, pp. 11-3.

ISG, Interactive Sports Games., 2005. Trackman R&D, 20 slide powerpoint presentation, shown at Loughborough University, 15<sup>th</sup> of November.

Isokawa, M., and Lees, A., 1988. A biomechanical analysis of the instep kick motion in soccer. *Science and Football: Proceedings of the First World Congress of Science and Football*, London: E & FN Spon, pp. 449-55.

ITTF, International table tennis federation, 2003. ITTF handbook, 2.03 the ball, updated 15<sup>th</sup> of July 2003, ittf.com, accessed 15<sup>th</sup> December 2006.

## Laser based tracking and spin measurement

Johansmann, M., Siegmund, G., and Pineda, M., 2005. Targeting the limits of LDV, *Proceedings of IDEMA*, Santa Clara, California, USA, pp. 1-12.

Johnson, H., and Foster, M., C., 2003. Golf ball tracking device. *World Wide patent*, WO03032006, patented April 17<sup>th</sup>.

Knowles, S., Mather, J., S., and Brooks, R., 1996. Cricket bat design and analysis through impact vibration modelling. *The Engineering of Sport*, **1**, pp. 339-46.

Kurtus, R., 2007. Beat frequency in sound. Website [http://www.school-for-champions.com/science/sound\\_beat.htm](http://www.school-for-champions.com/science/sound_beat.htm), accessed 17<sup>th</sup> June 2008.

Langmuir, R., 1963. Scattering of laser light. *Applied Physics Letters*, **2**, 2, 15<sup>th</sup> January, pp. 29-30.

Levis, I., 2006. The myths and realities of image acquisition. *Photonics Spectra*, November, pp. 70-2.

LOE, Laser Optical Engineering., 2007a. Diffractive optical elements. Web site accessed 10<sup>th</sup> of September 2007, <http://www.laseroptical.co.uk/kinofoms.html>.

LOE, Laser Optical Engineering, 2007b. Quote for purpose built DOE. Personal communication with Professor John Tyrer, 5<sup>th</sup> March 2007.

Maccoll, J., 1928. Aerodynamics of a spinning sphere. *Royal Aeronautical Society*, **32**, pp. 777-91.

Macmillan, M., 1975. Determinants of the flight of the kicked football. *Research Quarterly*, **46**, pp. 48-57.

Marinelli, D., 2000. Speed, spin rate, curve measuring device. *United States patent* 6,418,271, Silicon Pie Incorporation, patented November 14<sup>th</sup>.

McReary, I., McLachlan, P., and Kellet, J., 2005. Method of determining a flight trajectory and extracting flight data for a trackable golf ball. *United States patent application*, 20050233815, HBL Limited, patented October 20<sup>th</sup>.

Mehta, R., D., 1985. Aerodynamics of sports balls. *Annual Review of Fluid Mechanics*, **17**, pp. 151-89.

MFA/Como drills, UK, 2008. Online brochure, [www.mfacomodrills.com](http://www.mfacomodrills.com) accessed 25<sup>th</sup>, April.

Michelson, A., A., and Morley, E., W., 1887. On the real motion of earth and the luminiferous ether. *The American Journal of Science*, **34**, 3, pp. 333-45.

Mihran, R., T., 2001. Spin determination for a rotating object. *United States patent* 6,244,97, the DistanceCaddy company, LLC, patented June 12<sup>th</sup>.

Miles, T., J., Lucas, M., and Rothberg, S., 1996. Bending vibration measurement on rotors by laser vibrometry. *Optics Letters*, **21**, 4, February, pp. 296-8.

Miles, T., J., Lucas, M., Halliwell, N., A., and Rothberg, S., 1999. Torsional and bending vibration measurement on rotors using laser technology. *Journal of Sound and Vibration*, **226**, 3, pp. 441-67.

MLB, Major League Baseball, 2006. Official info, official rules, 1.00 objectives of the game. [www.mlb.com](http://www.mlb.com), accessed 15<sup>th</sup> December 2006.

Morales, W., Fusaro, R., and Kascak, A., 2003. Permanent magnetic bearing for spacecraft applications. *Tribology Transactions*, **46**, 3, pp. 460-4.

Muybridge, E., J., 1883. Method and apparatus for photographing changing or moving objects. *United States patent*, 279,878, patented June 19<sup>th</sup>.

Muybridge, E., J., 1878. The horse in motion. Adapted from still image, Library of congress prints and photographs division, Washington, DC 20540, USA. Internet website, <http://www.loc.gov/rr/print/list/picamer/paMotPic.html>, accessed 7th February 2008.

Naruo, T., and Mizota, T., 2004. Trajectory analysis and optimum trajectory of a golf ball. *The Engineering of Sport*, **5**, pp. 432-9.

Nathan, A.M., Hopkins, J., Chong, L. and Kacmarski, H., 2006. The effect of spin on the flight of a baseball. *The Engineering of Sport*, **6**, *Developments for sports*, (1), pp. 23-8.

Neilson, P., J., 2003. The dynamic testing of soccer balls. *PhD Thesis*. Chapter 4 – Determination of soccer ball performance parameters, pp. 59-74.

Neilson, P., Jones, R., Kerr, D., and Sumpter, C., 2004a. An automated system for the measurement of soccer ball flight characteristics. *Engineering of Sport*, **5**, (2), pp. 180-6.

Neilson, P., Jones, R., Kerr, D., and Sumpter, C., 2004b. An image recognition system for the measurement of soccer ball spin characteristics. *Institute of Physics Publishing, Measurement Science and Technology*, **15**, pp. 2239-47.

## Laser based tracking and spin measurement

- NFL, National Football League, 2006. NFL fans, digest of rules, the ball, internet website [www.nfl.com](http://www.nfl.com), accessed 15<sup>th</sup> December 2006.
- Nike., Nike Incorporation., 2007. Nike's total ninety laser: Designed for shooting accuracy. Press Release, received in personal communication 5<sup>th</sup> November.
- Norby, J., 2005. Petawatt lasers aim for relativistic phenomena. *Laser Focus World*, January, pp. 34-7.
- Nowak, C., J., 2003. Flight data recorder for the American football. *MSc*, State University of New York at Buffalo, submitted May 25<sup>th</sup>.
- Nunome, H., Asai, T., Ikegami, Y., and Sakurai, S., 2002. Three-dimensional kinetic analysis of side-foot and instep soccer kicks. *Medicine and Science in Sports and Exercise*, **34**, 12, pp. 2028-36.
- Oldengarm, J., Krieken, A., H., and Raterink, H., J., 1973. Laser Doppler velocimeter with optical frequency shifting. *Optics and Laser Technology*, **5**, December, pp. 249-52.
- Oliver, B., M., 1963, Sparkling spots and random diffraction. *Proceedings of the IEEE*, January, pp. 220-1.
- Pallis, J., M., 1998. US open professional player ball spin work, cooperative agreement between NASA and Cislunar aerospace, internet website accessed 12th December 2006, <http://wings.avkids.com/Tennis/Project/index.html>.
- Parsons, D., 2005. Personal communication. Spin bowling at the England Cricket Academy, England Cricket Board (ECB), 24<sup>th</sup>, November.
- Perrin, S., Cassinelli, A., Ishikawa, M., 2003. Laser-based finger tracking system suitable for MOEMS integration. *Image and vision computing, IVCNZ*, Massey, New Zealand, November.
- Perrin, S., Cassinelli, A., Ishikawa, M., 2004. Gesture recognition using laser-based tracking system. *6<sup>th</sup> International Conference on Automatic Face Recognition*, Seoul, Korea, 17<sup>th</sup> -19<sup>th</sup> May.
- Pickering, C., J., Halliwell, N., A., and Wilmshurst, T., H., 1986. The laser vibrometer: A Portable instrument. *Journal of Sound and Vibration*, **107**, 3, pp. 471-85.
- Plagenhoef, S., 1971. The patterns of human motion, a cinematographic analysis. Englewood Cliffs, Prentice-Hall, ISBN 01365178.



Polytec GmbH, 2006. Rotational vibrometer 4000 series brochure.

Prandtl, L., 1905. Theory of lifting surfaces. *National Advisory Committee for Aeronautical Technical Notes*, 10, pp. 451-77.

Precision Graphics., 2000. The lens. *The American Heritage Dictionary of the English Language*, 4<sup>th</sup> Edition, Website <http://www.bartleby.com/61/imagepages/A4lens.html> accessed 17<sup>th</sup> June 2008.

Price, D., S., Neilson, P., J., Harland, A., R., and Jones, R., 2003. Measurement of out of balance forces in soccer balls. *5<sup>th</sup> World Congress of Science and Football*, Lisbon, April, pp. 11-5.

Price, D., S., 2005. Advanced modelling of soccer balls. *PhD Thesis*, Loughborough University.

Quinspin, 2006. Promotional image. [www.quinspin.com](http://www.quinspin.com), accessed 7<sup>th</sup> February 2008.

Rae, W., J., 2003. Flight dynamics of an American football in a forward pass. *Journal of Sports Engineering*, 6, pp. 149-63.

Rapp, P., 2004. Speeds and feeds for standard solid carbide drills and high speed steel twist drills. *Engineers Black Book*, 2<sup>nd</sup> edition, ISBN 0-9580571-1-7, pp. 43-4.

Rasband, W., 2006. ImageJ software, Version 1.36b, *National Institute of Health*, USA, open source application, Java 1.3.1\_13.

Reilly, T., P., Bangsbo, J., and Franks, A., 2000. Anthropometric and physiological predispositions for elite soccer. *Journal of Sports Sciences*, 18, pp. 669-83.

Reilly, T., P., 2008. Maximal kicking power related to age. Personal communication received on 15<sup>th</sup> January 2008.

Rhodes, D., R., 1959. Introduction to monopulse. McGraw-Hill. ISBN: 0890060916.

Rigden, J., D., and Gordon, E., I., 1962. The granularity of scattered optical maser light. *Proceedings of the I.R.E.*, November, pp. 2367-8.

Roberts, J., R., 2002. Mechanical and psychological influences on the 'feel' of a golf shot. *PhD Thesis*, Loughborough University.

Roberts, E., M., and Metcalfe, A., 1968. Mechanical analysis of kicking. *Biomechanics I*, Baltimore University press, pp. 513-9.

- Ronkainen, J., A., 2004. Acoustic assessment of soccer ball impacts. *BSc Final Year Project*, pp. 21-3.
- Ronkainen, J., A., and Harland, A., 2006. Soccer ball modal analysis using a scanning laser Doppler vibrometer. *The Engineering of Sport, Developments for Sports* **6**, (1), pp. 357-362.
- Rothberg, S., Baker, J., and Halliwell, N., 1989. Laser vibrometry: pseudo vibrations. *Journal of Sound and Vibration*, **135** (3), pp. 516-22.
- Rothberg, S., and Halliwell, N., A., 1993. Laser vibrometry on solid surfaces: the effects of laser speckle. *Journal of Laser Applications*, **6**, pp. 38-41.
- Rothberg, S., and Halliwell, N., A., 1994. Vibration measurements on rotating machinery using laser Doppler velocimetry. *Journal of Vibration and Acoustics*. **116**, pp. 326-31.
- Rothberg, S., and Halkon, B., 2004. Laser vibrometry meets laser speckle. *SPIE, Sixth International Conference on Vibration Measurements by Laser Techniques*, **5503**, pp. 280-91.
- Rothberg, S., 2006. Numerical simulation of speckle noise in laser Vibrometry. *Applied Optics*, **45**, 19, pp. 4523-33.
- Scitec Instruments., 2007. DPSS Laser price catalogue, web site, accessed 7<sup>th</sup> of September 2007, <http://www.scitec.uk.com/lasers/>.
- SGMA, Sporting Goods Manufacturing Association., 2008. Manufacturers sales by category report, US wholesale value of annual manufacturers' shipments (\$millions). Online reports. Accessed April 18<sup>th</sup> 2008, [www.sgma.com](http://www.sgma.com).
- Shirinzadeh, B., 1998. Laser interferometry based tracking for dynamic measurements. *Industrial Robot*, **25**, 1, pp. 35-41.
- Smits, A., J., and Ogg, S., 2004. Golf ball aerodynamics. *The Engineering of Sport*, **5**, (1), pp. 3-12..
- Soccer Ball World., 2007. adidas and Cairos test new goal line technology during FIFA club World Cup, Japan. Web Press release, accessed 6<sup>th</sup> February 2008. [Soccerballworld.com/Teamgeist\\_II.htm](http://Soccerballworld.com/Teamgeist_II.htm), 13<sup>th</sup> December.
- Sriram, P., Hanagud, S., Craig, J., and Komerath, N., M., 1990. Scanning laser Doppler technique for velocity profile sensing on a moving surface. *Applied Optics*, **29**, 16, pp. 2409-17.

- Srixon, 2003. Srixon golf science center brochure, BCS theory, published July.
- Srixon, 2008. Brand history, Website [www.srixon.co.uk/story.aspx](http://www.srixon.co.uk/story.aspx), accessed 15<sup>th</sup> April 2008.
- Stachura, M., 2006. The 17 yard secret. *Golf Digest Magazine*, December, pp. 76-81.
- Stanbridge A., and Ewins, D., 1995. Modal testing of rotating discs using a scanning LDV. *Design Engineering Technical Conferences*, **3**, B, ASME, pp. 1207-13.
- Stanbridge, A., Sever, I., and Ewins, D., 2002a. Vibration measurements in a rotating blisk test rig using an LDV. *Fifth International Conference on Vibration Measurements by Laser Techniques*, Ancona, Italy, pp. 1-8.
- Stanbridge, A., Martarelli, M., and Ewins, D., J., 2002b. Continuous-scan vibration measurements on moving components. *IMAC*, Los Angeles, California, USA, pp. 1519-25.
- Sumitomo Rubber Industries Ltd., 2006. Financial summary, August 29<sup>th</sup>, flash report, pp. 7.
- Sumpter, C., 1993. Golf ball flight path digitiser for windows. Version 1.01, CMS Consultancy.
- Takai, N., Iwai, T., and Asakura, T., 1983. Correlation distance of dynamic speckles. *Applied Optics*, **22**, 1, pp. 170-7.
- Tamaki, T., Sugino, T., and Yamamoto, M., 2004. Measuring ball spin by image registration. *FCV: The 10th Korea-Japan Joint Workshop on Frontiers of Computer Vision*, Fukuoka, Japan, pp. 269-74.
- Tavares, G., Shannon, K., and Melvin, T., 1998. Golf ball spin decay model based on radar measurements. *Science and Golf III: Proceedings of the World Scientific Congress on Golf*, St Andrews, Scotland, human kinetics, pp. 464-72.
- Theobalt, C., Albrecht, I., Haber, J., Magnor, M., and Seidel, H-P., 2004. Pitching a baseball- tracking high speed motion with multi-exposure images. *ACM, Transactions on Graphics, Special Issue SIGGRAPH*, **23**, 3, August, pp. 540-7.
- Thomas, G., Deiters, T., Best, C., 1995. Simulating golf club performance using modal analysis. *Proceedings of the 13<sup>th</sup> International Modal Analysis Conference, SEM*, Nashville, Tennessee, United States, February, 13 – 16<sup>th</sup>, pp. 989-95.
- Trackman, 2006. Interactive Sports Games A/S, [www.trackman.dk](http://www.trackman.dk), accessed 15<sup>th</sup> December 2006.

- Trethewey, M., W., Sommer, H., J., and Cafeo, J., A., 1993. A dual beam laser vibrometer for measurement of dynamic structural rotations and displacements. *Journal of Sound and Vibration*, **164**, 1, pp. 67-84.
- Tsai, C-Z., and Wu, E., 1998. A transient laser Doppler anemometry for measurement of rapidly changing velocities of solid bodies. *Experimental Mechanics*, **38**, 4, December, pp. 1-9.
- Tsaousidis, N., and Zatsiorsky, V., M., 1996. Two types of ball-effector interaction and their relative contribution to soccer kicking. *Human Movement Science*, **15**, 6, pp. 861-76.
- Tuxen, F., 2005. A method of and an apparatus for determining information relating to a projectile, such as a golf ball. *World Wide patent*, WO2005116678, Interactive Sports Games AS, patented December 8<sup>th</sup>.
- UKAS, United Kingdom Accreditation Service., 1997. M3003, The expression of uncertainty and confidence in measurement. Crown copyright, **1**, December, pp. 10-15.
- USGA, United States Golf Association, 2006. Club and ball rules, equipment testing, appendix III – the ball, [www.usga.org](http://www.usga.org), accessed 15<sup>th</sup> December 2006.
- Varoto, P., S., and McConnell, K., G., 1995. Using modal analysis to evaluate golf club performance. *Sound and Vibration*, **29**, 3, pp. 1962-6.
- Vignola, J., and Houston, B., 1993. The design of a three dimensional laser vibrometer. *The American Society of Mechanical Engineers*, **42**, pp. 1-10.
- Wagner, W., E., III., 2007. Using SPSS for social statistics and research methods. London: Sage Publication Ltd, ISBN: 9781412940771.
- Walter, E., 2005. Football force measurement unit has pressure and three axis acceleration sensors with radio link to processor and display. *German patent*, DE10338620, patented March 24<sup>th</sup>.
- Watts, R., and Moore, G., 2003. The drag force on an American football. *American Association of Physics Teachers*, **71**, (8), pp. 791-3.
- Watts, R., and Sawyer, E., 1975. Aerodynamics of a knuckleball. *American Journal of Physics*, **43**, (11), pp. 960-3.
- Wány, M., 2007. Trends in CMOS and CCD image sensors. *Machine Vision Design*, April, pp. 31-35.

- Wei, X., F., and Grill, W., M., 2005. Current density distribution, field distributions and impedance analysis of segmented deep brain stimulation electrodes. *Institute of Physics Publishing, Journal of Neural Engineering*, 2, pp. 139-47.
- Wicks, A., L., Knight, C., E., Braunwart, P., and Neighbors, J., 1999. The dynamics of a golf club. *The 17<sup>th</sup> International Modal Analysis Conference*, Kissimmee, Florida, United States, February, 8– 11<sup>th</sup>, pp. 503-8.
- Williamson, M., 2006. Selecting image-transfer techniques for high speed imaging. *Europhotonics*, October/November, pp. 30-1.
- Wilson, A., 2006. Product focus – PCI express captures frame-grabber designs. *Vision Systems Design*, November, pp. 95-101.
- Wilson, A., 2007a. Product focus – Standards propel gigabit ethernet to the forefront. *Vision Systems Design*, February, pp. 31-38.
- Wilson, A., 2007b. Product focus – Understanding camera performance specs. *Vision Systems Design*, July, pp. 39-45.
- Winfield, D., C., 2002. Method of image processing of paint dots on golf balls. *United States patent*, 6,390,934, Acushnet company, March 29<sup>th</sup>.
- Yeh, Y., and Cummins, H., Z., 1964. Localized fluid flow measurements with an He-Ne laser spectrometer. *Applied Physics Letters*, 4, 10, May, pp. 176-8.
- Zeleny, R., 2004. Choosing the right galvo for your application requires understanding system requirements. *SPIE's Magazine*, May, pp. 30-2.
- Zeng, X., Wicks, A., and Mitchell, L., 1994. The determination of the position and orientation of a scanning laser vibrometer for a laser-based mobility measurement system. *Proceedings of SPIE – The International Society for Optical Engineering*, Bellingham, Washington, USA, 2358, pp.81-92.
- Zhang, Z., 1999. Flexible camera calibration by viewing a plane from unknown orientations. *Proceedings of International Conference on Computer Vision*, Corfu, Greece, September, pp. 666–73.
- Zhang, Z., 2000. A flexible new technique for camera calibration. *IEEE, Transactions on Pattern Analysis and Machine Intelligence*, 22, 11, pp. 1330–4.



